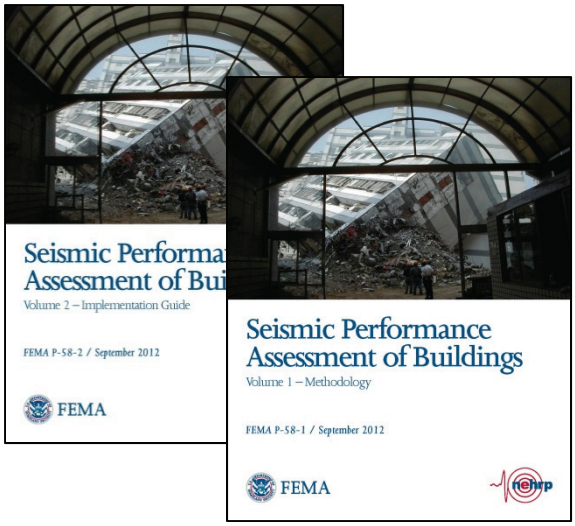

Background Document

FEMA P-58/BD-3.8.9

Fragility Functions for Slender Reinforced Concrete Walls

Prepared by

Anna C. Birely, Laura N. Lowes, and Dawn E. Lehman
Department of Civil and Environmental Engineering
214B More Hall
University of Washington
Seattle, Washington 98195

Submitted to

APPLIED TECHNOLOGY COUNCIL
201 Redwood Shores Parkway, Suite 240
Redwood City, California 94065
www.ATCouncil.org

Prepared for

FEDERAL EMERGENCY MANAGEMENT AGENCY
U.S. Department of Homeland Security
500 C Street, SW
Washington, D.C. 20472

June 7, 2011

FEMA

nehrp

Background Documentation

FEMA P-58 Background Documents are a series of reports documenting the technical background and source information for key aspects of the FEMA P-58 methodology and its implementation. These reports were developed over the course of the 10-year ATC-58/ATC-58-1 Projects funded under FEMA Contracts EMW-2001-RP-0056 and HSFEHQ-06-D-1105.

Background Documents were developed by consultants, serving at various levels within the project hierarchy, reporting the results of: (1) decisions on technical development protocols; (2) focused studies on the development of key aspects of the methodology; (3) documentation of recommended procedures; and (4) collection of available data for the development of structural and nonstructural fragilities. They were initially intended to serve as a record of the technical state-of-knowledge at the time they were produced, and as resources for the development of the eventual project reports. As such, they represent a snapshot in time, and may, or may not, match the technical content, recommended procedures, or data incorporated into the final methodology and its implementation.

This Background Document is intended for the purpose of providing supplemental knowledge to users of the FEMA P-58 methodology. Information contained herein has not been independently verified for accuracy as a stand-alone document, and may have been superseded in its final implementation within the methodology. Users of information in this document assume all liability arising from such use.

Notice

Cover illustration – Primary resource documents for the FEMA P-58 *Seismic Performance Assessment of Buildings, Methodology and Implementation* series of products: FEMA P-58-1, *Volume 1 – Methodology*, and FEMA P-58-2, *Volume 2 – Implementation Guide*.

Contents

Chapter 1

Introduction

This report discusses the development of and presents compiled fragility functions for slender reinforced concrete walls, where slender is defined as a shear span ratio equal to or exceeding two (2.0). The presented fragility functions are part of the ATC-58 project and were developed following the procedures outlined in *Guidelines for Seismic Performance Assessment of Buildings: ATC-58* 50% *draft.* [1].

Fragility functions for performance based earthquake engineering (PBEE) are functional relationships defining the likelihood that a specific method of repair (MOR) will be required given a specific magnitude of engineering demand parameter (EDP) experienced by a structural component or system. The methods of repair are associated with specific damage states (DS). The MORs are intended to provided a basis for quantifying the economic impact of structural damage resulting from a seismic event. The fragility functions were developed using experimental data and expert opinion.

The layout of this report is as follows: Chapter 1 provides an introduction, including a brief description of prior research focusing on fragility functions for reinforced concrete walls. Chapter 2 describes the database of experimental tests used to develop the fragility functions. Chapter 3 evaluates suitability of a suite of engineering demand parameters (EDPs). Chapter 4 describes the damage states (DSs) and associated methods of repair (MORs). Chapter 5 presents the development of the fragility functions recommended for use in the ATC-58 project. A summary of the work and recommendations is provided in Chapter 6.

1.1 Prior Research on Damage Estimating for RC Walls

Fragility functions for reinforced concrete structural walls has been the focus of a couple different studies. Gulec et al. [14, 15] developed fragility functions for squat walls. Brown [8] developed fragility functions for squat and slender walls. A summary of the results of these studies are provided in the following sections.

1.1.1 Fragilities for Squat Walls

Gulec et al. [14, 15] investigated fragility functions for squat reinforced concrete walls with aspect ratio less than or equal to 2.0, where aspect ratio is defined as the ratio of the effective wall height to the wall length. Fifty-one specimens had rectangular cross sections, 32 had barbell cross sections, and 28 had flanged cross-sections.

Table 1.1 lists the damage states and methods of repair used in the study. Four methods of repair were specified. The first, cosmetic repair, is associated with initial cracking. The second, epoxy-resin injection of cracks, is associated with initial yielding and cracks less than 0.12 inches (3.0 mm) but greater than 0.02 inches (0.5 mm). The third, partial wall replacement, is associated with concrete crushing (toe or web) and bar buckling. The forth, full wall replacement, is associated with sliding shear, widespread concrete crushing, and bar fracture.

The engineering demand parameters considered were i) drift, ii) dissipated hysteretic energy, and iii) a functional form of maximum story drift and number of load cycles [9],[34]; ultimately drift was used to develop the fragility functions. The impact of wall geometry, aspect ratio, reinforcement ratios, and axial load on damage progression and the fragilities were considered, but only wall geometry was found to significantly affect the progression of damage. Separate sets of fragilities were developed for walls with rectangular, barbell, and flanged cross sections.

For wall tests with multiple occurrences of a damage state, all were recorded. Fragilities were developed twice, once using all occurrences of a damage state and once using only the first occurrence of a damage state. Minimal differences were observed in the fragilities. The fragilities were created using the lognormal distribution and the Method of Maximum Likelihood; they were evaluated using the Lilliefors test. Figure 1.1 shows the fragility functions developed for rectangular squat walls by Gulec et al. [14, 15].

1.1.2 Fragilities for Squat and Slender Walls

Brown [8] developed fragilities for walls without consideration for slenderness. Only data from tests of walls with rectangular and barbell shaped cross sections were used. The data set used had 45 tests from 10 research programs.

Table 1.2 provides a summary of the damage states and methods of repair used. Five methods of repair were specified. The first cosmetic repair, is associated with initial horizontal cracks. The second, epoxy injection of cracks, is associated with initial diagonal cracks and initial yield of reinforcement. The third method of repair, concrete patching, is associated with initial spalling of the cover concrete. The forth, replacement of concrete, is associated with crushing of the concrete in the web. The fifth method of repair,

Table 1.1: Damage states and methods of repair for structural walls by Gulec et. al. [15][14]

Damage States	Method of Repair
DS1 - Initial cracking and crack widths less than 0.02 inches (0.5 mm)	MOR-1 - **Cosmetic repair** of surface finishes to restore aesthetic appearance, maintain first resistance and prevent water infiltration into wall
DS2 - Initiation of yielding in reinforcement (boundary element, web, or horizontal) and cracks less than 0.12 inches (3.0 mm)	MOR-2 - **Epoxy-resin injection** of cracks to restore component stiffness and strength
DS3 - Concrete crushing at toe or in web; Vertical cracking in toe; Buckling of longitudinal reinforcement; Flexural cracks exceeding 0.12 inches (3 mm)	MOR-3 - **Partial wall replacement** requiring removal and replacement of damaged concrete
DS4 - Sliding at base of wall; Wide diagonal cracks; Widespread concrete crushing; Reinforcement fracture; Shear cracks exceeding 0.12 inches (3 mm)	MOR-4 - **Wall replacement**

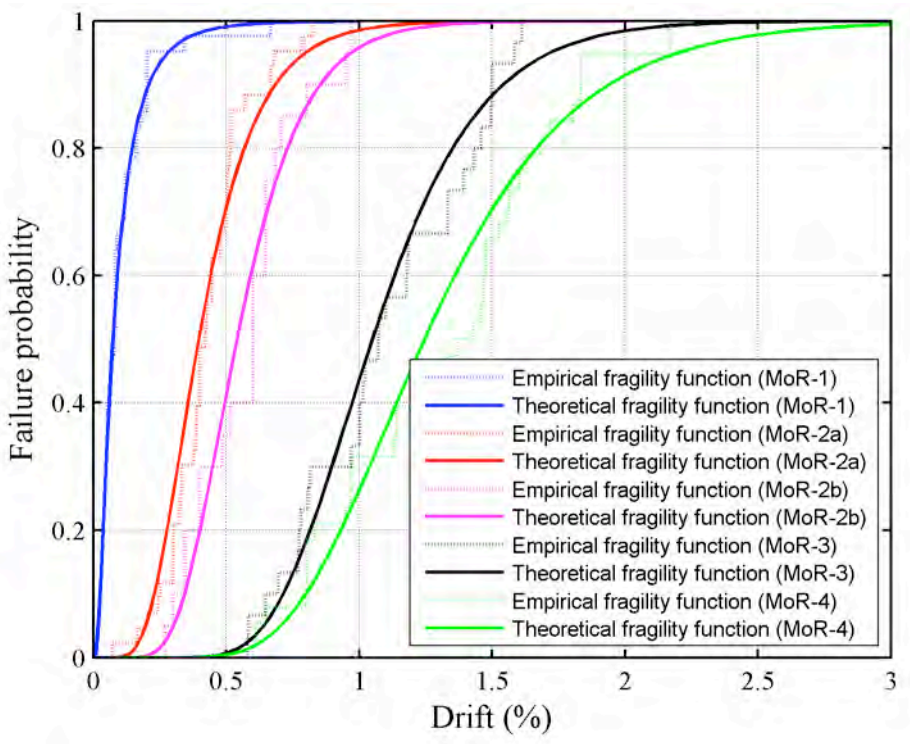

Figure 1.1: Fragility functions developed by Gulec et al. [14, 15] for rectangular squat walls.

replacement of steel, is associated with bar buckling and damage resulting in loss of lateral strength of at least 20%.

Brown considered the impact of the following engineering demand parameters: i) story drift, ii) number

of load cycles, iii) displacement ductility, and iv) plastic rotation. Drift was identified as the best predictor of damage progression and was used to develop fragility functions. The impact on damage progression of design parameters such as shape, aspect ratio, and shear demand-capacity ratio were evaluated. Of the parameters considered, only shape was found to impact damage progression, and in particular only the median drifts at which web crushing and extreme damage occurred. Separate fragilities were not developed due to insufficient data.

Fragility functions were developed using a lognormal distribution and the Method of Maximum Likelihood. Goodness-of-fit testing was done using the Lilliefors test. Figure 1.2 shows the final fragility functions developed by Brown [8].

Table 1.2: Damage states and methods of repair for structural walls by Brown[8]

Damage States	Method of Repair	Repair
DS.0 - First recorded horizontal crack	MOR.0 - Cosmetic Repair	Replace and repair finishes
DS.1 - First recorded diagonal crack DS.2 - Recorded and/or measured yield of extreme reinforcement	MOR.1 - Epoxy injection	Inject cracks with epoxy and replace finishes
DS.3 - Initial spalling of concrete cover	MOR.2 - Patching	Patch spalled concrete, epoxy inject cracks and replace finishes
DS.4 - Crushing of web concrete	MOR.3 - Replace concrete	Remove and replace damaged concrete, replaces finishes
DS.5 - Extreme damage, including buckling of longitudinal reinforcement or damage resulting in reduction of lateral strength by 20%	MOR.4 - Replace steel	Replace damaged reinforcing steel, remove and replace concrete, and replace finishes

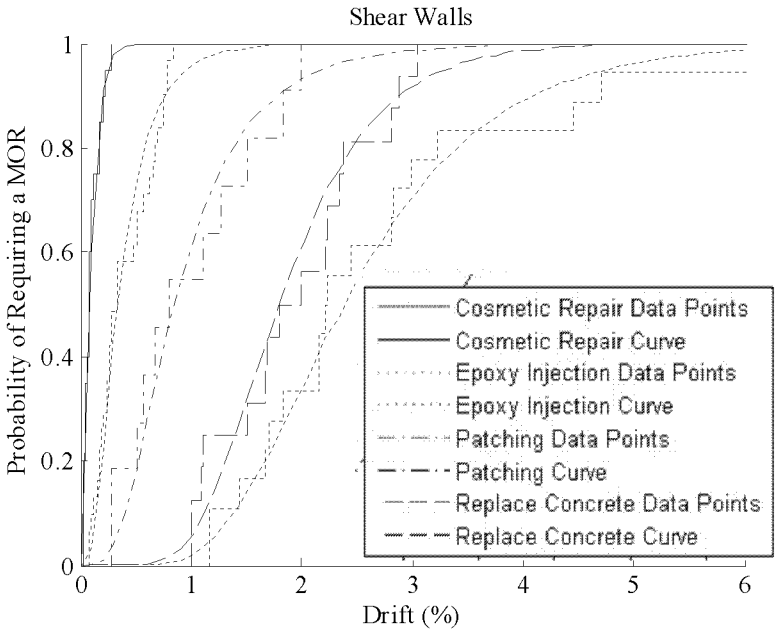

Figure 1.2: Fragility functions developed by Brown [8] for reinforced concrete walls.

Chapter 2

Experimental Data Used to Develop Fragilities

The objective of this study was to develop fragility functions for slender walls. Fragilities were developed using data from experimental tests of slender wall subassemblages. Wall slenderness was defined on the basis of the shear span ratio.

Typically, wall subassemblages are tested to assess earthquake response by applying a lateral (shear) load at the top of the laboratory test specimen. However, in some cases, to provide improved simulation of the earthquake load distribution in a wall, lateral load and moment are applied at the top of the test specimen. To capture the effect of these different loading schemes, "slenderness" was assessed on the basis of shear span ratio, defined as $M/(Vl_w)$ where l_w is the length of the wall, M is the base moment, and V is the base shear. The ratio M/V is the effective height of loading. Wall subassemblages were considered "slender" if the shear span ratio was greater than or equal to 2.0.

Any wall determined slender, that did not contain openings, and for which damage and load-displacement data were provided was included in the dataset. The database compromised 66 walls from 18 test programs, with 42 rectangular, 13 barbell, 5 C-shaped, 2 H-shape, and 4 T-shape. Fifty walls were tested with cyclic uni-directional loading, 11 with monotonic uni-directional loading, and 5 with bi-directional cyclic loading.

The sections that follow provide an overview of the test programs used to develop the database (Section 2.1), a description of the data collected from each test (Section 2.2), and a discussion of the design and response parameters included in the database (Section 2.3).

2.1 Test Programs

The following sections provide a brief overview of the test programs used to develop the database for slender walls. For each test program, the following information is provided: i) objective of the test program, ii) number of specimens tested, iii) study parameters, iv) shear span ratio, and v) load conditions. The summaries of the test programs are presented in chronological order.

Oesterle et al.

Oesterle et al. [33, 32, 31] tested two flanged walls (*F1*, *F2*), two rectangular walls (*R1*, *R2*), and ten barbell walls (*B1-B10*). The parameters varied were i) axial load, ii) amount of flexural, horizontal and confining reinforcement, iii) load history, and iv) concrete strength. All walls were 1/3 scale with a shear span ratio of 2.40. A constant axial load ratio was applied to each wall varied from 0.0-0.13$A_g f'_c$. Lateral load was applied to the top of the walls. The tests were force-controlled prior to yielding and displacement-controlled at levels beyond yielding. Most walls were loaded cyclically, however two barbell walls were loaded monotonically.

Shiu et al.

Shiu et al. [40] tested one-third scale rectangular walls with and without openings to explore the impact of openings in walls. Only the wall without openings (*C1*) was included in the database. The shear span ratio was 2.88. Axial load was not applied. Load load was displacement controlled and applied in a reverse cyclic pattern by a lateral load at the top of the wall.

Morgan et al.

Morgan et al. [29][30] tested a barbell wall subassemblage as part of a joint US-Japan research program focused on testing large-scale structures. The wall was designed at a 1:3.5 scale. The shear span ratio of the wall was 2.79. A constant axial load of $0.05A_g f'_c$ and a displacement-controlled reverse cyclic lateral load was applied to the top of the wall.

Lefas et al.

Lefas et al. [20, 21, 22] tested ten one-fifth scale rectangular walls. The study sought to investigate the impact of horizontal reinforcement ratio and repair techniques. Six walls were tested under monotonic loading and four walls were tested under reverse cyclic loading[1]. The shear span ratio of the walls was 2.0. Constant axial

[1]Due to the very limited amount of cyclic loading applied to these walls, they were considered monotonic tests when entered into the database

loads were applied, and for individual walls, varied from $0.0A_g f'_c$ to $0.21A_g f'_c$. A lateral load was applied to the top of the wall and the tests were force controlled.

Ali and Wight

Ali and Wight [4] tested one-quarter scale barbell walls. A control wall (*W1*) without openings was also tested and was included in the database. The shear span ratio of the wall was 3.04. A constant axial load ratio of $0.08A_g f'_c$ was applied to the wall. The loading of the wall was reverse cyclic under displacement control and was applied as a lateral load at the top of the wall.

Pilakoutas and Elnashai

Pilakoutas and Elnashai [36, 37, 38][38] tested six rectangular walls (*SW4-SW9*) at a scale of approximately one-fifth scale to investigate the impact of shear reinforcement ratios. The shear span ratio of the walls was 2.0. No axial load was applied to the walls. Lateral load was applied to the top of the wall. The test was displacement controlled with reverse cyclic loading.

Thomsen and Wallace

Thomsen and Wallace [42, 43] tested one-quarter scale rectangular (*RW1* and *RW2*) and T-shaped (*TW1* and *TW2*) walls to verify results of displacement-based design of slender walls. The rectangular walls were identical with the exception that *RW2* had less confining reinforcement in the boundary regions. The T-shaped walls were similar, with *TW2* having a longer boundary element at the tip of the web. The shear span ratio of the walls was 3.0. The walls were subjected to constant axial loads of approximately $0.10A_g f'_c$ and uni-directional, reversed cyclic displacement histories. The tests were displacement-controlled with a single lateral force was applied to the top of the walls.

Tupper

Tupper [44] tested rectangular walls (approximately 1/2 scale) with structural steel boundary elements. A reference specimen of a conventional wall was also tested. Only the conventionally reinforced wall, W3, was included in the damage database. Specimen *W3* had a shear span of 3.75. A constant axial load of $0.1A_g f'_c$ was applied. A reversed-cyclic lateral load history was applied to the wall, with the initial cycles force-controlled and later cycles displacement-controlled.

Tasnimi

Tasnimi [41] tested four identical one-eighth scale rectangular walls to evaluate the behavior of walls designed using the Iranian seismic design code. The shear span ratio of the walls was 2.2. No axial load was applied. The walls were tested with different load histories under force-controlled, reverse cyclic loading. Load was applied as a single lateral load near the top of the walls.

Mobeen

Mobeen [28] tested three barbell walls (approximately 2/3 scale) to study the effect of double headed studs as boundary element confining reinforcement. One wall was constructed using conventional reinforcement. The study concluded that the walls confined with double headed studs improved the displacement ductility of the walls. Only the wall with conventional reinforcement, W1, was included in the damage database. W1 had a shear span of 2.74 and a constant axial load of $0.15A_g f'_c$. The wall was tested with a displacement-controlled quasi-static load history with a lateral load only applied to the wall.

Riva et al.

Riva et al. [39] tested a full-scale rectangular wall representative of European construction. Lateral loads were applied in two locations to create an effective loading height representative of a triangular load distribution on a four-story wall. This resulted in a shear span ratio of 3.17. No axial load was applied. Loads were applied under reverse cyclic loading. The test was force-controlled to yield and displacement controlled thereafter.

Liu

Liu [24] tested two approximately two-thirds scale rectangular walls to investigate the use of high strength concrete. The walls were identical except for the compressive strength of the concrete and the shear reinforcement ratio. The walls had with a shear span ratio of 3.13 and constant axial loads of $0.04A_g f'_c$ and $0.08A_g f'_c$. Lateral load was applied to the top of the wall and the test was displacement controlled with a reverse cyclic displacement history.

Khalil and Ghobarah/Elnady

Khalil and Ghobarah [19] and Elnady [13] tested rectangular walls of approximately one-third scale to investigate the seismic rehabilitation of walls. Three control walls that were not retrofitted were included in the database. The design of the walls represented pre-1970 design and had unconfined boundary regions.

Two walls had lap splices (*CW1* and *CW2*). The tested subassemblages were intended to represent the plastic hinge region of a ten-story wall; the shear span ratios varied from 2.25 to 5.0. A constant axial load of approximately $0.075A_g f'_c$ was applied to the walls. The tests were force controlled until yield of the longitudinal reinforcement and displacement controlled thereafter.

Ile and Reynouard

Ile and Reynouard [18] tested three identical, approximately full-scale, U-shaped walls to investigate the impact of load direction and uni-directional versus bi-directional loading. The shear span ratio of the walls was 2.4 for strong-axis bending and 2.88 for weak-axis bending. Constant axial loads of approximately $0.1A_g f'_c$ were applied. Cyclic lateral loads were applied under displacement control to the top of the walls.

Beyer et al.

Two half-scale U-shaped walls (*TUA* and *TUB*) were tested under constant axial load and cyclic, bidirectional lateral loading at ETH Zurich [6]. The thickness of the walls was the primary variable for the test program. The walls had a strong-axis bending shear span ratio of 2.58 and were subjected to constant axial loads of $0.02A_g f'_c$ and $0.04A_g f'_c$. No axial load was applied. Lateral loads only were applied at the top of the wall in a 'clover-leaf' pattern. Early cycles were force-controlled; cycles beyond the elastic range were displacement-controlled.

Brueggen

Brueggen [10] tested two half scale T-shaped walls to investigate the effects of multi-directional loading. The test specimens were one-half scale and represented the bottom 4 (*NTW1*) and 2 (*NTW2*) stories of a six-story prototype specimen. Test specimens included a portion of the floor slab at each story. The walls had a shear span ratio of 3.47 and were loaded with a constant axial load equal to $0.03A_g f'_c$ and subjected to cyclic, bi-directional, lateral displacement history (displacement controlled). Moment and shear were applied to the top of the specimens to simulate loading from the upper stories. Loads were controlled such that the relationship between the base moment and shear simulated a triangular load distribution for the six-story prototype. This resulted in a shear span ratio of 3.47.

Dazio et al.

Dazio et al. [11, 12] tested six half scale rectangular walls under reverse cyclic loading to examine the impact of longitudinal reinforcement ratio, steel ductility, and confining reinforcement. The shear span ratio for

Table 2.1: Summary of Database Properties

Parameter	Mean	Min.	Max.	Std. Dev.	Coeff. of Var.
Scale	0.37	0.16	0.98	0.18	0.48
f'_c, ksi	5.5	3.0	11.3	1.6	0.3
f_y, ksi	67	40	87	10	0
ρ_{be}, %	3.5	0.8	11.4	2.3	0.7
ρ_{web}, %	0.71	0.17	2.49	0.70	0.99
ρ_h, %	0.46	0.17	1.38	0.22	0.49
ρ_{con}, %	1.62	0.00	5.93	1.64	1.01
λ_N	0.05	0.00	0.21	0.05	1.04
$M/(V\ell_w)$	2.46	1.99	5.00	0.53	0.21
v_n	6.4	3.5	14.3	2.3	0.4
v_u	4.8	1.1	11.0	2.3	0.5
V_u/V_n	0.7	0.2	1.4	0.3	0.4

the walls was 2.28. A constant axial load ranging from $0.05A_g f'_c$-$0.13A_g f'_c$ was applied to each wall. Cyclic displacement controlled loading was applied by a single lateral force at the top of the walls.

Lowes et al.

Lowes et al. [7, 25] tested four, modern, ACI 318 [2] compliant one-third scale planar walls. The parameters explored by the test program were i) lateral load distribution, ii) longitudinal reinforcement layout and iii) the use of lap splices above the wall-foundation interface. The shear span ratios of the walls ranged from 2.0 to 2.85. A constant axial load of approximately $0.1A_g f'_c$ was applied to each wall. Lateral forces and overturning moments were applied to the top of the specimen to simulate the effect of additional stories. Specimens were intended to represent the bottom 3 stories of a 10-story wall. Actuators applied additional lateral forces at the story levels. Lateral loading was cyclic and applied under displacement control.

2.2 Assembled Test Data

For each specimen, the following data were included in the database: i) measured material properties (such as concrete compressive strength and steel yield strength), ii) specimen geometry and reinforcement layout, iii) positive and negative load-displacement envelopes and iv) damage information, such as cracking, cover spalling, and yielding, buckling and fracture of reinforcing bars. The following sections provide a more detailed discussion on each type of data included in the database. The data are summarized in Table 2.1 and provided in detail in Appendix A.

2.2.1 Material Properties

Measured concrete compressive strength, f'_c, and measured steel tensile yield strength, f_y, were reported by researchers. For walls constructed in multiple lifts, the compressive strength of the concrete in the lowest lift of the wall was used. The distribution of compressive concrete strengths are shown in Figure 2.1a and the distribution of tensile steel strengths are shown in Figures 2.1b.

In addition to tensile yield strength of the steel, values useful in reproducing the stress-strain response of the steel were also recorded, including i) modulus of elasticity (E_s), ii) yield strain (ε_y), iii) strain at onset of strain hardening (ε_{sh}), iv) tangent stiffness at on-set of strain hardening (E_{sh}), v) ultimate stress (f_u) and vi) ultimate strain (ε_u). These values are provided in Table A.2 in the Appendix. When available, tabulated values were recorded. Occasionally, only figures showing the stress-strain response of the steel were provided. In these cases, the values were obtained by digitizing the response curve and selecting the appropriate values.

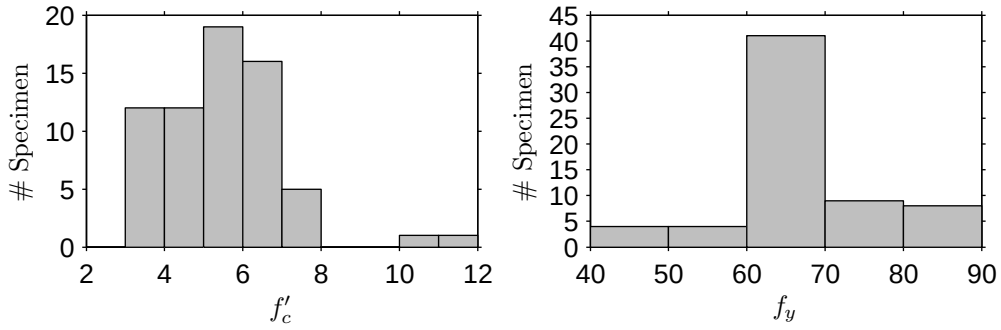

(a) Concrete compressive strength (b) Steel yield strength

Figure 2.1: Histograms of material strengths

2.2.2 Geometry and Reinforcement Layout

In recording the geometry of the walls, the height of the wall (h_w) was defined as the distance from the bottom of the wall (top of foundation block) to the height of the instrument recording the lateral displacement of the wall. Wall length, l_w, and wall thickness, t_w, were recorded for all walls. For barbell walls, the width, b_f, and the thickness, h_f, of the boundary elements were recorded. For flanged walls, h_f, is the thickness of the flange and b_f is the width of the flange.

Cross sections showing the reinforcement layouts of the walls were provided for all test specimens. However, for some walls, information such as reinforcement spacing or cover dimensions was not specified. In this case, dimensions were estimated from the provided drawings. The reinforcing bar properties and lay-

out/spacing were recorded for longitudinal boundary element and web reinforcement, horizontal reinforcement, and boundary element confining steel. The length of the boundary elements, ℓ_{be}, was defined as the distance between the centers of the extreme boundary element longitudinal bars plus twice the distance from the center of the outermost bar to the surface of the wall.

2.2.3 Load-Displacement Response

Load and displacement points defining the positive and negative envelopes to the load-displacement histories were recorded. For some walls, the forces and displacements/drifts were tabulated by the researcher; for these walls, the values at the peaks for the first cycle for each displacement demand level in the load history were recorded in the database. If the values were not tabulated, the load-displacement plots were used to determine load-displacement points defining the response envelope with the aide of digitizing software.

The factor α_{load} was defined as the factor by which the height of the wall, h_w, was multiplied to get the effective height, ℓ_{eff}, of loading for the walls, and thus the shear span ratio was defined by Eq. 2.1. For most walls, this factor was equal to unity, as the load was applied at the same height where the lateral displacement was measured. For walls loaded with a moment and shear at the top of the wall, α_{load} was greater than unity (Section 3 discusses how the drift at the effective loading height is determined for these walls).

$$\frac{M}{V\ell_w} = \frac{\alpha_{load} h_w}{\ell_w} = \frac{h_{eff}}{\ell_w} \tag{2.1}$$

2.2.4 Damage Information

For each test, damage information was recorded if any of the following were reported by the researchers: i) initiation of cracking (distinctions were made between horizontal and inclined, or diagonal, cracking), ii) yielding of reinforcement (tensile or compressive), iii) spalling of concrete, with distinctions made between cover spalling and spalling exposing longitudinal reinforcement, iv) vertical cracks or splitting of concrete, v) crushing of core concrete in the boundary region, vi) web crushing, vii) bar buckling, viii) bar fracture, and ix) shear failure. The organization of the reported damage into damage states and the association with methods of repair (MORs) is discussed in further detail in Chapter 4.

For each recorded instance of damage, the load-displacement point associated with the damage occurrence was recorded. Whenever available, the load-displacement at the exact occurrence of the damage was recorded, however, in many instances, only the load-displacement point at the peak of the cycle in which the damage occurred was reported. If the damage occurred during the unload phase of a cycle, the load-displacement

information corresponding to the maximum historic displacement was recorded.

2.2.4.1 Calculation of Flexural Yielding

One of the damage states used to characterize performance of the walls was the onset of tensile yielding of the extreme longitudinal reinforcement in the wall. Several different approaches may be used to determine the onset of yield, e.g. measurement of steel strains in excess of the yield strain or the application of load in excess of a calculated yield load. To maintain a consistent definition of yield for the development of the fragility functions, a theoretical yield force was calculated for each wall and the yield drift was defined as the drift corresponding to this measured force.

The theoretical yield forces were determined from moment-curvature analysis of the wall cross section using a fiber model. These analyses were conducted using OpenSees [27]. The cross section models used the measured material strengths and reinforcement layouts reported in the literature. The concrete fiber response was modeled using the modified Kent-Park [35] response curve (*Concrete01* material model in OpenSees). The measured compressive strength was assumed to correspond to a compressive strain of -0.002. The impact of confining reinforcement on the compressive response of the concrete was not considered, and it was assumed that concrete in tension did not contribute to the strength. The discretization of concrete fibers was 50-by-10 for wall webs or rectangular cross-sections, 10-by-30 for barbell boundary elements or C-wall flanges, and 10-by-40 for other flanges. The reinforcing bars for the boundary and web longitudinal steel were modeled using either the *Steel01* (bilinear response) or *ReinforcingSteel* (reflects the shape of typical rebar stress-strain response) uniaxial material models available in OpenSees, depending upon the measured steel stress-strain response provided in the reference material. In some cases, insufficient steel material information was provided in the literature and it was necessary to make assumptions about various steel material properties. Table A.2 in the appendix contains the steel properties for each specimen, with assumed values denoted with a *.

2.2.4.2 Crack Width Information

For each recorded damage state, crack widths were recorded when reported. Whenever possible, a distinction was made between crack widths of horizontal and diagonal cracks. Additionally, any reported cracks widths corresponding to both peak displacements and residual displacement of the wall (at approximately zero force) were recorded. This was done to allow for later consideration of damage states based on widths of cracks. When sufficient information was available, crack spacing and the height over which cracking occurred was recorded. The recorded crack widths are provided in Appendix A.

Unfortunately, there is not an extensive amount of crack width data for slender walls, especially residual

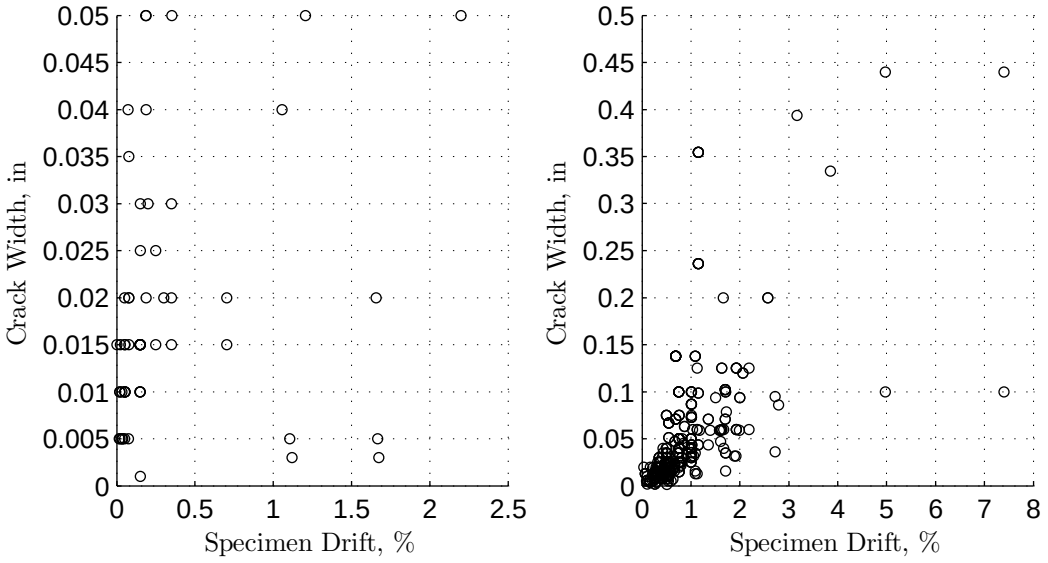

(a) Residual (b) Cycle max

Figure 2.2: Reported crack widths

crack widths, which are the most applicable to development of fragility functions as observation of damage following an earthquake will only provide data on residual crack widths. Only 59 instances of residual crack widths were available for the entire data sets, with all but 6 coming from walls tests by Lowes et al. [25][2]. All residual crack widths were less than 1/16 in (1.6 mm), the largest measuring 0.05 inches (1.3 mm) at maximum historic drifts ranging from 0.2%-2.2%.

Figure 2.2a shows residual crack widths as a function of maximum historic drift. Figure 2.2b shows the crack widths at cycle peaks with markers denoted by damage state; two cracks were measured as having widths greater than 0.5 inches (12.7 mm) at drifts of 3.2% and 7.0% and are not shown.

2.3 Design Parameters

Various design parameters could be expected to affect damage progression in walls. The parameters discussed in the following sections were computed for each specimen. Their impact on damage progression is presented in Section 5.4. Table A.1 provides values for each wall subassembly. Table 2.1 provides summary statistics. Figures 2.3 - 2.6 are histograms showing the distributions of the design parameters.

[2]The crack width data included for the walls tested by Lowes et al. were measured and recorded during testing. Hart[17] provides additional information on crack widths and spacing obtained from digitized crack maps and Metris displacement measurements.

2.3.1 Reinforcement ratios

Longitudinal reinforcement ratios for the boundary element (the boundary element length, ℓ_{be}, was defined as the length between the centers of the extreme longitudinal bars in the boundary element plus twice the distance from the center of the outermost bar to the surface of the wall), ρ_{be}, and web, ρ_{web}, were calculated as the ratio of the total area of steel for the respective area to the respective concrete area. The boundary element confining reinforcement ratio, ρ_{con}, was calculated as the ratio of the volume of steel to the volume of concrete. The horizontal reinforcement ratio, ρ_h, was calculated as the area of steel in one row of reinforcement to the area of concrete formed by the thickness of the wall and the spacing of the horizontal reinforcement. Figure 2.3 shows the distribution of reinforcement ratios for the database.

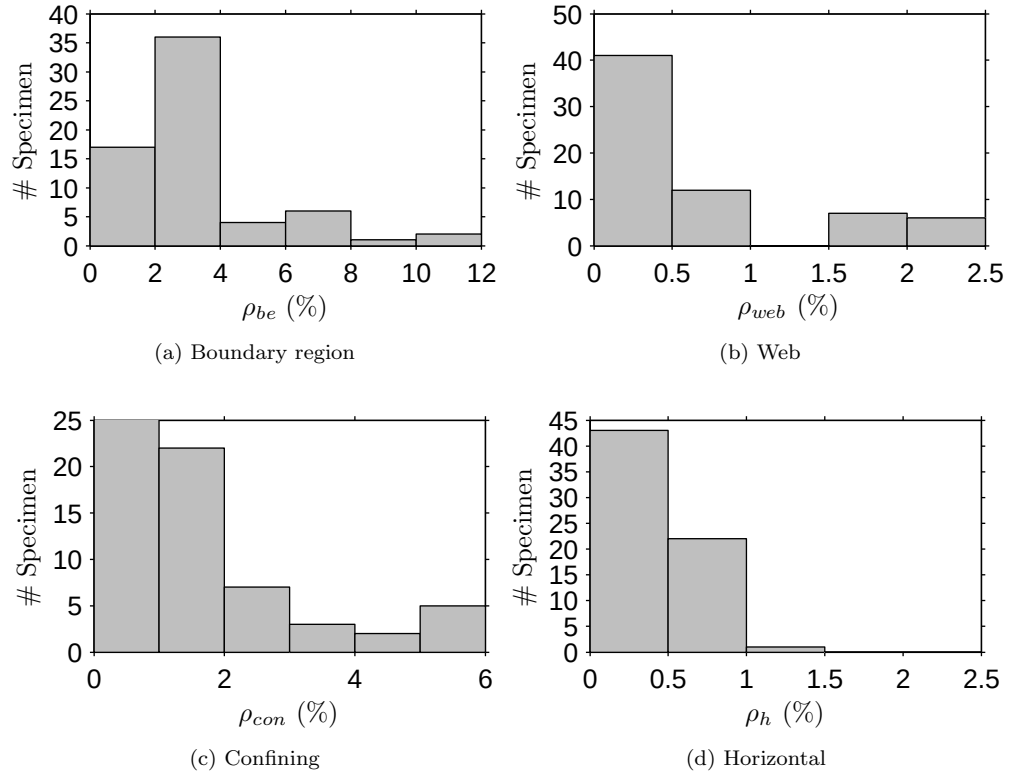

(a) Boundary region (b) Web

(c) Confining (d) Horizontal

Figure 2.3: Histograms of reinforcement ratios

2.3.2 Scale

It was found that different researchers defined the scale of their test specimens in different ways. To provide a consistent measure of specimen scale, a full-scale wall was assumed to be 12 inches (305 mm) thick. Brown [8] reviewed existing structures and determined that 12 inches represented a lower bound on typical wall thickness. Gulec et al. [15] used a minimum thickness of 8 inches to define a scale for their squat wall

database. For this study, specimen scale was defined as web thickness, t_w, divided by 12 inches; an upper bound of 1.0 was specified for the scale. Figure 2.4 shows the distribution of the wall scales used here.

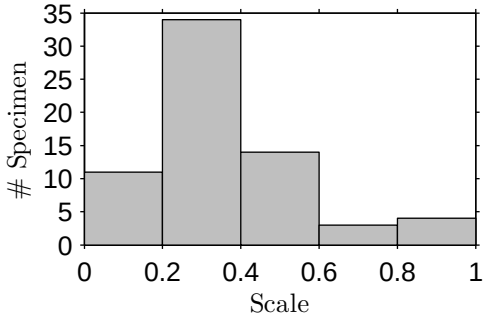

Figure 2.4: Histogram of wall scale

Shear Span Ratio

The shear span ratio, $M/(V\ell_w)$, is the ratio of the effective load height to the wall length and is used to characterize the slenderness of the wall. For flanged walls loaded subjected to weak-axis bending, the length of the wall ℓ_w was replaced by the flange width, b_f, however, the value corresponding to strong-axis bending is typically the value considered, and is shown in Figure 2.5a.

$$(\frac{M}{V\ell_w})_{strong} = \frac{\alpha_{load} h_w}{\ell_w} \tag{2.2a}$$

$$(\frac{M}{V\ell_w})_{weak} = \frac{\alpha_{load} h_w}{b_f} \tag{2.2b}$$

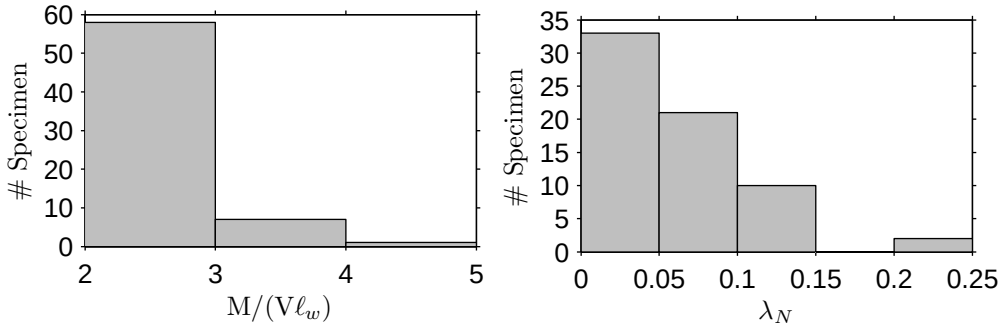

(a) Shear span ratio (b) Axial load ratio

Figure 2.5: Histograms of load characteristics.

Axial Load Ratio

The axial load ratio, λ_n, or ratio of applied axial load (P), to gross section capacity ($A_g f'_c$) varied from 0.0 to 0.21. Figure 2.5b shows the distribution of axial load ratio for the database.

$$\lambda_n = \frac{P}{A_g f'_c} \tag{2.3}$$

Shear Capacity

Nominal shear strength of the walls was defined using ACI 318-08 Chapter 21 (21.9.4.1) [2]:

$$V_n = A_{cv}\left(\alpha_c \sqrt{f'_c} + \rho_h f_{yh}\right) \tag{2.4}$$

where f'_c is the reported concrete compressive strength, f_{yh} is the reported yield strength of the horizontal reinforcement, ρ_h is the horizontal reinforcement ratio. The variable α_c is intended to account for the wall aspect ratio and is equal to 2.0 for the walls in the database. A_{cv} is the shear area of the wall, computed as the length of the wall, ℓ_w, multiplied by the web thickness, t_w; for flanged walls under weak-axis loading, the wall length, ℓ_w, is replaced by the flange width b_f.

To enable comparison of the shear capacity of different walls, a normalized shear stress capacity was also computed as the nominal shear strength normalized by the shear area, A_{cv}, and the square of the concrete compressive strength, $\sqrt{f'_c}$.

$$v_n = \frac{V_n}{A_{cv}\sqrt{f'_c}} \tag{2.5}$$

The distribution of shear stress capacity ratio is plotted in Figure 2.6a.

Shear Demand

The shear demand, V_u, was the maximum shear force reported by the researchers. To enable comparison of walls, a normalized shear stress demand, v_u, was calculated

$$v_u = \frac{V_u}{A_{cv}\sqrt{f'_c}} \tag{2.6}$$

where all parameters are as defined previously. Figure 2.6b shows the distribution of shear stress demand ratio.

Shear Demand-Capacity Ratio

The shear demand-capacity ratio was computed as V_u/V_n. The distribution of this ratio in the database is shown in Figure 2.6c.

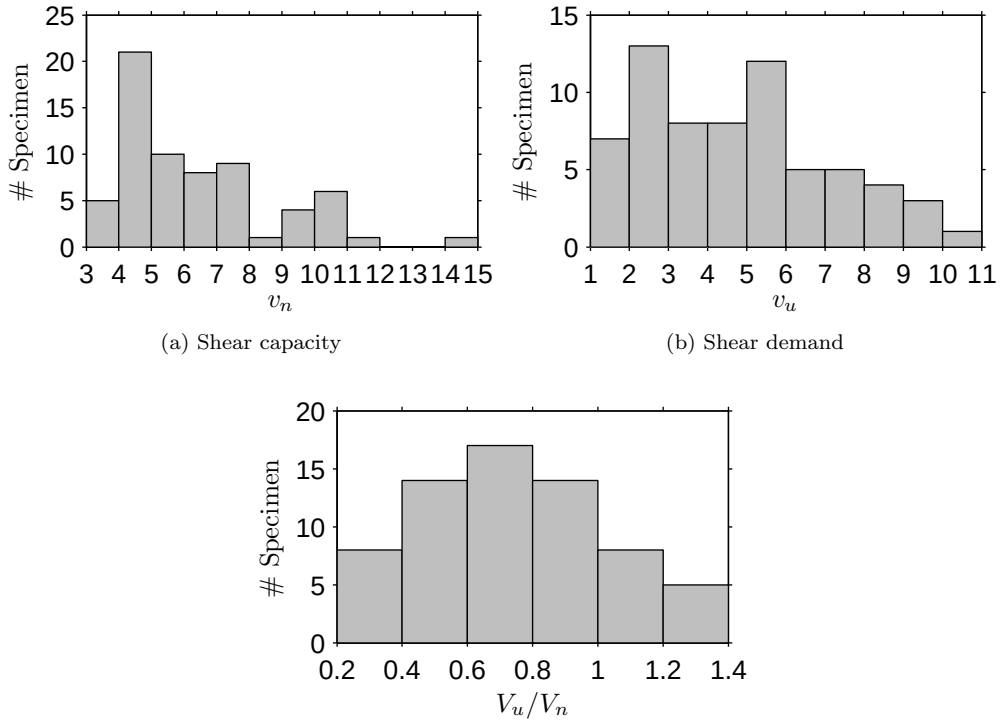

(a) Shear capacity

(b) Shear demand

(c) Shear demand-capacity ratio

Figure 2.6: Histograms of shear demand and capacity

Chapter 3

Demand Parameters

Multiple earthquake demand parameters were investigated with the objective of determining the most efficient predictor of earthquake damage. All parameters considered can be computed using analysis software employed commonly in practice, and thus could easily be employed by practitioners considering a performance-based design or evaluation. The parameters considered are discussed in the following sections.

3.1 Drift

The specimen drift was computed as the lateral displacement at the plane of loading divided by the height above the fixed base of the wall. No consideration was made for the type of load (i.e. pure shear or shear and moment) applied at the load plane.

Drift is the simplest demand measure and can be computed using either a linear or nonlinear model.

3.2 Rotation Demand

The rotation demand was calculated as the rotation required to achieve the experimental drift given the applied loading and using a lumped-plasticity model of the wall. The lumped-plasticity model comprised a rotational hinge at the base of the wall with a hinge length of one-half the length of the wall (ℓ_w) with the remainder of the wall modeled as elastic. The region of the wall above the plastic hinge was assumed to deform in flexure and shear. An effective flexural stiffness of $0.5E_cI_g$ and an effective shear stiffness of $0.4E_cI_g$ were used for computing rotations for all damage states except DS1 (initial cracking and initial yielding). For DS1, these effective stiffnesses resulted in overly large elastic deformation and negative rotation demands. Thus, for DS1, the gross flexural stiffness, E_cI_g, was used.

Rotation demand is the most complicated demand parameter considered in the study and requires use of a nonlinear response model for application in practice.

3.3 Drift at Effective Height

The experimental test programs used to create the slender wall database loaded specimens using one of three different configurations, shown in Figure 3.1: i) lateral force applied at the top of the specimen (most common load configuration), ii) lateral forces applied at the top of the specimen and at one or more additional locations along the height of the specimen, and iii) lateral force and overturning moment applied at the top of the specimen. Because these different load distributions imply specimens represent different portions of the real wall, it could be expected that the drift at the top of the specimen would be different for the different load distributions. The only consistent known height for the specimens is the effective height of the applied load (h_{eff}), calculated as the ratio of the base moment to the base shear. Thus, drift at the effective height (referred to as "effective drift") was computed for all specimens in an effort to provide a more consistent engineering demand parameter.

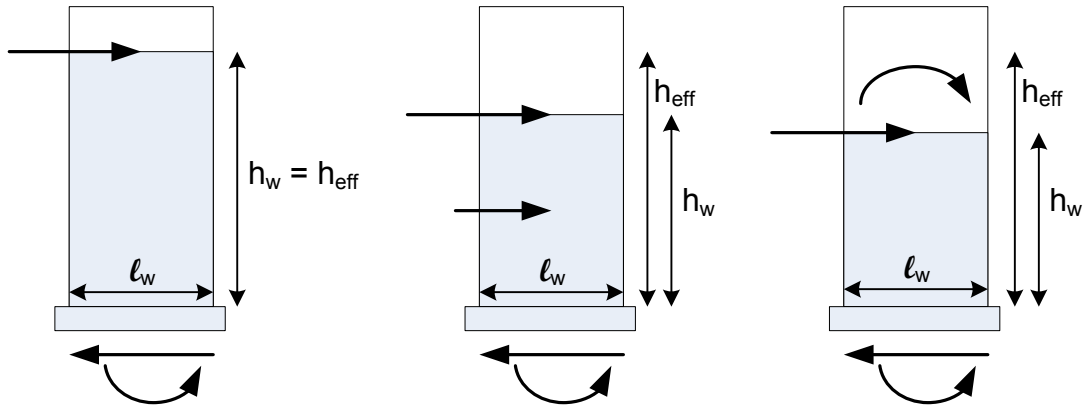

(a) Lateral force at top of specimen (b) Distribution of lateral forces (c) Lateral force and overturning moment at top of specimen

Figure 3.1: Equal base reactions for a real wall (white box) can be achieved for different specimen (gray box) heights (h_w) by changing the configuration of the applied loading.

For walls loaded with only a lateral force at the top of the specimen, the specimen height is equal to the effective height, thus, the specimen drift is equal to the effective drift. For walls with other loading conditions, the drift at the effective height of the loading was calculated. To estimate the effective drift, the model used to calculate the rotation demand (see Section 3.2) was extended to a height equal to the effective height of loading. Thus, the model (shown in Figure 3.2) compromised a plastic hinge with a hinge length

equal to half the wall length and rotation equal to the "rotation demand" computed above, topped by an elastic element with an effective shear stiffness of $0.4E_cA_g$ and an effective flexural stiffness of E_cI_g for DS1 and $0.5E_cI_g$ for all other damage states. This method of estimating the roof drift ensured that the model used for the estimation accurately simulated the experimental drift and provided a reasonable estimate of rotation at the top of the experimental specimen, as this information was not available for all tests.

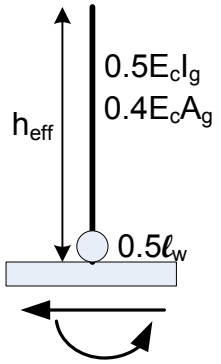

Figure 3.2: Model used to estimate the drift at the effective height of the wall.

Chapter 4

Damage States & Methods of Repair

In performance based design, there is an interest in being able to estimate the cost of returning the structure to its pre-damaged condition. This is achieved by relating methods of repair, for which costs can be estimated, to engineering demand parameters. This relationship is typically established using experimental data. The primary focus during an experimental test is on damage, therefore a critical component of performance based design is linking the salient damage state(s) with the methods of repair. The methods of repair and associated damage states established for the present study is presented in this chapter.

FEMA 308 Repair of Earthquake Damaged Concrete and Masonry Wall Buildings [5], ACI 546-98 Concrete Repair Guide [3], and previous research to develop fragility functions for RC components ([8, 9, 14, 26, 34]) were used to guide the selection of repair methods and to link damage states to methods of repair. Four methods of repair, ranging from cosmetic repair to wall replacement were identified. Table 4.1 provides a summary of the methods of repair identified and the associated damage states. Figure 4.1 shows the damage states versus the EDPs of drift, effective drift, and rotation demand[1].

In the sections that follow the four methods of repair are discussed. Each section includes i) a description of the method of repair, ii) the reason the repair is necessary to restore structural integrity, iii) an overview of the repair process, iv) data necessary to estimate the potential cost of repair, and v) a summary of each damage state associated with the method of repair. Section 4.1 discusses MOR1, cosmetic repair, which is associated with initial concrete cracking and initial yield of longitudinal and/or horizontal reinforcement. Section 4.2 discusses MOR2, epoxy injection and patching, which is associated with vertical cracks and spalling of cover concrete that does not reveal the longitudinal reinforcement. Section 4.3 discusses MOR3, replacement of concrete, which is associated with spalling of cover concrete that exposes the longitudinal reinforcement. Section 4.4 discusses MOR4, replacement of steel and concrete, which is associated with web

[1] Outliers are indicated with gray shading. Section 5.2 discusses how outliers are determined

crushing, boundary element core crushing, bar fracture, bar buckling, and bond slip.

Table 4.1: Damage States and Methods of Repair

Method of Repair	Damage State	Description
Cosmetic repair	DS1a	Initial cracking
	DS1b	Initial flexural cracking
	DS1c	Initial shear cracking
	DS1d	Tensile yield of extreme longitudinal steel
	DS1e	Compression yield of longitudinal steel
	DS1f	Tensile yield of horizontal reinforcement
Epoxy injection and concrete patching	DS2a	Spalling of boundary region cover concrete (not revealing longitudinal reinforcement)
	DS2b	Spalling of patched concrete
	DS2c	Spalling of web concrete
	DS2d	Vertical cracks/splitting
Replace concrete	DS3a	Spalling revealing longitudinal reinforcement
Replace wall	DS4a	Core crushing (boundary element)
	DS4b	Bar buckling
	DS4c	Compressive failure of boundary element
	DS4d	Failure by core crushing (boundary element)
	DS4e	Bar fracture
	DS4f	Failure due to bar buckling
	DS4g	Failure due to bar fracture
	DS4i	Shear failure
	DS4k	Web crushing
	DS4m	Failure due to web crushing
	DS4o	Failure by bond slip
	DS4p	Core crushing in confined boundary element of flange tips (bi-directional tests only)
	DS4q	Confining reinforcement open or fractured

4.1 MOR 1: Cosmetic Repair

The first method of repair, MOR1, cosmetic repair, is associated with damage states for which structural integrity is not compromised. Cosmetic repair consists of the painting or application of alternative surface coating/architectural finishes to conceal the presence of cracks and to provide a barrier against water. FEMA 308 [5] identifies this repair as CR1, cosmetic patching, and limits the effectiveness of painting to cracks equal to or less than 0.06 inches (1.5 mm) in width.

Cosmetic repair requires repair of the surface area of a wall only. The amount of surface area cracked could be as large as the entire surface area of the wall. The cost of material needed for cosmetic repair is largely dependent on the type of surface covering required for the wall, e.g. paint, drywall, etc.

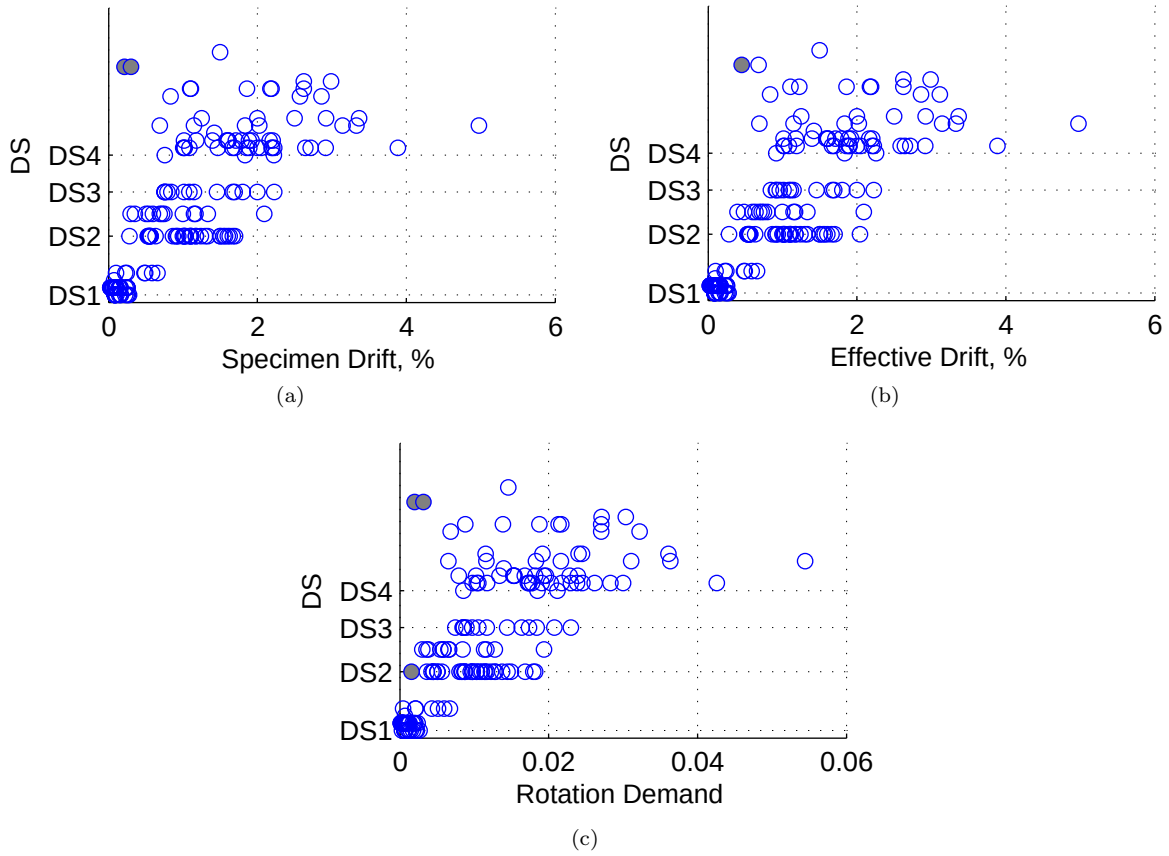

Figure 4.1: Damage state (DS) versus engineering demand parameter (EDP). Outliers are indicated by filled marker.

4.1.1 Concrete Cracking

Concrete cracking is the first damage state observed in walls subjected to earthquake loading. The presence of cracks significantly impacts the stiffness of a wall. In evaluating post-earthquake damage of a building, the width of the residual cracks determines the repair method necessary. Experimental tests typically report crack widths at peak displacement but rarely report residual crack widths. Thus, it can be difficult to pair damage states with methods of repair based solely on the crack width.

For the data set used in this study, *maximum* crack widths associated with initial cracking (DS1a, DS1b, and DS1c) do not exceed 0.012 inches (0.3 mm). As this is well below the 0.06 inches (1.5 mm) limit provided by FEMA 308 [5], these damage states are associated with MOR1.

4.1.2 Yield of Reinforcement

Yield of reinforcement in an experimental test can be reported in a number of ways, such as when steel strain gauges indicate strains in excess of the yield strain or when the applied load exceeds a predetermined yield

load. Because yield definitions can vary between test programs, a theoretical yield point was identified for each specimen to provide consistency among the data. To determine this theoretical yield point, the yield force corresponding to initial yield was determined from a moment-curvature analysis of the cross-sections. Details of this calculation are provided in Section 2.2.4.1.

Although there are no crack width measurements directly associated with the theoretical yield, it was observed that for most walls, the drift at the theoretical yield is similar to the experimentally observed drift, for which some crack width observations are available. The maximum observed crack widths do not exceed 0.05 inches (1.3 mm), with only two measurements exceeding 0.025 inches (0.6 mm). These widths are consistent with the widths associated with cosmetic repair of walls, and thus association of the yield damage state with MOR1 is appropriate.

4.2 MOR 2: Epoxy Injection and Patching

MOR2, epoxy injection of cracks and patching of spalled cover concrete, is necessary to restore the structural integrity of the wall but does not require replacement of the steel and concrete.

Epoxy injection of cracks is necessary to restore the stiffness of a wall, to prevent corrosion of steel, and to restore fire resistance. The literate contains a range of cracks widths at which it is believed that epoxy injection is required. FEMA 308 [5] states that epoxy injection is required for cracks wider than 0.06 inches (1.5 mm), but can be achieved at crack widths as low as 0.002 inches (0.05 mm). Gulec et al. [14] suggested epoxy injection for squat walls is necessary for cracks equal to or exceeding 0.02 inches (0.5 mm). Discussions by Pagni and Lowes [34] for the repair of reinforced concrete beam-column joints suggests that widths of 0.025 inches (0.6 mm), 1/32 inches (0.8 mm) or 1/16 inches (1.6 mm) are commonly used by structural engineers. In this study, experimentally observed crack widths were not explicitly used in establishing methods of repair and it is suggested that the FEMA 308 guidelines be used.

To estimate the cost of repairing a wall by epoxy injection of the cracks, it is necessary to provide an estimate of the linear length of cracks for a given surface area of wall. This can be determined from the descriptions of damage and crack maps provided by researchers[2]. The amount of linear crack spacing requiring epoxy injection was estimated as $150 - 220$ feet of linear cracks per 100 square feet of surface area and was based on the following experimental observations:

- Cracks extend the length of the wall, ℓ_w
- Cracks extend as high as ℓ_w-$2\ell_w$ from the point of maximum moment demand

[2]The information reported for DS2 damage states was used to estimate the linear footage of cracks requiring epoxy injection because experimental damage states corresponding to crack widths were not used.

- Crack spacing ranges from 3-10 inches (76-254 mm), with a mean and median of 5.5 inches (140 mm)

Patching of cover concrete is necessary for partial spalling of the cover concrete. This repair is primarily necessary to restore corrosion protection of the steel and assumes the bond between steel and concrete is still intact. Patching of the cover concrete should not require the use of course aggregates, thus, the repair method is similar to SR3 for shallow spalls (less than 0.75 inches (19 mm) deep) in FEMA 308 [5].

The information provided in the literature related to cover spalling for slender walls suggests that the volume of concrete requiring patching is no more than 0.625 cubic feet per 100 square feet of wall. This was determined assuming a depth of 0.75 inches (19 mm), upper limit of depth defining shallow spalling in FEMA 308, and a surface area of no more than $\ell_w^2/10$, where ℓ_w is the length of the wall.

4.2.1 Cover Spalling

Three damage states (DS2a, DS2b, and DS2c) were considered to be spalling of the cover concrete in which the longitudinal reinforcement is not exposed. Because the longitudinal reinforcement is not exposed, it is assumed that the bond between the steel and concrete is still intact. Thus, these damage states were associated with MOR2. Figure 4.2a shows an example of cover spalling.

4.2.2 Vertical Cracks

The vertical crack damage state, DS2d, was grouped with cover spalling, and consequently, MOR2, because the two damage states were often reported together by researchers and the median drifts for vertical cracks and cover spalling were very similar. Vertical cracks reported by researchers typically occurred while the wall was in compression.

4.3 MOR 3: Replace Concrete

Replacement of concrete was considered necessary for spalling revealing longitudinal reinforcement (see Figure 4.2b). Simply patching was considered inadequate because most of the cover is gone, which necessitates restoration of the bond and compressive capacities. Consequently, this repair state requires the use of coarse aggregate (FEMA 308 [5]).

To replace the concrete, the following steps are necessary:

1. Shore wall.

2. Remove all concrete in damaged regions.

3. Replace damaged concrete.

The volume of concrete requiring replacement was estimated to be 4-10 square feet per 100 square feet of walls. This was computed assuming a wall thickness of 12 inches (305 mm). The surface area requiring replacement of concrete was determined based on damage information reported by researchers, was approximately the same as that for patching of cover concrete, and ranged from $l_w^2/25$ to $l_w^2/10$.

(a) Cover spalling (b) Exposed longitudinal reinforcement

Figure 4.2: Examples of spalling damage states [7].

4.4 MOR 4: Replace Steel and Concrete

MOR4 comprises the replacement of steel and concrete. This repair state was associated with web crushing, damage to confined core concrete, bar buckling or fracture, shear failure, and bond-slip failure. This repair method is required when damage to the steel and/or concrete limits the remaining strength and stiffness of the wall. The extent of the wall area in need of repair depends on the extent of the damage.

To replace the steel and concrete, the following steps are necessary:

1. Shore floor and wall.

2. Remove all concrete and steel from damaged region.

3. Remove all concrete and steel approximately one development length away from the damaged region (either direction).

4. Replace removed steel and concrete. Jacket dimensions must be adequate to ensure anchorage of the steel.

The costs associated with replacing the steel and concrete is dependent on i) partial or full wall replacement, ii) the height and length over which the damage occurs, iii) the size of the reinforcement and the development length needed to anchor the steel, iv) use of lap splices or mechanical splices, and v) reinforcement ratios.

4.4.1 Core Damage

Damage to the confined core of the boundary region is shown in Figure 4.3a. Like deep spalling, this requires replacement of the concrete. However, core concrete damage was associated with MOR4, replacement of steel and concrete. In walls where core damage occurs prior to visible damage of longitudinal reinforcement, the stresses required to damage the core likely have also compromised the integrity of the steel and replacement of the steel is likely necessary.

4.4.2 Web Crushing

Because the concrete in the web is not confined and typically does not experience crushing until the test has reached drift capacity or significant damage has occurred in the boundary region, crushing of web concrete are associated with damage to core concrete. Figure 4.3b shows an example of web crushing.

4.4.3 Bar Buckling/Fracture

Buckling or fracture of the longitudinal reinforcement (DS4b, DS4e, DS4f, and DS4g), requires replacement of the steel to restore the strength of the wall and replacement of concrete to ensure bond and shear capacity is available. Thus, any damage to the wall reinforcing steel is associated with MOR4, replacement of steel and concrete. Figures 4.3c and 4.3d show examples of fractured and buckled bars, respectively.

4.4.4 Bond Failure

There only two instances of bond failure in the data set used for this study. These walls were designed to represent older construction (they do not satisfy the current ACI design provisions) and were tested as control walls for evaluating retrofitting methods. Because a bond failure is likely to only occur in older walls, repair of the wall would likely require a full replacement of the wall. Thus, bond failure is associated with MOR4, replacement of steel and concrete. It should be noted that the bond failure damage states occur at EDPs that are sufficiently low such that they were ultimately determined as outliers.

(a) Core damage

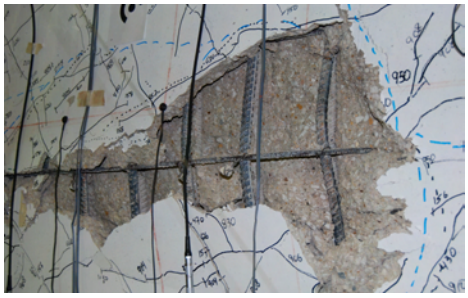

(b) Web crushing

(c) Bar fracture

(d) Bar buckling

Figure 4.3: Examples of damage states associated with MOR4 [7]. The damage states shown are severe examples to provide clear illustration of the damage states.

4.4.5 Shear Failure

Walls that fail in shear typically sustain damage the full width of the wall and have reduced strength and limited drift capacity. Thus, shear failure damage states (DS4i) require MOR4, replacement of steel and concrete, to restore strength and stiffness of the wall. Shear failure can include i) diagonal shear failure, ii) fracture of shear reinforcement, and iii) sliding shear failure. Figure 4.4 shows examples of diagonal shear and sliding shear failures.

(a) Diagonal shear failure [19].

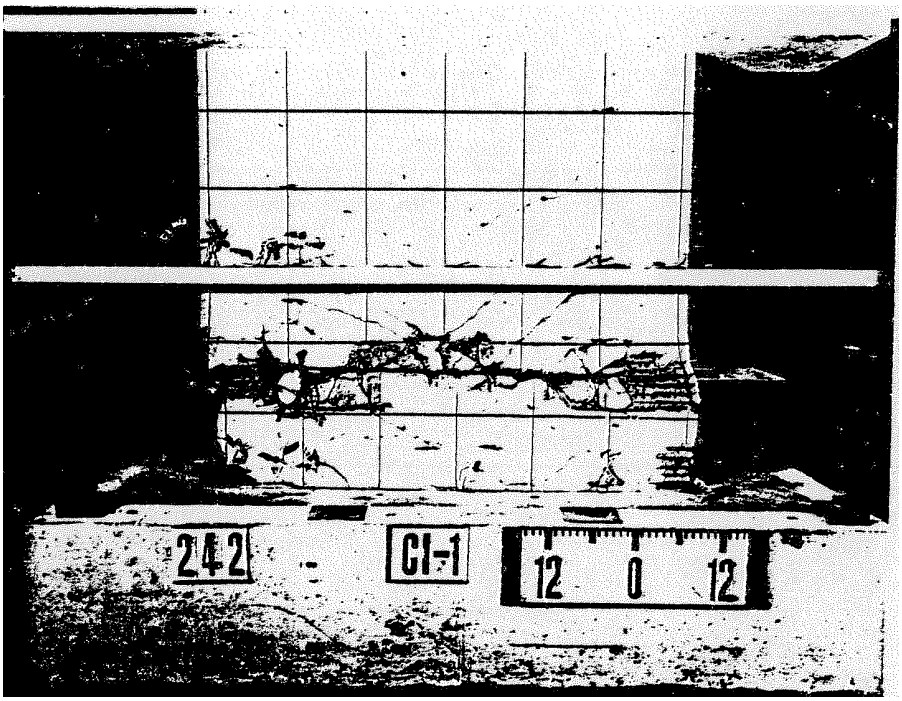

(b) Sliding shear failure [40].

Figure 4.4: Examples of shear failures associated with MOR4.

Chapter 5

Development of Fragility Functions

In this study, fragility functions were developed to quantify the probability of a specific damage state occurring and method of repair being required. Fragility functions are essentially CDF's and can be empirical or functional. Here, lognormal cumulative probability distributions are used to define functional CDFs. The engineering demand parameters described earlier were used to define the fragility functions.

To develop the proposed fragility functions for slender walls subject to earthquake motion, the full data set described in Section 2 was analyzed to remove specific data points that might inappropriately skew the results. First, outliers were identified using Pierce's criterion and removed (see Section 5.2). Then data set statistics (mean, median, coefficient of variation) were computed for all walls and for walls grouped by load history (monotonic or cyclic) and test specimen scale. Ultimately, data for walls subjected to monotonic loading were eliminated. The reduced data set for the proposed fragilities is discussed in Section 5.3. The reduced data set was then used to assess the impact of the design parameters (shape, aspect ratio, shear demand, axial demand, etc) on the damage progression (Section 5.4).

Section 5.5 provides a brief overview of the theory used in developing fragility functions. Section 5.6 discusses the calculate and evaluation of fragility functions for the slender walls evaluated in this study.

5.1 Analysis of the Full Dataset

Table 5.1 shows statistics for the full database, excluding outliers. The median EDP (drift, effective drift, or rotation demand) is shown for each data set, as well as the mean, standard deviation, coefficient of variation, minimum and maximum.

For all EDPs, there is a clear increase in the median value as the severity of the damage states increase, although the separation between DS2 and DS3 is less than elsewhere. For DS1 (initial cracking and initial

yielding), the coefficients of variation range from 1.0-1.2; for other damage states, the coefficient of variation ranges from 0.3-0.45. Comparison of the specimen drift and the effective drift indicates that there is not too much statistical difference between the two EDPs for the full data set.

Table 5.1: Median EDP values of damage states using full database. Outliers not removed.

		All						
		#	Median	Mean	Std. Dev.	Coeff. of Var.	Min.	Max.
Specimen Drift	DS1	66	0.0836	0.133	0.132	0.991	0.0223	0.658
	DS2	48	1.02	1	0.423	0.424	0.283	2.09
	DS3	14	1.12	1.29	0.513	0.399	0.753	2.23
	DS4	60	1.87	1.93	0.866	0.448	0.212	4.97
Effective Drift	DS1	66	0.0856	0.138	0.131	0.949	0.0223	0.658
	DS2	48	1.02	1.02	0.426	0.417	0.283	2.09
	DS3	14	1.13	1.35	0.455	0.339	0.843	2.23
	DS4	60	1.89	1.97	0.85	0.431	0.449	4.97
Hinge Rotation	DS1	66	0.000658	0.00113	0.00133	1.17	0.000139	0.00674
	DS2	48	0.00916	0.00924	0.00428	0.463	0.00157	0.0194
	DS3	14	0.0111	0.0132	0.00517	0.393	0.00746	0.023
	DS4	60	0.0189	0.0197	0.00947	0.481	0.00201	0.0545

5.2 Removal of Outliers

When developing fragility functions using experimental data, it is possible to have a value that does not reflect the true behavior of real walls. This can be the result of experimental error or a test specimen that does not accurately represent real walls. To account for such point, the ATC-58 [1] guidelines require evaluation of the data for outliers using Pierce's criterion. A detailed outline of the procedure can be found in the ATC-58 guidelines. The general approach to checking for outliers is the following:

1. Determine the median, θ, and dispersion, β, of the data set
2. Assume one doubtful observation
3. Determine the value R ($R = |ln(d) - ln(\theta)|/\beta$). This is a tabulated value based on the number of doubtful observations and the number of walls in the data set being evaluated.
4. Determine the maximum allowable deviation of a measurement d from the median: $|ln(d) - ln(\theta)|$
5. Determine the distance of each measurement, d_i, from
6. Eliminate the data point d_i if the distance from the median exceeds the allowable
7. If any outliers are detected, return to Step 2 and increase the number of doubtful observations, D. Repeat until no more outliers are detected.

8. Determine new median and dispersion for the data set

Table 5.2 provides the same information as Table 5.1, but values were determined after outliers were removed from the data set. When considering the full dataset, few outliers were detected, and when removed, did not have much effect on the median EDP values but did reduce the coefficient of variation some. Although minimal impact is seen in the outliers here, it is import to remove them as the Method of Maximum Likelihood, which is sensitive to outliers, was used to determine the fragility functions in this study.

Table 5.2: Median EDP values of damage states using the full database, with outliers removed.

		All						
		#	Median	Mean	Std. Dev.	Coeff. of Var.	Min.	Max.
Specimen Drift	DS1	66	0.0836	0.133	0.132	0.991	0.0223	0.658
	DS2	48	1.02	1	0.423	0.424	0.283	2.09
	DS3	14	1.12	1.29	0.513	0.399	0.753	2.23
	DS4	58	1.89	1.99	0.822	0.413	0.688	4.97
Effective Drift	DS1	66	0.0856	0.138	0.131	0.949	0.0223	0.658
	DS2	48	1.02	1.02	0.426	0.417	0.283	2.09
	DS3	14	1.13	1.35	0.455	0.339	0.843	2.23
	DS4	59	1.89	2	0.833	0.417	0.678	4.97
Hinge Rotation	DS1	66	0.000658	0.00113	0.00133	1.17	0.000139	0.00674
	DS2	47	0.00951	0.0094	0.00418	0.444	0.00302	0.0194
	DS3	14	0.0111	0.0132	0.00517	0.393	0.00746	0.023
	DS4	58	0.0191	0.0203	0.00907	0.447	0.00655	0.0545

5.3 Reduction of Dataset

The check for outliers discussed in Section 5.2 removes data based on statistical analysis. It is also desired to remove any data that is not representative of full scale walls subjected to seismic loading. Thus, the impact of load history and test specimen scale on damage progression were evaluated. When evaluating subsets of the data set, outliers were removed, following the procedure outlined in Section 5.2, prior to presenting the final statistics.

First, the impact of load history on damage progression was investigated. The data were separated into three categories: i) walls subjected to monotonic loading, ii) walls subjected to uni-directional cyclic loading, and iii) walls subjected to bi-directional cyclic loading. Dataset statistics are listed in Table 5.3. Eleven wall specimens (the full dataset comprised 66 specimens) were subjected to monotonic loading; ten were from same test program [20]. The drift corresponding to DS5 was expected to higher for these walls than for those subjected to cyclic loading. However, the data in Table 5.3 show that this was not the case, with the median EDPs for onset of DS5 for monotonic loading was approximately 80% of the EDPs for cyclic loading. On the basis of this unexpected behavior, the monotonic tests were considered to provide damage

data unrepresentative of earthquake damage and it was decided to remove the monotonic tests from the data set. The median EDP was higher for bi-direction tests than for uni-direction tests, which is likely because there were relatively few data points available for for bi-directional tests. Additionally, the bi-directional tests in the data set tended to have fewer cycles at larger displacement increments than did uni-directional tests, and the researchers tended to report damage only at the cycle peaks. Thus, the damage was not reported at the drift at which damage actually initiated, but rather at the much larger drifts, thus resulting in unrealistically high median EPPs. It was concluded that there was insufficient information to create a seperate set of fragility functions for bi-direction loading.

Table 5.3: Median EDP values of damage states (walls sorted by load history)

		Monotonic			Cyclic			Bi-Dir.		
		#	Median	c.v.	#	Median	c.v.	#	Median	c.v.
Specimen Drift	DS1	11	0.0462	0.31	50	0.097	0.715	5	0.494	0.751
	DS2	4	0.978	0.0863	40	1.01	0.453	4	1.4	0.274
	DS3	0	NaN	NaN	13	1.08	0.411	1	1.8	0
	DS4	9	1.61	0.196	43	2	0.399	4	2.11	0.0735
Effective Drift	DS1	11	0.0462	0.31	50	0.103	0.672	5	0.494	0.729
	DS2	4	0.978	0.0863	40	1.01	0.43	4	1.41	0.349
	DS3	0	NaN	NaN	13	1.11	0.346	1	1.8	0
	DS4	9	1.61	0.196	44	1.95	0.404	5	2.26	0.154
Hinge Rotation	DS1	11	0.000244	0.386	50	0.000711	0.798	5	0.00514	0.777
	DS2	4	0.0086	0.17	39	0.00951	0.469	4	0.0131	0.303
	DS3	0	NaN	NaN	13	0.0106	0.403	1	0.0184	0
	DS4	9	0.0153	0.26	43	0.0191	0.419	4	0.0214	0.0839

Next, the impact of test specimen scale was investigated, as it is often thought that small scale specimens result in unrealistic damage progression. Four subdivisions, shown in Table 5.4, were considered. The median values of walls with scale less than or equal to 0.25 (which were primarily the result of one test program), were not consistently less than or greater than those walls with a scale less than 0.33, and the medians were often very similar to those with a scale greater than 0.33. Due to this lack of consistency, it was determined that there was insufficient reason to develop suites of fragility functions based on the scale of the wall. No walls were removed from the data set on the basis of scale.

5.4 Impact of Design Parameters on Damage Progression

The impact of various design parameters on damage progression was investigated. In part, this was conducted to investigate the development of multiple suites of fragility functions. The reduced data set (monotonic tests excluded) was used. The following parameters were considered: a) shape, b) shear-span ration, c) axial load ratio, d) shear stress demand, and e) shear demand/capacity ratio. The specific design parameter values used to sub-divide the data set were determined via an iterative process. Only the final subdivisions

Table 5.4: Median EDP values of damage states for reduced data set (walls sorted by scale)

		Scale $\leq$ 0.25			0.25 < Scale $\leq$ 0.33			Scale > 0.33		
		#	Median	c.v.	#	Median	c.v.	#	Median	c.v.
Specimen Drift	DS1	11	0.0833	0.348	19	0.135	0.937	24	0.105	0.832
	DS2	10	1.33	0.254	15	0.75	0.323	18	1.08	0.5
	DS3	2	1.73	0.222	3	1.8	0.154	9	0.843	0.314
	DS4	6	1.83	0.139	17	2.5	0.236	22	1.78	0.427
Effective Drift	DS1	11	0.0833	0.348	19	0.135	0.937	24	0.153	0.737
	DS2	10	1.33	0.254	15	0.75	0.323	18	1.08	0.472
	DS3	2	1.73	0.222	3	1.8	0.154	8	0.986	0.108
	DS4	6	1.83	0.139	17	2.5	0.236	23	1.85	0.443
Hinge Rotation	DS1	11	0.000651	0.276	19	0.00097	1.17	24	0.00105	0.949
	DS2	9	0.0128	0.221	15	0.00661	0.39	18	0.00975	0.502
	DS3	2	0.0176	0.255	3	0.0184	0.175	9	0.00896	0.294
	DS4	6	0.0184	0.177	18	0.0241	0.301	22	0.0174	0.418

are presented here. For each sub-division, an outlier check was performed using the procedure discussed in the previous section. In evaluating the sub-divisions, the following were considered: i) increasing median value as the damage level increases, ii) difference between the median values for different sub-divisions, iii) the number of outliers in each sub-division, and iv) are there sufficient data points in each sub-division to ensure confidence that the observations are a function of the design parameter considered and is not a misrepresentation of the behavior due to a few data points significantly affecting the median.

Table 5.5 shows the median values and coefficients of variation for the database sorted by shape (rectangular (32), barbell(12), and flange (11; C-walls, T-walls, and H-walls)). While there are distinct differences in the median values for each shape, there are not a sufficient number of data points for the barbell and flanged walls to consider them independently.

Table 5.5: Median EDP values of damage states (walls sorted by shape)

		Rectangle			Barbell			Flange		
		#	Median	c.v.	#	Median	c.v.	#	Median	c.v.
Specimen Drift	DS1	32	0.0848	0.781	12	0.105	0.64	11	0.245	0.787
	DS2	26	1.03	0.436	11	0.597	0.507	7	1.11	0.289
	DS3	10	0.927	0.4	3	1.67	0.223	1	1.8	0
	DS4	26	1.83	0.429	10	2.21	0.296	10	2.04	0.197
Effective Drift	DS1	32	0.0946	0.712	12	0.105	0.64	11	0.245	0.775
	DS2	26	1.03	0.4	11	0.597	0.507	7	1.11	0.359
	DS3	10	1.05	0.323	3	1.67	0.223	1	1.8	0
	DS4	28	1.83	0.465	10	2.21	0.296	10	2.04	0.207
Hinge Rotation	DS1	31	0.000703	0.636	12	0.00052	0.795	11	0.00214	0.87
	DS2	26	0.00975	0.447	10	0.00537	0.499	7	0.0104	0.333
	DS3	10	0.00933	0.392	3	0.0164	0.249	1	0.0184	0
	DS4	26	0.0184	0.432	10	0.0223	0.333	9	0.0216	0.151

Shear span ratio, Eq. 2.2, was considered because one could expect that walls with a lower shear span ratio to have lower drift demands. The data in Table 5.6 shows that, for walls with a shear span ratio

less than or equal to three, the median EDPs for all damage states (except DS1 for drift and rotation) are significantly smaller than those for walls with shear span ratios greater than three. However, there are at present too few experimental data on walls with larger aspect ratios to conclude that multiple suites of fragility functions are necessary for slender walls based on shear span ratio.

Table 5.6: Median EDP values of damage states for reduced data set (walls sorted by shear span)

		$M/(V\ell_w) \leq 3$			$M/(V\ell_w) > 3$		
		#	Median	c.v.	#	Median	c.v.
Specimen Drift	DS1	47	0.101	0.915	7	0.0941	0.629
	DS2	37	0.905	0.416	5	1.6	0.0414
	DS3	14	1.12	0.399	0	NaN	NaN
	DS4	42	1.88	0.393	6	2.78	0.148
Effective Drift	DS1	47	0.104	0.883	7	0.106	0.504
	DS2	37	0.905	0.39	7	1.6	0.172
	DS3	14	1.13	0.339	0	NaN	NaN
	DS4	42	1.9	0.385	6	2.78	0.115
Hinge Rotation	DS1	47	0.000719	1.08	7	0.000666	0.558
	DS2	36	0.00857	0.456	7	0.0137	0.239
	DS3	14	0.0111	0.393	0	NaN	NaN
	DS4	42	0.0189	0.42	6	0.0254	0.144

Axial load ratio was considered because one could expect that higher compressive loads will delay the onset of initial cracking and yield but could decrease the demand at which bar buckling and core crushing occur. Axial load ratios were divided as less than or greater than 10% of the gross capacity, with most walls falling into the former category. Table 5.7 provides the median values for each damage state and EDP. Walls with lower axial loads have significantly higher EDPs for DS5 and DS4, and lower drift and roof drift for DS1. However, there are relatively few data for walls with axial loads in excess of 10% of the gross capacity and more experimental data would be needed to support the developement of multiple suites of fragility functions on the basis of axial load ratio.

Table 5.7: Median EDP values of damage states for reduced data set (walls sorted by axial load ratio)

		$\lambda_N < 0.10$			$\lambda_N \geq 0.10$		
		#	Median	c.v.	#	Median	c.v.
Specimen Drift	DS1	45	0.0941	0.913	9	0.104	0.526
	DS2	34	1.1	0.375	9	0.566	0.584
	DS3	9	1.67	0.308	5	0.756	0.17
	DS4	38	2.18	0.345	10	1.27	0.435
Effective Drift	DS1	45	0.102	0.871	9	0.108	0.451
	DS2	34	1.1	0.38	9	0.597	0.512
	DS3	9	1.67	0.267	5	0.921	0.0942
	DS4	39	2.17	0.362	10	1.32	0.394
Hinge Rotation	DS1	45	0.000719	1.05	9	0.000719	0.662
	DS2	34	0.0105	0.408	9	0.00453	0.453
	DS3	9	0.0164	0.31	5	0.00853	0.13
	DS4	38	0.0217	0.369	10	0.0139	0.36

No trends were observed for the impact of shear demand. Table 5.8 provides three groups of shear demand, walls with a demand less than or equal to $2.5A_{cv}\sqrt{f'_c}$, walls with a demand greater than or equal to $7A_{cv}\sqrt{f'_c}$, and those between. The walls with low shear demands have a higher median drift for DS3 and DS5 than do the walls with a mid-range shear demand. However, the median drift for DS5 has a very similar value for low and high shear demands. The higher drift for high shear demands is a result of all but one of the walls with this higher shear demand coming from the same test program (Oesterle et al. [33, 32]), which had a median drift at DS5 higher than than for the full data set.

Table 5.8: Median EDP values of damage states for reduced data set (walls sorted by shear demand)

		$v_u \leq 2.5$			$2.5 < v_u < 7$			$v_u \geq 7$		
		#	Median	c.v.	#	Median	c.v.	#	Median	c.v.
Specimen Drift	DS1	13	0.0522	0.636	32	0.105	0.829	9	0.108	0.541
	DS2	12	1.12	0.407	24	1.01	0.429	8	0.615	0.462
	DS3	1	1.15	0	12	1.05	0.43	1	1.67	0
	DS4	9	2.64	0.442	30	1.87	0.339	8	2.41	0.221
Effective Drift	DS1	13	0.0522	0.663	32	0.139	0.782	9	0.108	0.541
	DS2	12	1.12	0.407	24	1.01	0.415	8	0.615	0.462
	DS3	1	1.15	0	12	1.1	0.361	1	1.67	0
	DS4	10	2.42	0.511	30	1.9	0.337	8	2.41	0.221
Hinge Rotation	DS1	13	0.000512	0.648	32	0.00105	0.975	8	0.000818	0.586
	DS2	12	0.0115	0.405	24	0.00911	0.444	8	0.00466	0.592
	DS3	1	0.0117	0	12	0.0101	0.424	1	0.0164	0
	DS4	9	0.0262	0.462	30	0.0188	0.342	8	0.0244	0.247

Table 5.9 contains the median values for the database sub-divided by shear demand-capacity ratio of the walls. There are no trends observed that indicate a need for separate suites of fragility functions.

Table 5.9: Median EDP values of damage states for reduced data set (walls sorted by shear demand ratio)

		$V_u/V_n < 0.5$			$0.5 \leq V_u/V_n \leq 0.75$			$0.75 \leq V_u/V_n \leq 1.0$			$V_u/V_n > 1.0$		
		#	Median	c.v.	#	Median	c.v.	#	Median	c.v.	#	Median	c.v.
Specimen Drift	DS1	14	0.0736	0.648	17	0.23	0.737	12	0.0833	1.14	11	0.101	0.266
	DS2	11	1.09	0.37	13	1.01	0.435	12	0.828	0.447	8	0.871	0.553
	DS3	1	1.46	0	5	1.08	0.293	7	1.67	0.442	1	0.756	0
	DS4	11	2.2	0.432	13	2.03	0.339	11	1.89	0.28	12	2.1	0.39
Effective Drift	DS1	14	0.0851	0.63	17	0.23	0.696	12	0.0833	1.11	11	0.108	0.26
	DS2	11	1.09	0.37	13	1.01	0.436	12	0.828	0.412	8	0.871	0.528
	DS3	1	1.46	0	5	1.11	0.229	7	1.67	0.391	1	0.96	0
	DS4	12	2.03	0.487	13	2.03	0.33	12	1.88	0.306	12	2.1	0.396
Hinge Rotation	DS1	13	0.000456	0.611	17	0.00174	0.82	12	0.000719	1.27	11	0.00085	0.309
	DS2	11	0.00978	0.384	13	0.00973	0.481	12	0.00767	0.486	8	0.00772	0.619
	DS3	1	0.0144	0	5	0.0106	0.286	7	0.0164	0.438	1	0.00841	0
	DS4	11	0.0238	0.464	13	0.0213	0.325	12	0.0195	0.336	11	0.0212	0.383

5.5 Fragility Function Theory

The fragility functions presented here are defined by the lognormal cumulative probability distribution (CDF). Experimental data provides discrete information that can be used to create an empirical CDF; however, the empirical CDF is defined by the entire dataset and use of the empirical CDF requires the entire dataset. The lognormal CDF is defined by two parameters. These parameters may be estimated in two ways from the empirical data [16]. The first method, the Method of Moments, uses the mean and variance of the empirical data set. The Method of Moments introduces error associated with estimating population statistics (i.e. distribution parameters) from the sample that is the data set. The second method, the Method of Maximum Likelihood, uses a likelihood function to estimate the distribution parameters which are most likely to produce the empirical values. Unlike the Method of Moments, this produces a higher probability that the CDF accurately represents the empirical data. However, because the Method of Maximum Likelihood considers the individual empirical values, it is more sensitive to the presence of outliers.

The lognormal distribution was used for the development of fragility functions in this study. Researchers have investigated other distributions (beta, gamma, Weibull) for use in earthquake damage predictions ([34], [15]), however, these have not been shown to provide significant improvement, over the lognormal distribution for damage prediction in structural elements. Further, the lognormal distribution is being used in the ATC-58 project for all structural and non-structural element.

The appropriateness of a chosen distribution can be evaluated using goodness-of-fit tests. Pagni and Lowes [34] discuss in detail three such tests: the chi-squared (χ^2), Kolmogorov-Smirnov (K-S), and the Lilliefors [23] tests. The χ^2 test is not appropriate for small sample sizes. The K-S test is appropriate for any sample size but is not exact and provides unconservative results if the distribution parameters are defined by the empirical data set. The K-S test can be modified to provide exact results for the case of distribution parameters defined by the empirical dataset and a small data set; the Lilliefors [23] test does this for the case of the normal distribution. Here, the Lilliefors test was used to evaluate the appropriateness of the lognormal distributions used to define the fragility functions.

To perform the Lilliefors test, the maximum difference between the theoretical CDF, F_X, and the emperical CDF, S_n, is determined:

$$D_n = max(|F_X(x_i) - S_n|) \tag{5.1}$$

where x_i is the i^{th} observation of each CDF. If value of D_n is less than or equal to a tabulated value of D_n^α, then the distribution tested is acceptable at the significance level α. The difference between the K-S and

Lilliefors tests are the tabulated values of D_n^α.

5.6 Fragility Functions for Slender Walls

The proposed fragility functions (functional CDF's) were developed using the reduced data set (no monotonic tests). Outliers were removed using Pierce's criterion. As discussed in Section 5.5, a log-normal probability distributions were used to define the fragilty functions and the distribution parameters were determined using the method of maximum likelihood. This was achieved through the use of the Matlab statistics toolbox *lognfit* function, which returns the mean (μ) and standard deviation (σ) of the associated normal distribution. The median of the lognormal distribution (θ) is equal to e^μ and the dispersion (β_d) can be approximated as σ.

Dispersion is a measure of uncertainty in the data. ATC 58 [1] requires consideration for two sources of dispersion. The first of these, β_d, is the dispersion of the experimental data determined using the method of maximum likelihood. The second, β_u, accounts for uncertainty that experimental tests represent the conditions of a real building component. ATC 58 specifies that the fragility function dispersion, β, be calculated as the square root of the sum of the squares (SRSS) of β_d and β_u:

$$\beta = \sqrt{\beta_u^2 + \beta_d^2} \tag{5.2}$$

For the slender wall dataset, the only condition for which β_u was not equal to 0.10 was when five or fewer specimens were used for a particular damage state, in which case 0.25 was used per the ATC 58 guidelines. The lognormal distribution parameters are provided in Table 5.10. Figure 5.1 shows empirical data and the fitted lognormal curve (including consideration for the uncertainty parameter).

The Lilliefors test with a significance level of 5% was used to evaluate the appropriateness of the lognormal distribution. The test was done using the Matlab function *lillietest*. Because the Lilliefors test was developed for a normal distribution, the log of the emperical data was used. The test indicated that the log-normal distribution was appropriate for all EDPs and MOR combinations except MOR2 and MOR4 for experimental drift.

Table 5.10: Lognormal distribution parameters for cyclically loaded walls

		All Walls					
		θ	β_d	β_u	β	Correct CDF	p
Specimen Drift	DS1	0.111	0.779	0.1	0.786	T	0.0764
	DS2	0.897	0.495	0.1	0.505	F	0.00917
	DS3	1.19	0.398	0.1	0.41	T	0.355
	DS4	1.86	0.419	0.1	0.431	F	0.0335
Effective Drift	DS1	0.118	0.755	0.1	0.762	T	0.5
	DS2	0.927	0.465	0.1	0.476	F	0.0469
	DS3	1.28	0.326	0.1	0.341	T	0.129
	DS4	1.86	0.43	0.1	0.441	F	0.0196
Hinge Rotation	DS1	0.000869	0.877	0.1	0.882	T	0.0529
	DS2	0.00841	0.501	0.1	0.511	T	0.0564
	DS3	0.0123	0.382	0.1	0.395	T	0.425
	DS4	0.0189	0.44	0.1	0.451	F	0.0145

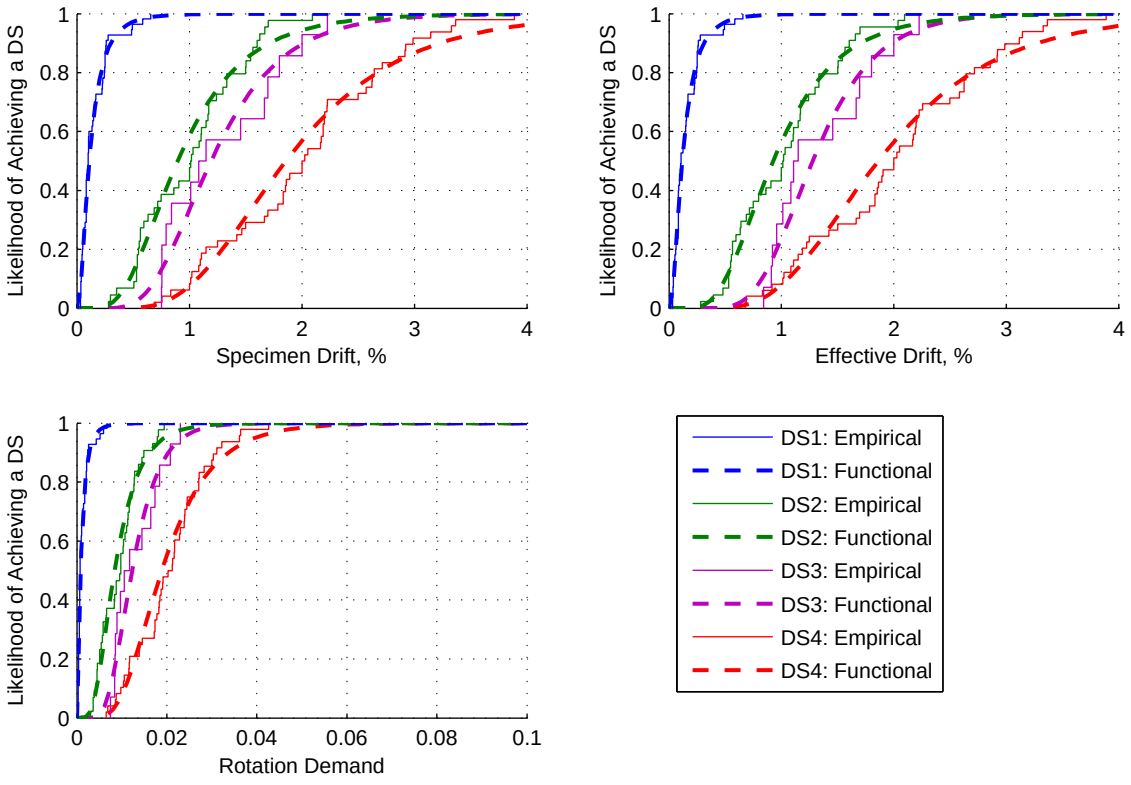

Figure 5.1: Fragility functions for cyclically loaded walls

Chapter 6

Recommendations and Conclusions

This report presented the development of fragility functions for slender RC walls. Experimental data from 66 test programs was used to associate damage states and methods of repair with engineering demand parameters for walls. Rectangular, barbell, and flanged walls with shear span ratios of two or greater were considered. It was determined that it was necessary to remove the damage data for monotonically loaded walls, and the final fragilities were developed using 55 cyclic tests. One set of fragility functions was developed as there was not sufficient data in individual categories to develop multiple sets of fragility functions. The engineering demand parameters considered were experimentally reported drift, drift at effective height of loading, and rotation demand. Recommendations to the ATC-58 committee were made using rotation demand, and are summarized in Table 6.1 (with median values rounded to two significant figures and dispersions to the nearest 0.05), however, effective drift values provided in Tables 5.10 could also be used.

Table 6.1: Recommended fragility function parameters

Method of Repair	Damage State	θ	β_d	β_u	β
MOR-1: Cosmetic Repair	DS1: Initial cracking and yielding	0.00087	0.90	0.10	0.90
MOR-2: Epoxy Injection and Patching	DS2: Cover spalling, vertical cracks	0.0084	0.50	0.10	0.50
MOR-3: Replace Concrete	DS3: Exposed longitudinal reinforcement	0.012	0.40	0.10	0.40
MOR-4: Replace Steel and Concrete	DS4: Bar fracture or buckling, core damage, bond slip, crushed web, shear failure	0.019	0.45	0.10	0.45

List of Symbols

A_{cv}	Area of wall resisting shear	21
A_g	Total cross-sectional area of wall	10
E_c	Elastic modulus of concrete	23
E_s	Modulus of elasticity	15
E_{sh}	Tangent stiffness at on-set of strain hardening	15
I_g	Cross section moment of inertia	23
M	Base moment	9
$\frac{M}{V\ell_w}$	Shear span ratio	9
$(\frac{M}{V\ell_w})_{strong}$	Shear span ratio for strong axis bending	20
$(\frac{M}{V\ell_w})_{weak}$	Shear span ratio for weak axis bending	20
P	Axial force	21
V	Base shear	9
V_n	ACI 318 nominal shear strength	21
V_u	Maximum experimental shear strength	21
V_u/V_n	Shear demand-capacity ratio	22
b_f	Width of boundary element (barbell wall); Flange width (flanged wall)	15
f'_c	Concrete compressive strength	10
f_y	Rebar yield stress	15
f_u	Rebar ultimate stress	15
h_f	Thickness of boundary element (barbell wall); Flange thickness (flanged wall)	15
h_w	Height of wall specimen	15
h_{eff}	Effective height of load	24
ℓ_{be}	Boundary element length	16
ℓ_w	Wall length	9

Bibliography

[1] A. 58. Guidelines for seismic performance assesment of buildings. ATC 58 50% Draft, 2009.

[2] ACI Committee 318. *Building code requirements for structural concrete (ACI 318-08) and commentary (ACI 318R-08)*. American Concrete Institute, 2008.

[3] ACI Committee 546. *ACI 546R-96: Concrete Repair Guide*. American Concrete Institute, Farmington Hills, MI, 1996.

[4] A. Ali. *Reinforced concrete structural walls with staggered opening configurations under reversed cyclic loading*. PhD thesis, University of Michigan, 1990.

[5] Applied Technology Council. *FEMA 308: Repair of Earthquake Damaged Concrete and Masonry Wall Buildings*. FEMA, Washington, D.C., 1998.

[6] K. Beyer, A. Dazio, and M. Priestley. Quasi-static cyclic tests of two U-shaped reinforced concrete walls. *Journal of Earthquake Engineering*, 12:1023–1053, 2008.

[7] A. Birely. *Seismic Performance of Slender Reinforced Structural Concrete Walls*. PhD thesis, University of Washington, 2012 (expected).

[8] P. Brown. Probabilistic earthquake damage predictions for reinforced concrete building components. Master's thesis, University of Washington, 2008.

[9] P. Brown and L. Lowes. Fragility functions for modern reinforced concrete beam-column joints. *Earthquake Spectra*, 23(2):263–289, May 2007.

[10] B. Brueggen. *Performance of T-shaped Reinforced Concrete Structural Walls under Multi-Directional Loading*. PhD thesis, University of Minnesota, August 2009.

[11] A. Dazio, K. Beyer, and H. Bachmann. Quasi-static cyclic tests and plastic hinge analysis of RC structural walls. *Engineering Structures*, 31:1556–1571, 2009.

[12] A. Dazio, T. Wenk, and H. Bachmann. Versuche an stahlbetontragwaden unter zyklish-statischer Einwirkung (tests on RC walls under cyclic-static action). Technical Report 239, IBK, 1999. http://e–collection.ethbib.ethz.ch/view/eth:23296.

[13] M. Elnady. *Seismic Rehabilitation of RC Structural Walls*. PhD thesis, McMaster University, 2008.

[14] C. Gulec, A. Whittaker, and J. Hooper. Fragility functions for low aspect ratio reinforced concrete walls. *Engineering Structures*, 32:2894–2901, September 2010.

[15] K. Gulec, A. Whittaker, and J. Hooper. Damage states and fragility curves for low aspect ratio reinforced concrete walls. Prepared for the Applied Technology Council Project ATC–58, 2009.

[16] A. Halder and S. Mahadevan. *Probability, Reliability and Statistical Methods in Engineering Design*. John Wiley and Sons, Inc., New York, 2000.

[17] C. Hart. *Tensile Response of Reinforced Concrete Structural Walls Under Reversed Cyclic Loading*. PhD thesis, University of Illinois Urbana-Champaign, 2011 (expected).

[18] N. Ile and J. Reynouard. Behaviour of U-shaped walls subjected to uniaxial and biaxial cyclic lateral loading. *Journal of Earthquake Engineering*, 9(1):67–94, 2005.

[19] A. Khalil and A. Ghobarah. Behaviour of rehabilitated structural walls. *Journal of Earthquake Engineering*, 9(3):371–391, 2005.

[20] I. Lefas. *Behaviour of Reinforced Concrete Structural Walls and Its Implication for Ultimate Limit State Design*. PhD thesis, University of London, February 1988.

[21] I. Lefas and M. Kotsovos. Strength and deformation characteristics of reinforced concrete walls under load reversals. *ACI Structural Journal*, 87(6):716–726, 1990.

[22] I. Lefas, M. Kotsovos, and N. Ambraseys. Behavior of reinforced concrete structural walls: Strength, deformation characteristics, and failure mechanism. *ACI Structural Journal*, 87(1):23–31, 1990.

[23] H. Lilliefors. On the K-S test for normality with mean and variance unknown. *Journal of the American Statistical Association*, 62:399–402, 1967.

[24] H. Liu. Effect of concrete strength on the response of ductile shear walls. Master's thesis, McGill University, 2004.

[25] L. Lowes, B. A., K. Marley, C. Hart, D. Kuchma, and D. Lehman. Investigation of the seismic response of slender planar concrete walls. In *9th US National and 10th Canadian Conference on Earthquake Engineering*, 2010.

[26] L. Lowes, J. Li, and A. . S. Team. Fragility functions for reinforced concrete moment frames. Report to Applied Technology Council Project ATC–58, 2010.

[27] S. Mazzoni, F. McKenna, G. Fenves, and et al. Open system for earthquake engineering simulation user manual. http://opensees.berkeley.edu, 2010.

[28] S. Mobeen. Cyclic tests of shear walls confined with double head studs. Master's thesis, University of Alberta, 2002.

[29] B. Morgan, H. Hiraishi, and W. Corley. U.s.–Japan quasi-static test of isolated wall planar reinforced concrete structure, volume I. Technical report, National Science Foundation, 1986.

[30] B. Morgan, H. Hiraishi, and W. Corley. U.s.–Japan quasi-static test of isolated wall planar reinforced concrete structure, volume II. Technical report, National Science Foundation, 1986.

[31] R. Oesterle. *Inelastic Analysis for In-plane Strength of Reinforced Concrete Shear Walls*. PhD thesis, Northwestern University, June 1986.

[32] R. Oesterle, J. Aristizabal-Ochoa, A. Fiorato, H. Russell, and W. Corley. Earthquake resistant structural walls – tests of isolated walls – phase II. Technical report, National Science Foundation, 1979.

[33] R. Oesterle, A. Fiorato, L. Johal, J. Carpenter, H. Russell, and W. Corley. Earthquake resistant structural walls – tests of isolated walls. Technical report, National Science Foundation, 1976.

[34] C. Pagni and L. Lowes. Fragility functions for older reinforced concrete beam-column joints. *Earthquake Spectra*, 22(1):215–238, February 2006.

[35] R. Park, M. Priestly, and W. Gill. Ductility of square-confined concrete columns. *Journal of the Structural Division*, 108:135–137, 1982.

[36] K. Pilakoutas. *Earthquake Resistant Design of Reinforced Concrete Walls*. PhD thesis, University of London, May 1990.

[37] K. Pilakoutas and A. Elnashai. Cyclic behavior of reinforced concrete cantilever walls, part I: Experimental results. *ACI Structural Journal*, 92(3):271–281, May–June 1995.

[38] K. Pilakoutas and A. Elnashai. Cyclic behavior of reinforced concrete cantilever walls, part II: Discussions and theoretical comparisons. *ACI Structural Journal*, 92(4):425–281, July–August 1995.

[39] P. Riva, A. Meda, and E. Giuriani. Cyclic behaviour of a full scale RC structural wall. *Engineering Structures*, 25:835–845, 2003.

[40] K. Shiu, J. Daniel, J. Aristizabal-Ochoa, A. Fiorato, and W. Corley. Earthquake resistant structural walls – tests of walls ith and without openings. Technical report, National Science Foundation, 1981.

[41] A. Tasnimi. Strength and deformation of mid-rise shear walls under load reversal. *Engineering Structures*, 22:311–322, 2000.

[42] J. Thomsen, IV and J. Wallace. Displacement-based design of reinforced concrete structural walls: Experimental studies of walls with rectangular and T–shaped cross sections. Technical Report 95/06, Department of Civil and Environmental Engineering, Clarkson University, Potsdam, N.Y., 1995.

[43] J. Thomsen, IV and J. Wallace. Displacement-based design of slender reinforced concrete structural walls – experimental verification. *Journal of Structural Engineering*, 130(4):618–630, April 2004.

[44] B. Tupper. Seismic response of reinforced concrete walls with steel boundary elements. Master's thesis, McGill University, 1999.

Appendix A

Database

Table A.1 contains a summary of the walls used in this study. Table A.2 provides a summary of the reinforcing steel properties, including i) the location in the wall where there steel is used (B = boundary element longitudinal steel, W = web longitudinal steel, H = horizontal steel, and C = confining steel) ii) the material model used for OpenSees fiber models, *ReinforcingSteel* (reinfStl) or *Steel01* (Steel01), and iii) estimated material properties (see Section 2.2.4.1), which are denoted by a '*'.

Sections A.1 through A.66 provide summaries of the individual wall tests. For each specimen, the following is provided:

- A table listing the recorded damage states. The damage states are sorted in alpha-numeric order. When developing the fragility functions, only one damage state for each method of repair was used and was selected to be the damage state with the lowest magnitude of drift, which is not necessarily the first damage state listed for each damage state. The damage states, which were listed in the main body of the report in Table 4.1 is reiterated here in Table A.3 and contains damage states that were entered into the database but which were not used in developing the fragility functions. These damage states begin with the the letters 'DSr', are primarily related to crack width measurements, and are included in the appendix for completeness.

- A table listing recorded crack width measurements. Any crack width measurements entered into the slender wall database were included here. The tables indicate the i) associated damage state, ii) the drift and force at the measurement, iii) if the measurement corresponds to the exact drift or the maximum cycle drift for the occurrence of the damage, iv) if the crack measurement is for an inclined crack (shear), a horizontal crack (flexure), or an unspecified crack (any), and v) the maximum and/or residual crack widths. Crack widths that were reported but not associated with a particular damage state are indicated by the letter 'C' and a number corresponding to the number of the reading.

- A figure showing the positive and negative load-drift envelopes (and the full hysteresis if available), with markers indicating the occurrences of the damage states. The markers shown in the legends correspond to the cycle peak where the damage occurred. Smaller markers of the same shape and color indicate the exact point on the load displacement envelope where the damage occurred, if available.

- Any figures (photos, sketches, crack maps) collected and added to the slender wall database to provide a visual reference for the damage data. Figure captions contain the name of the specimen, the damage state the photo is associated with, and a description of the figure.

Table A.1: Properties for slender walls included in database

Source	Specimen Name	Database Name	Shape	Loading	AR	$M/(V\ell_w)$	Scale	λ_n	v_n	v_u	V_u/V_n	f'_c ksi (MPa)	ρ_{be} %	ρ_{web} %	ρ_h %	ρ_{con} %
Pilakoutas and Elnashai	SW4	PilaSW4	Rect.	cyclic	2.00	2.00	0.20	0.00	6.2	5.7	0.92	5.4 (37)	6.85	0.75	0.39	1.54
	SW5	PilaSW5	Rect.	cyclic	2.00	2.00	0.20	0.00	5.0	7.0	1.40	4.6 (32)	11.41	0.79	0.35	0.88
	SW6	PilaSW6	Rect.	cyclic	2.00	2.00	0.20	0.00	4.7	5.8	1.24	5.6 (39)	6.85	0.75	0.35	0.71
	SW7	PilaSW7	Rect.	cyclic	2.00	2.00	0.20	0.00	6.6	7.5	1.15	4.6 (32)	11.08	0.79	0.39	1.85
	SW8	PilaSW8	Rect.	cyclic	2.00	2.00	0.20	0.00	5.0	4.7	0.94	6.6 (46)	7.14	0.75	0.42	0.85
	SW9	PilaSW9	Rect.	cyclic	2.00	2.00	0.20	0.00	6.6	5.3	0.79	5.6 (39)	7.14	0.75	0.60	1.22
Tasnimi	SHW1	TasSHW1	Rect.	cyclic	2.20	2.20	0.16	0.00	3.6	1.6	0.45	3.1 (22)	3.23	0.28	0.28	0.00
	SHW2	TasSHW2	Rect.	cyclic	2.20	2.20	0.16	0.00	3.6	2.1	0.57	3.1 (22)	3.23	0.28	0.28	0.00
	SHW3	TasSHW3	Rect.	cyclic	2.20	2.20	0.16	0.00	3.6	1.7	0.47	3.3 (22)	3.23	0.28	0.28	0.00
	SHW4	TasSHW4	Rect.	cyclic	2.20	2.20	0.16	0.00	3.5	2.3	0.66	3.4 (23)	3.23	0.28	0.28	0.00
Thomsen and Wallace	RW1	ThomRW1	Rect.	cyclic	3.00	3.00	0.33	0.10	5.1	2.6	0.50	4.6 (32)	2.93	0.33	0.33	1.06
	RW2	ThomRW2	Rect.	cyclic	3.00	3.00	0.33	0.07	5.0	2.6	0.53	4.9 (34)	2.93	0.33	0.33	1.21
	TW1	ThomTW1	T-wall	cyclic	3.00	3.00	0.33	0.07	4.7	4.3	0.92	6.3 (44)	3.27	0.33	0.33	1.06
	TW2	ThomTW2	T-wall	cyclic	3.00	3.00	0.33	0.07	4.7	5.5	1.16	6.0 (42)	2.51	0.45	0.33	0.89
Dazio et al.	WSH1	DazioWSH1	Rect.	cyclic	2.28	2.28	0.49	0.05	4.6	2.0	0.44	6.5 (45)	1.57	0.30	0.25	1.08
	WSH2	DazioWSH2	Rect.	cyclic	2.28	2.28	0.49	0.06	4.3	2.3	0.53	5.9 (41)	1.57	0.30	0.25	1.12
	WSH3	DazioWSH3	Rect.	cyclic	2.28	2.28	0.49	0.06	4.4	2.9	0.67	5.7 (39)	1.74	0.54	0.25	1.04
	WSH4	DazioWSH4	Rect.	cyclic	2.28	2.28	0.49	0.06	4.5	2.8	0.63	5.9 (41)	1.74	0.54	0.25	0.00
	WSH5	DazioWSH5	Rect.	cyclic	2.28	2.28	0.49	0.13	4.5	2.9	0.63	5.6 (38)	0.77	0.27	0.25	1.00
	WSH6	DazioWSH6	Rect.	cyclic	2.26	2.26	0.49	0.11	4.3	3.5	0.81	6.6 (46)	1.74	0.54	0.25	1.68
Lefas et al.	SW21	LefasSW21	Rect.	monotonic	2.00	2.00	0.21	0.00	10.8	6.2	0.57	5.0 (34)	2.99	2.49	0.82	0.56
	SW22	LefasSW22	Rect.	monotonic	2.00	2.00	0.21	0.12	10.7	7.2	0.68	5.1 (35)	2.99	2.49	0.82	0.56
	SW23	LefasSW23	Rect.	monotonic	2.00	2.00	0.21	0.21	10.3	8.3	0.80	5.6 (39)	2.99	2.49	0.82	0.56
	SW24	LefasSW24	Rect.	monotonic	2.00	2.00	0.21	0.00	10.7	5.8	0.54	5.1 (35)	2.99	2.49	0.82	0.56
	SW25	LefasSW25	Rect.	monotonic	2.00	2.00	0.21	0.21	10.5	7.1	0.67	5.3 (37)	2.99	2.49	0.82	0.56
	SW26	LefasSW26	Rect.	monotonic	2.00	2.00	0.21	0.00	7.2	7.1	0.99	3.5 (24)	2.99	2.49	0.41	0.56
	SW30	LefasSW30	Rect.	monotonic	2.00	2.00	0.21	0.00	6.6	6.8	1.03	3.5 (24)	2.99	1.55	0.36	0.49
	SW31	LefasSW31	Rect.	monotonic	2.00	2.00	0.21	0.00	6.3	6.2	0.99	4.1 (28)	2.99	1.55	0.36	0.49
	SW32	LefasSW32	Rect.	monotonic	2.00	2.00	0.21	0.00	5.5	4.9	0.89	6.0 (42)	2.99	1.55	0.36	0.49
	SW33	LefasSW33	Rect.	monotonic	2.00	2.00	0.21	0.00	5.7	5.2	0.91	5.4 (37)	2.99	1.55	0.36	0.49

Table A.1: Database properties (con't)

Source	Specimen Name	Database Name	Shape	Loading	AR	$M/(VL)$	Scale	λ_n	α_{V_n}	α_{V_u}	V_u/V_n	f'_c ksi (MPa)	ρ_{be} %	ρ_{web} %	ρ_h %	ρ_{con} %
Oesterle et al.	R1	OestR1	Rect.	cyclic	2.40	2.40	0.33	0.00	4.9	1.1	0.22	6.5 (45)	1.47	0.28	0.31	0.00
	R2	OestR2	Rect.	cyclic	2.40	2.40	0.33	0.00	5.0	2.0	0.40	6.7 (46)	4.00	0.28	0.31	3.99
	B1	OestB1	Barbell	cyclic	2.40	2.40	0.33	0.00	4.7	2.3	0.49	7.7 (53)	1.11	0.28	0.31	0.48
	B2	OestB2	Barbell	cyclic	2.40	2.40	0.33	0.00	7.5	5.8	0.77	7.8 (54)	3.67	0.28	0.63	0.42
	B3	OestB3	Barbell	cyclic	2.40	2.40	0.33	0.00	7.2	2.5	0.34	6.9 (47)	1.11	0.28	0.63	4.75
	B4	OestB4	Barbell	monotonic	2.40	2.40	0.33	0.00	7.7	3.1	0.41	6.5 (45)	1.11	0.28	0.63	4.75
	B5	OestB5	Barbell	cyclic	2.40	2.40	0.33	0.00	7.6	7.0	0.93	6.6 (45)	3.67	0.28	0.63	5.91
	B6	OestB6	Barbell	cyclic	2.40	2.40	0.33	0.13	10.2	11.0	1.07	3.2 (22)	3.67	0.28	0.63	3.57
	B7	OestB7	Barbell	cyclic	2.40	2.40	0.33	0.08	7.2	8.7	1.20	7.2 (49)	3.67	0.28	0.63	5.91
	B8	OestB8	Barbell	cyclic	2.40	2.40	0.33	0.09	14.3	9.4	0.66	6.1 (42)	3.67	0.28	1.38	5.91
	B9	OestB9	Barbell	cyclic	2.40	2.40	0.33	0.09	7.2	9.2	1.27	6.4 (44)	3.67	0.28	0.63	5.91
	B10	OestB10	Barbell	cyclic	2.40	2.40	0.33	0.08	7.3	9.0	1.24	6.6 (46)	1.97	0.28	0.63	5.93
	F1	OestF1	H-wall	cyclic	2.40	2.40	0.33	0.00	9.3	8.4	0.90	5.6 (38)	3.89	0.28	0.71	1.11
	F2	OestF2	H-wall	cyclic	2.40	2.40	0.33	0.07	6.5	8.2	1.25	6.6 (46)	5.01	0.24	0.55	3.15
Morgan et. al.	W1	Morgan	Barbell	cyclic	2.86	2.79	0.19	0.05	6.8	2.5	0.37	4.6 (32)	1.11	0.42	0.44	1.20
Liu	W1	LiuW1	Rect.	cyclic	3.08	3.13	0.66	0.08	5.9	2.3	0.39	4.8 (33)	3.00	0.33	0.40	2.32
	W2	LiuW2	Rect.	cyclic	3.08	3.13	0.66	0.04	5.1	1.7	0.33	10.3 (71)	3.00	0.33	0.47	2.32
Ali, Wight	W1	AliW1	Barbell	cyclic	2.92	3.04	0.25	0.08	5.3	3.7	0.69	4.7 (32)	3.20	0.28	0.28	2.67
Tupper	W3	TupperW3	Rect.	cyclic	3.90	3.75	0.50	0.10	8.9	4.3	0.48	5.6 (39)	5.36	0.44	0.73	0.96
Mobeen	W1	MobeenW1	Barbell	cyclic	2.98	2.74	0.66	0.15	11.4	3.8	0.34	3.5 (24)	1.60	0.67	1.00	2.15
Riva et al.	W1	RivaW1	Rect.	cyclic	4.11	3.17	0.98	0.00	4.0	2.0	0.51	4.7 (33)	2.30	0.17	0.17	0.96
Shiu et al.	C1	ShiuC1	Rect.	cyclic	2.88	2.88	0.33	0.00	6.3	4.3	0.69	3.4 (23)	5.58	0.24	0.37	2.78
Khalil	C1	KhaC1	Rect.	cyclic	1.10	2.25	0.39	0.07	5.2	5.9	1.14	5.5 (38)	10.00	0.83	0.27	0.00
Elnady and	CW2	ElnCW2	Rect.	cyclic	1.10	5.00	0.39	0.08	4.9	1.6	0.33	5.4 (37)	6.41	1.67	0.26	0.00
Ghobarah	CW3	ElnCW3	Rect.	cyclic	1.10	2.25	0.39	0.08	4.9	3.5	0.71	5.4 (38)	6.41	1.67	0.26	0.00
Ile et al.	X	IleX	C-wall	cyclic	2.40	2.40	0.82	0.10	9.4	6.0	0.64	3.4 (24)	0.98	0.25	0.54	1.09
	Y	IleY	C-wall	cyclic	2.40	2.40	0.82	0.10	9.4	3.0	0.32	3.4 (24)	0.98	0.25	0.54	1.09
	XY	IleXY	C-wall	cyclic	2.40	2.40	0.82	0.11	9.9	6.0	0.60	3.0 (21)	0.98	0.25	0.54	1.09
Beyer et al.	TUA	TUA	C-wall	cyclic	2.58	2.58	0.49	0.02	4.1	3.2	0.79	11.3 (78)	1.29	0.25	0.30	1.64
	TUB	TUB	C-wall	cyclic	2.58	2.58	0.33	0.04	5.8	5.7	0.99	7.9 (55)	2.17	0.38	0.45	2.44
Brueggen	NTW1	NTW1	T-wall	cyclic	3.20	3.47	0.50	0.03	4.5	4.9	1.09	7.3 (50)	3.78	0.28	0.29	1.13
	NTW2	NTW2	T-wall	cyclic	1.60	3.47	0.50	0.03	7.5	5.4	0.72	6.6 (45)	2.64	0.86	0.61	1.12
Lowes et al.	PW1	PW1	Rect.	cyclic	1.20	2.85	0.50	0.10	4.9	3.6	0.73	5.2 (36)	3.33	0.29	0.28	2.10
	PW2	PW2	Rect.	cyclic	1.20	2.15	0.50	0.13	4.8	5.0	1.05	5.8 (40)	3.50	0.29	0.28	1.86
	PW3	PW3	Rect.	cyclic	1.20	2.00	0.50	0.10	5.0	4.5	0.89	5.0 (34)	2.01	1.59	0.28	1.86
	PW4	PW4	Rect.	cyclic	1.20	1.99	0.50	0.12	5.2	4.6	0.89	4.3 (29)	3.50	0.29	0.28	1.86

Table A.2: Rebar Properties (* denotes assumed value)

Name	Bar Size	Location	Area in^2 (mm^2)	d_b in (mm)	Material Model	E ksi (GPa)	E_{sh} ksi (MPa)	f_y ksi (MPa)	ε_y	ε_{sh}	f_u ksi (MPa)	ε_u
PilaSW4	d12	B	0.18 (113)	0.47 (12.0)	Steel01	29028 (200)	228 (1573)	68 (470)	0.0024	-	87 (600)	0.085
	d6	WHC	0.04 (28)	0.24 (6.0)	Steel01	29028 (200)	378 (2605)	79 (545)	0.0027	-	86 (590)	0.02
PilaSW5	d16	B	0.31 (201)	0.63 (16.0)	Steel01	29753 (205)	110 (760)	78 (535)	0.0026	-	86 (590)	0.075
	d6	BW	0.04 (28)	0.24 (6.0)	Steel01	29028 (200)	378 (2605)	79 (545)	0.0027	-	86 (590)	0.02
	d4	HC	0.02 (13)	0.16 (4.0)	Steel01	29028 (200)	150 (1034)	58 (400)	0.002	-	67 (460)	0.06
PilaSW6	d12	B	0.18 (113)	0.47 (12.0)	Steel01	29028 (200)	228 (1573)	68 (470)	0.0024	-	87 (600)	0.085
	d6	W	0.04 (28)	0.24 (6.0)	Steel01	29028 (200)	378 (2605)	79 (545)	0.0027	-	86 (590)	0.02
	d4	HC	0.02 (13)	0.16 (4.0)	Steel01	29028 (200)	150 (1034)	58 (400)	0.002	-	67 (460)	0.06
PilaSW7	d16	B	0.31 (201)	0.63 (16.0)	Steel01	29753 (205)	110 (760)	78 (535)	0.0026	-	86 (590)	0.075
	d6	BWHC	0.04 (28)	0.24 (6.0)	Steel01	29028 (200)	378 (2605)	79 (545)	0.0027	-	86 (590)	0.02
PilaSW8	d10	B	0.12 (79)	0.39 (10.0)	Steel01	29028 (200)	838 (5772)	62 (430)	0.0022	-	96 (660)	0.042
	d6	W	0.04 (28)	0.24 (6.0)	Steel01	29028 (200)	378 (2605)	79 (545)	0.0027	-	86 (590)	0.02
	d4	HC	0.02 (13)	0.16 (4.0)	Steel01	29028 (200)	150 (1034)	58 (400)	0.002	-	67 (460)	0.06
PilaSW9	d10	B	0.12 (79)	0.39 (10.0)	Steel01	29028 (200)	838 (5772)	62 (430)	0.0022	-	96 (660)	0.042
	d6	W	0.04 (28)	0.24 (6.0)	Steel01	29028 (200)	378 (2605)	79 (545)	0.0027	-	86 (590)	0.02
	d4	HC	0.02 (13)	0.16 (4.0)	Steel01	29028 (200)	150 (1034)	58 (400)	0.002	-	67 (460)	0.06
TasSHW1	d6	B	0.04 (28)	0.24 (6.0)	Steel01	29000 (145)*	293 (2018)	40 (276)	0.0014	-	69 (475)	0.10*
	d3	WH	0.01 (7)	0.12 (3.0)	Steel01	29000 (145)*	148 (1021)	31 (216)	0.0011	-	46 (317)	0.10*
TasSHW2	d6	B	0.04 (28)	0.24 (6.0)	Steel01	29000 (145)*	293 (2018)	40 (276)	0.0014	-	69 (475)	0.10*
	d3	WH	0.01 (7)	0.12 (3.0)	Steel01	29000 (145)*	148 (1021)	31 (216)	0.0011	-	46 (317)	0.10*
TasSHW3	d6	B	0.04 (28)	0.24 (6.0)	Steel01	29000 (145)*	293 (2018)	40 (276)	0.0014	-	69 (475)	0.10*
	d3	WH	0.01 (7)	0.12 (3.0)	Steel01	29000 (145)*	131 (900)	31 (216)	0.0011	-	44 (305)	0.10*
TasSHW4	d6	B	0.04 (28)	0.24 (6.0)	Steel01	29000 (145)*	293 (2018)	40 (276)	0.0014	-	69 (475)	0.10*
	d3	WH	0.01 (7)	0.12 (3.0)	Steel01	29000 (145)*	131 (900)	31 (216)	0.0011	-	44 (305)	0.10*
ThomRW1	no3	B	0.11 (71)	0.38 (9.5)	reinfStl	29000 (200)	1450 (9991)	63 (433)	0.0022	0.017	93 (639)	0.094
	no2	WH	0.05 (32)	0.25 (6.3)	Steel01	29000 (200)	397 (2733)	64 (438)	0.0022	-	85 (588)	0.057
ThomRW2	no3	B	0.11 (71)	0.38 (9.5)	reinfStl	29000 (200)	1450 (9991)	63 (433)	0.0022	0.017	93 (639)	0.094
	no2	WH	0.05 (32)	0.25 (6.3)	Steel01	29000 (200)	397 (2733)	64 (438)	0.0022	-	85 (588)	0.057
ThomTW1	no3	B	0.11 (71)	0.38 (9.5)	reinfStl	29000 (200)	1450 (9991)	63 (433)	0.0022	0.017	93 (639)	0.094
	no2	BWH	0.05 (32)	0.25 (6.3)	Steel01	29000 (200)	397 (2733)	64 (438)	0.0022	-	85 (588)	0.057
ThomTW2	no3	B	0.11 (71)	0.38 (9.5)	reinfStl	29000 (200)	1450 (9991)	63 (433)	0.0022	0.017	93 (639)	0.094
	no2	BW	0.05 (32)	0.25 (6.3)	Steel01	29000 (200)	397 (2733)	64 (438)	0.0022	-	85 (588)	0.057
DazioWSH1	d10	B	0.12 (79)	0.39 (10.0)	Steel01	29000 (200)	178 (1228)	79 (545)	0.0027	-	89 (612)	0.057
	d6	WHC	0.04 (28)	0.24 (6.0)	Steel01	29000 (200)	154 (1060)	83 (569)	0.0028	-	86 (590)	0.023
DazioWSH2	d10	B	0.12 (79)	0.39 (10.0)	Steel01	29000 (200)	318 (2190)	84 (580)	0.0029	-	108 (746)	0.079
	d6	WHC	0.04 (28)	0.24 (6.0)	Steel01	29000 (200)	117 (808)	70 (483)	0.0024	-	78 (534)	0.065

Table A.2: Rebar properties (con't)

Test	Bar Size	Location	Area in^2 (mm^2)	d_b in (mm)	Material Model	E ksi (GPa)	E_{sh} ksi (MPa)	f_y ksi (MPa)	ε_y	ε_{sh}	f_u ksi (MPa)	ε_u
DazioWSH3	d12	B	0.18 (113)	0.47 (12.0)	Steel01	29000 (200)	218 (1504)	87 (599)	0.003	-	105 (723)	0.085
	d8	W	0.08 (50)	0.31 (8.0)	Steel01	29000 (200)	240 (1655)	83 (569)	0.0028	-	101 (699)	0.082
	d6	HC	0.04 (28)	0.24 (6.0)	Steel01	29000 (200)	143 (985)	71 (488)	0.0024	-	80 (552)	0.068
DazioWSH4	d12	B	0.18 (113)	0.47 (12.0)	Steel01	29000 (200)	163 (1125)	83 (574)	0.0029	-	98 (672)	0.09
	d8	W	0.08 (50)	0.31 (8.0)	Steel01	29000 (200)	262 (1806)	85 (583)	0.0029	-	103 (713)	0.075
	d6	H	0.04 (28)	0.24 (6.0)	Steel01	29000 (200)	108 (741)	75 (518)	0.0026	-	81 (558)	0.058
DazioWSH5	d8	B	0.08 (50)	0.31 (8.0)	Steel01	29000 (200)	262 (1806)	85 (583)	0.0029	-	103 (713)	0.075
	d6	WH	0.04 (28)	0.24 (6.0)	Steel01	29000 (200)	108 (741)	75 (518)	0.0026	-	81 (558)	0.058
DazioWSH6	d12	B	0.18 (113)	0.47 (12.0)	Steel01	29000 (200)	163 (1125)	83 (574)	0.0029	-	98 (672)	0.09
	d8	W	0.08 (50)	0.31 (8.0)	Steel01	29000 (200)	262 (1806)	85 (583)	0.0029	-	103 (713)	0.075
	d6	HC	0.04 (28)	0.24 (6.0)	Steel01	29000 (200)	108 (741)	75 (518)	0.0026	-	81 (558)	0.058
LefasSW21	d8	BW	0.08 (50)	0.31 (8.0)	Steel01	23077 (159)	142 (979)	68 (470)	0.003	-	82 (565)	0.10*
	d6.25	H	0.05 (31)	0.25 (6.3)	Steel01	21771 (150)	135 (932)	75 (520)	0.0035	-	89 (610)	0.10*
LefasSW22	d8	BW	0.08 (50)	0.31 (8.0)	Steel01	23077 (159)	142 (979)	68 (470)	0.003	-	82 (565)	0.10*
	d6.25	H	0.05 (31)	0.25 (6.3)	Steel01	21771 (150)	135 (932)	75 (520)	0.0035	-	89 (610)	0.10*
LefasSW23	d8	BW	0.08 (50)	0.31 (8.0)	Steel01	23077 (159)	142 (979)	68 (470)	0.003	-	82 (565)	0.10*
	d6.25	H	0.05 (31)	0.25 (6.3)	Steel01	21771 (150)	135 (932)	75 (520)	0.0035	-	89 (610)	0.10*
LefasSW24	d8	BW	0.08 (50)	0.31 (8.0)	Steel01	23077 (159)	142 (979)	68 (470)	0.003	-	82 (565)	0.10*
	d6.25	H	0.05 (31)	0.25 (6.3)	Steel01	21771 (150)	135 (932)	75 (520)	0.0035	-	89 (610)	0.10*
LefasSW25	d8	BW	0.08 (50)	0.31 (8.0)	Steel01	23077 (159)	142 (979)	68 (470)	0.003	-	82 (565)	0.10*
	d6.25	H	0.05 (31)	0.25 (6.3)	Steel01	21771 (150)	135 (932)	75 (520)	0.0035	-	89 (610)	0.10*
LefasSW26	d8	BW	0.08 (50)	0.31 (8.0)	Steel01	23077 (159)	142 (979)	68 (470)	0.003	-	82 (565)	0.10*
	d6.25	H	0.05 (31)	0.25 (6.3)	Steel01	21771 (150)	135 (932)	75 (520)	0.0035	-	89 (610)	0.10*
LefasSW30	d8	BW	0.08 (50)	0.31 (8.0)	Steel01	23077 (159)	142 (979)	68 (470)	0.003	-	82 (565)	0.10*
	d6.25	H	0.05 (31)	0.25 (6.3)	Steel01	21771 (150)	135 (932)	75 (520)	0.0035	-	89 (610)	0.10*
LefasSW31	d8	BW	0.08 (50)	0.31 (8.0)	Steel01	23077 (159)	142 (979)	68 (470)	0.003	-	82 (565)	0.10*
	d6.25	H	0.05 (31)	0.25 (6.3)	Steel01	21771 (150)	135 (932)	75 (520)	0.0035	-	89 (610)	0.10*
LefasSW32	d8	BW	0.08 (50)	0.31 (8.0)	Steel01	23077 (159)	142 (979)	68 (470)	0.003	-	82 (565)	0.10*
	d6.25	H	0.05 (31)	0.25 (6.3)	Steel01	21771 (150)	135 (932)	75 (520)	0.0035	-	89 (610)	0.10*
LefasSW33	d8	BW	0.08 (50)	0.31 (8.0)	Steel01	23077 (159)	142 (979)	68 (470)	0.003	-	82 (565)	0.10*
	d6.25	H	0.05 (31)	0.25 (6.3)	Steel01	21771 (150)	135 (932)	75 (520)	0.0035	-	89 (610)	0.10*
OestR1	no3	B	0.11 (71)	0.38 (9.5)	Steel01	27800 (192)	386 (2660)	74 (511)	0.0027	-	111 (765)	0.098
	d6	WH	0.05 (32)	0.25 (6.3)	Steel01	31400 (216)	216 (1486)	76 (522)	0.0024	-	102 (699)	0.12
OestR2	no4	B	0.20 (129)	0.50 (12.7)	Steel01	26900 (185)	310 (2137)	65 (450)	0.0024	-	103 (708)	0.12
	d6	WHC	0.05 (32)	0.25 (6.3)	Steel01	32600 (225)	186 (1280)	78 (535)	0.0024	-	100 (690)	0.12

Table A.2: Rebar properties (con't)

Test	Bar Size	Location	Area in^2 (mm^2)	d_b in (mm)	Material Model	E ksi (GPa)	E_{sh} ksi (MPa)	f_y ksi (MPa)	ε_y	ε_{sh}	f_u ksi (MPa)	ε_u
OestB1	no4	B	0.20 (129)	0.50 (12.7)	Steel01	28300 (195)	327 (2253)	65 (449)	0.0023	-	103 (708)	0.12
	d6	WH	0.05 (32)	0.25 (6.3)	Steel01	32500 (224)	242 (1665)	76 (520)	0.0023	-	101 (695)	0.11
OestB2	no6	B	0.44 (284)	0.75 (19.1)	Steel01	30200 (208)	315 (2172)	60 (410)	0.002	-	101 (695)	0.13
	d6	WH	0.05 (32)	0.25 (6.3)	Steel01	32100 (221)	245 (1688)	77 (532)	0.0024	-	102 (700)	0.1
OestB3	no4	B	0.20 (129)	0.50 (12.7)	Steel01	25900 (178)	352 (2425)	64 (438)	0.0025	-	101 (696)	0.11
	d6	WHC	0.05 (32)	0.25 (6.3)	Steel01	30400 (209)	228 (1568)	69 (478)	0.0023	-	96 (658)	0.12
OestB4	no4	B	0.20 (129)	0.50 (12.7)	Steel01	27500 (189)	322 (2217)	65 (450)	0.0024	-	103 (706)	0.12
	d6	WHC	0.05 (32)	0.25 (6.3)	Steel01	31900 (220)	207 (1426)	73 (504)	0.0023	-	99 (681)	0.13
OestB5	no6	B	0.44 (284)	0.75 (19.1)	Steel01	29500 (203)	324 (2229)	64 (444)	0.0022	-	106 (733)	0.13
	d6	WHC	0.05 (32)	0.25 (6.3)	Steel01	31400 (216)	207 (1428)	73 (502)	0.0023	-	97 (671)	0.12
OestB6	no6	B	0.44 (284)	0.75 (19.1)	Steel01	28500 (196)	383 (2638)	64 (440)	0.0022	-	106 (732)	0.11
	d6	WH	0.05 (32)	0.25 (6.3)	Steel01	30400 (209)	266 (1831)	74 (511)	0.0024	-	98 (675)	0.092
OestB7	no6	B	0.44 (284)	0.75 (19.1)	Steel01	28400 (196)	401 (2765)	66 (457)	0.0023	-	109 (750)	0.11
	d6	WHC	0.05 (32)	0.25 (6.3)	Steel01	28500 (196)	296 (2036)	71 (489)	0.0025	-	101 (696)	0.1
OestB8	no6	B	0.44 (284)	0.75 (19.1)	Steel01	27500 (189)	410 (2824)	65 (447)	0.0024	-	108 (745)	0.11
	d6	WC	0.05 (32)	0.25 (6.3)	Steel01	28200 (194)	220 (1518)	66 (453)	0.0023	-	89 (615)	0.11
	no3	H	0.11 (71)	0.38 (9.5)	Steel01	25000 (172)	405 (2789)	70 (482)	0.0028	-	106 (728)	0.091
OestB9	no6	B	0.44 (284)	0.75 (19.1)	Steel01	27600 (190)	414 (2853)	62 (429)	0.0023	-	107 (734)	0.11
	d6	WHC	0.05 (32)	0.25 (6.3)	Steel01	28600 (197)	219 (1506)	67 (461)	0.0023	-	89 (613)	0.1
OestB10	no5	B	0.31 (200)	0.63 (15.9)	Steel01	27100 (187)	477 (3286)	55 (378)	0.002	-	108 (746)	0.11
	no4	B	0.20 (129)	0.50 (12.7)	Steel01	27000 (186)	328 (2259)	64 (438)	0.0024	-	102 (706)	0.12
	d6	WHC	0.05 (32)	0.25 (6.3)	Steel01	31300 (216)	210 (1444)	69 (475)	0.0022	-	92 (632)	0.11
OestF1	no4	B	0.20 (129)	0.50 (12.7)	Steel01	28100 (194)	338 (2329)	65 (444)	0.0023	-	103 (707)	0.12
	d6	WHC	0.05 (32)	0.25 (6.3)	Steel01	31300 (216)	256 (1764)	76 (525)	0.0024	-	102 (704)	0.1
OestF2	no4	B	0.20 (129)	0.50 (12.7)	Steel01	28100 (194)	338 (2329)	65 (444)	0.0023	-	103 (707)	0.12
	d6	BWHC	0.04 (28)	0.24 (6.0)	Steel01	29400 (203)	190 (1306)	67 (464)	0.0023	-	88 (607)	0.11
Morgan	d6	B	0.04 (28)	0.24 (6.0)	Steel01	29000 (145)*	107 (739)	65 (448)	0.0022	-	86 (593)	0.2
	D3	WH	0.03 (19)	0.20 (5.0)	Steel01	29000 (145)*	134 (925)	74 (510)	0.0026	-	84 (579)	0.077
LiuW1	20M	B	0.47 (300)	0.77 (19.5)	reinfStl	28029 (193)	1401 (9656)	66 (458)	0.0024	0.015	88 (606)	0.18
	10M	WHC	0.16 (100)	0.44 (11.3)	reinfStl	23485 (162)	1174 (8091)	67 (464)	0.0029	0.022	80 (552)	0.17
LiuW2	20M	B	0.47 (300)	0.77 (19.5)	reinfStl	28029 (193)	1401 (9656)	66 (458)	0.0024	0.015	88 (606)	0.18
	10M	WHC	0.16 (100)	0.44 (11.3)	reinfStl	23485 (162)	1174 (8091)	67 (464)	0.0029	0.022	80 (552)	0.17
AliW1	no4	B	0.20 (129)	0.50 (12.7)	reinfStl	29037 (200)	1452 (10003)	78 (540)	0.0027	0.01	110 (756)	0.07
	no2	WH	0.05 (32)	0.25 (6.3)	Steel01	29107 (201)	2911 (20055)*	82 (562)	0.0028	-	364 (2511)*	0.10*

Table A.2: Rebar properties (con't)

Test	Bar Size	Location	Area in^2 (mm^2)	d_b in (mm)	Material Model	E ksi (GPa)	E_{sh} ksi (MPa)	f_y ksi (MPa)	ε_y	ε_{sh}	f_u ksi (MPa)	ε_u
TupperW3	20M	B	0.47 (300)	0.77 (19.5)	reinfStl	26556 (183)	1328 (9148)	65 (450)	0.0025	0.015	87 (600)	0.17
	10M	WH	0.16 (100)	0.44 (11.3)	reinfStl	24841 (171)	1242 (8558)	71 (488)	0.0029	0.017	79 (547)	0.23
MobeenW1	15M	B	0.31 (200)	0.63 (16.0)	reinfStl	27576 (190)	1379 (9500)	57 (395)	0.0021	0.01	80 (553)	0.094
	10M	WHC	0.16 (100)	0.44 (11.3)	reinfStl	27431 (189)	1372 (9450)	56 (384)	0.002	0.015	77 (527)	0.16
RivaW1	d20	B	0.49 (314)	0.79 (20.0)	Steel01	29000 (145)*	143 (985)	81 (560)	0.0028	-	93 (640)	0.084
	d8	BWHC	0.08 (50)	0.31 (8.0)	Steel01	29000 (145)*	143 (985)	81 (560)	0.0028	-	93 (640)	0.084
ShiuC1	no4	B	0.20 (129)	0.50 (12.7)	Steel01	26100 (180)	425 (2930)	69 (476)	0.0026	-	111 (761)	0.10*
	d6	WHC	0.04 (28)	0.24 (6.0)	Steel01	29500 (203)	263 (1813)	69 (473)	0.0023	-	94 (650)	0.10*
KhaC1	20M	B	0.47 (300)	0.77 (19.5)	Steel01	29000 (145)*	2900 (19981)*	68 (470)	0.0024	-	351 (2421)*	0.10*
	10M	W	0.16 (100)	0.44 (11.3)	Steel01	29000 (145)*	2900 (19981)*	68 (470)	0.0024	-	351 (2421)*	0.10*
	6M	H	0.05 (29)	0.24 (6.1)	Steel01	29000 (145)*	2900 (19981)*	87 (600)	0.003	-	368 (2538)*	0.10*
ElnCW2	15M	BW	0.31 (200)	0.63 (16.0)	Steel01	29000 (145)*	460 (3171)	65 (450)	0.0023	-	110 (760)	0.10*
	15M	Web	0.31 (200)	0.63 (16.0)	Steel01	29000 (145)*	460 (3171)	65 (450)	0.0023	-	110 (760)	0.10*
	d6	H	0.04 (28)	0.24 (6.0)	Steel01	29000 (145)*	69 (474)	83 (570)	0.0029	-	89 (616)	0.10*
ElnCW3	15M	BW	0.31 (200)	0.63 (16.0)	Steel01	29000 (145)*	460 (3171)	65 (450)	0.0023	-	110 (760)	0.10*
	d6	H	0.04 (28)	0.24 (6.0)	Steel01	29000 (145)*	69 (474)	83 (570)	0.0029	-	89 (616)	0.10*
IleX	d12	B	0.18 (113)	0.47 (12.0)	Steel01	29000 (145)*	59 (403)	75 (516)	0.0026	-	89 (615)	0.25
	d10	W	0.12 (79)	0.39 (10.0)	Steel01	29000 (145)*	56 (384)	76 (525)	0.0026	-	90 (617)	0.24
	d8	HC	0.08 (50)	0.31 (8.0)	Steel01	29000 (145)*	50 (344)	81 (557)	0.0028	-	93 (642)	0.25
IleY	d12	B	0.18 (113)	0.47 (12.0)	Steel01	29000 (145)*	59 (403)	75 (516)	0.0026	-	89 (615)	0.25
	d10	W	0.12 (79)	0.39 (10.0)	Steel01	29000 (145)*	56 (384)	76 (525)	0.0026	-	90 (617)	0.24
	d8	HC	0.08 (50)	0.31 (8.0)	Steel01	29000 (145)*	50 (344)	81 (557)	0.0028	-	93 (642)	0.25
IleXY	d12	B	0.18 (113)	0.47 (12.0)	Steel01	29000 (145)*	59 (403)	75 (516)	0.0026	-	89 (615)	0.25
	d10	W	0.12 (79)	0.39 (10.0)	Steel01	29000 (145)*	56 (384)	76 (525)	0.0026	-	90 (617)	0.24
	d8	HC	0.08 (50)	0.31 (8.0)	Steel01	29000 (145)*	50 (344)	81 (557)	0.0028	-	93 (642)	0.25
TUA	d12	B	0.18 (113)	0.47 (12.0)	reinfStl	29000 (145)*	1450 (10)*	71 (488)	0.0024	0.024	86 (595)	0.13
	d6	BWHC	0.04 (28)	0.24 (6.0)	Steel01	29000 (145)*	291 (2002)	75 (518)	0.0026	-	99 (681)	0.084
TUB	d12	B	0.18 (113)	0.47 (12.0)	reinfStl	29000 (145)*	1450 (10)*	68 (471)	0.0024	0.032	83 (574)	0.13
	d6	BWHC	0.04 (28)	0.24 (6.0)	Steel01	29000 (145)*	291 (2002)	75 (518)	0.0026	-	99 (681)	0.084
NTW1	no6	B	0.44 (284)	0.75 (19.1)	Steel01	28700 (198)	194 (1338)	64 (438)	0.0022	-	92 (636)	0.15
	no5	B	0.31 (200)	0.63 (15.9)	reinfStl	28000 (193)	1400 (9646)	63 (434)	0.0022	0.0046	92 (630)	0.15
	no3	BWH	0.11 (71)	0.38 (9.5)	Steel01	29000 (200)	237 (1634)	73 (502)	0.0025	-	106 (727)	0.14
NTW2	no6	B	0.44 (284)	0.75 (19.1)	Steel01	29600 (204)	238 (1641)	67 (460)	0.0023	-	101 (695)	0.14
	no5	BW	0.31 (200)	0.63 (15.9)	reinfStl	27700 (191)	1385 (9543)	66 (456)	0.0024	0.0069	103 (706)	0.14
	no4	BW	0.20 (129)	0.50 (12.7)	Steel01	29000 (145)*	222 (1532)	75 (513)	0.0026	-	106 (727)	0.14
	no3	BWH	0.11 (71)	0.38 (9.5)	Steel01	29000 (145)*	229 (1577)	73 (504)	0.0025	-	105 (723)	0.14

Table A.2: Rebar properties (con't)

Test	Bar Size	Location	Area in^2 (mm^2)	d_b in (mm)	Material Model	E ksi (GPa)	E_{sh} ksi (MPa)	f_y ksi (MPa)	ε_y	ε_{sh}	f_u ksi (MPa)	ε_u
PW1	no4	B	0.20 (129)	0.50 (12.7)	reinfStl	29000 (200)	1450 (9991)	84 (579)	0.0029	0.015	91 (628)	0.12
	no2	WHC	0.05 (32)	0.25 (6.3)	reinfStl	29000 (200)	1450 (9991)	76 (522)	0.0026	0.015	76 (526)	0.058
PW2	no4	B	0.20 (129)	0.50 (12.7)	reinfStl	29000 (200)	1450 (9991)	84 (579)	0.0029	0.015	91 (628)	0.12
	no2	WHC	0.05 (32)	0.25 (6.3)	reinfStl	29000 (200)	1450 (9991)	76 (522)	0.0026	0.015	76 (526)	0.058
PW3	no4	BW	0.20 (129)	0.50 (12.7)	reinfStl	29000 (200)	1450 (9991)	51 (353)	0.0018	0.012	70 (484)	0.2
	no2	HC	0.05 (32)	0.25 (6.3)	reinfStl	29000 (200)	1450 (9991)	76 (522)	0.0026	0.015	76 (526)	0.058
PW4	no4	B	0.20 (129)	0.50 (12.7)	reinfStl	29000 (200)	1450 (9991)	67 (462)	0.0023	0.0075	99 (682)	0.13
	no2	WHC	0.05 (32)	0.25 (6.3)	reinfStl	29000 (200)	1450 (9991)	76 (522)	0.0026	0.015	76 (526)	0.058

Table A.3: Damage States and Methods of Repair

Method of Repair	Damage State	Description
Cosmetic repair	DS1a	Initial cracking
	DS1b	Initial flexural cracking
	DS1c	Initial shear cracking
	DS1d	Tensile yield of extreme longitudinal steel
	DS1e	Compression yield of longitudinal steel
	DS1f	Yield of horizontal reinforcement
Epoxy injection and concrete patching	DS2a	Spalling of boundary region cover concrete (not revealing longitudinal reinforcement)
	DS2b	Spalling of patched concrete
	DS2c	Spalling of web concrete
	DS2d	Vertical cracks/splitting
Replace concrete	DS3a	Spalling revealing longitudinal reinforcement
Replace wall	DS4a	Core crushing (boundary element)
	DS4b	Bar buckling
	DS4c	Compressive failure of boundary element
	DS4d	Failure by core crushing (boundary element)
	DS4e	Bar fracture
	DS4f	Failure due to bar buckling
	DS4g	Failure due to bar fracture
	DS4i	Shear failure
	DS4k	Web crushing
	DS4m	Failure due to web crushing
	DS4o	Failure by bond slip
	DS4p	Core crushing in confined boundary element of flange tips (bi-directional tests only)
	DS4q	Confining reinforcement open or fractured
Not used for development of fragility functions	DSr1	First yield of flexural reinforcement
	DSr2	Residual cracks $\leq 1/16$ inches
	DSr3	Wall fully cracked
	DSr4	Large shear cracks
	DSr5	Shear cracks extending most of length of wall
	DSr9	Cracks $\geq 1/16$ inches
	DSr10	Cracks $\geq 1/8$ inches
	DSr11	Cracks $\geq 1/4$ inches
	DSr12	Cracks $\geq 1/2$ inches
	DSr13	Cracks ≥ 1 inch
	DSr14	Stirrup yield

A.1 PilaSW4

Table A.4: PilaSW4 damage information

MOR	DS	% Drift	Force, kips (kN)	Description	Figure
1	DS1a	0.08%	4.2 (18.8)	Occurred before 1mm disp, halfway to first maximum (p. 102)	Fig. A.2
	DS1d	-0.56%	-19.4 (-86.2)	As determined from moment-curvature analysis	
2	DS2d	1.33%	22.7 (100.9)	Vertical cracks in boundary element at base, at location of long. reinf. (p. 102); Identical other than description to large shear crack width damage state for same wall	Fig. A.7
4	DS4a	1.83%	22.4 (99.8)	Concrete confined by lowest 2 B.E. hoops spalling (p. 102)	Fig. A.4
	DS4d	-2.00%	-20.3 (-90.3)	Failure by core crushing in boundary elements (p. 102); No load history reported at this drift (LVDT maxed out). Load is extrapolated from the negative envelope, as the envelope and figure of damage suggests the left side (compression under (-) drift) is the side that saw compressive failure	Fig. A.5
	DSr1	0.46%	17.1 (76.0)	Occurred before 6mm disp (cycle peak) (p. 102); exact values reported in Table 7.2 (p. 193)	Fig. A.6
	DSr4	1.33%	22.7 (100.9)	Lower web crack widths larger than others at end of 16mm cycle, as noted by researchers (p. 102)	Fig. A.7

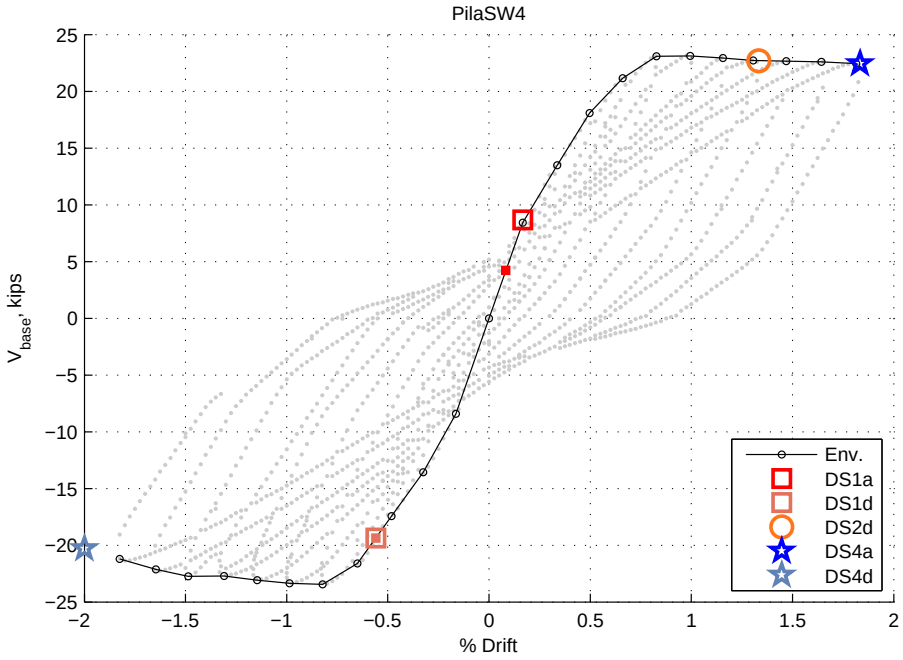

Figure A.1: Envelope for PilaSW4

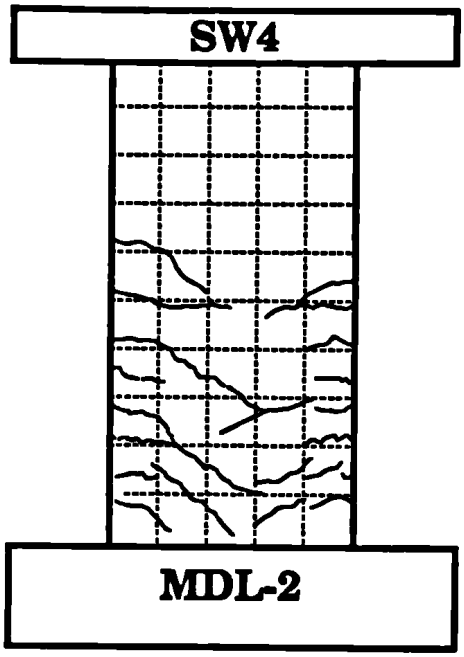

Figure A.2: PilaSW4: DS1a - cracks at MDL-2 (peak after initial cracking)

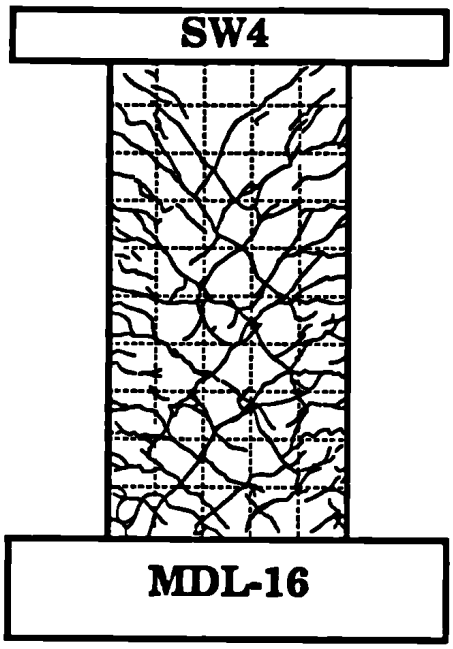

Figure A.3: PilaSW4: DS2d - cracks at MDL-16 (larger shear crack widths)

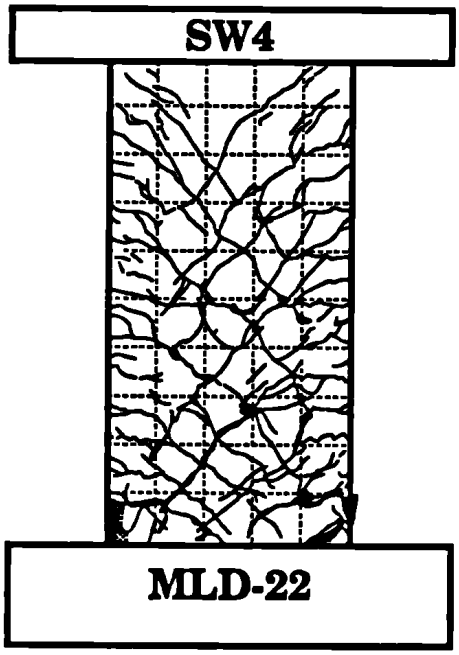

Figure A.4: PilaSW4: DS4a - cracks at MDL-22 (core crushing)

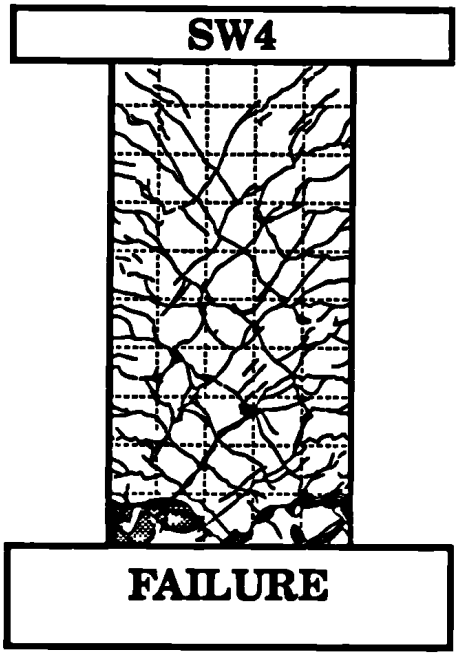

Figure A.5: PilaSW4: DS4d - cracks at MDL-22 (core crushing)

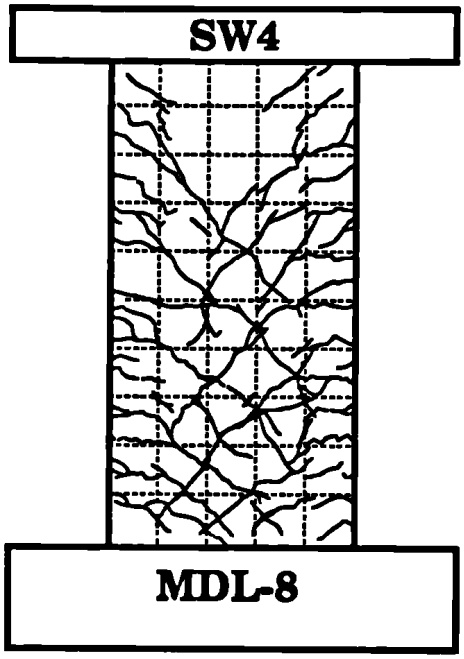

Figure A.6: PilaSW4: DSr1 - cracks at MDL-8 (peak of cycle following yield cycle)

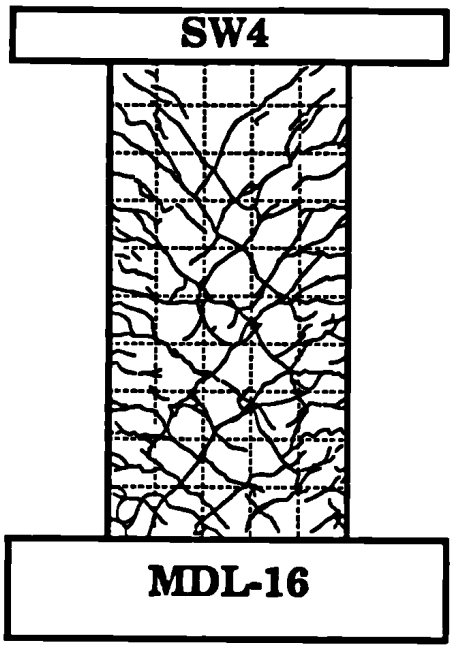

Figure A.7: PilaSW4: DSr4 - cracks at MDL-16 (larger shear crack widths)

A.2 PilaSW5

Table A.5: PilaSW5 damage information

MOR	DS	% Drift	Force, kips (kN)	Description	Figure
1	DS1a	0.08%	4.8 (21.1)	Occurred before 1mm disp, halfway to first maximum; cracks 3/4 of wall at end of cycle; more cracks in B.E. than web; web cracks 30 degrees (p. 105)	Fig. A.9
	DS1d	0.75%	25.5 (113.5)	As determined from moment-curvature analysis	
	DS1f	0.83%	26.0 (115.8)	Shear reinf. yielded (flex. not yielded) (p. 106)	Fig. A.12
4	DS4i	-0.83%	-23.0 (-102.4)	Loss of shear capacity on way to neg. peak; shear cracks significantly open; researcher noted failure due to lower shear crack extending into boundary element in compression (extending from nearly top corner to lower corner) (p. 106)	Fig. A.12
	DSr1	0.69%	24.7 (110.0)	Yield of flexural reinforcement, from force reported in Table 7.2 (p. 193)	
	DSr5	0.67%	24.4 (108.7)	Shear cracks extend most of wall length (p. 107)	Fig. A.12

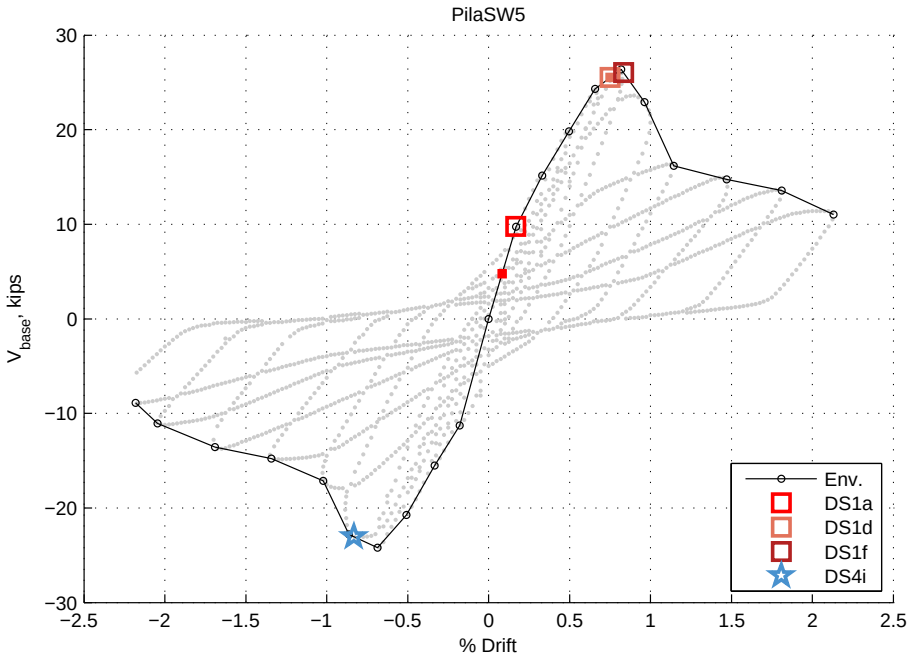

Figure A.8: Envelope for PilaSW5

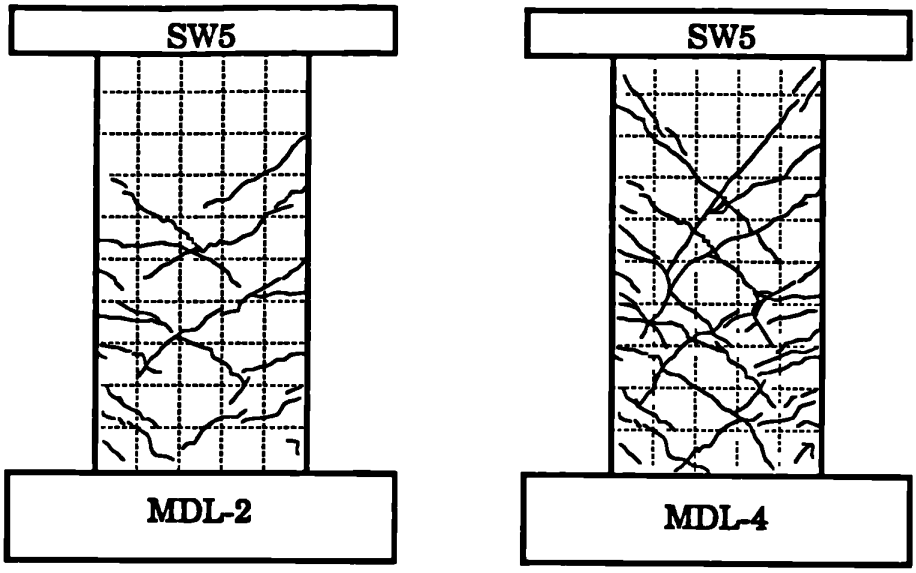

Figure A.9: PilaSW5: DS1a - cracks at MDL-2 (peak after initial cracking) and MDL-4 (wall fully cracked)

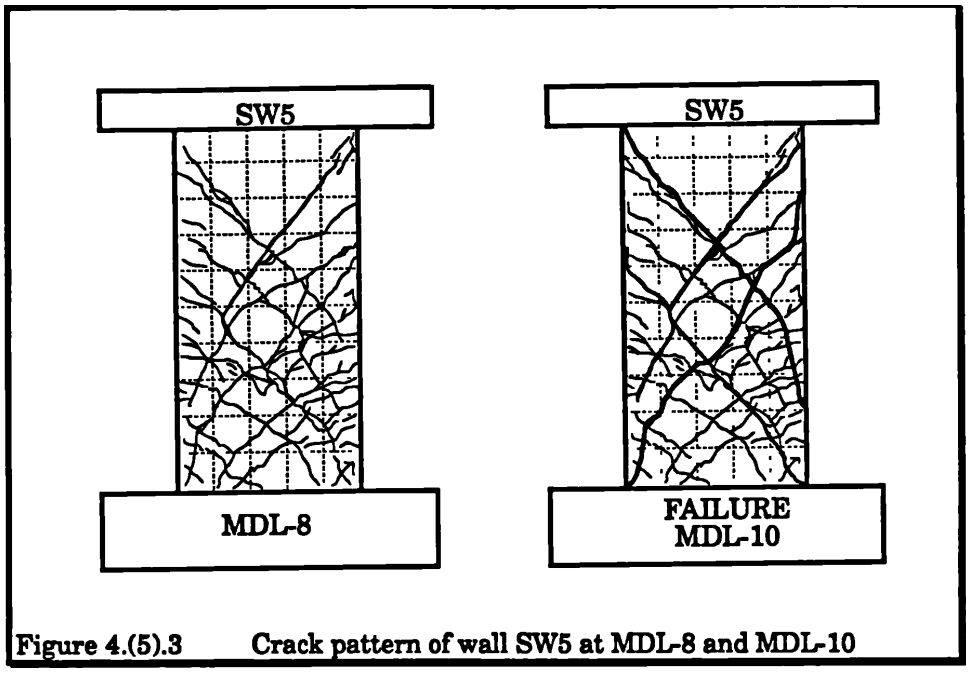

Figure A.10: PilaSW5: DS1f - cracks at MDL-8 (shear cracks extend length of wall) and MDL-10 (shear reinf. yield)

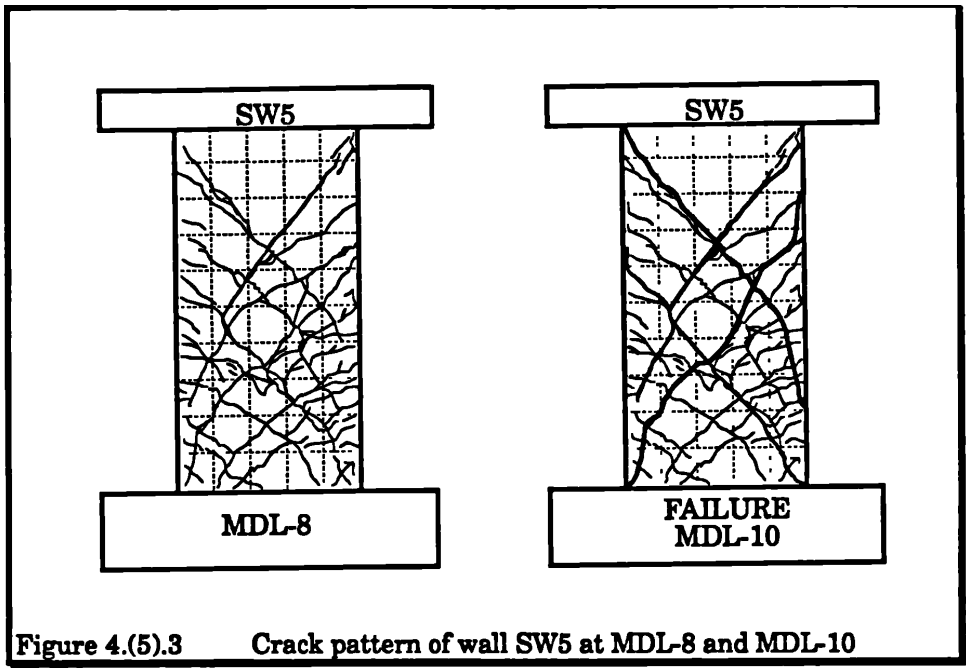

Figure A.11: PilaSW5: DS4i - cracks at MDL-8 (shear cracks extend length of wall) and MDL-10 (shear reinf. yield)

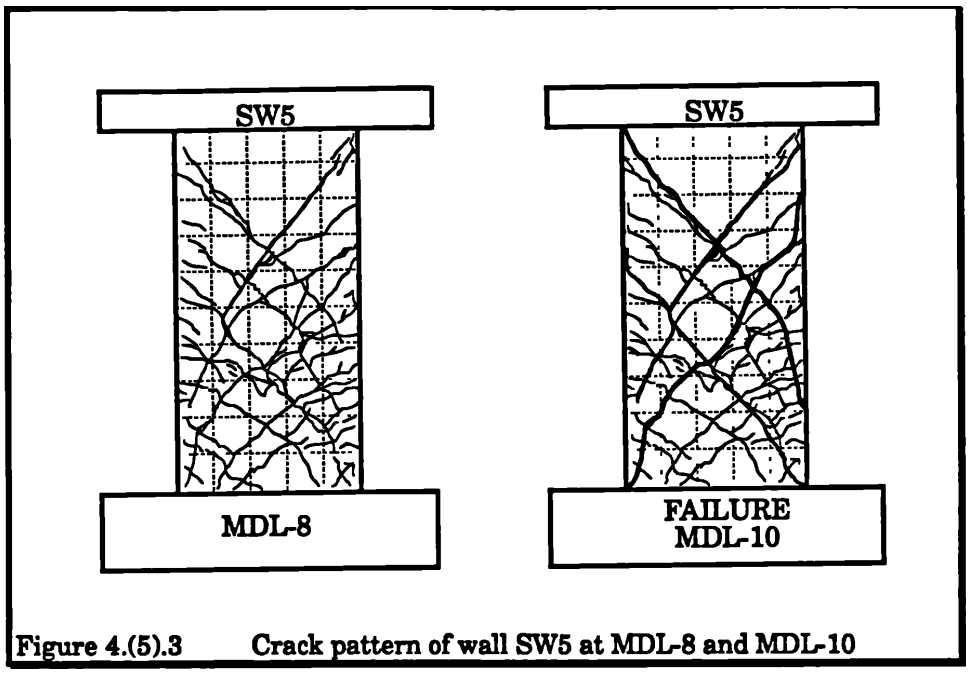

Figure A.12: PilaSW5: DSr5 - cracks at MDL-8 (shear cracks extend length of wall) and MDL-10 (shear reinf. yield)

A.3 PilaSW6

Table A.6: PilaSW6 damage information

MOR	DS	% Drift	Force, kips (kN)	Description	Figure
1	DS1a	0.08%	4.5 (20.0)	Occurred before 1mm disp, halfway to first maximum; flexure and shear (extending into b.e.) (p. 109)	Fig. A.14
	DS1d	0.58%	18.7 (83.2)	As determined from moment-curvature analysis	
2	DS2a	1.33%	23.9 (106.2)	Spalling at base of wall; diagonal cracks extending into boundary element; maximum load occurred (p. 110);	Fig. A.17
4	DS4a	1.83%	20.3 (90.2)	Crushing initiated (p. 111)	
	DS4d	1.83%	20.2 (89.7)	Wide crack in B.E. (not specified as shear and flexure); Cycle wall failed at (p. 111)	
	DS4q	1.50%	24.1 (107.4)	Stirrup opened; cracks extending into compressed region (p. 111)	Fig. A.16
	DSr1	0.47%	16.6 (74.0)	Occurred just before 6mm disp (cycle peak) (p. 109); exact reported in Table 7.2 (p. 193)	Fig. A.17

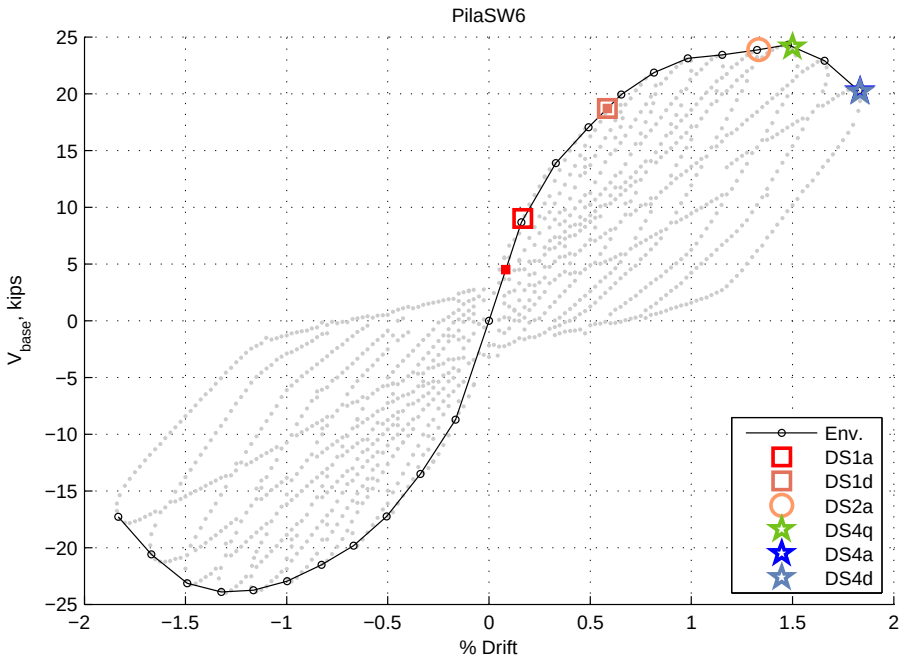

Figure A.13: Envelope for PilaSW6

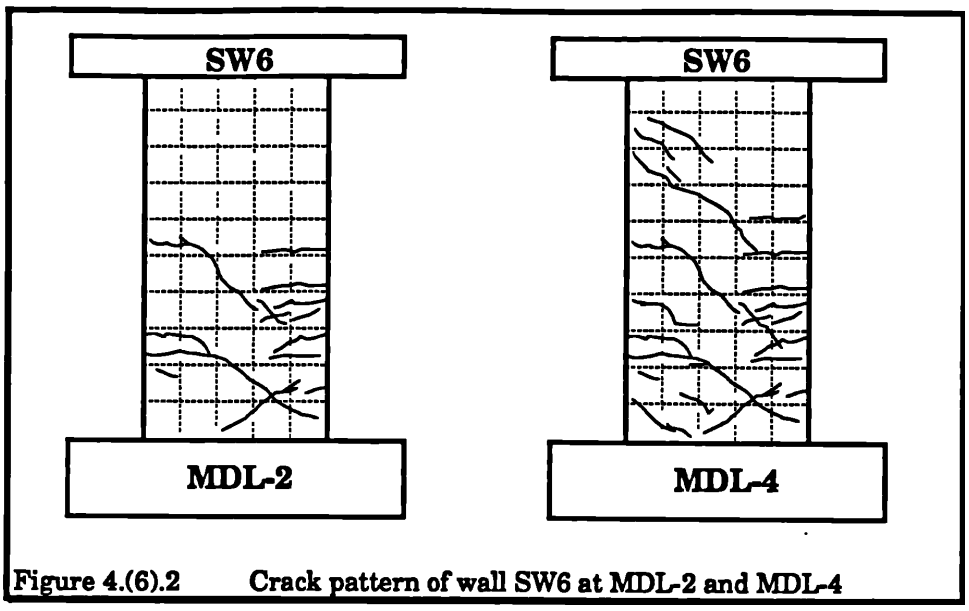

Figure A.14: PilaSW6: DS1a - cracks at MDL-2 (peak after initial cracking) and MDL-4 (fully cracked)

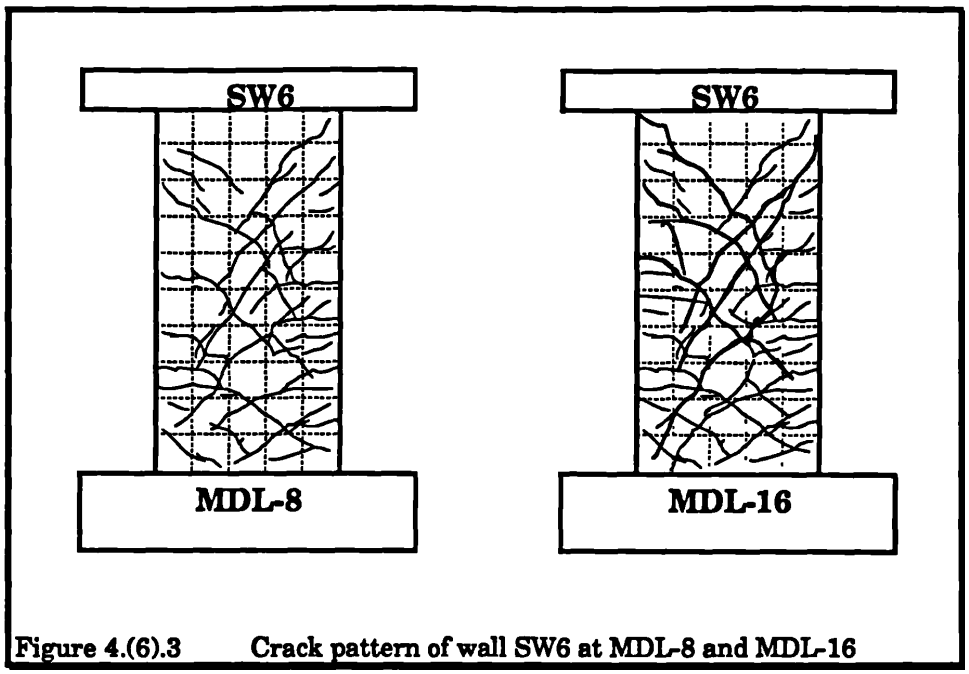

Figure A.15: PilaSW6: DS2a - cracks at MDL-8 (yield) and MDL-16 (spalling/maximum load)

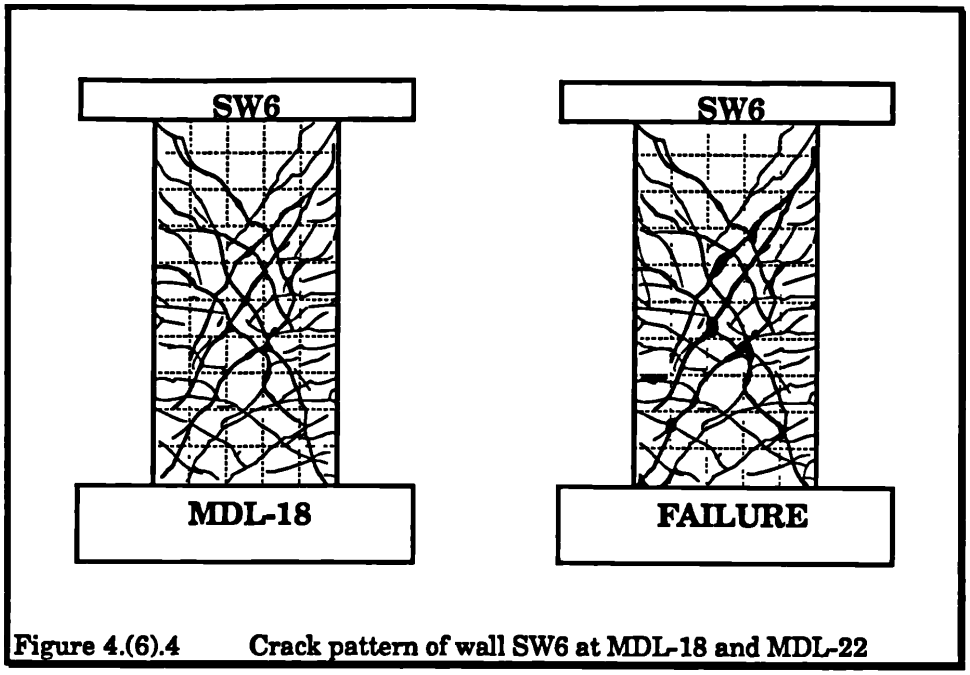

Figure A.16: PilaSW6: DS4q - cracks at MDL-18 (open stirrup) and Failure

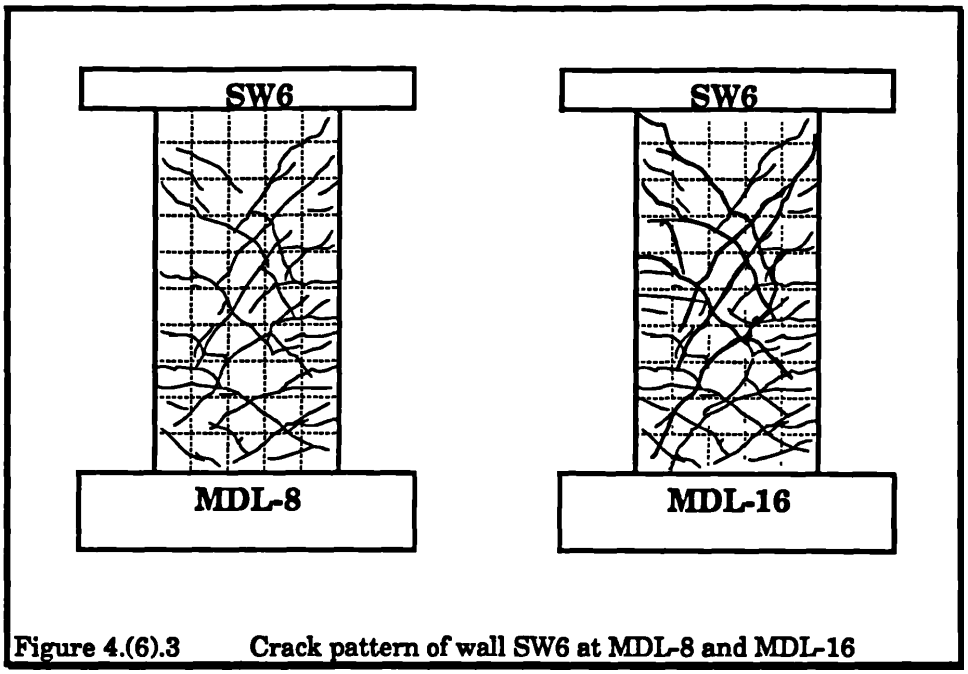

Figure A.17: PilaSW6: DSr1 - cracks at MDL-8 (yield) and MDL-16 (spalling/maximum load)

A.4 PilaSW7

Table A.7: PilaSW7 damage information

MOR	DS	% Drift	Force, kips (kN)	Description	Figure
1	DS1a	0.08%	4.5 (20.1)	Occurred before 1mm disp, halfway to first maximum; flexure and shear cracks 3/4 of wall height (p. 113)	Fig. A.19
	DS1d	-0.62%	-25.5 (-113.5)	As determined from moment-curvature analysis	
4	DS4e	-1.83%	-22.8 (-101.5)	Fracture of 6mm reinf. bar (2 fractured by end of cycle to LHS) (p. 115)	Fig. A.20
	DSr1	0.68%	24.1 (107.0)	Yield of flexural reinforcement, from force reported in Table 7.2 (p. 193)	
	DSr5	1.17%	27.6 (123.0)	Main web cracks extend into compressive area (figure validates classification as extending nearly full length of wall) (p. 115)	Fig. A.21

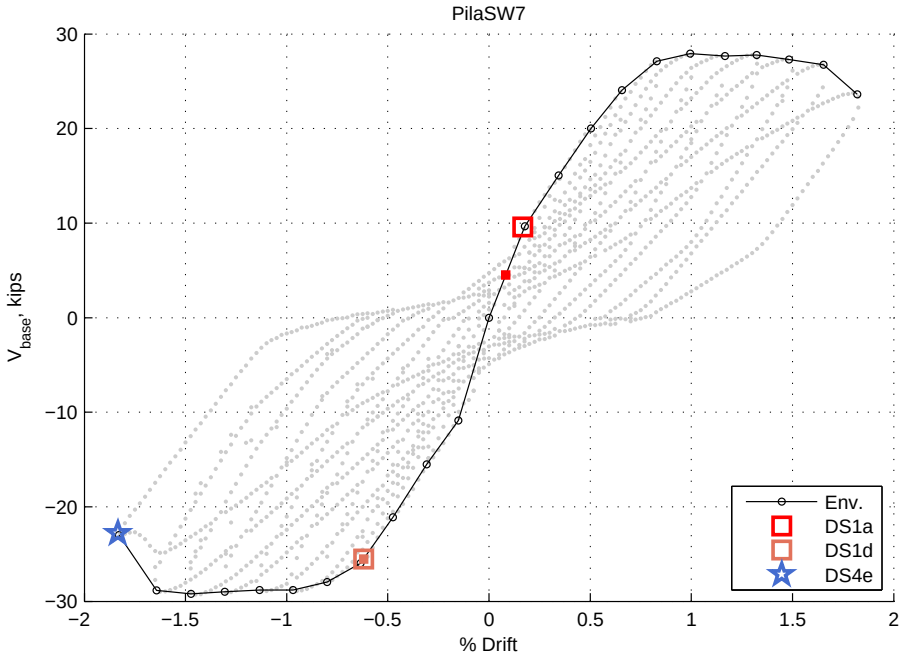

Figure A.18: Envelope for PilaSW7

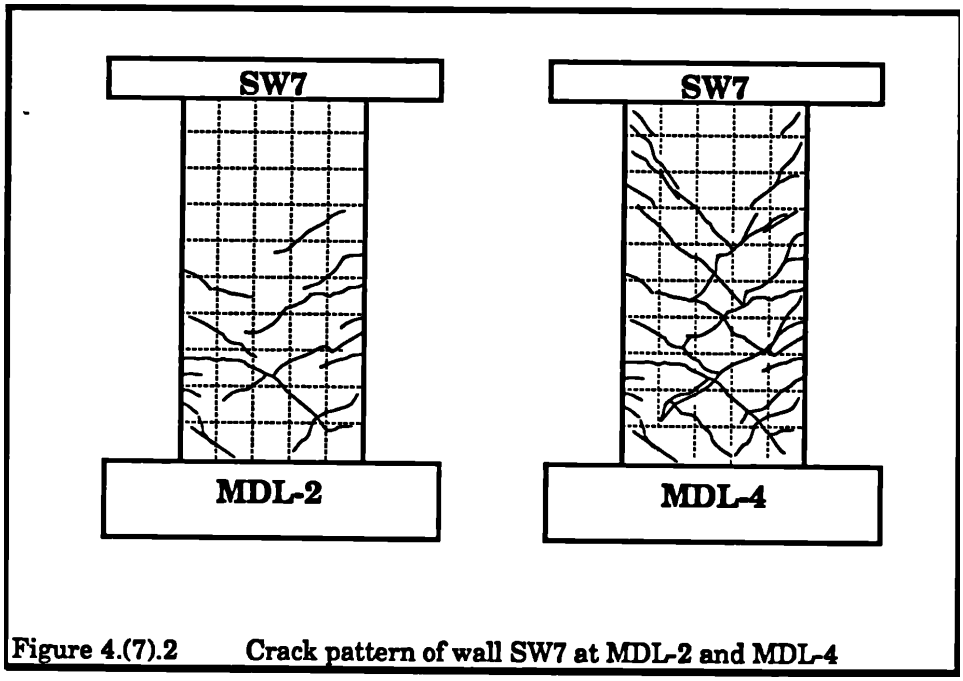

Figure A.19: PilaSW7: DS1a - cracks at MDL-2 (peak after initial cracking) and MDL-4 (fully cracked)

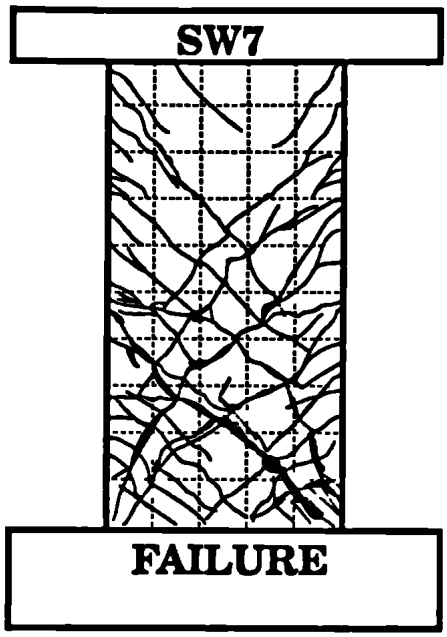

Figure A.20: PilaSW7: DS4e - cracks at MDL-22 (failure due to bar fracture)

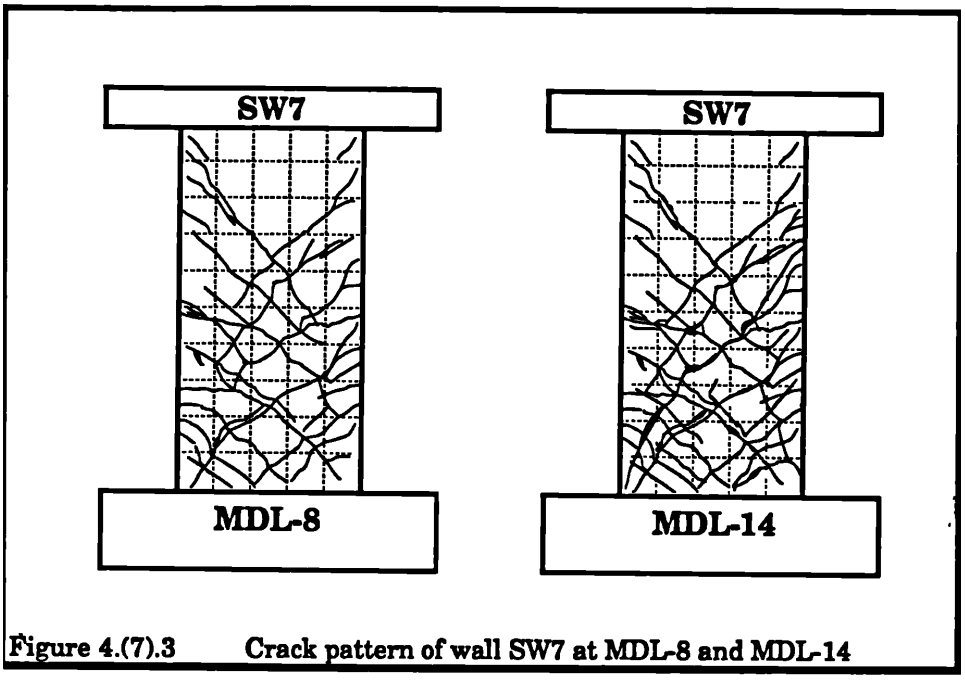

Figure A.21: PilaSW7: DSr5 - cracks at MDL-8 and MDL-4 (shear cracks in b.e.)

A.5 PilaSW8

Table A.8: PilaSW8 damage information

MOR	DS	% Drift	Force, kips (kN)	Description	Figure
1	DS1a	0.08%	4.1 (18.3)	Occurred before 1mm disp, halfway to first maximum; flexure and shear cracks 1/2 of wall height (p. 117)	Fig. A.23
	DS1d	-0.46%	-17.2 (-76.5)	As determined from moment-curvature analysis	
2	DS2a	1.50%	21.3 (94.8)	Spalling at interior of B.E. (p. 119)	Fig. A.24
	DS2d	1.17%	20.8 (92.5)	Vertical cracks at bottom end main reinforcement (p. 119)	
3	DS3a	2.00%	21.2 (94.4)	Flexural reinforcement exposed at extreme bottom parts of wall (p. 119)	
4	DS4c	2.17%	19.8 (87.9)	Assummed failure mode. Loss of lateral load capacity dropped to 75% of max	
	DSr1	0.44%	16.0 (71.0)	Yield of flexural reinforcement, from force reported in Table 7.2 (p. 193)	
	DSr4	1.00%	21.1 (93.8)	Wider web cracks without change in crack pattern (p. 118)	Fig. A.25

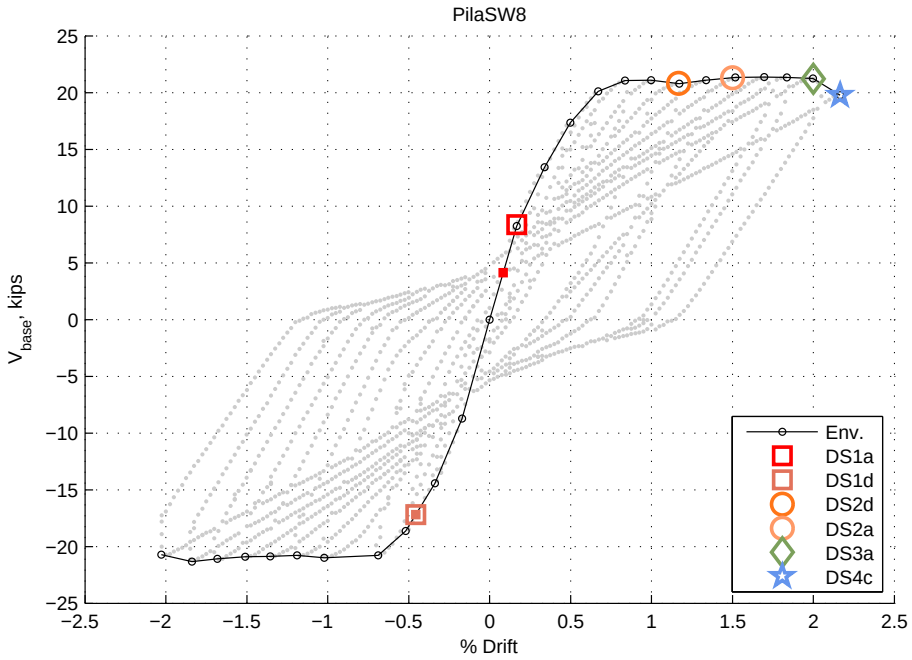

Figure A.22: Envelope for PilaSW8

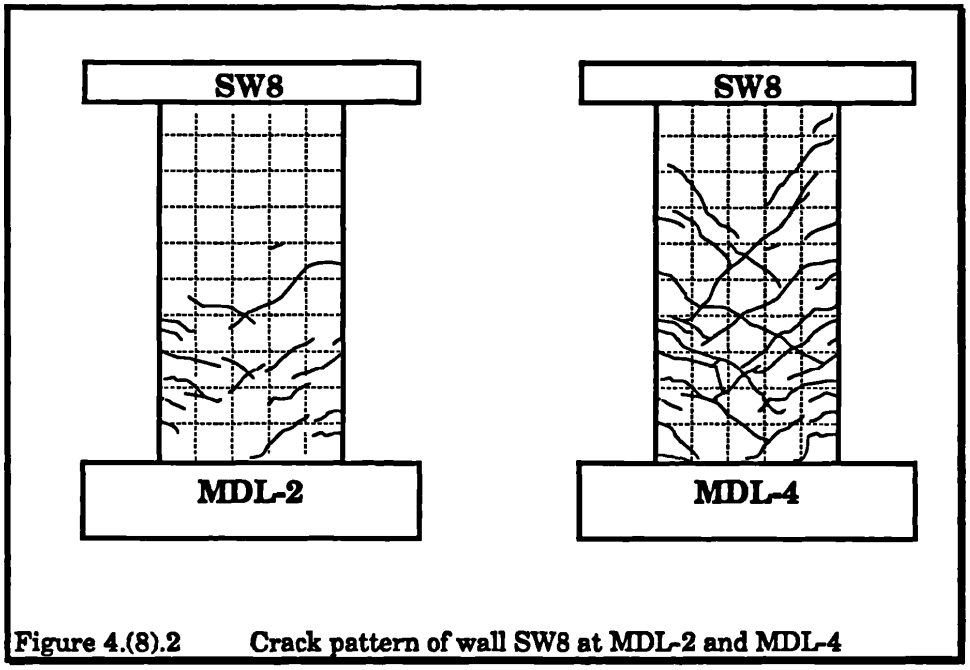

Figure A.23: PilaSW8: DS1a - cracks at MDL-2 (peak after initial cracking) and MDL-4 (fully cracked)

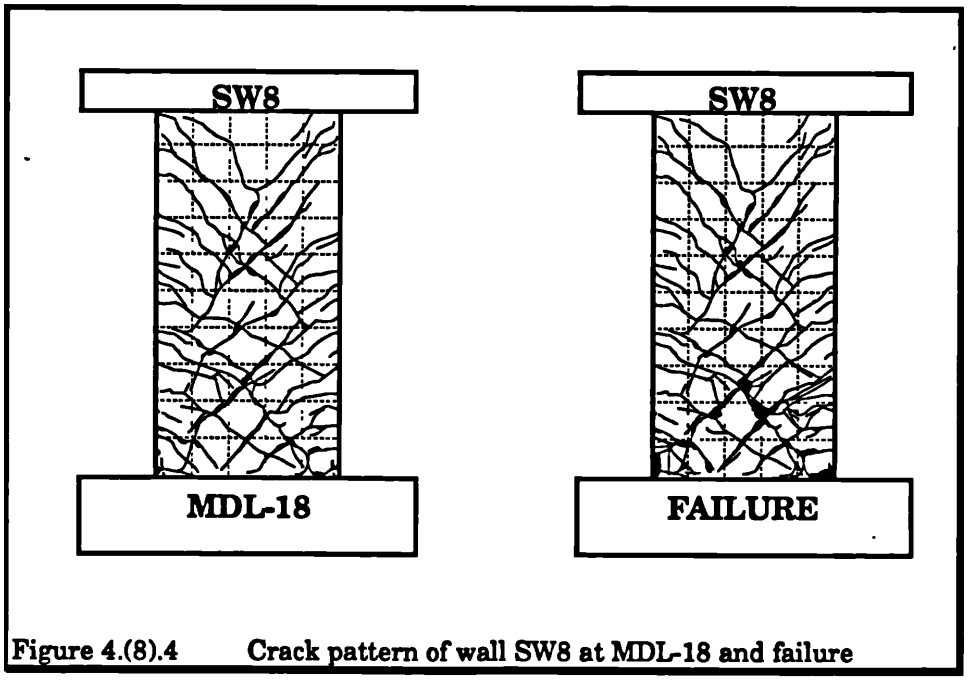

Figure A.24: PilaSW8: DS2a - cracks at MDL-18 (spalling) and Failure

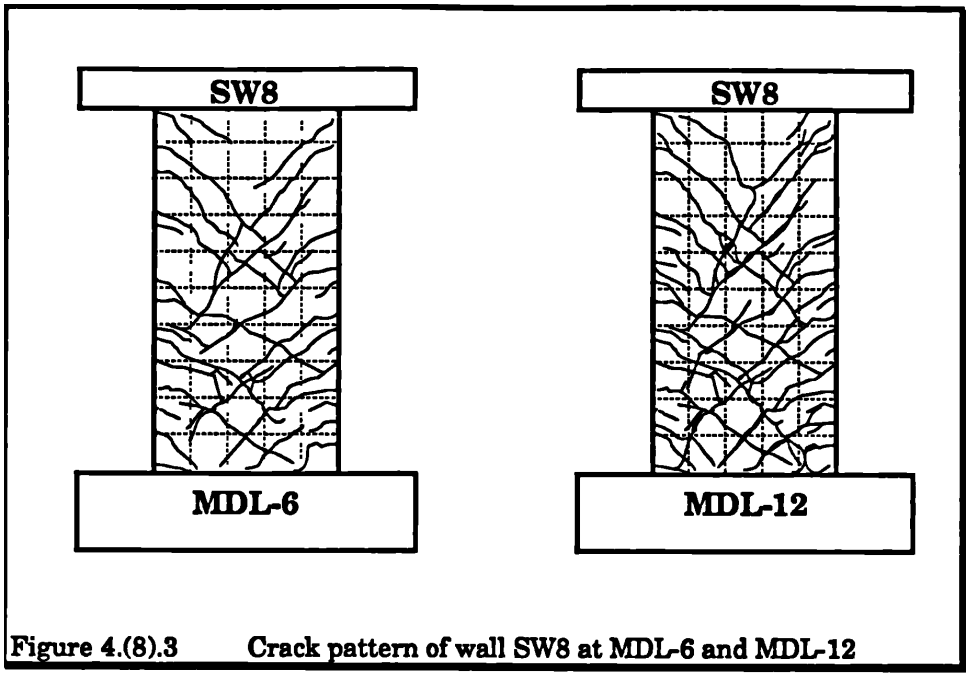

Figure A.25: PilaSW8: DSr4 - cracks at MDL-6 and MDL-12

A.6 PilaSW9

Table A.9: PilaSW9 damage information

MOR	DS	% Drift	Force, kips (kN)	Description	Figure
1	DS1a	0.08%	4.1 (18.1)	Occurred before 1mm disp, halfway to first maximum; flexure and shear cracks 1/2 of wall height (p. 120)	Fig. A.27
	DS1d	-0.42%	-17.0 (-75.7)	As determined from moment-curvature analysis	
2	DS2a	1.50%	20.9 (93.0)	Spalling at intersection of main cracks in web (p. 122)	Fig. A.28
4	DS4c	2.20%	12.2 (54.1)	Assummed failure mode. Loss of lateral load capacity dropped to 75% of max	
	DSr1	0.41%	15.7 (70.0)	Yield of flexural reinforcement, from force reported in Table 7.2 (p. 193)	
	DSr4	1.17%	20.5 (91.0)	Wider web cracks and opening fast (p. 122)	Fig. A.29

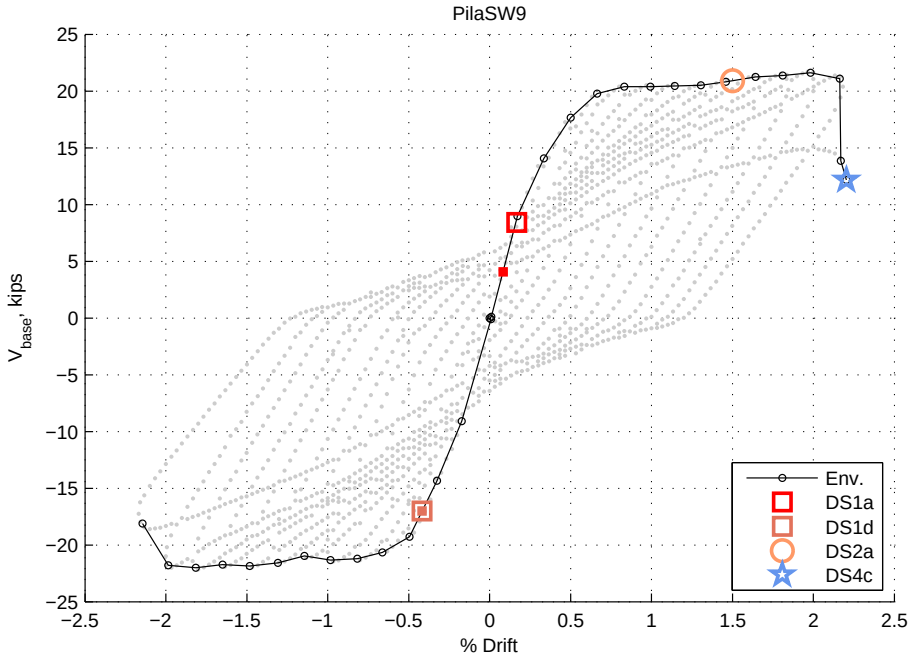

Figure A.26: Envelope for PilaSW9

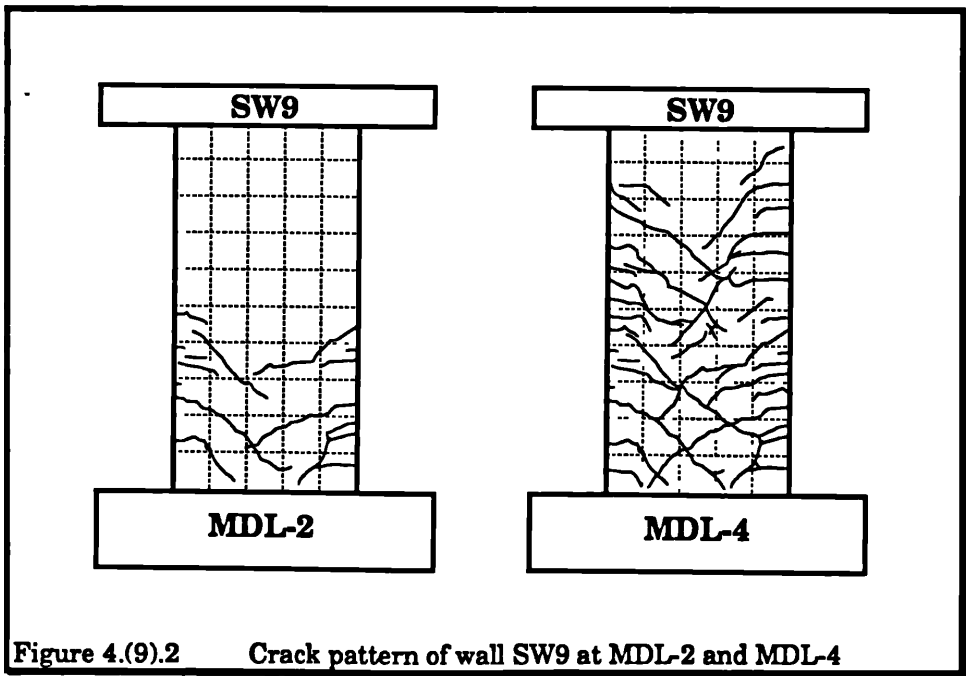

Figure A.27: PilaSW9: DS1a - cracks at MDL-2 (peak after initial cracking) and MDL-4 (fully cracked)

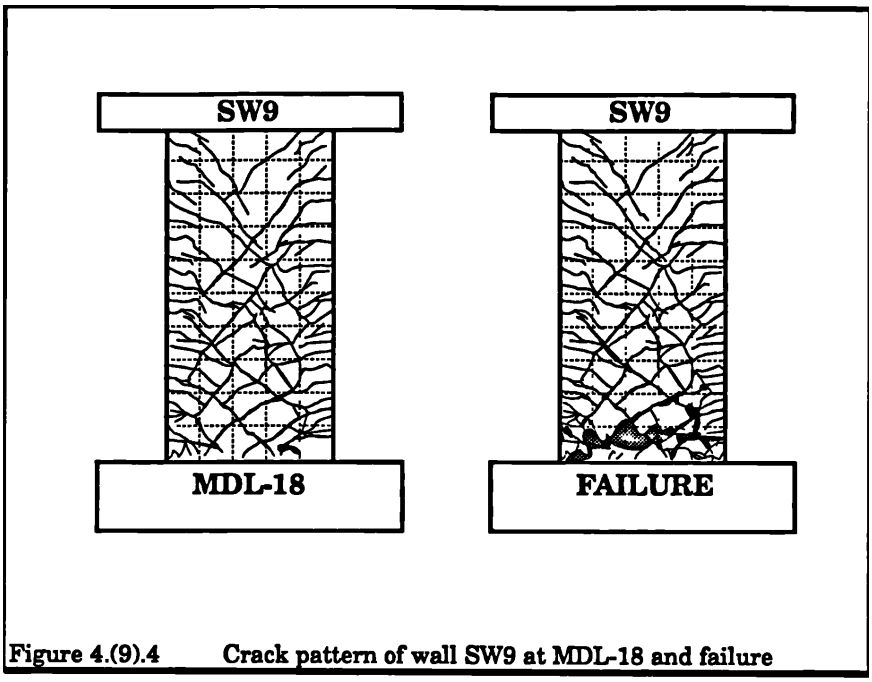

Figure A.28: PilaSW9: DS2a - cracks at MDL-18 (spalling) and Failure

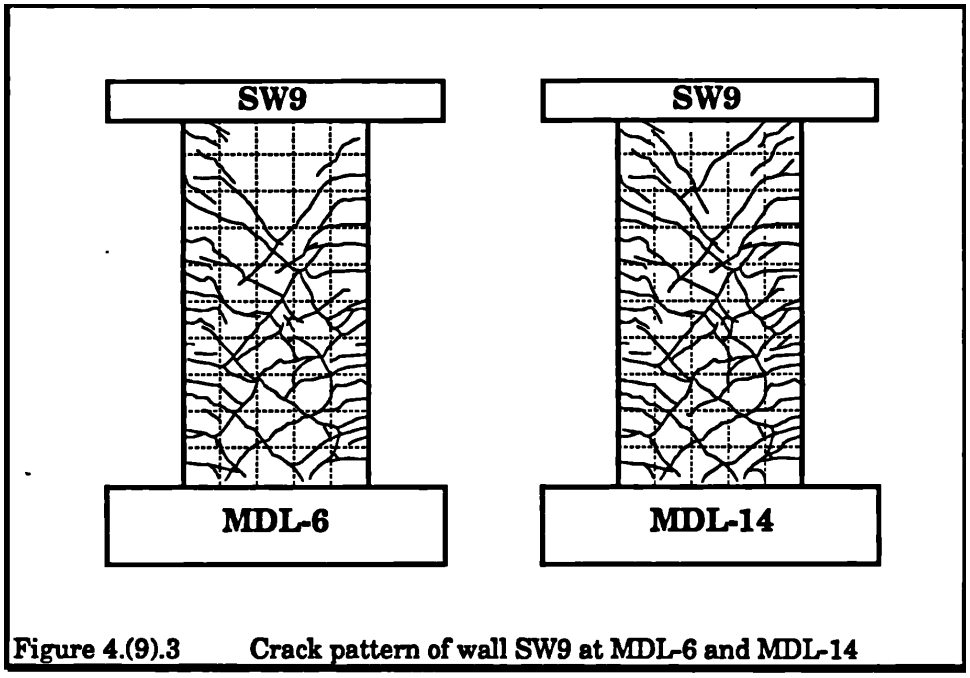

Figure A.29: PilaSW9: DSr4 - cracks at MDL-6 and MDL-14

A.7 TasSHW1

Table A.10: TasSHW1 damage information

MOR	DS	% Drift	Force, kips (kN)	Description	Figure
1	DS1b	0.04%	0.3 (1.5)	flexural cracks initiate at 10% of wall capacity	
	DS1c	0.38%	2.0 (9.1)	significant inclined cracking initiated at 62% of maximum load	
	DS1d	-0.52%	-2.6 (-11.4)	As determined from moment-curvature analysis	
2	DS2a	1.56%	3.3 (14.5)	A few semi-vertical cracks and spalling in compressive zone just prior to failure	
	DS2d	1.56%	3.3 (14.5)	A few semi-vertical cracks and spalling in compressive zone just prior to failure	
	DSr1	-0.41%	-2.3 (-10.3)	Yield displacement reported in Table 8 of paper	

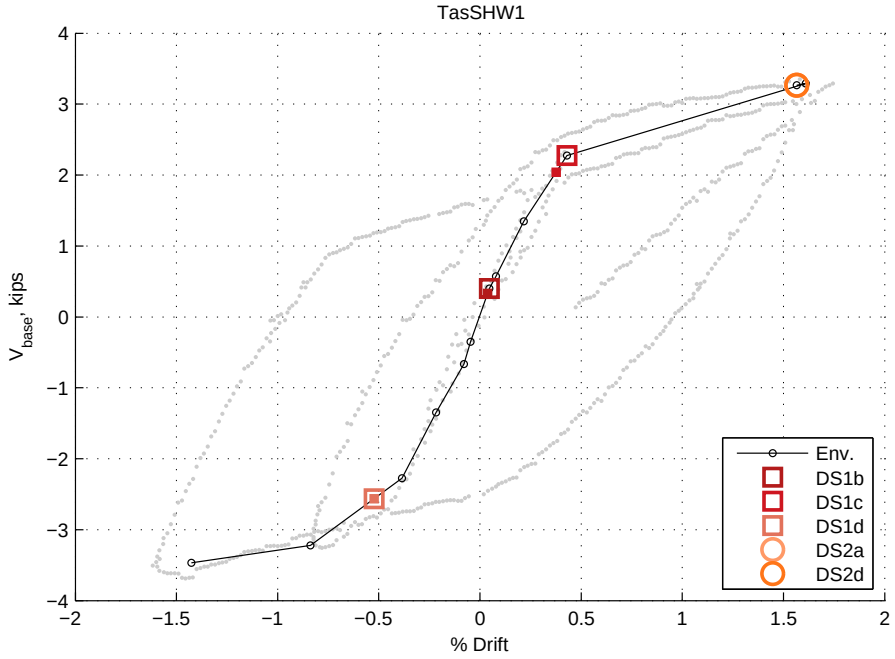

Figure A.30: Envelope for TasSHW1

A.8 TasSHW2

Table A.11: TasSHW2 damage information

MOR	DS	% Drift	Force, kips (kN)	Description	Figure
1	DS1b	0.04%	0.4 (1.8)	flexural cracks initiate at 10% of wall capacity	
	DS1c	0.34%	2.5 (11.3)	significant inclined cracking initiated at 62% of maximum load	
	DS1d	0.35%	2.6 (11.4)	As determined from moment-curvature analysis	
2	DS2a	0.86%	3.9 (17.3)	A few semi-vertical cracks and spalling in compressive zone just prior to failure	
	DS2d	0.86%	3.9 (17.3)	A few semi-vertical cracks and spalling in compressive zone just prior to failure	
	DSr1	0.31%	2.4 (10.6)	Yield displacement reported in Table 8 of paper	

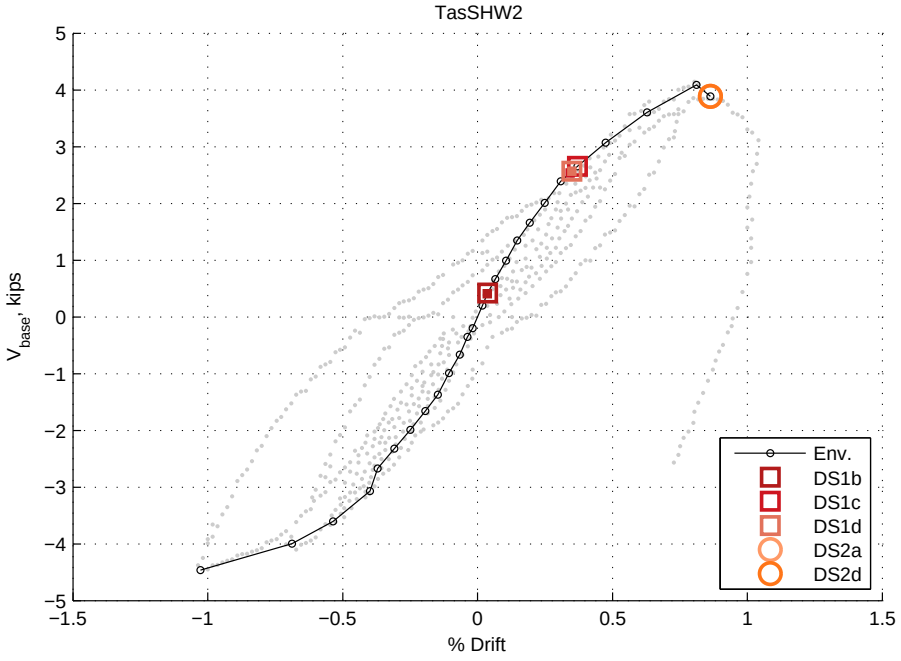

Figure A.31: Envelope for TasSHW2

A.9 TasSHW3

Table A.12: TasSHW3 damage information

MOR	DS	% Drift	Force, kips (kN)	Description	Figure
1	DS1b	0.03%	0.3 (1.5)	flexural cracks initiate at 10% of wall capacity	
	DS1c	0.39%	2.1 (9.4)	significant inclined cracking initiated at 62% of maximum load	
	DS1d	-0.42%	-2.6 (-11.5)	As determined from moment-curvature analysis	
2	DS2a	-1.03%	-3.7 (-16.4)	A few semi-vertical cracks and spalling in compressive zone just prior to failure	
	DS2d	-1.03%	-3.7 (-16.4)	A few semi-vertical cracks and spalling in compressive zone just prior to failure	
	DSr1	-0.46%	-2.7 (-12.1)	Yield displacement reported in Table 8 of paper	

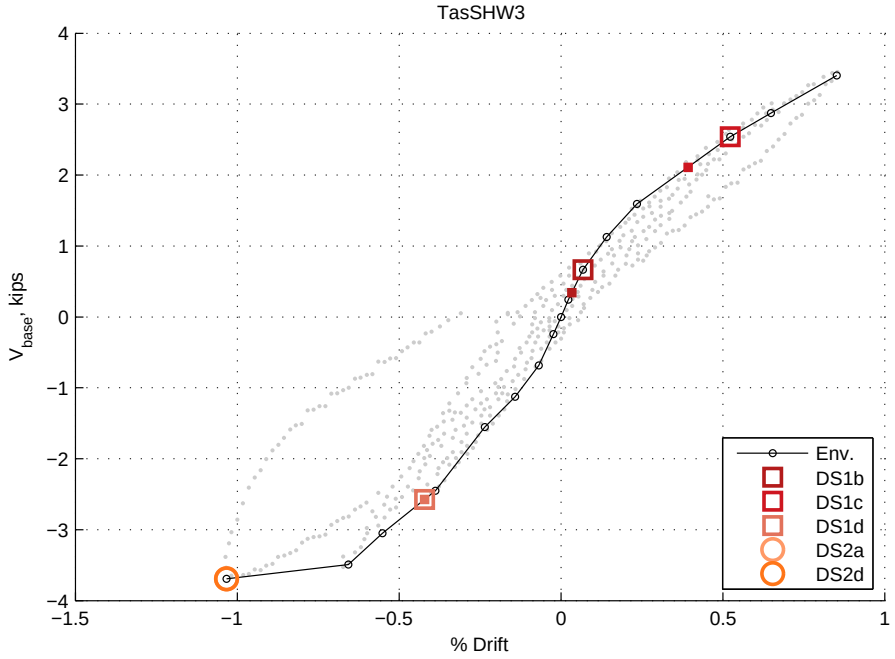

Figure A.32: Envelope for TasSHW3

A.10 TasSHW4

Table A.13: TasSHW4 damage information

MOR	DS	% Drift	Force, kips (kN)	Description	Figure
1	DS1b	0.05%	0.4 (2.0)	flexural cracks initiate at 10% of wall capacity	
	DS1c	0.56%	2.8 (12.3)	significant inclined cracking initiated at 62% of maximum load	
	DS1d	0.50%	2.6 (11.5)	As determined from moment-curvature analysis	
2	DS2a	-1.70%	-5.3 (-23.5)	A few semi-vertical cracks and spalling in compressive zone just prior to failure	
	DS2d	-1.70%	-5.3 (-23.5)	A few semi-vertical cracks and spalling in compressive zone just prior to failure	
	DSr1	0.43%	2.4 (10.7)	Yield displacement reported in Table 8 of paper	

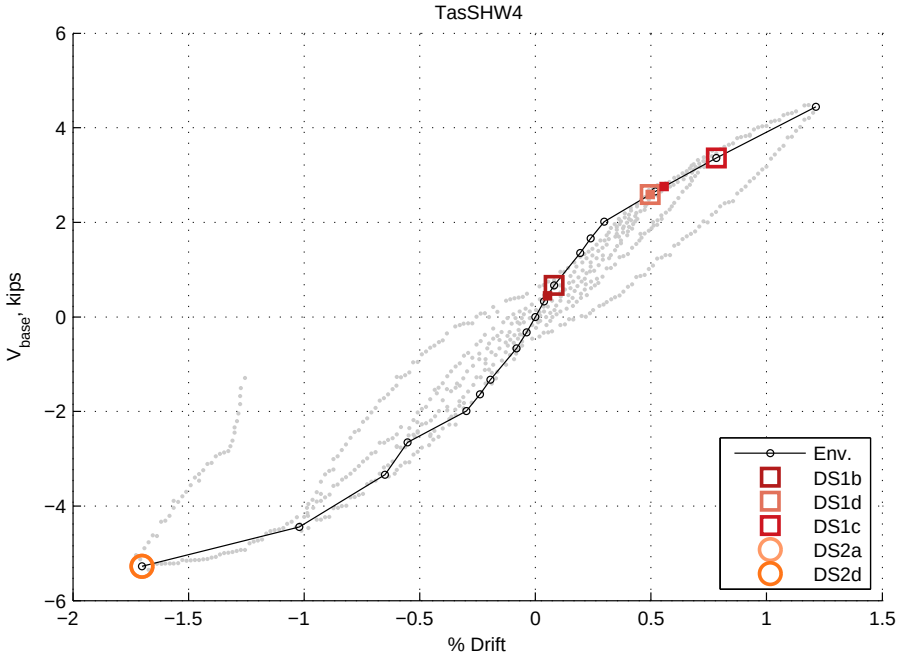

Figure A.33: Envelope for TasSHW4

A.11 ThomRW1

Table A.14: ThomRW1 damage information

MOR	DS	% Drift	Force, kips (kN)	Description	Figure
1	DS1b	-0.25%	-14.7 (-65.3)	Flexural cracking over first floor at approximately 0.25% drift; also horizontal cracks at construction joints	
	DS1c	-0.50%	-26.8 (-119.4)	Flexural cracks extend to become shear-flexure cracks	
	DS1d	-0.74%	-30.2 (-134.2)	As determined from moment-curvature analysis	
2	DS2a	-1.00%	-31.7 (-140.9)	Vertical splitting and minor crushing at wall edge at approximately 1.0% drift (first cycle)	
	DS2d	-1.00%	-31.7 (-140.9)	Vertical splitting and minor crushing at wall edge at approximately 1.0% drift (first cycle)	
4	DS4b	-2.00%	-33.4 (-148.3)	Slight buckling of edge boundary bars observed in first cycle at 2.0% drift; extensive spalling & crushing in B.E.	Fig. A.35
	DS4f	2.22%	30.6 (135.9)	Loss of lateral load carrying capacity due to buckling at 2.5% drift (first excursion)	
	DSr1	-0.75%	-30.3 (-135.0)	Yielding of reinforcement at approximately 0.75% drift	
	DSr10	-1.50%	-32.8 (-145.7)	Crack widths measured at 3/32”	

Table A.15: ThomRW1 crack width information

					Crack Width, in (mm)	
DS	% Drift	Force, kips (kN)	Exact/Max	Crack Type	Max.	Resid.
DSr10	-1.50%	-32.8 (-145.7)	Max	Any	0.094 (2.4)	
DS4b	-2.00%	-33.4 (-148.3)	Max	Any	0.094 (2.4)	

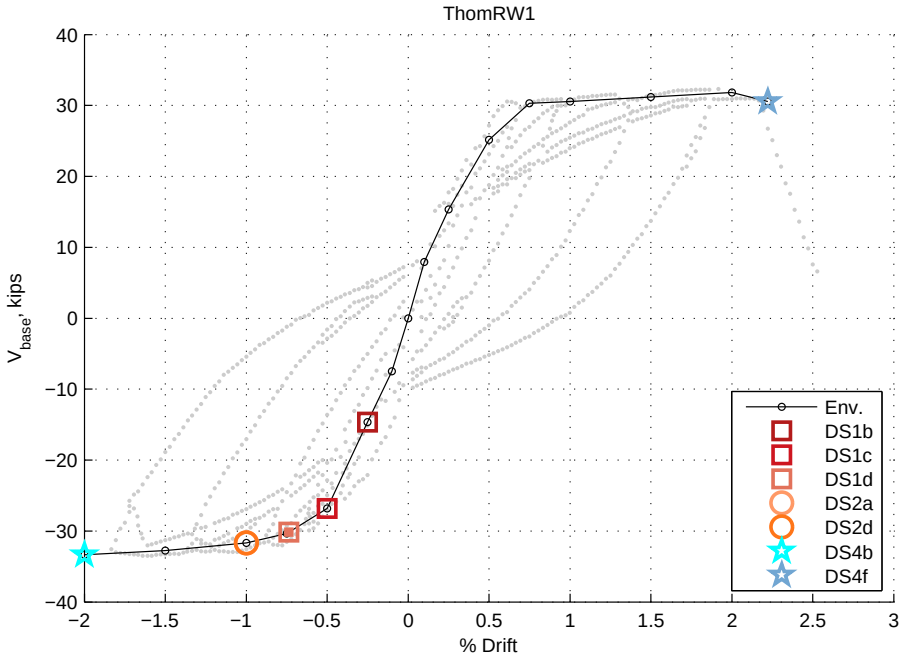

Figure A.34: Envelope for ThomRW1

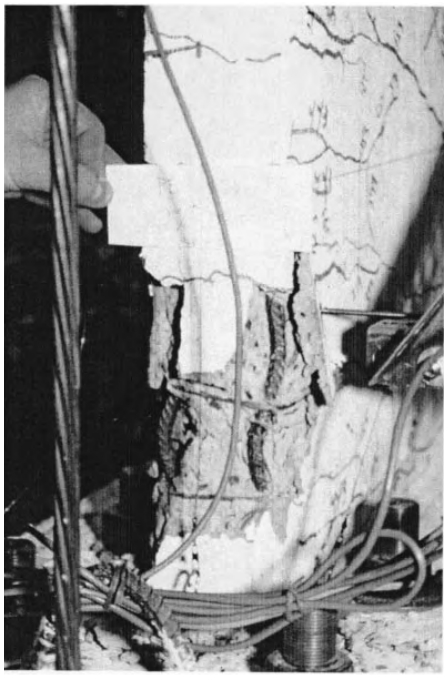

Figure A.35: ThomRW1: DS4b - Slight buckling of RW1 bars at 2% drift

A.12 ThomRW2

Table A.16: ThomRW2 damage information

MOR	DS	% Drift	Force, kips (kN)	Description	Figure
1	DS1b	-0.25%	-17.5 (-77.8)	Flexural cracking over first floor at approximately 0.25% drift	
	DS1c	-0.50%	-25.3 (-112.5)	Flexural cracks extend to become shear-flexure cracks	
	DS1d	-0.63%	-27.7 (-123.1)	As determined from moment-curvature analysis	
	DS1e	-0.75%	-29.9 (-132.8)	Compression yielding of reinforcement at approximately 0.75% drift (tension yielding occurs in same cycle)	
2	DS2a	-1.50%	-32.2 (-143.4)	Minor crushing and spalling of cover concrete during first cycle to 1.5% drift (vertical cracking was extensive in boundary regions)	
	DS2d	-1.00%	-31.0 (-137.9)	Vertical splitting during first cycle to 1.0% drift	
4	DS4f	-2.50%	-35.2 (-156.4)	Loss of lateral load carrying capacity due to buckling at 2.5% drift (second excursion); multiple bars (8) buckled simultaneously; core crushing was also occuring	Fig. A.37
	DSr1	-0.75%	-29.9 (-132.8)	Tensile yielding of reinforcement at approximately 0.75% drift (compression yielding occurs in same cycle)	
	DSr10	-2.00%	-34.0 (-151.1)	Crack widths measured at 3/32" (2.0% drift)	

Table A.17: ThomRW2 crack width information

					Crack Width, in (mm)	
DS	% Drift	Force, kips (kN)	Exact/Max	Crack Type	Max.	Resid.
DSr10	-2.00%	-34.0 (-151.1)	Max	Any	0.094 (2.4)	

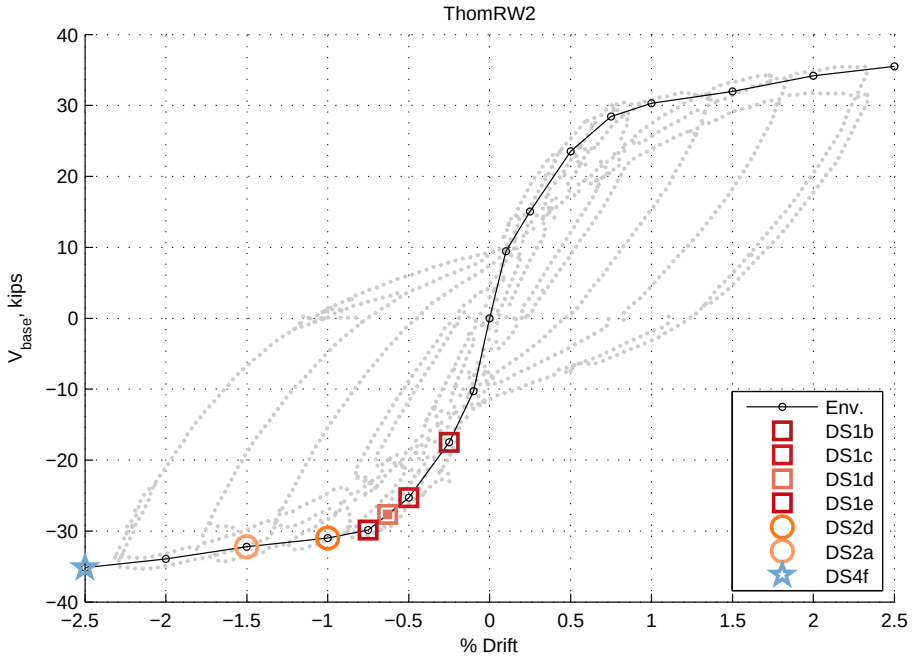

Figure A.36: Envelope for ThomRW2

Figure A.37: ThomRW2: DS4f - RW2 damage at 2.5% drift

A.13 ThomTW1

Table A.18: ThomTW1 damage information

MOR	DS	% Drift	Force, kips (kN)	Description	Figure
1	DS1b	0.25%	19.8 (88.2)	Initial flexural cracking during second drift level	
	DS1c	0.50%	30.0 (133.6)	Initial shear cracking seen in south web boundary element during cycle to 0.5% drift	
	DS1d	-0.39%	-33.5 (-148.9)	As determined from moment-curvature analysis	
2	DS2d	-0.75%	-48.9 (-217.6)	Onset of vertical splitting of web boundary element	
4	DS4f	-1.25%	-65.4 (-290.8)	Loss of lateral load carrying capacity due to buckling of web and B.E. reinforcement on way to 1.25% drift	Fig. A.39
	DSr1	0.75%	38.0 (169.1)	Longitudinal steel in web b.e. yielding in tension	

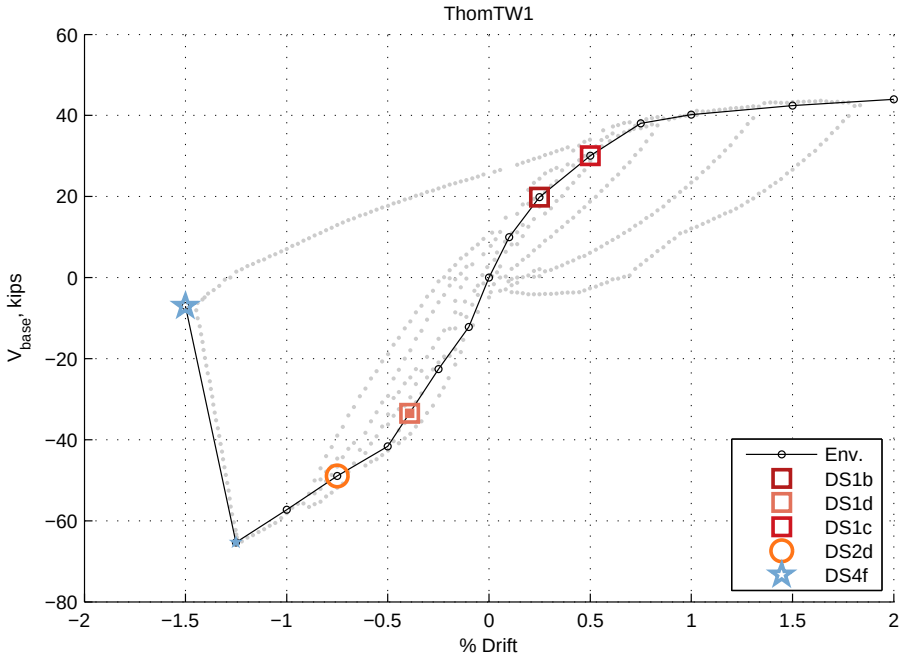

Figure A.38: Envelope for ThomTW1

Figure A.39: ThomTW1: DS4f - TW1 damage at 1.25% drift

A.14 ThomTW2

Table A.19: ThomTW2 damage information

MOR	DS	% Drift	Force, kips (kN)	Description	Figure
1	DS1d	-0.24%	-33.2 (-147.5)	As determined from moment-curvature analysis	
4	DS4f	-2.00%	-81.3 (-361.5)	Loss of lateral load carrying capacity due to buckling over several hoop spacing in web boundary compression zone	Fig. A.41

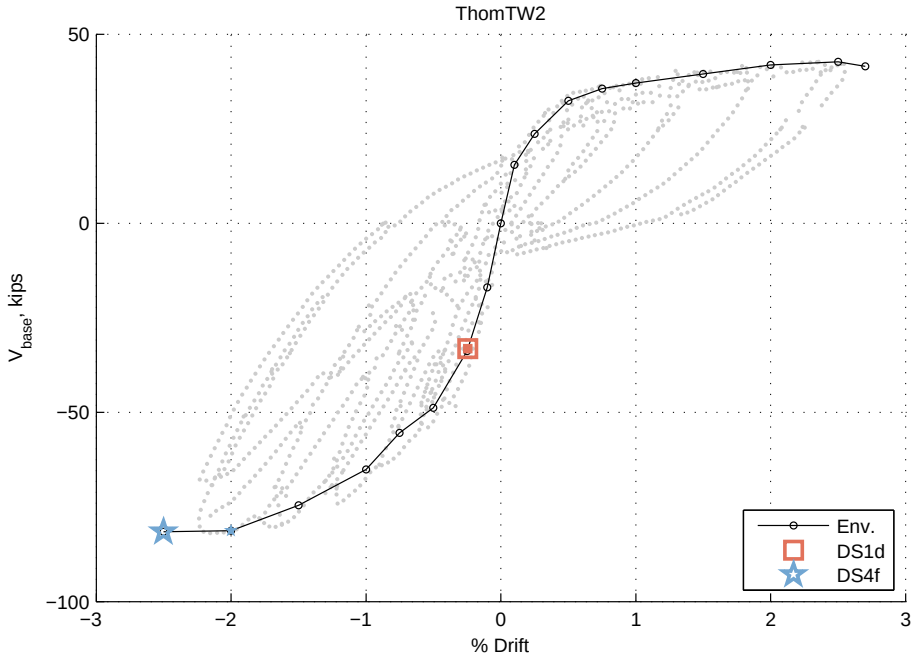

Figure A.40: Envelope for ThomTW2

Figure A.41: ThomTW2: DS4f - TW2 damage at 2.5% drift

A.15 DazioWSH1

Table A.20: DazioWSH1 damage information

MOR	DS	% Drift	Force, kips (kN)	Description	Figure
1	DS1a	0.17%	52.4 (233.1)	First cracking (from data downloaded for project)	
	DS1d	-0.21%	-58.4 (-259.7)	As determined from moment-curvature analysis	
2	DS2d	0.69%	74.7 (332.4)	Vertical cracks in cover at base of wall (same time as web reinf. rupture)	
4	DS4e	0.69%	74.7 (332.4)	Bar rupture in web reinforcement (vertical cracking beginning to appear)	
	DSr1	0.18%	53.6 (238.3)	First yield as reported in paper Table 4 (Δ_y^b)	
	DSr10	0.69%	74.7 (332.4)	Cracks exceeding or equal to 1/8" (determined from download crack data)	
	DSr9	0.69%	74.7 (332.4)	Cracks exceeding or equal to 1/16" (determined from download crack data)	

Table A.21: DazioWSH1 crack width information

					Crack Width, in (mm)	
DS	% Drift	Force, kips (kN)	Exact/Max	Crack Type	Max.	Resid.
DS1a	0.17%	52.4 (233.1)	Max	Shear	0.0039 (0.1)	
				Flexure	0.0039 (0.1)	
				Any	0.0039 (0.1)	
DSr1	0.47%	74.7 (332.4)	Max	Shear	0.016 (0.4)	
				Flexure	0.024 (0.6)	
				Any	0.024 (0.6)	
DSr9	0.69%	74.7 (332.4)	Max	Shear	0.071 (1.8)	
				Flexure	0.14 (3.5)	
				Any	0.14 (3.5)	
DSr10	0.69%	74.7 (332.4)	Max	Shear	0.071 (1.8)	
				Flexure	0.14 (3.5)	
				Any	0.14 (3.5)	
DS4e	0.69%	74.7 (332.4)	Max	Shear	0.071 (1.8)	
				Flexure	0.14 (3.5)	
				Any	0.14 (3.5)	
DS2d	0.69%	74.7 (332.4)	Max	Shear	0.071 (1.8)	
				Flexure	0.14 (3.5)	
				Any	0.14 (3.5)	

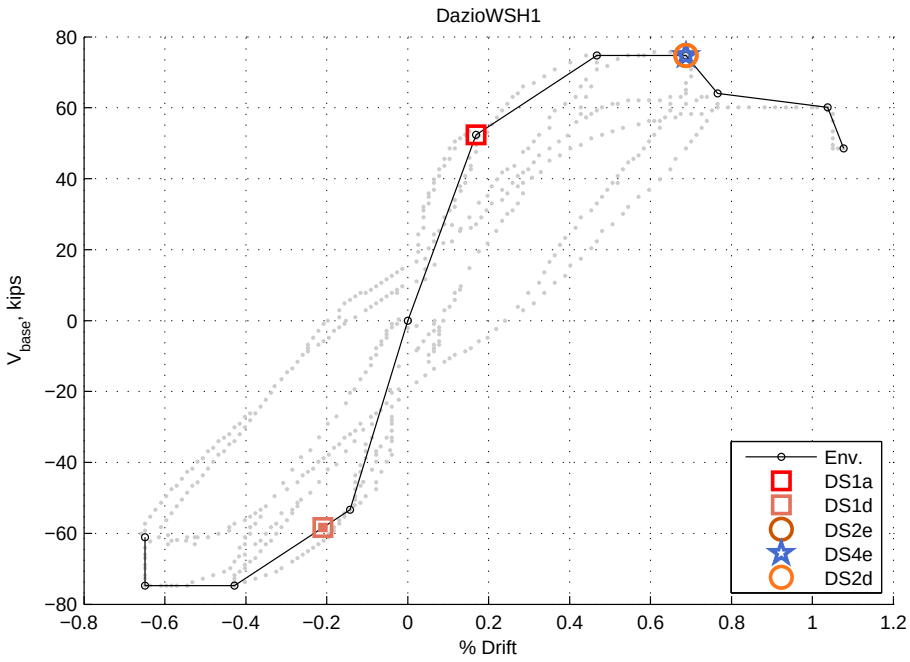

Figure A.42: Envelope for DazioWSH1

A.16 DazioWSH2

Table A.22: DazioWSH2 damage information

MOR	DS	% Drift	Force, kips (kN)	Description	Figure
1	DS1a	0.16%	54.3 (241.7)	First cracking (from data downloaded for project)	
	DS1d	0.23%	59.5 (264.5)	As determined from moment-curvature analysis	
2	DS2d	1.15%	77.6 (345.3)	Vertical cracking beginning to appear (web bar fracture also occurs)	
3	DS3a	-1.15%	-72.8 (-323.7)	Cover spalled fell off, revealing buckled bars (buckling recorded as independent damage state)	
4	DS4b	-1.15%	-72.8 (-323.7)	Initial buckling seen; revealed by cover spalling (independent damage states)	
	DS4e	1.15%	77.6 (345.3)	Bar rupture in web reinforcement (vertical cracking beginning to appear)	
	DS4g	1.40%	66.0 (293.5)	Previously buckled bars ruptured causing loss of load carrying capacity	
	DSr1	0.17%	55.4 (246.3)	First yield as reported in paper Table 4 (Δ_y^b)	

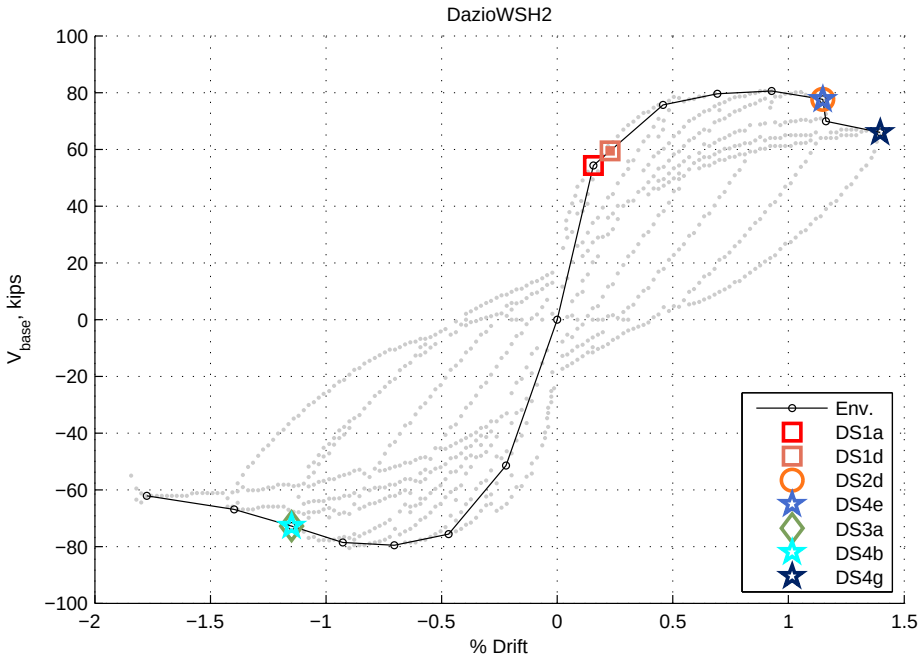

Figure A.43: Envelope for DazioWSH2

Table A.23: DazioWSH2 crack width information

					Crack Width, in (mm)	
DS	% Drift	Force, kips (kN)	Exact/Max	Crack Type	Max.	Resid.
DS1a	0.16%	54.3 (241.7)	Max	Shear	0.0039 (0.1)	
				Flexure	0.0059 (0.15)	
				Any	0.0059 (0.15)	
DSr1	0.46%	75.7 (336.7)	Max	Shear	0.018 (0.45)	
				Flexure	0.024 (0.6)	
				Any	0.024 (0.6)	
DS2d	1.15%	77.6 (345.3)	Max	Shear	0.043 (1.1)	
				Flexure	0.24 (6)	
				Any	0.24 (6)	
DS4e	1.15%	77.6 (345.3)	Max	Shear	0.043 (1.1)	
				Flexure	0.24 (6)	
				Any	0.24 (6)	
DS3a	-1.15%	-72.8 (-323.7)	Max	Shear	0.35 (9)	
				Flexure	0.098 (2.5)	
				Any	0.35 (9)	
DS4b	-1.15%	-72.8 (-323.7)	Max	Shear	0.35 (9)	
				Flexure	0.098 (2.5)	
				Any	0.35 (9)	

A.17 DazioWSH3

Table A.24: DazioWSH3 damage information

MOR	DS	% Drift	Force, kips (kN)	Description	Figure
1	DS1a	0.26%	67.9 (302.2)	First cracking (from data downloaded for project)	
	DS1d	-0.37%	-75.1 (-334.1)	As determined from moment-curvature analysis	
2	DS2a	1.02%	100.9 (448.9)	Initial spalling, but long. reinf. NOT seen	
3	DS3a	1.70%	101.9 (453.2)	Cover continued to spall, revealing long. reinf. for first time (initial buckling also seen)	
4	DS4b	1.70%	101.9 (453.2)	Initial buckling seen when spalling first revealed long. reinf. (indep. damage state)	
	DS4g	2.04%	101.9 (453.2)	Bar rupture in corner bar (previously buckled) shortly before cycle peak	
	DSr1	0.25%	64.5 (286.8)	First yield as reported in paper Table 4 (Δ_y^b)	
	DSr9	1.36%	101.9 (453.2)	Cracks exceeding or equal to 1/16" (determined from download crack data)	

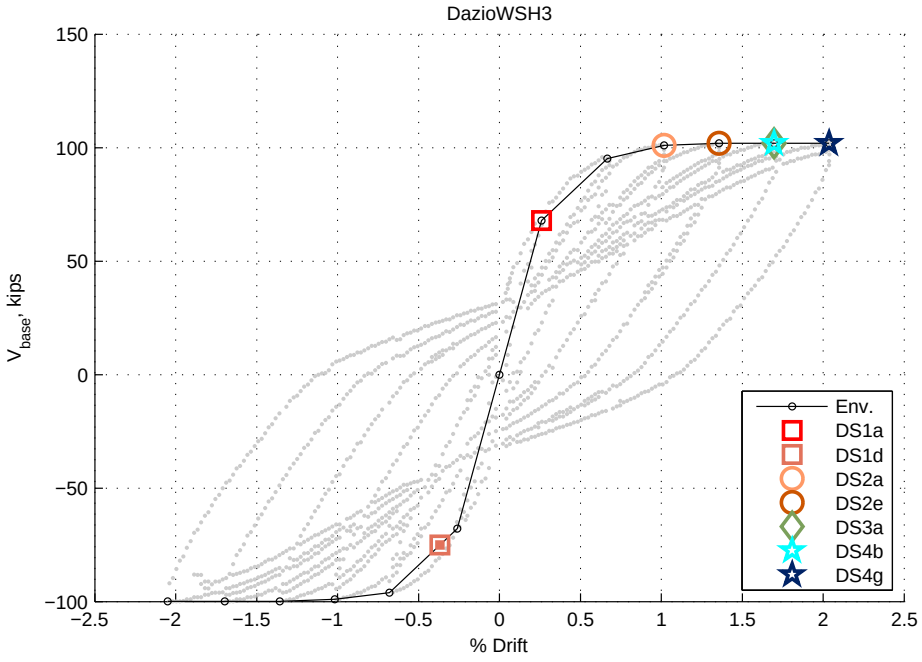

Figure A.44: Envelope for DazioWSH3

Table A.25: DazioWSH3 crack width information

					Crack Width, in (mm)	
DS	% Drift	Force, kips (kN)	Exact/Max	Crack Type	Max.	Resid.
DSr1	0.26%	67.9 (302.2)	Max	Shear	0.002 (0.05)	
				Flexure	0.0079 (0.2)	
				Any	0.0079 (0.2)	
DS1a	0.26%	67.9 (302.2)	Max	Shear	0.002 (0.05)	
				Flexure	0.0079 (0.2)	
				Any	0.0079 (0.2)	
DS2a	1.02%	100.9 (448.9)	Max	Shear	0.031 (0.8)	
				Flexure	0.043 (1.1)	
				Any	0.043 (1.1)	
DSr9	1.36%	101.9 (453.2)	Max	Shear	0.043 (1.1)	
				Flexure	0.071 (1.8)	
				Any	0.071 (1.8)	
DS3a	1.70%	101.9 (453.2)	Max	Shear	0.071 (1.8)	
				Flexure	0.1 (2.6)	
				Any	0.1 (2.6)	
DS4b	1.70%	101.9 (453.2)	Max	Shear	0.071 (1.8)	
				Flexure	0.1 (2.6)	
				Any	0.1 (2.6)	

A.18 DazioWSH4

Table A.26: DazioWSH4 damage information

MOR	DS	% Drift	Force, kips (kN)	Description	Figure
1	DS1a	0.25%	68.9 (306.5)	First cracking (from data downloaded for project)	
	DS1d	0.31%	73.5 (327.1)	As determined from moment-curvature analysis	
2	DS2a	-1.01%	-97.0 (-431.7)	Initial spalling, but long. reinf. not seen (initial buckling also occurs)	
3	DS3a	1.01%	100.0 (444.6)	Cover continued to spall, revealing long. reinf. for first time	
4	DS4b	-1.01%	-97.0 (-431.7)	Initial buckling seen at same time as initial spalling	
	DS4d	1.56%	90.2 (401.4)	Failure due to crushing of core concrete	
	DSr1	0.25%	69.1 (307.5)	First yield as reported in paper Table 4 (Δ_y^b)	
	DSr9	1.01%	100.0 (444.6)	Cracks exceeding or equal to 1/16" (determined from download crack data)	

Table A.27: DazioWSH4 crack width information

					Crack Width, in (mm)	
DS	% Drift	Force, kips (kN)	Exact/Max	Crack Type	Max.	Resid.
DS1a	0.25%	68.9 (306.5)	Max	Shear	0.0059 (0.15)	
				Flexure	0.012 (0.3)	
				Any	0.012 (0.3)	
DSr1	0.67%	98.0 (436.0)	Max	Shear	0.02 (0.5)	
				Flexure	0.047 (1.2)	
				Any	0.047 (1.2)	
DSr9	1.01%	100.0 (444.6)	Max	Shear	0.035 (0.9)	
				Flexure	0.073 (1.9)	
				Any	0.073 (1.9)	
DS2a	-1.01%	-97.0 (-431.7)	Max	Shear	0.043 (1.1)	
				Flexure	0.087 (2.2)	
				Any	0.087 (2.2)	
DS3a	1.01%	100.0 (444.6)	Max	Shear	0.035 (0.9)	
				Flexure	0.073 (1.9)	
				Any	0.073 (1.9)	
DS4b	-1.01%	-97.0 (-431.7)	Max	Shear	0.043 (1.1)	
				Flexure	0.087 (2.2)	
				Any	0.087 (2.2)	

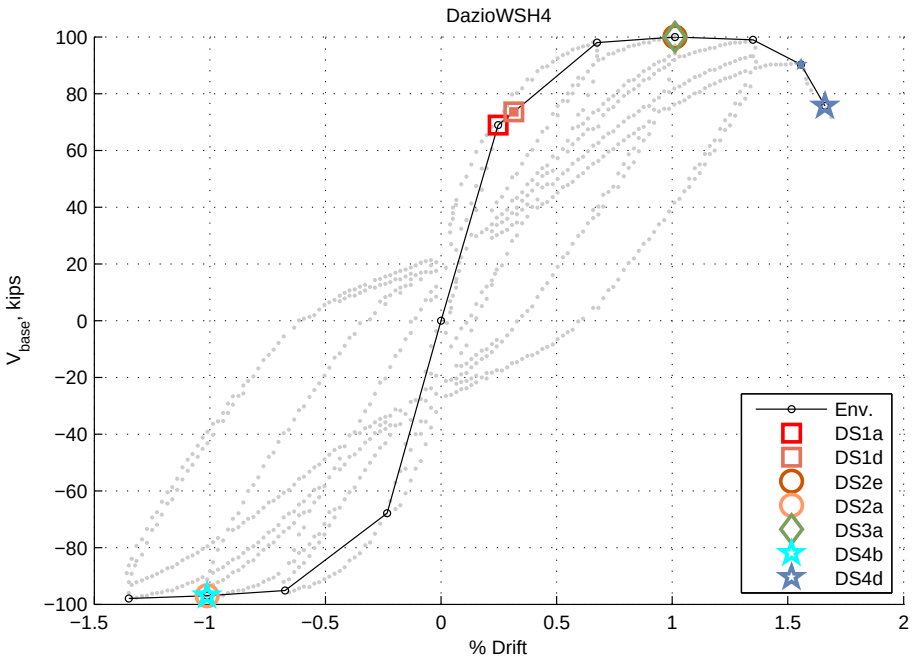

Figure A.45: Envelope for DazioWSH4

A.19 DazioWSH5

Table A.28: DazioWSH5 damage information

MOR	DS	% Drift	Force, kips (kN)	Description	Figure
1	DS1a	0.10%	66.0 (293.5)	First cracking (from data downloaded for project)	
	DS1d	0.19%	77.3 (344.0)	As determined from moment-curvature analysis	
2	DS2a	0.55%	95.1 (423.0)	Initial spalling	
3	DS3a	1.08%	94.1 (418.7)	Cover continued to spall, revealing long. reinf. for first time (B.E bars buckled and web bars fractured)	
4	DS4b	1.08%	94.1 (418.7)	Initial buckling of corner bars (spalling reveals reinf. for first time and web bars rupture)	
	DS4e	1.08%	94.1 (418.7)	Rupture of web bars (spalling reveals reinf. for first time and corner bars have initial buckling)	
	DS4g	1.54%	78.6 (349.6)	Failure due to rupture of bar (other had previously buckled/fractured)	
	DSr1	0.17%	74.7 (332.5)	First yield as reported in paper Table 4 (Δ_y^b)	
	DSr9	0.55%	95.1 (423.0)	Cracks exceeding or equal to 1/16" (determined from download crack data)	

Table A.29: DazioWSH5 crack width information

DS	% Drift	Force, kips (kN)	Exact/Max	Crack Type	Crack Width, in (mm) Max.	Resid.
DS1a	0.10%	66.0 (293.5)	Max	Shear	0.002 (0.05)	
				Flexure	0.0059 (0.15)	
				Any	0.0059 (0.15)	
DSr1	0.27%	88.3 (392.8)	Max	Shear	0.014 (0.35)	
				Flexure	0.016 (0.4)	
				Any	0.016 (0.4)	
DSr9	0.55%	95.1 (423.0)	Max	Shear	0.051 (1.3)	
				Flexure	0.067 (1.7)	
				Any	0.067 (1.7)	
DS2a	0.55%	95.1 (423.0)	Max	Shear	0.051 (1.3)	
				Flexure	0.067 (1.7)	
				Any	0.067 (1.7)	
DS3a	1.08%	94.1 (418.7)	Max	Shear	0.14 (3.5)	
DS4b	1.08%	94.1 (418.7)	Max	Shear	0.14 (3.5)	
DS4e	1.08%	94.1 (418.7)	Max	Shear	0.14 (3.5)	

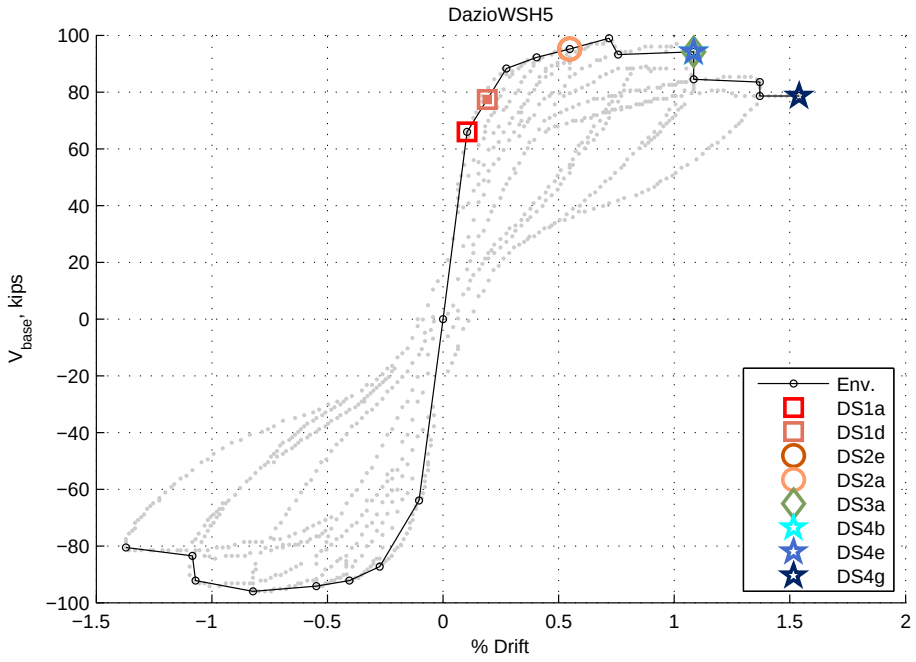

Figure A.46: Envelope for DazioWSH5

A.20 DazioWSH6

Table A.30: DazioWSH6 damage information

MOR	DS	% Drift	Force, kips (kN)	Description	Figure
1	DS1a	0.22%	90.2 (401.4)	First cracking (from data downloaded for project)	
	DS1d	-0.32%	-103.4 (-459.9)	As determined from moment-curvature analysis	
2	DS2a	0.57%	125.2 (556.8)	Initial spalling	
3	DS3a	0.84%	131.0 (582.7)	Spalling revealing corner bars but no bar buckling	
4	DS4b	-1.73%	-132.0 (-587.1)	Initial buckling of corner bars (spalling reveals reinf. for first time and web bars rupture)	
	DS4d	1.42%	132.0 (587.1)	Failure due to crushing of core concrete (occurred in negative direction after positive direction reached actuator displacement limit)	
	DSr1	0.22%	88.3 (392.7)	First yield as reported in paper Table 4 (Δ_y^b)	
	DSr9	-0.87%	-132.9 (-591.4)	Cracks exceeding or equal to 1/16" (determined from download crack data)	

Table A.31: DazioWSH6 crack width information

					Crack Width, in (mm)	
DS	% Drift	Force, kips (kN)	Exact/Max	Crack Type	Max.	Resid.
DS2a	0.57%	125.2 (556.8)	Max	Flexure	0.024 (0.6)	
DS3a	0.84%	131.0 (582.7)	Max	Flexure	0.045 (1.1)	
DSr9	-0.87%	-132.9 (-591.4)	Max	Shear	0.043 (1.1)	
				Flexure	0.063 (1.6)	
				Any	0.063 (1.6)	
DS4b	-1.73%	-132.0 (-587.1)	Max	Shear	0.079 (2)	

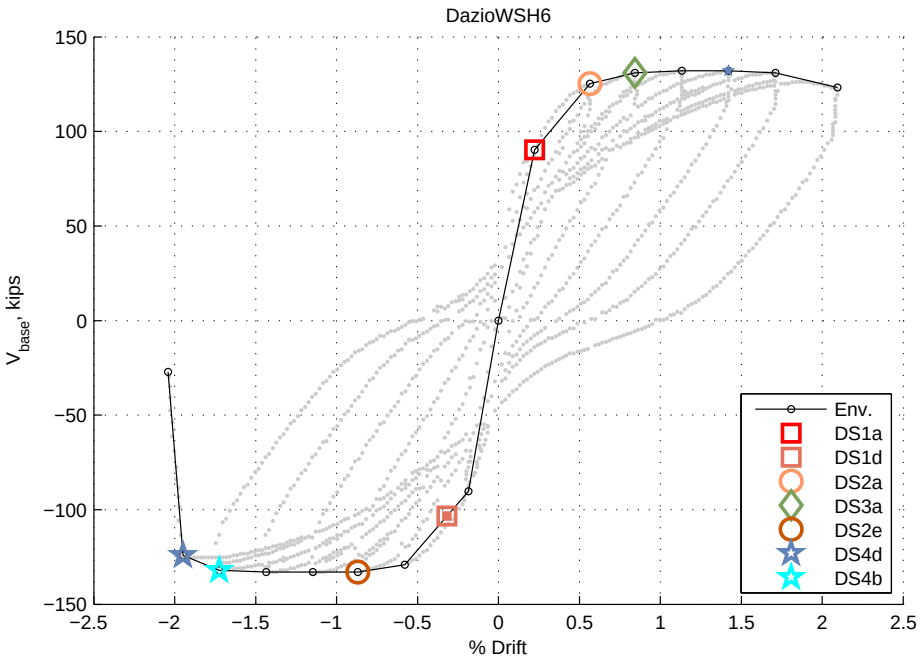

Figure A.47: Envelope for DazioWSH6

A.21 LefasSW21

Table A.32: LefasSW21 damage information

MOR	DS	% Drift	Force, kips (kN)	Description	Figure
1	DS1b	0.02%	2.2 (10.0)	First flexural cracking reported	
	DS1c	0.45%	18.0 (80.0)	First shear cracking reported	
	DS1d	0.38%	15.9 (70.5)	As determined from moment-curvature analysis	
2	DS2a	0.92%	25.7 (114.3)	Spalling at 90% of ultimate horizontal load (accompanied by large vertical crack in compressive B.E.)	
4	DS4c	1.59%	28.6 (127.0)	Compressive failure at ultimate load due to vertical cracking in compression zone	
	DSr1	0.45%	18.0 (80.0)	First flexural steel yielding reproted	

Table A.33: LefasSW21 crack width information

					Crack Width, in (mm)	
DS	% Drift	Force, kips (kN)	Exact/Max	Crack Type	Max.	Resid.
DS4c	1.59%	28.6 (127.0)	Max	Flexure	0.059 (1.5)	

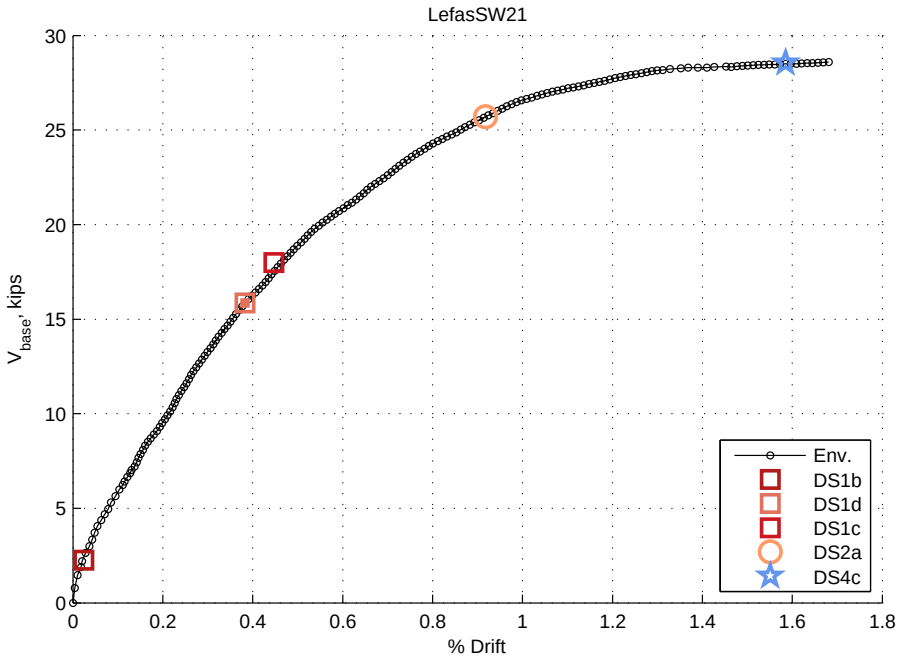

Figure A.48: Envelope for LefasSW21

A.22 LefasSW22

Table A.34: LefasSW22 damage information

MOR	DS	% Drift	Force, kips (kN)	Description	Figure
1	DS1b	0.03%	3.1 (14.0)	First flexural cracking reported	
	DS1c	0.38%	24.7 (110.0)	First shear cracking reported	
	DS1d	0.31%	21.8 (96.9)	As determined from moment-curvature analysis	
4	DS4c	1.18%	33.7 (150.0)	Compressive failure at ultimate load due to vertical cracking in compression zone	
	DSr1	0.38%	22.5 (100.0)	First flexural steel yielding reported	
	DSr5	0.59%	30.3 (135.0)	Inclined crack reaches within 200mm of wall edge (650mm wall length)	

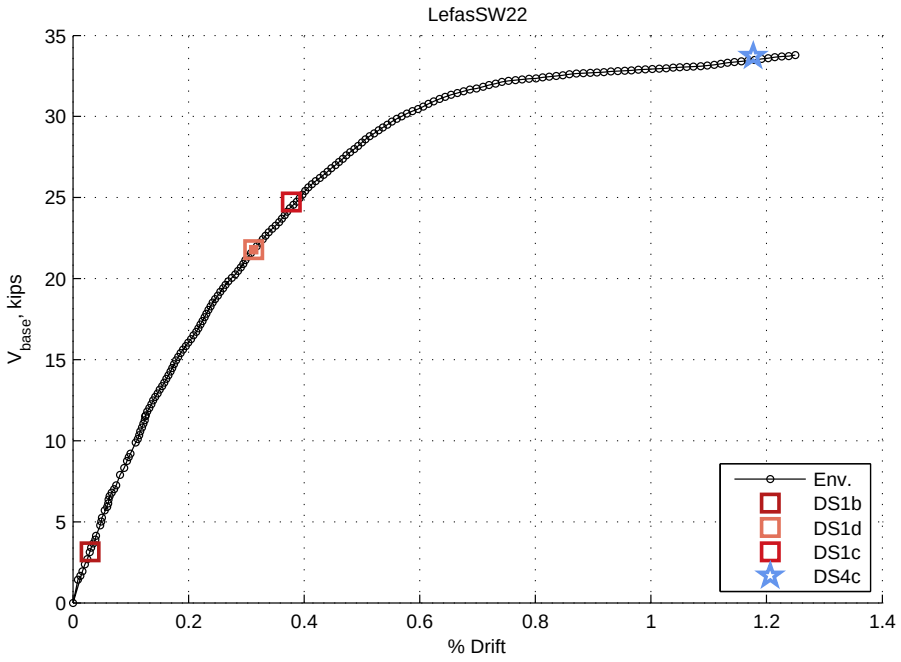

Figure A.49: Envelope for LefasSW22

A.23 LefasSW23

Table A.35: LefasSW23 damage information

MOR	DS	% Drift	Force, kips (kN)	Description	Figure
1	DS1b	0.04%	4.5 (20.0)	First flexural cracking reported	
	DS1c	0.40%	27.0 (120.0)	First shear cracking reported	
	DS1d	0.41%	26.7 (118.6)	As determined from moment-curvature analysis	
4	DS4c	1.01%	40.5 (180.0)	Compressive failure at ultimate load due to inclined crack becoming a vertical crack in compression zone, followed by immediate cruching	
	DSr1	0.40%	27.0 (120.0)	First flexural steel yielding	

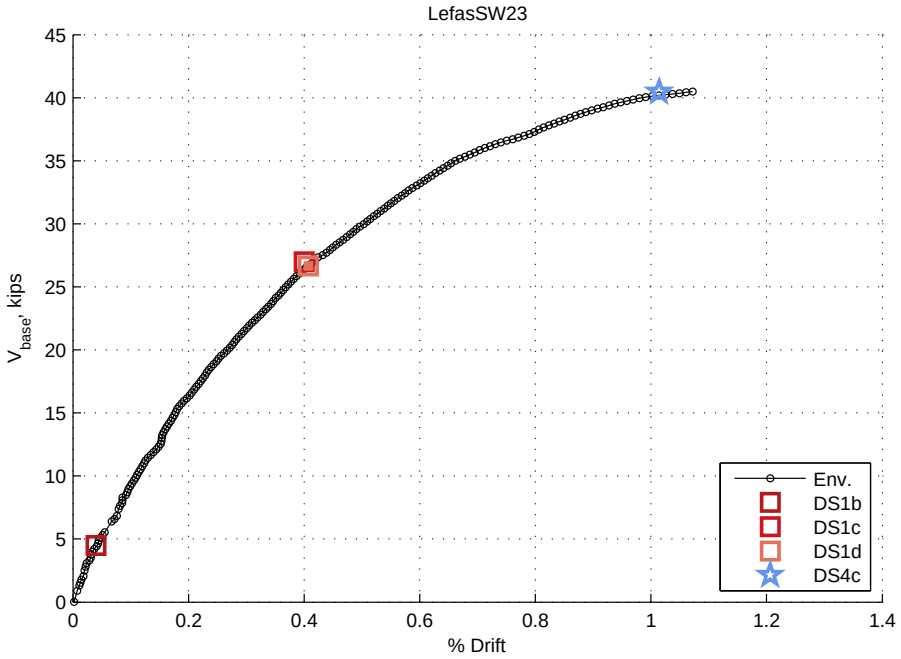

Figure A.50: Envelope for LefasSW23

A.24 LefasSW24

Table A.36: LefasSW24 damage information

MOR	DS	% Drift	Force, kips (kN)	Description	Figure
1	DS1b	0.02%	2.2 (10.0)	First flexural cracking reported	
	DS1c	0.48%	18.0 (80.0)	First shear cracking reported	
	DS1d	0.41%	15.7 (70.0)	As determined from moment-curvature analysis	
2	DS2a	0.94%	24.3 (108.0)	Spalling at 90% of ultimate horizontal load (accompanied by large vertical crack in compressive B.E.)	
4	DS4c	1.39%	27.0 (120.0)	Compressive failure at ultimate load due to vertical cracking in compression zone	
	DSr1	0.48%	18.0 (80.0)	First flexural steel yielding reported	

Table A.37: LefasSW24 crack width information

					Crack Width, in (mm)	
DS	% Drift	Force, kips (kN)	Exact/Max	Crack Type	Max.	Resid.
DS4c	1.39%	27.0 (120.0)	Max	Flexure	0.059 (1.5)	

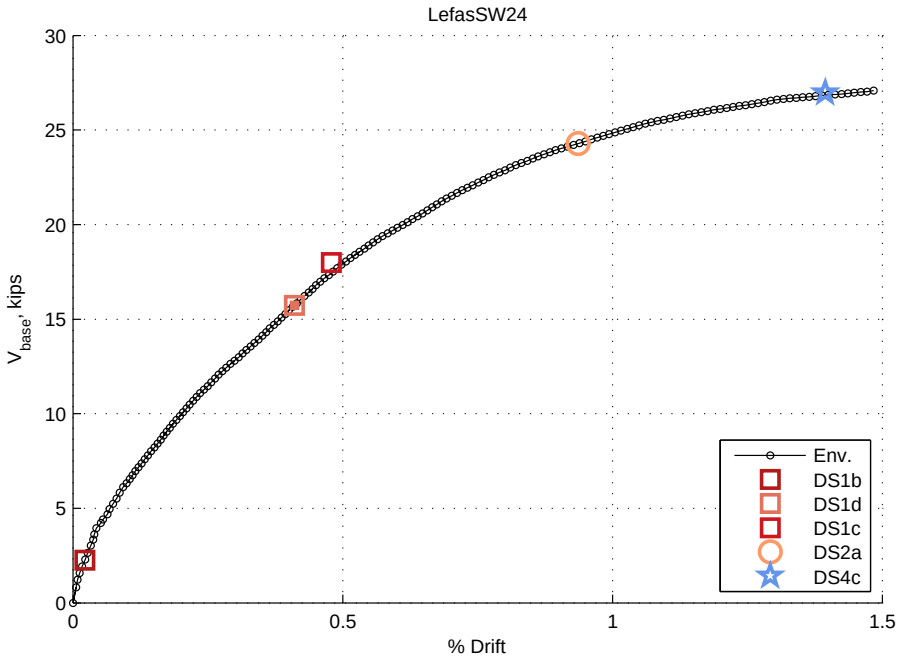

Figure A.51: Envelope for LefasSW24

A.25 LefasSW25

Table A.38: LefasSW25 damage information

MOR	DS	% Drift	Force, kips (kN)	Description	Figure
1	DS1b	0.05%	5.6 (25.0)	First flexural cracking reported	
	DS1c	0.45%	29.2 (130.0)	First shear cracking reported	
	DS1d	0.38%	26.0 (115.6)	As determined from moment-curvature analysis	
	DSr1	0.45%	29.2 (130.0)	First flexural steel yielding reported	

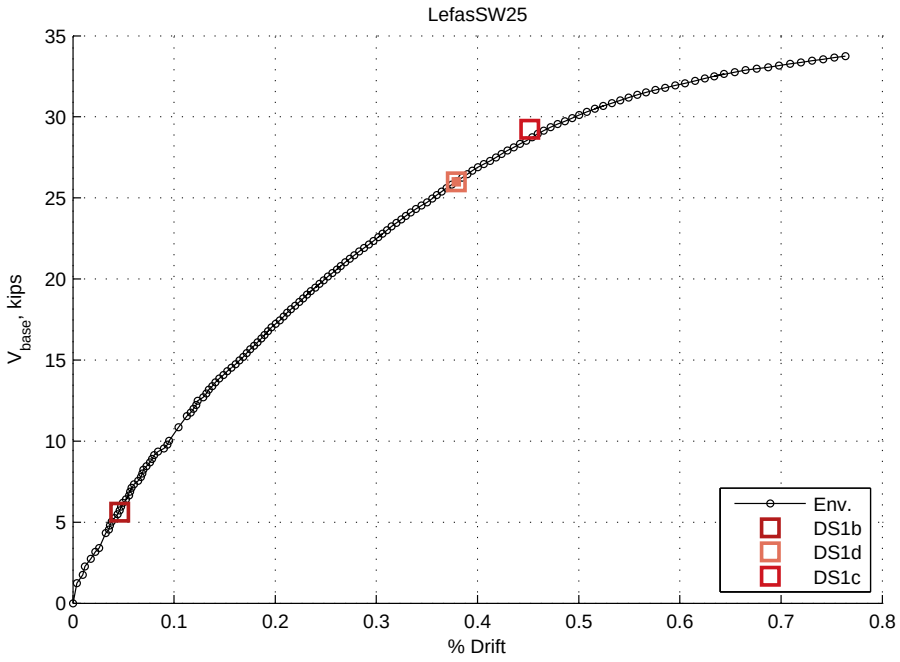

Figure A.52: Envelope for LefasSW25

A.26 LefasSW26

Table A.39: LefasSW26 damage information

MOR	DS	% Drift	Force, kips (kN)	Description	Figure
1	DS1b	0.03%	2.2 (10.0)	First flexural cracking reported	
	DS1c	0.42%	15.3 (68.0)	First shear cracking reported	
	DS1d	0.44%	15.1 (67.3)	As determined from moment-curvature analysis	
2	DS2a	1.02%	24.9 (110.7)	Spalling at 90% of ultimate horizontal load (accompanied by large vertical crack in compressive B.E.)	
4	DS4c	1.61%	27.7 (123.0)	Compressive failure at ultimate load due to vertical cracking in compression zone	
	DSr1	0.42%	15.3 (68.0)	First flexural steel yielding reported	

Table A.40: LefasSW26 crack width information

					Crack Width, in (mm)	
DS	% Drift	Force, kips (kN)	Exact/Max	Crack Type	Max.	Resid.
DS4c	1.61%	27.7 (123.0)	Max	Flexure	0.059 (1.5)	

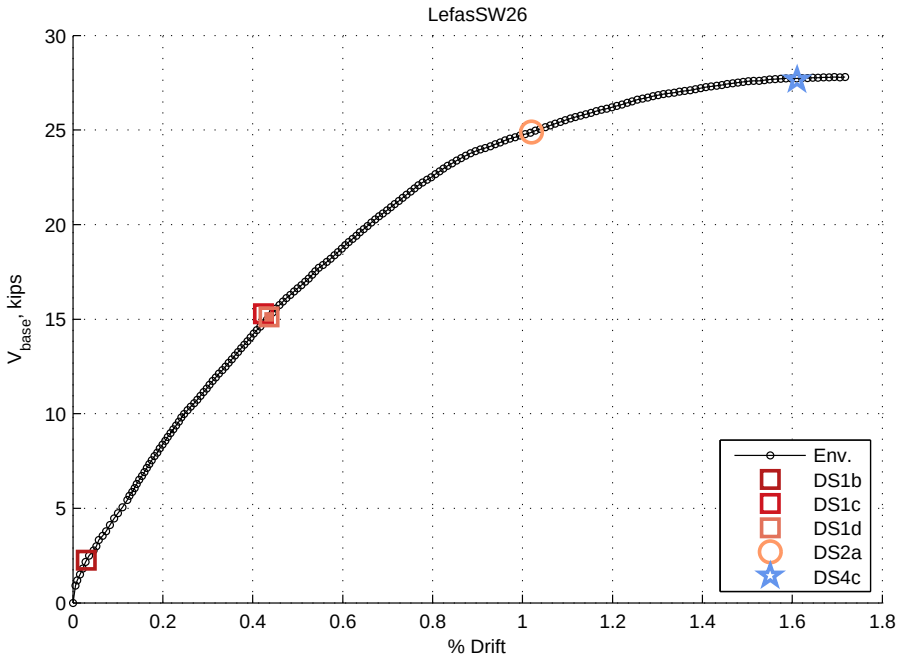

Figure A.53: Envelope for LefasSW26

A.27 LefasSW30

Table A.41: LefasSW30 damage information

MOR	DS	% Drift	Force, kips (kN)	Description	Figure
1	DS1b	0.06%	4.0 (17.7)	First flexural cracking occurred at 15% of maximum load (p. 722)	
	DS1c	0.06%	4.0 (17.7)	First shear cracking occurred at 60% of maximum load	
	DS1d	0.38%	13.8 (61.2)	As determined from moment-curvature analysis	
4	DS4c	1.61%	26.5 (117.7)	Spalling and vertical cracks in compressive b.e. ultimately led to loss of lateral load carrying capacity (p. 722-723)	

Table A.42: LefasSW30 crack width information

					Crack Width, in (mm)	
DS	% Drift	Force, kips (kN)	Exact/Max	Crack Type	Max.	Resid.
DS4c	1.61%	26.5 (117.7)	Max	Flexure	0.047 (1.2)	

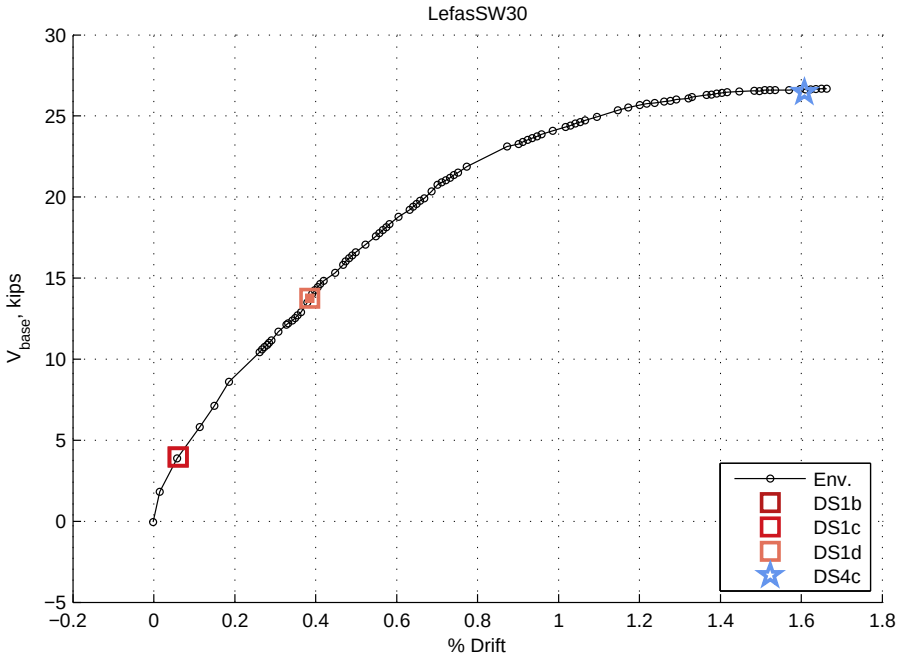

Figure A.54: Envelope for LefasSW30

A.28 LefasSW31

Table A.43: LefasSW31 damage information

MOR	DS	% Drift	Force, kips (kN)	Description	Figure
1	DS1b	0.05%	4.5 (20.0)	First flexural cracking (Table 8.3)	
	DS1c	0.32%	14.6 (64.9)	First shear cracking (Table 8.3)	
	DS1d	0.30%	14.0 (62.5)	As determined from moment-curvature analysis	
4	DS4c	1.71%	26.0 (115.8)	Spalling and vertical cracks in compressive b.e. ultimately led to loss of lateral load carrying capacity (p. 216)	
	DSr1	0.32%	14.6 (64.9)	First yield reported (Table 8.3)	

Table A.44: LefasSW31 crack width information

					Crack Width, in (mm)	
DS	% Drift	Force, kips (kN)	Exact/Max	Crack Type	Max.	Resid.
DS4c	1.71%	26.0 (115.8)	Max	Flexure	0.016 (0.4)	

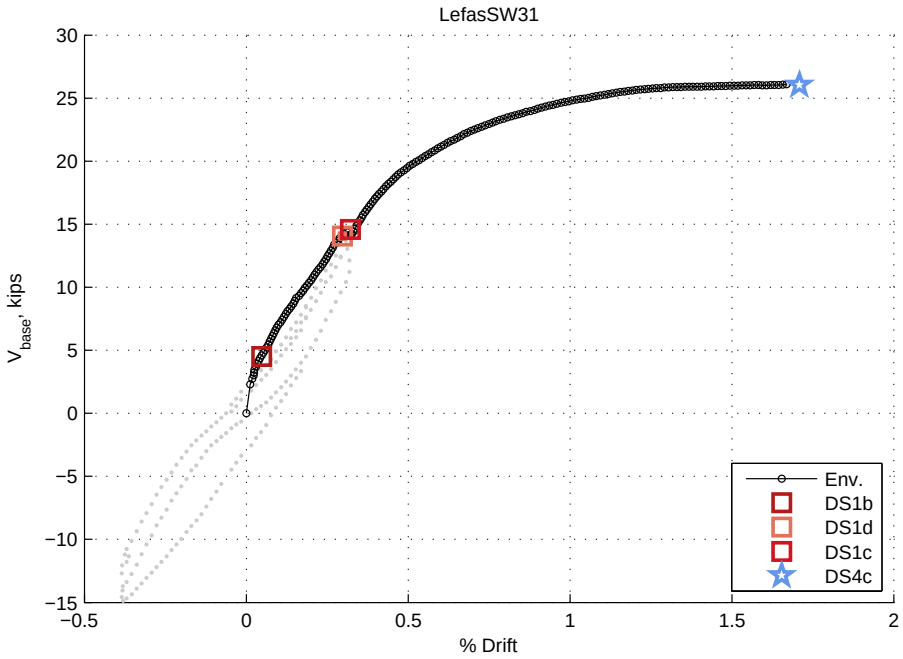

Figure A.55: Envelope for LefasSW31

A.29 LefasSW32

Table A.45: LefasSW32 damage information

MOR	DS	% Drift	Force, kips (kN)	Description	Figure
1	DS1b	0.05%	4.5 (20.0)	First flexural cracking (Table 8.3)	
	DS1c	0.34%	14.6 (64.9)	First shear cracking (Table 8.3)	
	DS1d	0.32%	14.4 (64.3)	As determined from moment-curvature analysis	
4	DS4c	1.89%	25.0 (111.0)	Spalling and vertical cracks in compressive b.e. ultimately led to loss of lateral load carrying capacity (p. 216)	
	DSr1	0.34%	14.6 (64.9)	First yield reported (Table 8.3)	

Table A.46: LefasSW32 crack width information

					Crack Width, in (mm)	
DS	% Drift	Force, kips (kN)	Exact/Max	Crack Type	Max.	Resid.
DS4c	1.89%	25.0 (111.0)	Max	Flexure	0.031 (0.8)	

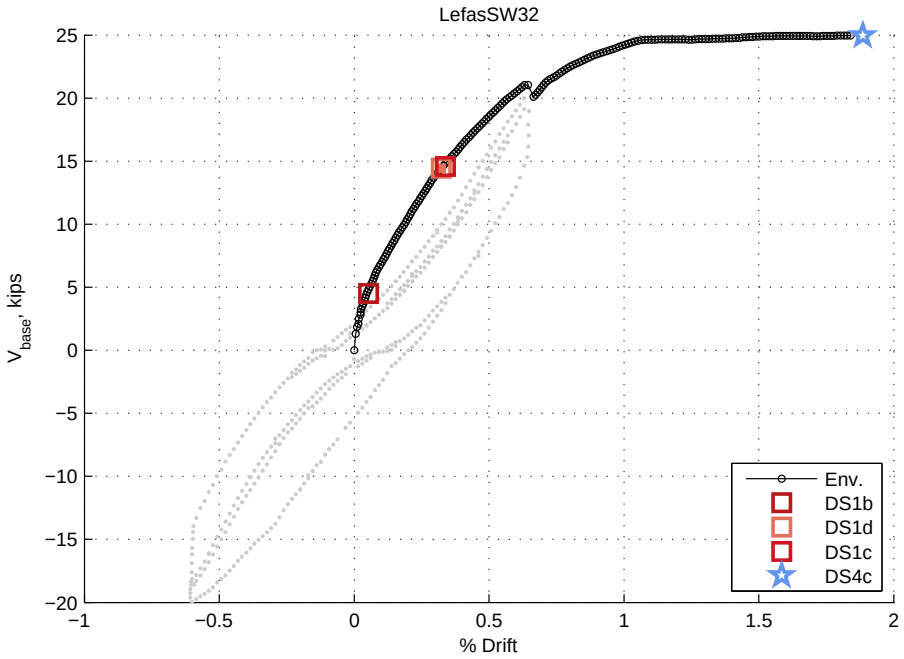

Figure A.56: Envelope for LefasSW32

A.30 LefasSW33

Table A.47: LefasSW33 damage information

MOR	DS	% Drift	Force, kips (kN)	Description	Figure
1	DS1b	0.05%	3.7 (16.4)	First flexural cracking (Table 8.3)	
	DS1c	0.44%	16.1 (71.5)	First shear cracking (Table 8.3)	
	DS1d	0.44%	16.1 (71.5)	Experimental reporting of yield used in place of theoretical calculation; First yield reported (Table 8.3)	
4	DS4c	1.92%	25.1 (111.5)	Spalling and vertical cracks in compressive b.e. ultimately led to loss of lateral load carrying capacity (p. 216)	
	DSr1	0.44%	16.1 (71.5)	First yield reported (Table 8.3)	

Table A.48: LefasSW33 crack width information

					Crack Width, in (mm)	
DS	% Drift	Force, kips (kN)	Exact/Max	Crack Type	Max.	Resid.
DS4c	1.92%	25.1 (111.5)	Max	Flexure	0.031 (0.8)	

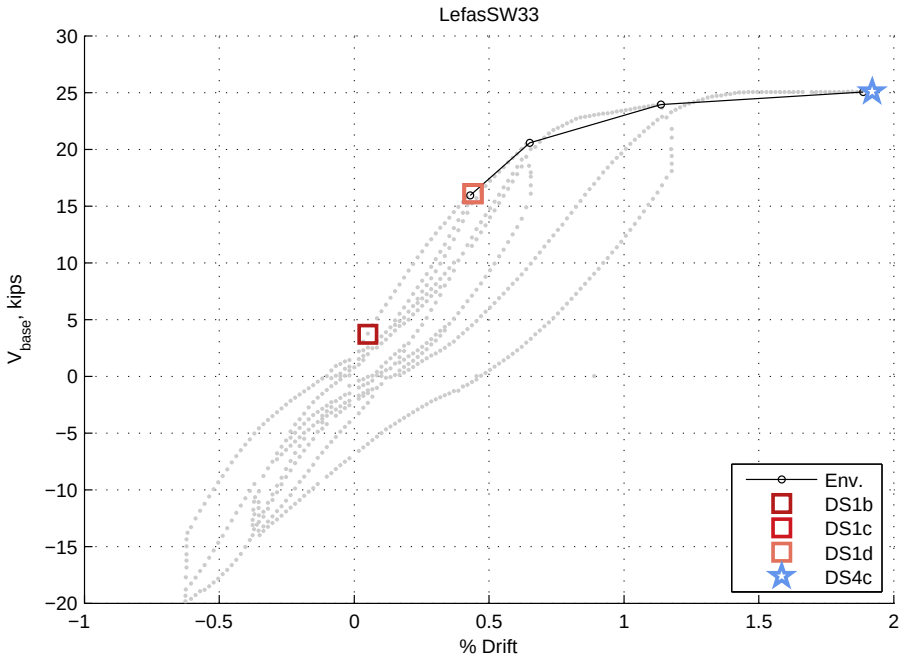

Figure A.57: Envelope for LefasSW33

A.31 OestR1

Table A.49: OestR1 damage information

MOR	DS	% Drift	Force, kips (kN)	Description	Figure
1	DS1b	0.04%	12.3 (54.8)	Initial flexural cracking; data taken from force-disp. figure of initial cycles	
	DS1d	-0.15%	-17.2 (-76.3)	As determined from moment-curvature analysis	
2	DS2a	-1.09%	-27.1 (-120.7)	Minor spalling and flaking along cracks observed in cycle 14 (data for cycle 13 used)	
4	DS4b	-2.20%	-27.2 (-121.0)	First buckling of main flex. reinf.: outer 2 bars in compression region buckled 15 inches above base (cycle 20 reported, info from cycle 19 on envelope is used)	
	DS4e	-2.75%	-20.0 (-89.0)	First bar fracture of bars that were first to buckle (cycle 26 is reported, info from cycle 25 on envelope is used)	
	DSr1	0.24%	20.1 (89.4)	Reported tensile yield	

Table A.50: OestR1 crack width information

					Crack Width, in (mm)	
DS	% Drift	Force, kips (kN)	Exact/Max	Crack Type	Max.	Resid.
DSr1	-0.57%	-25.3 (-112.7)	Max	Any	0.018 (0.46)	
DS4b	-2.20%	-27.2 (-121.0)	Max	Any		0.05 (1.3)
C1	-1.66%	-27.2 (-121.2)	Max	Flexure	0.2 (5.1)	0.02 (0.51)

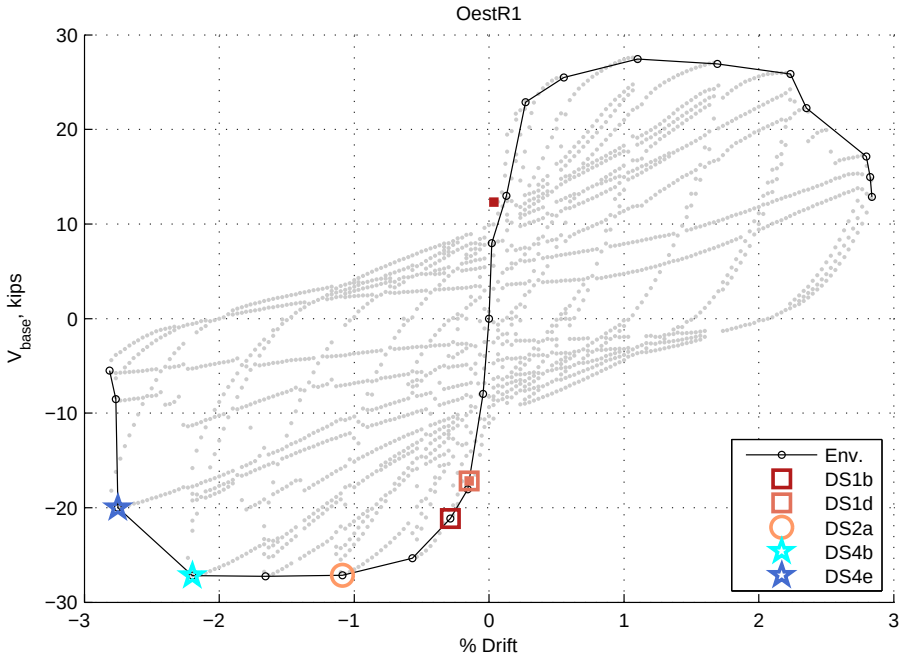

Figure A.58: Envelope for OestR1

A.32 OestR2

Table A.51: OestR2 damage information

MOR	DS	% Drift	Force, kips (kN)	Description	Figure
1	DS1b	0.06%	13.6 (60.5)	Initial flexural cracking; data taken from force-disp of initial cycles; cracking reported as occurring at 15 kips	
	DS1d	0.30%	32.6 (144.8)	As determined from moment-curvature analysis	
2	DS2a	-0.56%	-42.9 (-191.0)	Minor spalling and flaking along cracks observed in cycle 19 along horizontal web crack in lower 3ft	
4	DS4e	-3.33%	-29.3 (-130.2)	Several bars fractuctured during cycle 37	
	DSr1	0.33%	37.0 (164.6)	Reported tensile yield	
	DSr2	-1.67%	-49.4 (-219.9)	Residual cracks of 0.003 in	

Table A.52: OestR2 crack width information

					Crack Width, in (mm)	
DS	% Drift	Force, kips (kN)	Exact/Max	Crack Type	Max.	Resid.
DSr1	-0.56%	-42.9 (-191.0)	Max	Shear	0.019 (0.48)	
				Flexure	0.012 (0.3)	
DSr2	-1.67%	-49.4 (-219.9)	Max	Any		0.003 (0.076)

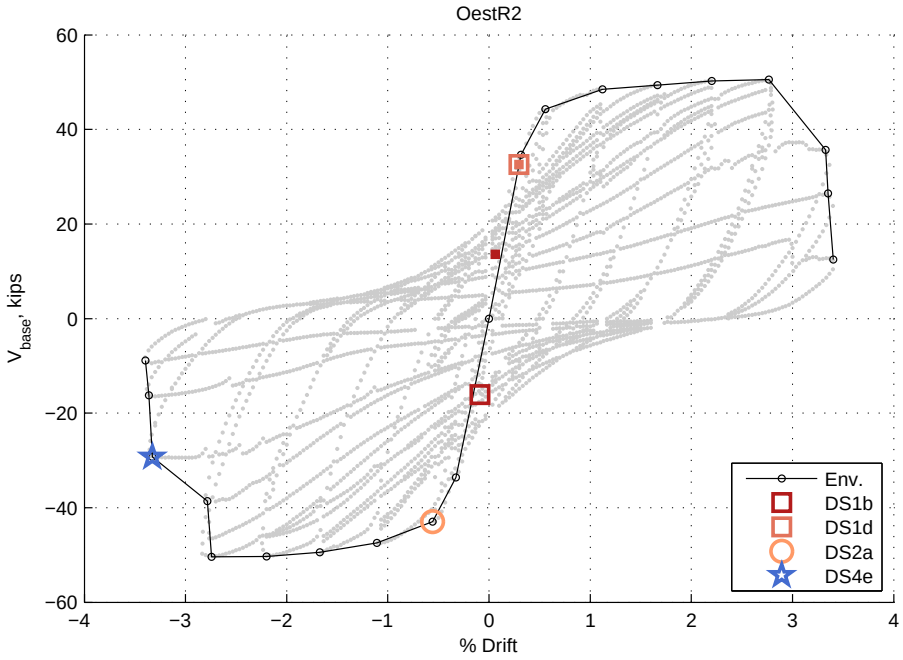

Figure A.59: Envelope for OestR2

A.33 OestB1

Table A.53: OestB1 damage information

MOR	DS	% Drift	Force, kips (kN)	Description	Figure
1	DS1b	0.05%	28.6 (127.4)	Initial flexural cracks; data taken from force-disp of initial cycles	
	DS1d	-0.17%	-42.1 (-187.1)	As determined from moment-curvature analysis	
2	DS2a	0.57%	54.1 (240.7)	Minor spalling and flaking along cracks observed in cycle 14 along web cracks (cycle 13 used for envelope data)	
4	DS4b	-1.67%	-65.0 (-289.0)	Corner bar near outer face of b.e. bowed out between ties	Fig. A.61
	DS4e	2.79%	56.6 (252.0)	First bar to fracture was first bar to buckle	
	DSr1	-0.27%	-45.1 (-200.6)	Reported tensile yield (only negative direction for cycle 10 considered; yield occurred in positive direction in cycle 13)	
	DSr2	1.11%	60.5 (269.0)	Residual cracks of 0.005 in	

Table A.54: OestB1 crack width information

					Crack Width, in (mm)	
DS	% Drift	Force, kips (kN)	Exact/Max	Crack Type	Max.	Resid.
DSr1	-0.25%	-49.9 (-222.2)	Max	Shear	0.014 (0.36)	
				Flexure	0.009 (0.23)	
DSr2	1.11%	60.5 (269.0)	Max	Any		0.005 (0.13)

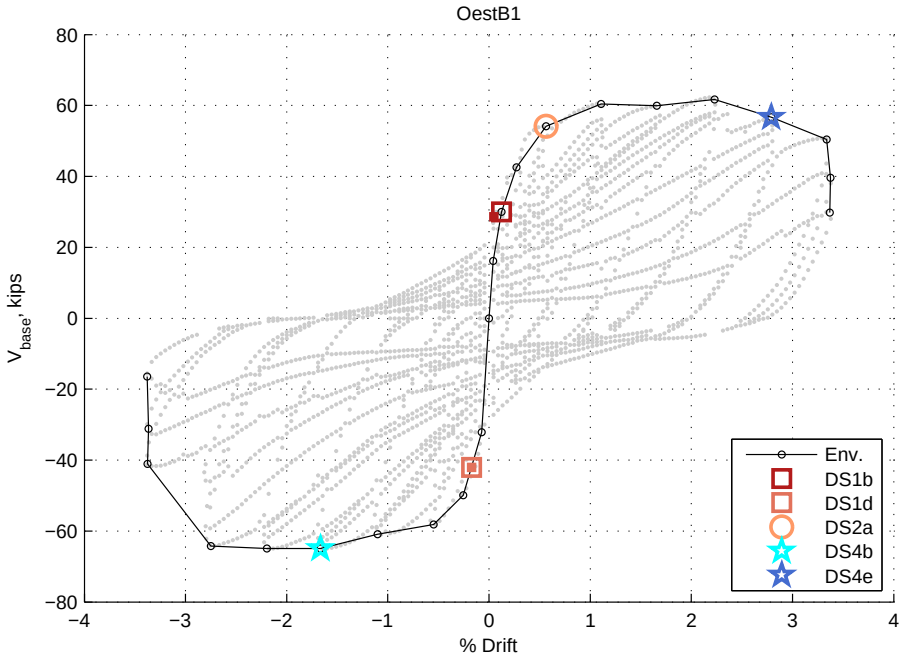

Figure A.60: Envelope for OestB1

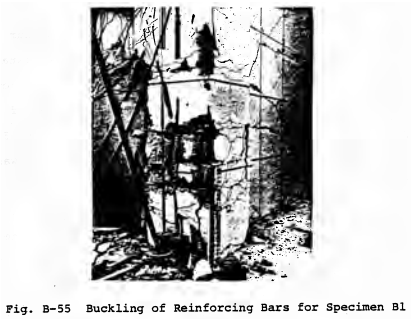
Fig. B-55 Buckling of Reinforcing Bars for Specimen B1

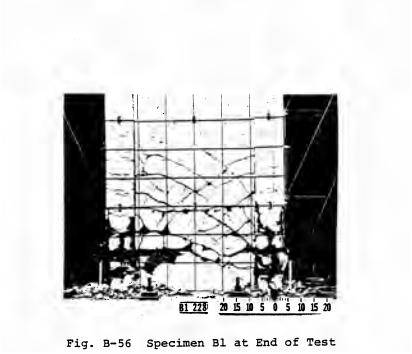
Fig. B-56 Specimen B1 at End of Test

Figure A.61: OestB1: DS4b - Buckling of reinforcing bars

A.34 OestB2

Table A.55: OestB2 damage information

MOR	DS	% Drift	Force, kips (kN)	Description	Figure
1	DS1b	0.04%	31.1 (138.4)	Initial flexural cracking; data taken from force-disp of initial cycles	
	DS1d	-0.38%	-112.0 (-498.4)	As determined from moment-curvature analysis	
2	DS2a	0.54%	121.0 (538.0)	Minor spalling and flaking along cracks observed in cycle 14 along diagonal cracks (cycle 13 used for envelope data)	
3	DS3a	2.23%	153.1 (681.2)	Considerable flaking and spalling in web during cycles 25 thru 27 (cycle 25 data used)	
4	DS4b	2.23%	153.1 (681.2)	Two bars buckled in lower 1 ft of wall in compression column under positive load () cycle 26	
	DS4k	-2.71%	-151.3 (-673.0)	Web failure occurred on way to -5 inch displacement in cycle 28	
	DSr1	0.47%	119.7 (532.5)	Reported tensile yield (only negative direction for cycle 10 considered; yield occurred in positive direction in cycle 13)	

Table A.56: OestB2 crack width information

					Crack Width, in (mm)	
DS	% Drift	Force, kips (kN)	Exact/Max	Crack Type	Max.	Resid.
DSr1	0.54%	121.0 (538.0)	Max	Shear	0.017 (0.43)	
				Flexure	0.005 (0.13)	
C1	-1.12%	-149.3 (-664.1)	Max	Flexure		0.003 (0.076)

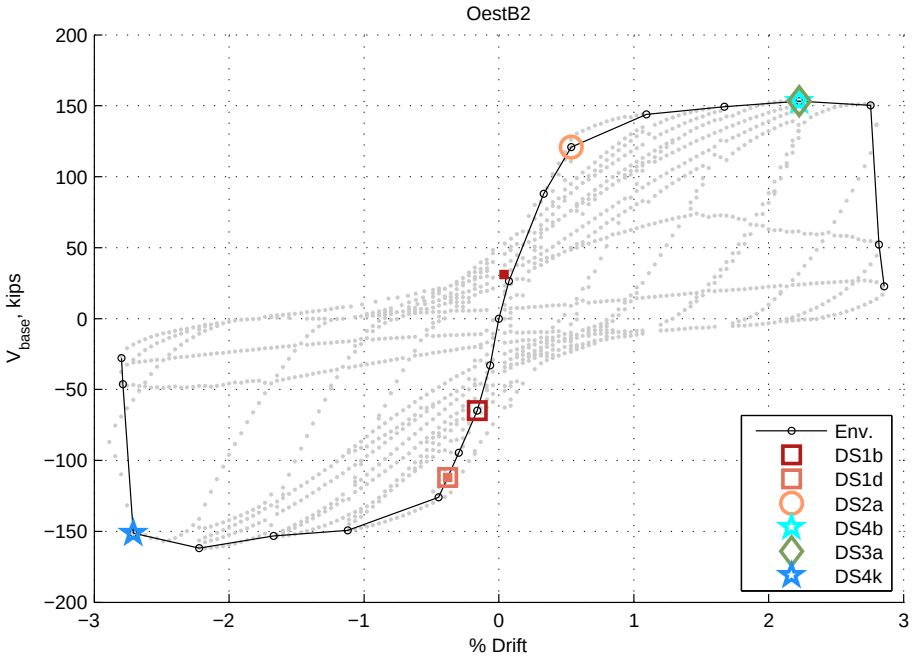

Figure A.62: Envelope for OestB2

A.35 OestB3

Table A.57: OestB3 damage information

MOR	DS	% Drift	Force, kips (kN)	Description	Figure
1	DS1b	0.04%	29.5 (131.2)	Initial flexural cracking; data taken from force-disp of initial cycles	
	DS1d	-0.23%	-41.0 (-182.6)	As determined from moment-curvature analysis	
4	DS4b	-3.89%	-62.2 (-276.9)	First buckling in cycle 38	
	DS4e	3.92%	57.6 (256.2)	Vertical bar fractured at base (cover still present)	
	DSr1	0.31%	45.2 (201.1)	Reported tensile yield	

Table A.58: OestB3 crack width information

					Crack Width, in (mm)	
DS	% Drift	Force, kips (kN)	Exact/Max	Crack Type	Max.	Resid.
DSr1	0.31%	45.6 (202.7)	Max	Shear	0.025 (0.64)	
				Flexure	0.012 (0.3)	

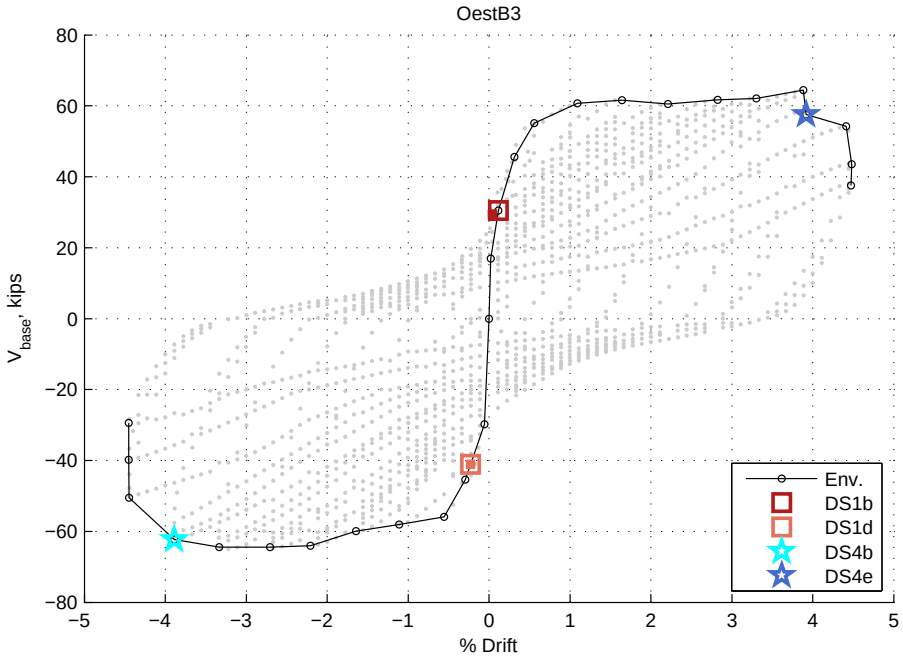

Figure A.63: Envelope for OestB3

A.36 OestB4

Table A.59: OestB4 damage information

MOR	DS	% Drift	Force, kips (kN)	Description	Figure
1	DS1b	0.05%	26.4 (117.6)	First cracking between steps 3 and 4 (called step 3.5 in envelope)	
	DS1d	0.23%	40.9 (182.1)	As determined from moment-curvature analysis	
2	DS2a	1.11%	64.7 (287.7)	Crushing of outer shell of compression face at load step 9	
4	DS4e	4.97%	78.6 (349.8)	Bar fracture of longitudinal bar in web at max load (point named 15.5)	
	DS4g	7.40%	15.6 (69.2)	All column bars (at diagonal crack) and 4 additional web bars fractured, causing drop in strength	
	DSr1	0.28%	45.2 (201.2)	First yield at load step 7	
	DSr13	6.97%	70.7 (314.6)	Largest shear crack 1.0"	

Table A.60: OestB4 crack width information

					Crack Width, in (mm)	
DS	% Drift	Force, kips (kN)	Exact/Max	Crack Type	Max.	Resid.
DSr1	0.28%	45.2 (201.2)	Max	Shear	0.02 (0.51)	
				Flexure	0.01 (0.25)	
DS4e	4.97%	78.6 (349.8)	Max	Shear	0.44 (11)	
				Flexure	0.1 (2.5)	
DSr13	6.97%	70.7 (314.6)	Max	Shear	1 (25)	
DS4g	7.40%	15.6 (69.2)	Max	Shear	0.44 (11)	
				Flexure	0.1 (2.5)	

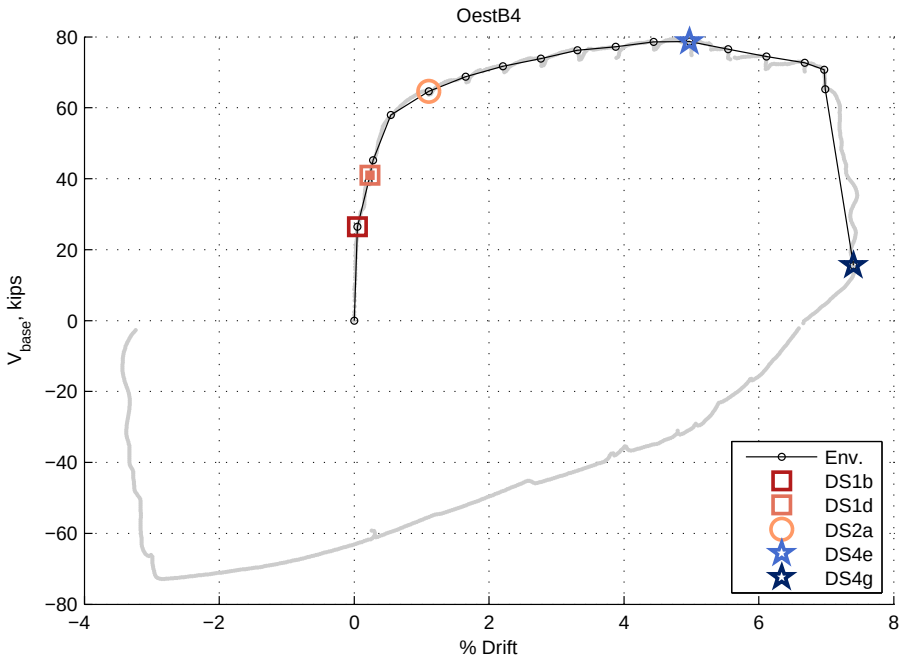

Figure A.64: Envelope for OestB4

A.37 OestB5

Table A.61: OestB5 damage information

MOR	DS	% Drift	Force, kips (kN)	Description	Figure
1	DS1b	-0.03%	-30.6 (-135.9)	Initial flexural cracking; data taken from force-disp of initial cycles	
	DS1d	-0.42%	-117.1 (-520.7)	As determined from moment-curvature analysis	
2	DS2a	0.53%	125.8 (559.5)	Minor spalling and flaking along diagonal cracks observed in cycle 16 along web cracks (cycle 13 used because this was maximum historic drift)	
3	DS3a	-1.67%	-165.6 (-736.7)	Significant spalling and crushing along right half of construction joint at 3 ft level	
4	DS4k	-2.62%	-165.1 (-734.3)	Web crushing in cycle 29 in negative direction	
	DSr1	0.47%	112.3 (499.5)	Reported tensile yield	

Table A.62: OestB5 crack width information

					Crack Width, in (mm)	
DS	% Drift	Force, kips (kN)	Exact/Max	Crack Type	Max.	Resid.
DSr1	0.53%	125.8 (559.5)	Max	Shear	0.025 (0.64)	
				Flexure	0.007 (0.18)	
DS3a	-1.67%	-165.6 (-736.7)	Max	Flexure		0.005 (0.13)

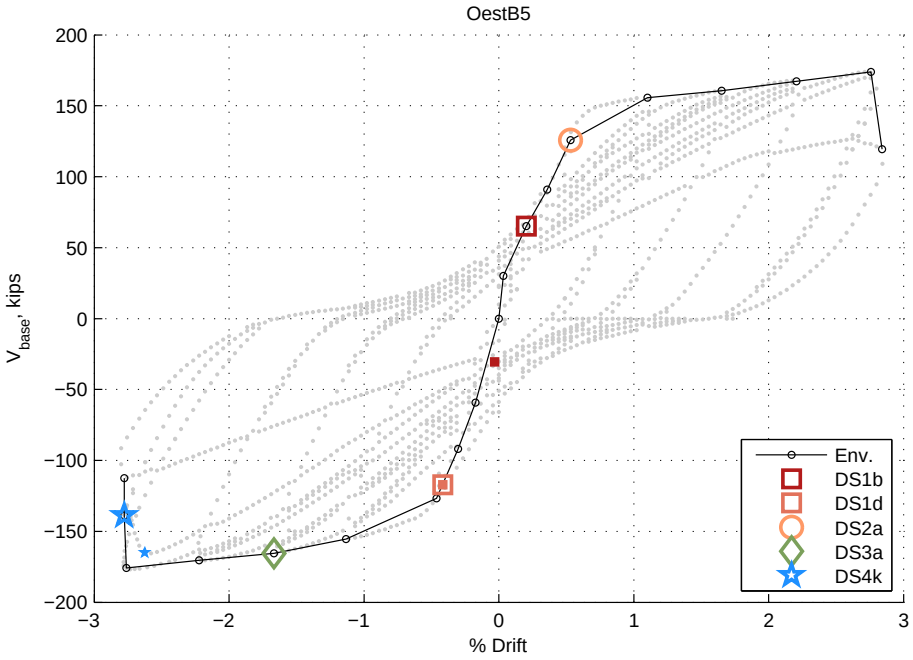

Figure A.65: Envelope for OestB5

A.38 OestB6

Table A.63: OestB6 damage information

MOR	DS	% Drift	Force, kips (kN)	Description	Figure
1	DS1b	-0.11%	-59.6 (-265.2)	Initial flexural cracking; data taken from force-disp of initial cycles	
	DS1d	-0.54%	-145.1 (-645.4)	As determined from moment-curvature analysis	
2	DS2a	1.11%	186.1 (827.8)	Crushing of concrete cover (cycle 22); Spalling & flaking along diagonal cracks (cycle 23)	
	DS2d	0.60%	145.7 (648.1)	Splitting of concrete cover in outer compression face	
4	DS4k	1.11%	186.1 (827.8)	Initial indication of crushing of compression strut in right side of web 18 in above base in cycle 24 (use cycle 22)	
	DS4m	1.41%	166.4 (740.4)	Several compression struts crushed simultaneously	
	DSr1	0.54%	144.2 (641.4)	Reported tensile yield	

Table A.64: OestB6 crack width information

					Crack Width, in (mm)	
DS	% Drift	Force, kips (kN)	Exact/Max	Crack Type	Max.	Resid.
DSr1	0.60%	145.7 (648.1)	Max	Shear	0.014 (0.36)	
				Flexure	0.005 (0.13)	

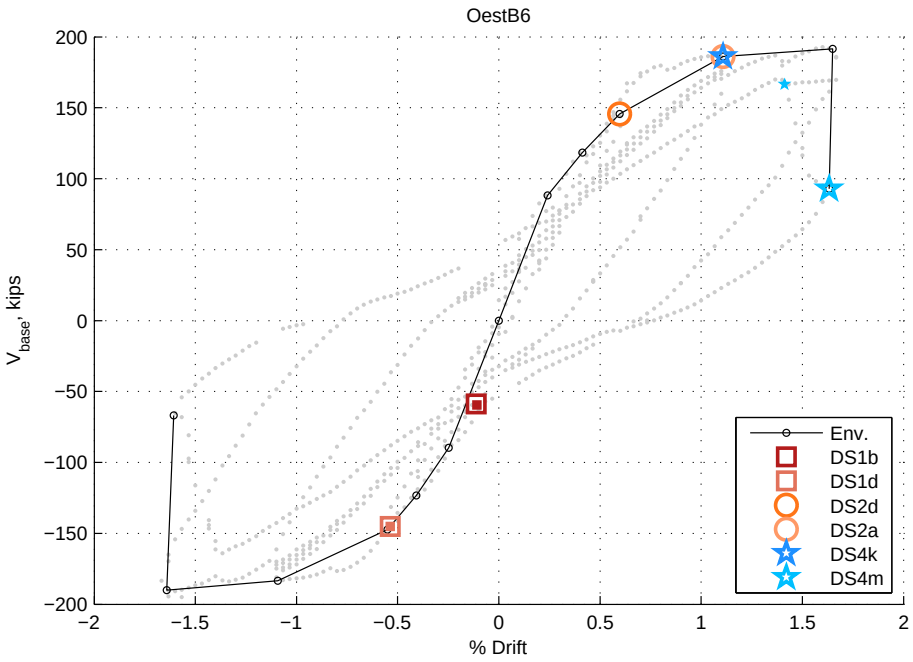

Figure A.66: Envelope for OestB6

A.39 OestB7

Table A.65: OestB7 damage information

MOR	DS	% Drift	Force, kips (kN)	Description	Figure
1	DS1b	0.15%	98.5 (438.0)	Initial flexural cracking; data taken from force-disp of initial cycles	
	DS1d	0.58%	165.7 (736.9)	As determined from moment-curvature analysis	
2	DS2a	0.28%	123.4 (549.0)	Spalling & flaking along diagonal cracks (cycle 10); Crushing of concrete cover (cycle 19)	
4	DS4k	2.19%	214.9 (955.9)	Initial indication of crushing of compression strut in right and left side of web	
	DS4m	2.71%	192.2 (854.8)	Several compression struts crushed simultaneously	
	DSr1	0.54%	161.2 (717.1)	Reported tensile yield	

Table A.66: OestB7 crack width information

					Crack Width, in (mm)	
DS	% Drift	Force, kips (kN)	Exact/Max	Crack Type	Max.	Resid.
DSr1	0.63%	174.2 (775.1)	Max	Shear	0.017 (0.43)	
				Flexure	0.007 (0.18)	

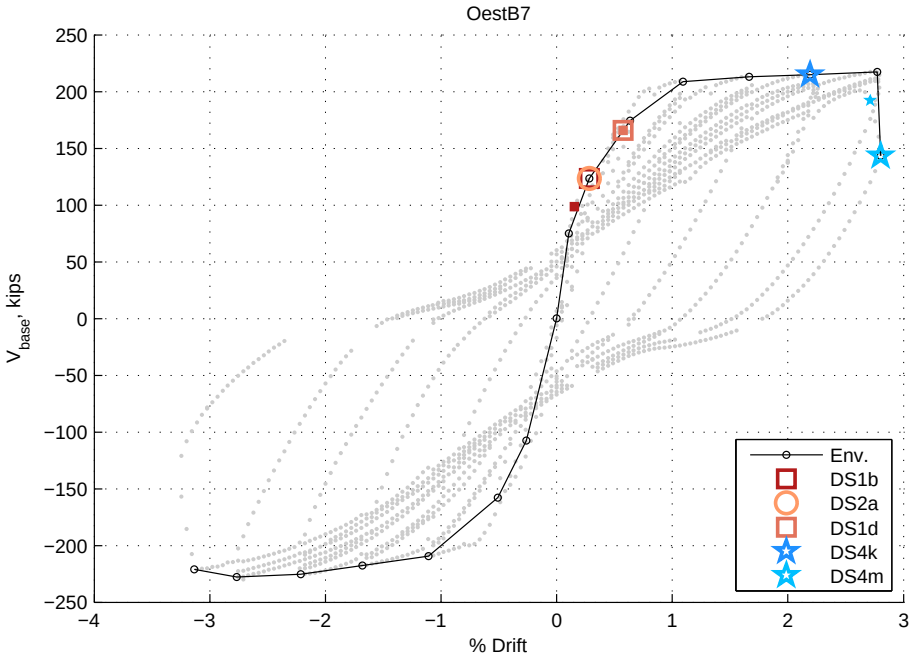

Figure A.67: Envelope for OestB7

A.40 OestB8

Table A.67: OestB8 damage information

MOR	DS	% Drift	Force, kips (kN)	Description	Figure
1	DS1b	-0.23%	-85.0 (-378.1)	Initial flexural cracking; data taken from force-disp of initial cycles	
	DS1d	-0.52%	-162.1 (-721.1)	As determined from moment-curvature analysis	
2	DS2a	-0.53%	-163.9 (-729.2)	Spalling & flaking along diagonal cracks (cycle 20); Crushing of concrete cover (cycle 14; use 13)	
4	DS4k	2.17%	211.2 (939.6)	Initial indication of crushing on both ends of horizontal crack formed along length of web 9 inches above the base (cycle 26; use 25)	
	DS4m	-3.21%	-235.5 (-1047.6)	Initial indication of crushing on both ends of horizontal crack formed along length of web 9 inches above the base (cycle 26; use 25)	
	DSr1	0.49%	155.4 (691.3)	Reported tensile yield	
	DSr9	-2.79%	-238.6 (-1061.5)	Diagonal cracks of 0.086 inches following cycle 28 displacement level	

Table A.68: OestB8 crack width information

					Crack Width, in (mm)	
DS	% Drift	Force, kips (kN)	Exact/Max	Crack Type	Max.	Resid.
DSr1	0.53%	158.0 (703.0)	Max	Shear Flexure	0.011 (0.28) 0.01 (0.25)	
DSr9	-2.79%	-238.6 (-1061.5)	Max	Shear	0.086 (2.2)	

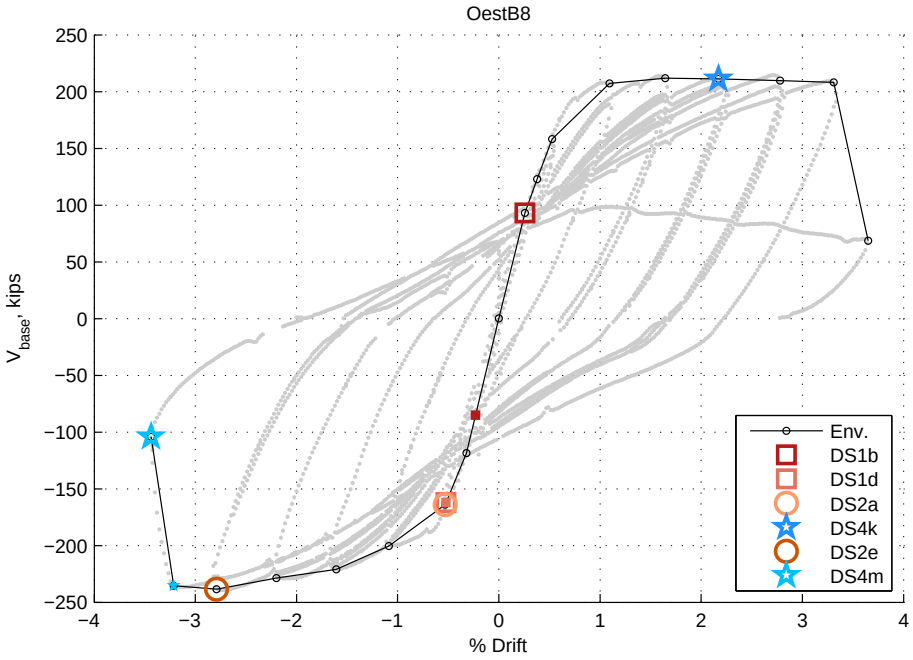

Figure A.68: Envelope for OestB8

A.41 OestB9

Table A.69: OestB9 damage information

MOR	DS	% Drift	Force, kips (kN)	Description	Figure
1	DS1b	0.16%	75.0 (333.6)	Initial flexural cracking; data taken from force-disp of initial cycles	
	DS1d	0.45%	156.1 (694.4)	As determined from moment-curvature analysis	
2	DS2a	1.24%	209.8 (933.3)	First indication of cover crushing on outer compression face (cycle 20)	
4	DS4m	-2.99%	-220.5 (-981.0)	Crushing of compression structs in lower left region; immediately followed by development of failure plane along diagonal crack (used maximum displacement of test due to unique disp. history)	
	DSr1	0.26%	158.0 (702.8)	Reported tensile yield	

Table A.70: OestB9 crack width information

					Crack Width, in (mm)	
DS	% Drift	Force, kips (kN)	Exact/Max	Crack Type	Max.	Resid.
DSr1	0.45%	157.5 (700.5)	Max	Shear	0.015 (0.38)	
				Flexure	0.011 (0.28)	

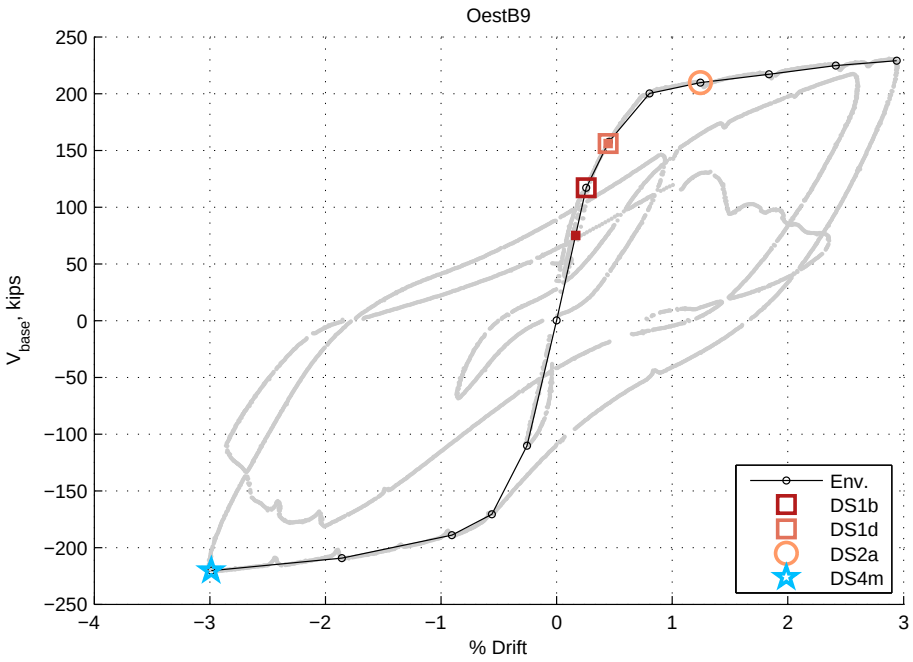

Figure A.69: Envelope for OestB9

A.42 OestB10

Table A.71: OestB10 damage information

MOR	DS	% Drift	Force, kips (kN)	Description	Figure
1	DS1b	0.14%	75.0 (333.6)	Initial flexural cracking occurred on way to cycle 2 stage 13 at 75 kips	
	DS1d	0.27%	102.9 (457.8)	As determined from moment-curvature analysis	
2	DS2a	0.63%	147.6 (656.7)	Crushing of concrete cover (cycle 2 load stage 15)	
	DS2b	-1.13%	-147.0 (-654.0)	Spalling of patched concrete (cycle 2 load stage 21)	
4	DS4f	-3.37%	-110.6 (-491.9)	Failure ultimately occurred due to damage of boundary element, including core crushing, bar buckling and bar fracture	
	DSr1	0.22%	120.0 (533.8)	Reported tensile yield	

Table A.72: OestB10 crack width information

					Crack Width, in (mm)	
DS	% Drift	Force, kips (kN)	Exact/Max	Crack Type	Max.	Resid.
DSr1	0.22%	94.3 (419.4)	Max	Shear	0.019 (0.48)	
				Flexure	0.011 (0.28)	
C1	0.37%	117.9 (524.4)	Max	Shear	0.019 (0.48)	
				Flexure	0.011 (0.28)	
C2	2.72%	169.8 (755.4)	Max	Shear	0.095 (2.4)	
				Flexure	0.036 (0.91)	

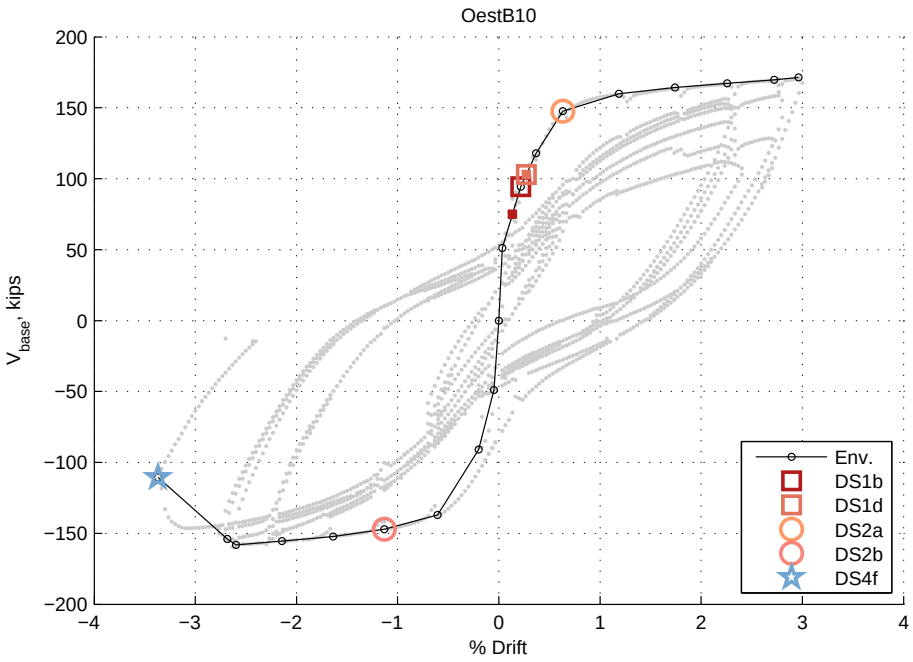

Figure A.70: Envelope for OestB10

A.43 OestF1

Table A.73: OestF1 damage information

MOR	DS	% Drift	Force, kips (kN)	Description	Figure
1	DS1b	0.05%	40.1 (178.2)	Initial flexural cracking; data taken from force-disp of initial cycles	
	DS1d	0.56%	147.6 (656.5)	As determined from moment-curvature analysis	
2	DS2a	-1.11%	-173.4 (-771.2)	Minor spalling and flaking along construction joint and diagonal cracks observed in cycle 20 (cycle 19 used because this was maximum historic drift)	
	DS2d	-1.11%	-173.4 (-771.2)	Vertical cracking in outer face of flange in cycle 20, possibly due to bowing caused by web expansion (cycle 19 used because this was maximum historic drift)	
4	DS4k	-1.86%	-173.5 (-771.8)	Steepest diagonal strut in web crushed and slipped (flange hinged to allow)	
	DSr1	0.56%	150.6 (669.9)	Reported tensile yield	

Table A.74: OestF1 crack width information

					Crack Width, in (mm)	
DS	% Drift	Force, kips (kN)	Exact/Max	Crack Type	Max.	Resid.
DSr1	-0.62%	-152.4 (-678.0)	Max	Shear	0.018 (0.46)	

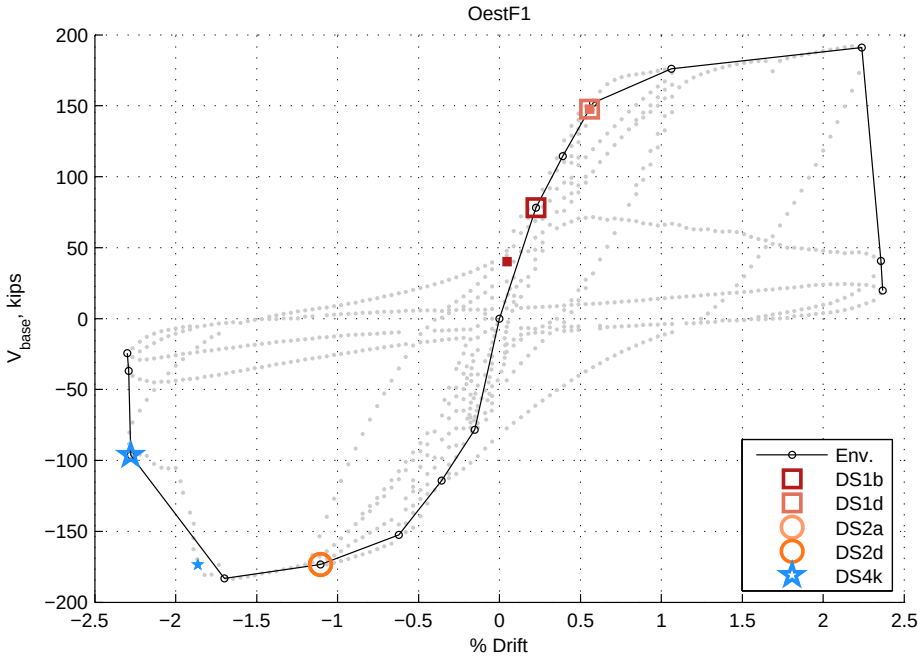

Figure A.71: Envelope for OestF1

A.44 OestF2

Table A.75: OestF2 damage information

MOR	DS	% Drift	Force, kips (kN)	Description	Figure
1	DS1b	0.09%	78.7 (350.0)	Initial flexural cracking; data taken from force-disp of initial cycles	
	DS1d	0.47%	159.9 (711.1)	As determined from moment-curvature analysis	
2	DS2a	-1.11%	-188.3 (-837.4)	Minor spalling and flaking along diagonal cracks	
	DS2d	-2.21%	-204.3 (-908.7)	Vertical cracking in lower 2.5 ft of flange	
4	DS4k	2.77%	205.7 (915.1)	Steepest diagonal strut in web crushed and slipped (flange hinged to allow this)	
	DS4m	-2.63%	-202.1 (-899.1)	Several struts in unconfined region crushed at once, immediately followed by shearing of compression flange and fracture of horizontal reinforcing bar	
	DSr1	0.46%	156.0 (693.9)	Reported tensile yield	

Table A.76: OestF2 crack width information

					Crack Width, in (mm)	
DS	% Drift	Force, kips (kN)	Exact/Max	Crack Type	Max.	Resid.
DSr1	0.52%	174.2 (774.8)	Max	Shear	0.012 (0.3)	
				Flexure	0.012 (0.3)	

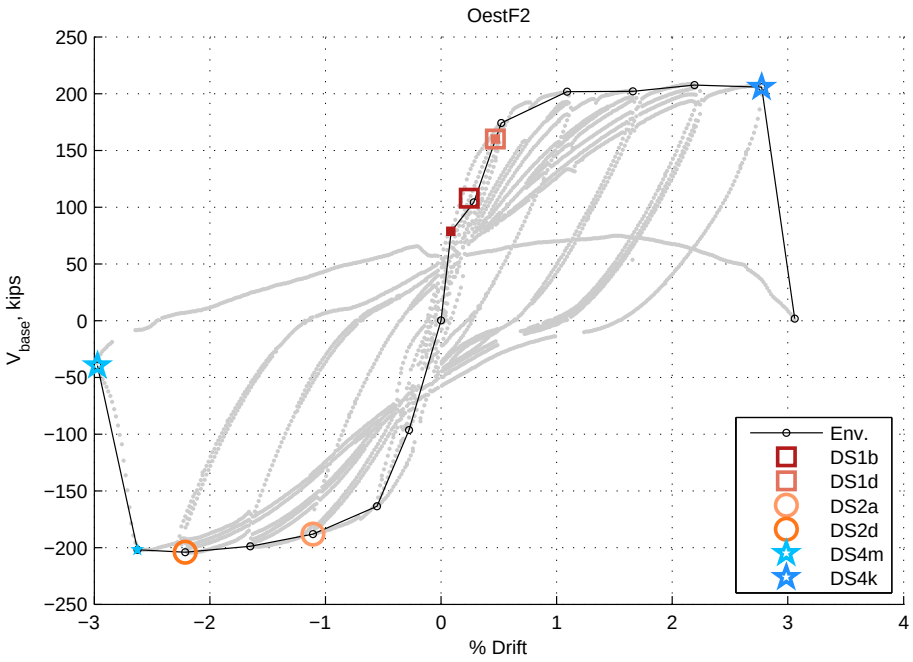

Figure A.72: Envelope for OestF2

A.45 Morgan

Table A.77: Morgan damage information

MOR	DS	% Drift	Force, kips (kN)	Description	Figure
1	DS1a	-0.11%	-12.2 (-54.3)	Crack map for first displacement level shows cracking occurred	Fig. A.74
	DS1d	0.10%	14.7 (65.3)	As determined from moment-curvature analysis	
2	DS2a	-1.10%	-20.9 (-92.8)	Crack map shows minor spalling occurred on way to steps 108/111; occurred approximately 1/3 way up first floor	Fig. A.75
	DS2d	0.72%	22.9 (102.1)	Crack map shows vertical cracking occurred on way to steps 88/91	Fig. A.76
3	DS3a	-1.46%	-17.6 (-78.2)	Crack map shows exposed reinforcement ccurred on way to steps 128/131	Fig. A.77
4	DS4c	1.79%	16.0 (71.0)	Assummed failure mode. Loss of lateral load capacity dropped less than 80% of max	
	DSr1	0.30%	19.7 (87.7)	Initial yield occurred in boundary element at 83% of maximum load. Data taken from positive envelope since 83% occurs on this in cycle sooner than on negative envelope	Fig. A.78

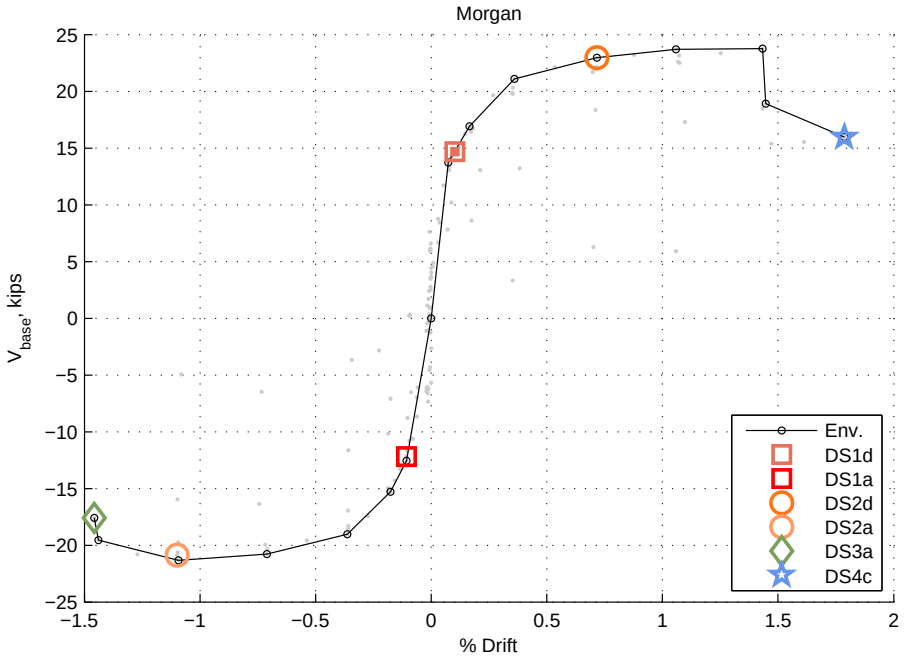

Figure A.73: Envelope for Morgan

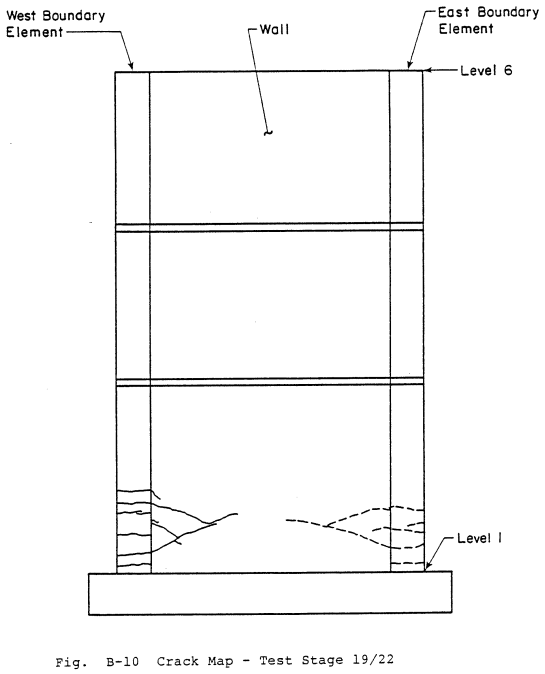

Fig. B-10 Crack Map - Test Stage 19/22

Figure A.74: Morgan: DS1a - crack map after steps 19/22

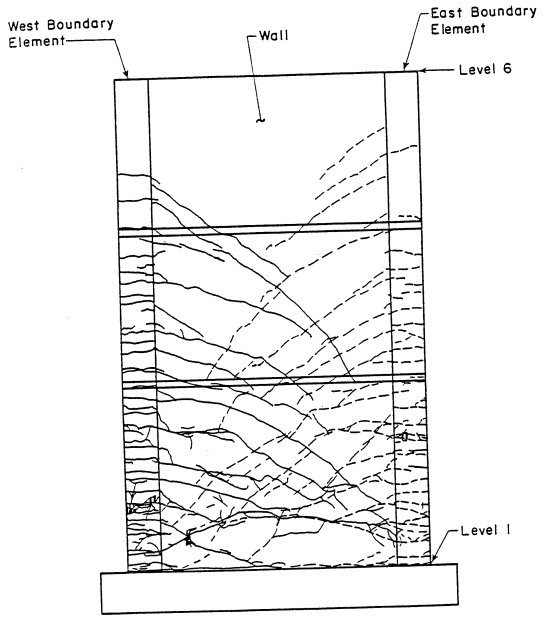

Fig. B-14 Crack Map - Test Stage 108/111

Figure A.75: Morgan: DS2a - crack map after steps 108/111

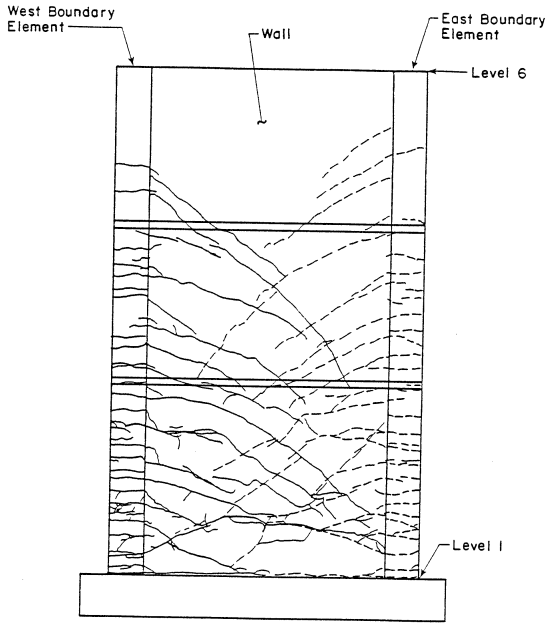

Fig. B-13 Crack Map - Test Stage 88/91

Figure A.76: Morgan: DS2d - crack map after steps 88/91

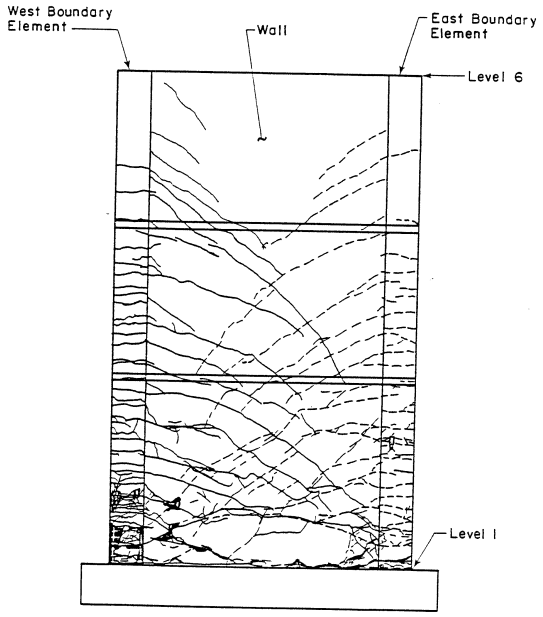

Fig. B-15 Crack Map - Test Stage 128/131

Figure A.77: Morgan: DS3a - crack map after steps 128/131

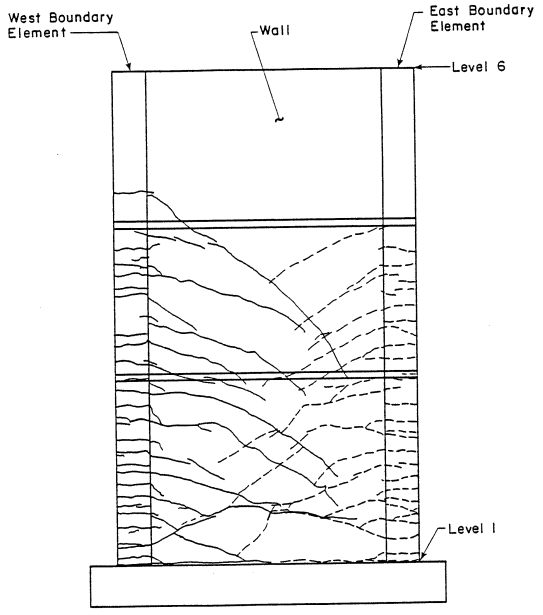

Fig. B-12 Crack Map - Test Stage 65/68

Figure A.78: Morgan: DSr1 - crack map after steps 65/68

A.46 LiuW1

Table A.78: LiuW1 damage information

MOR	DS	% Drift	Force, kips (kN)	Description	Figure
1	DS1b	-0.09%	-17.8 (-79.4)	Hairline crack at 150mm from base of wall at location of confining reinforcement; cycle 4a/4b (p. 39)	Fig. A.80
	DS1c	-0.28%	-34.4 (-153.2)	Shear crack developed from initial bottom flexural crack, inclined 45 degrees towards base; cycle 7a/7b (p. 39)	Fig. A.81
	DS1d	1.06%	58.1 (258.3)	As determined from moment-curvature analysis	
	DS1e	-1.16%	-57.6 (-256.1)	Compression yield ; cycle 20a (use data from 19a/b) (p. 41)	Fig. A.86
	DS1f	-3.02%	-55.5 (-246.8)	Shear yield; cycle 37a (p. 42)	
2	DS2a	1.50%	58.5 (260.3)	50mm above base in boundary region; Described as crushing, but interpretted to be spalling of cover and reinforcement not exposted; cycle 25a (p. 40)	
	DS2c	2.61%	56.9 (253.2)	Spalling in web; cycle 34a (p. 40)	Fig. A.83
4	DS4b	-2.64%	-57.3 (-254.7)	Longitudinal buckling of bars in boundary elements and spalling revealing confinement hoops; cycle 36b (p. 40)	Fig. A.84, **??**
	DS4f	2.98%	57.1 (253.8)	Loss of lateral load carrying capacity due to severe buckling of reinforcement and severe spalling and crushing of the concrete; cycle 40a (p. 41) but cycle 37a used for recording damage state b/c larger drift	Fig. A.85
	DSr1	0.54%	48.4 (215.2)	First yield in long. reinf. at base of wall; cycle 10a (p. 41)	Fig. A.86

Table A.79: LiuW1 crack width information

DS	% Drift	Force, kips (kN)	Exact/Max	Crack Type	Crack Width, in (mm) Max.	Resid.
DS1c	-0.28%	-34.4 (-153.2)	Max	Flexure	0.0039 (0.1)	
DSr1	0.54%	48.4 (215.2)	Max	Shear	0.016 (0.4)	
				Flexure	0.024 (0.6)	
C1	-0.28%	-34.4 (-153.2)	Max	Flexure	0.0039 (0.1)	
C2	-0.28%	-34.4 (-153.2)	Max	Flexure	0.0079 (0.2)	
C3	-0.58%	-48.0 (-213.6)	Max	Shear	0.016 (0.4)	
				Flexure	0.024 (0.6)	
C4	-0.79%	-56.7 (-252.0)	Max	Shear	0.022 (0.55)	
				Flexure	0.026 (0.65)	

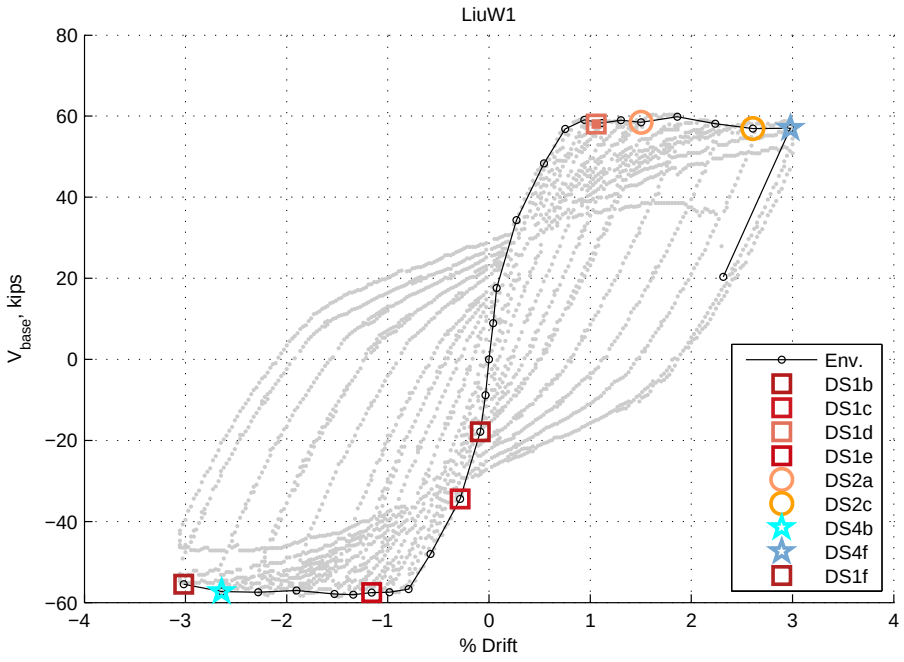

Figure A.79: Envelope for LiuW1

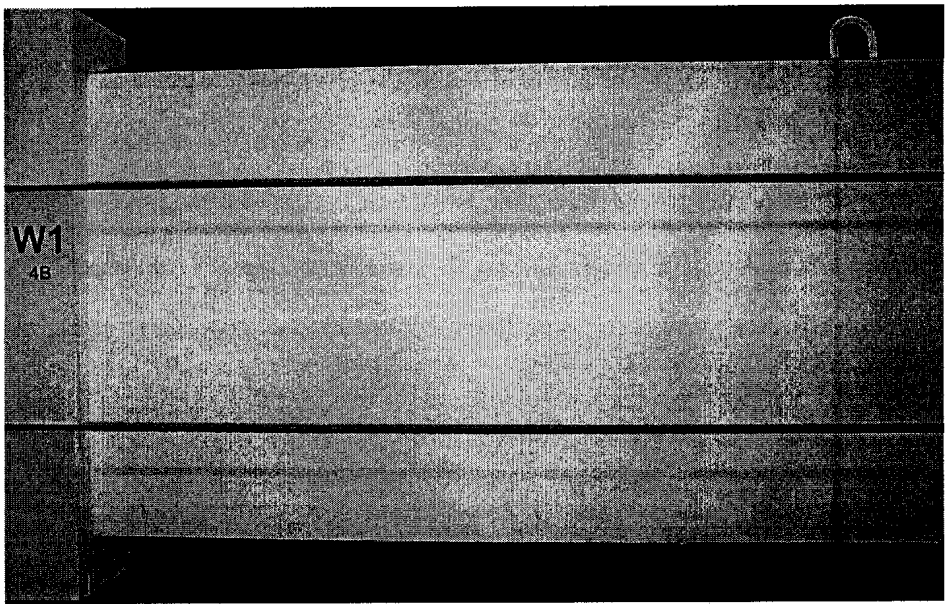

Figure A.80: LiuW1: DS1b - photo after initial cracking

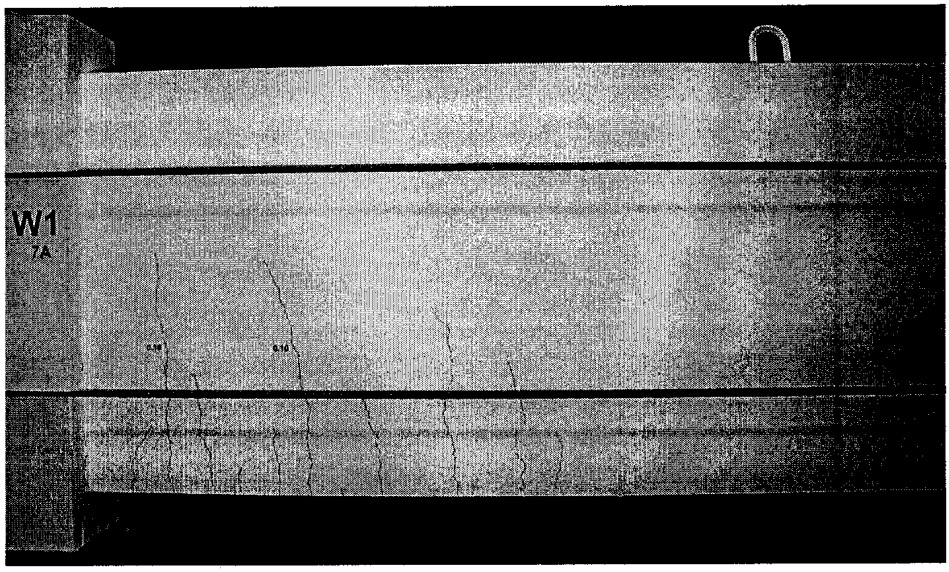

Figure A.81: LiuW1: DS1c - photo after 2.0Mcr cycles

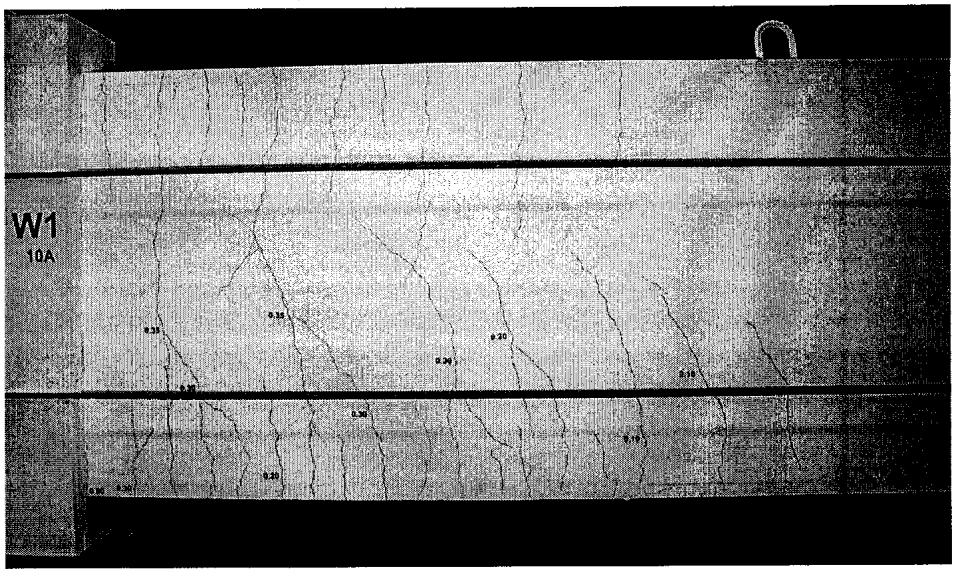

Figure A.82: LiuW1: DS1e - cracking of first yield

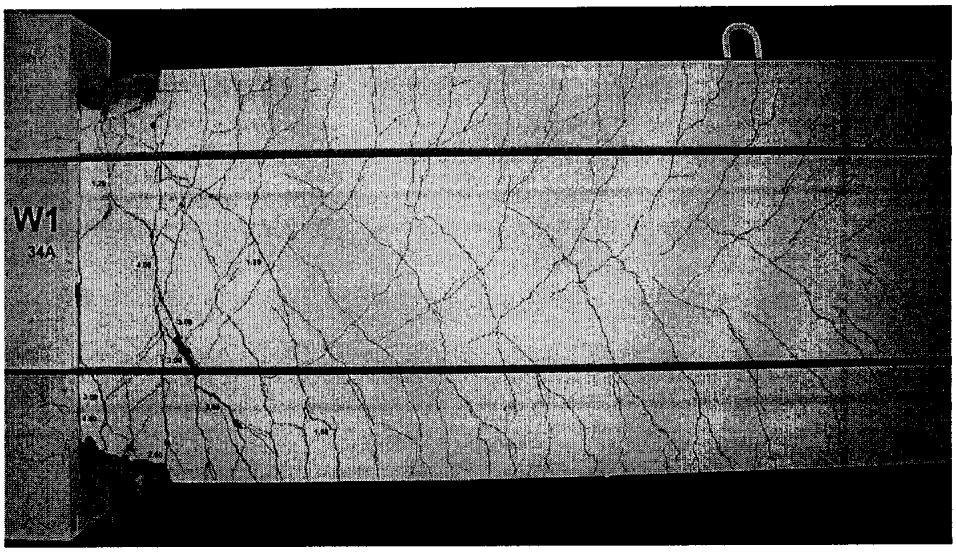

Figure A.83: LiuW1: DS2c - cracking at first cycle of 3.80 Delta_y; spalling in web

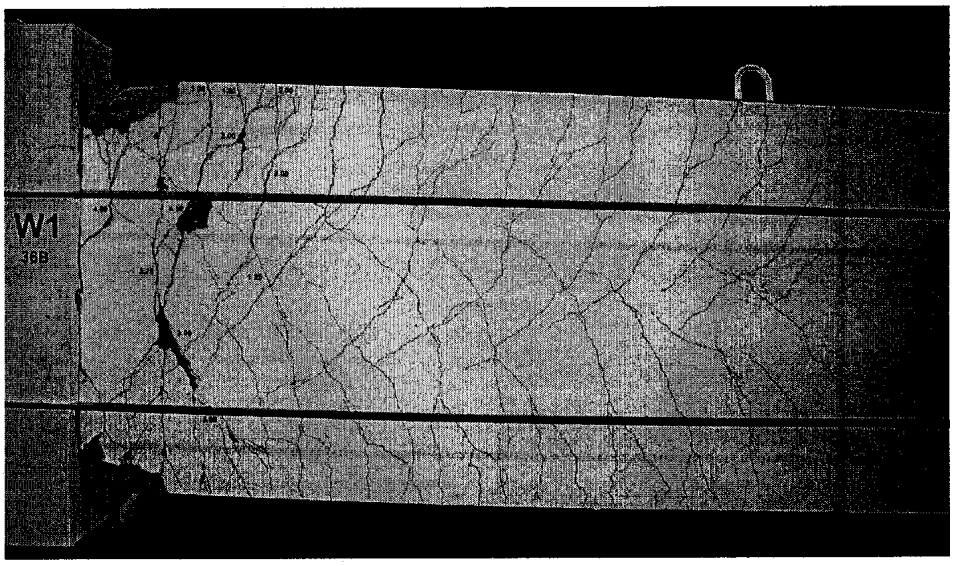

Figure A.84: LiuW1: DS4b - cracking after final cycle of 3.80 Delta_y; longitudinal buckling

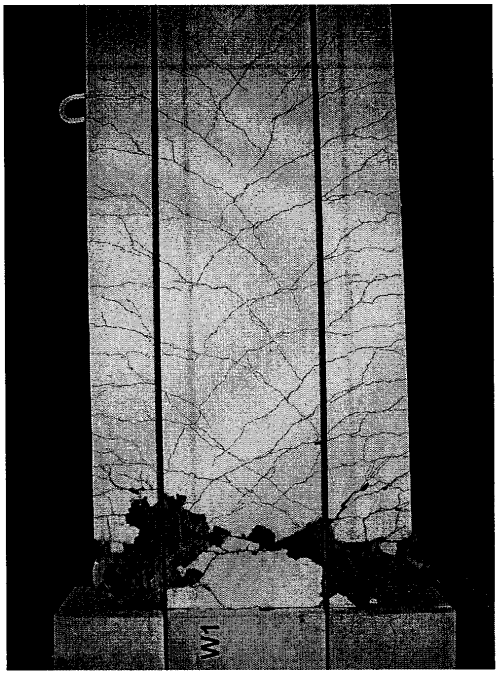

Figure A.85: LiuW1: DS4f - photo at failure

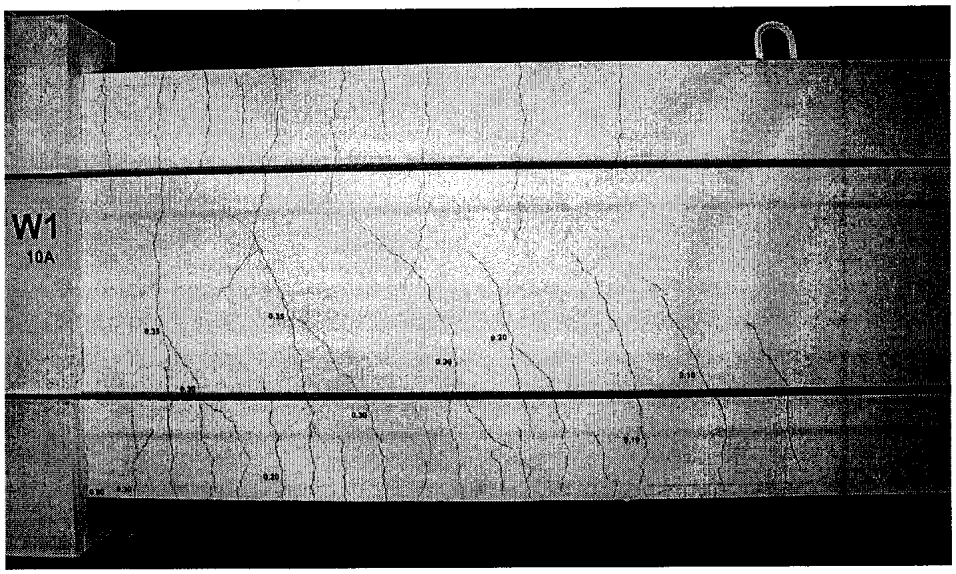

Figure A.86: LiuW1: DSr1 - cracking of first yield

A.47 LiuW2

Table A.80: LiuW2 damage information

MOR	DS	% Drift	Force, kips (kN)	Description	Figure
1	DS1b	0.09%	22.4 (99.6)	Hairline crack at 50mm from base of wall at location of confining reinforcement; cycle 4a/4b (p. 44)	Fig. A.88
	DS1c	-0.40%	-44.5 (-197.8)	Shear crack developed from initial bottom flexural crack, inclined 45 degrees towards base; cycle 7a/7b (p. 45)	Fig. A.89
	DS1d	1.24%	60.8 (270.6)	As determined from moment-curvature analysis	
	DS1f	1.95%	62.9 (279.7)	Shear yield; cycle 31a (p. 46)	Fig. A.92
2	DS2a	1.30%	61.1 (271.8)	150mm above base in boundary region; Described as crushing, but interpretted to be spalling of cover and reinforcement not exposted; cycle 25a (p. 45)	Fig. A.91
	DS2c	1.95%	62.9 (279.7)	Spalling in web; cycle 31a (p. 45)	Fig. A.92
4	DS4b	2.92%	57.4 (255.4)	Longitudinal buckling of bars in boundary elements and spalling revealing confinement hoops; cycle 40a (p. 45)	Fig. A.93, **??**
	DS4f	2.97%	46.9 (208.8)	Loss of lateral load carrying capacity due to severe buckling of reinforcement and severe spalling and crushing of the concrete; cycle 40a (p. 45-46)	Fig. A.94
	DSr1	0.66%	57.9 (257.7)	First yield in long. reinf. at base of wall; cycle 13a/b (p. 46)	Fig. A.95

Table A.81: LiuW2 crack width information

					Crack Width, in (mm)	
DS	% Drift	Force, kips (kN)	Exact/Max	Crack Type	Max.	Resid.
DS1c	-0.40%	-44.5 (-197.8)	Max	Flexure	0.0079 (0.2)	
DSr1	0.66%	57.9 (257.7)	Max	Shear	0.016 (0.4)	
				Flexure	0.024 (0.6)	
C1	-0.40%	-44.5 (-197.8)	Max	Flexure	0.0079 (0.2)	
C2	-0.40%	-44.5 (-197.8)	Max	Flexure	0.014 (0.35)	
C3	-0.45%	-46.5 (-207.1)	Max	Shear	0.016 (0.4)	
				Flexure	0.016 (0.4)	
C4	0.66%	57.9 (257.7)	Max	Shear	0.022 (0.55)	
				Flexure	0.024 (0.6)	

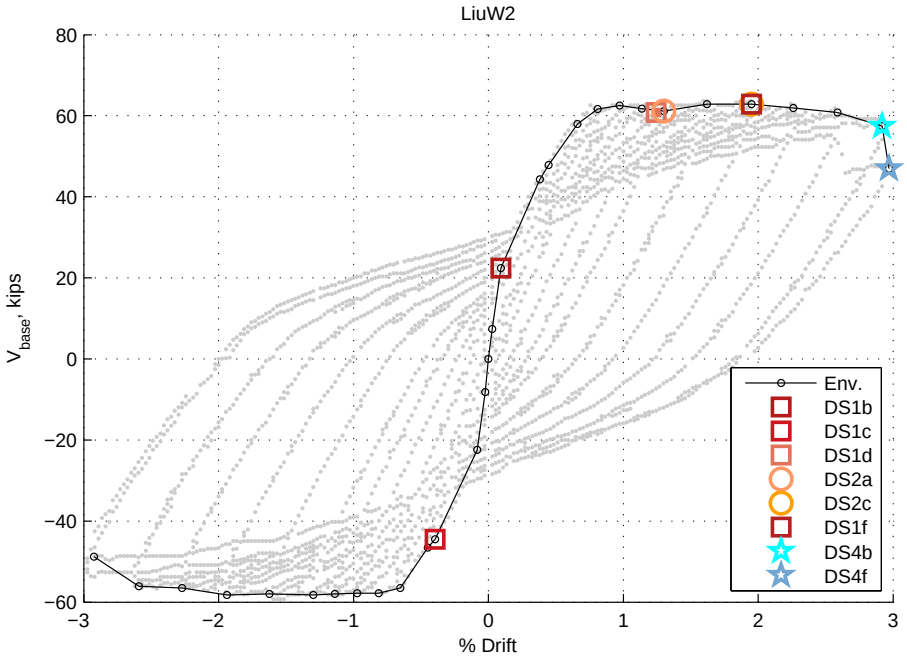

Figure A.87: Envelope for LiuW2

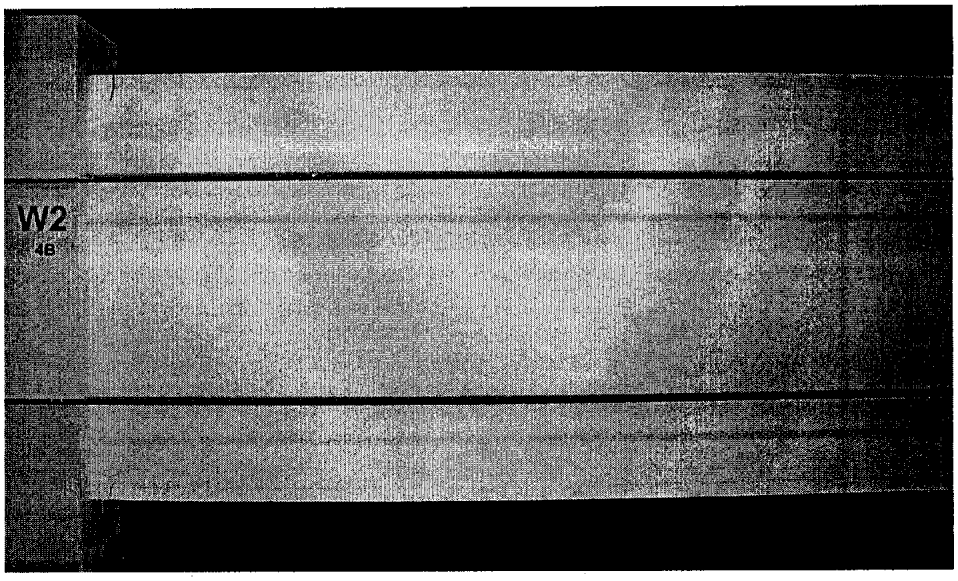

Figure A.88: LiuW2: DS1b - photo after initial cracking

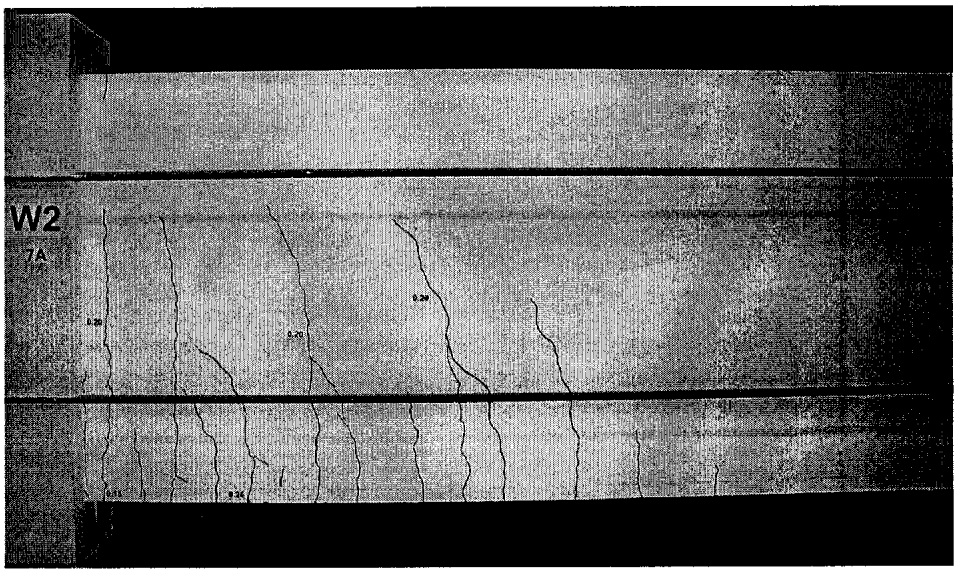

Figure A.89: LiuW2: DS1c - photo after 2.0Mcr cycles

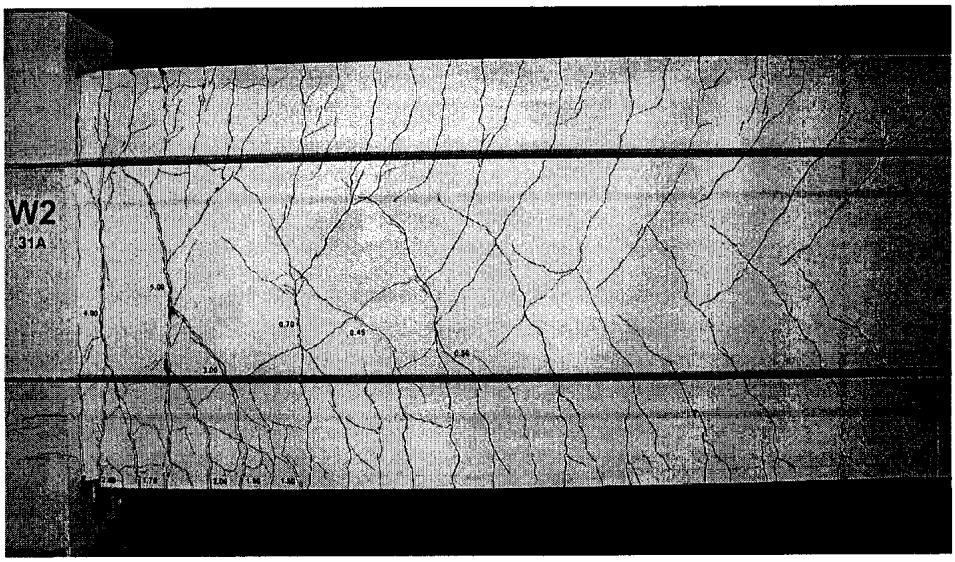

Figure A.90: LiuW2: DS1f - cracking of 3.38 Deltay

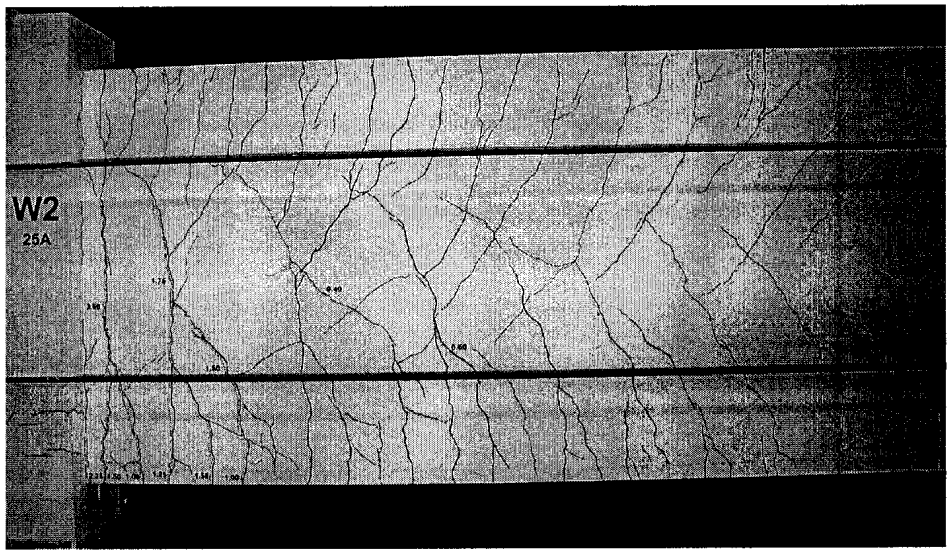

Figure A.91: LiuW2: DS2a - cracking of 2.25*Deltay

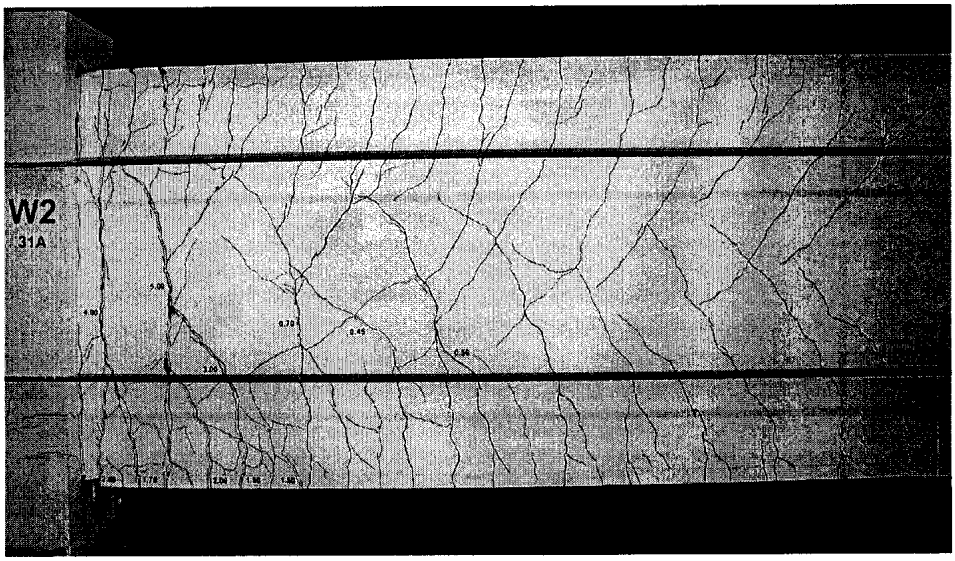

Figure A.92: LiuW2: DS2c - cracking at first cycle of 3.80 Delta_y; spalling in web

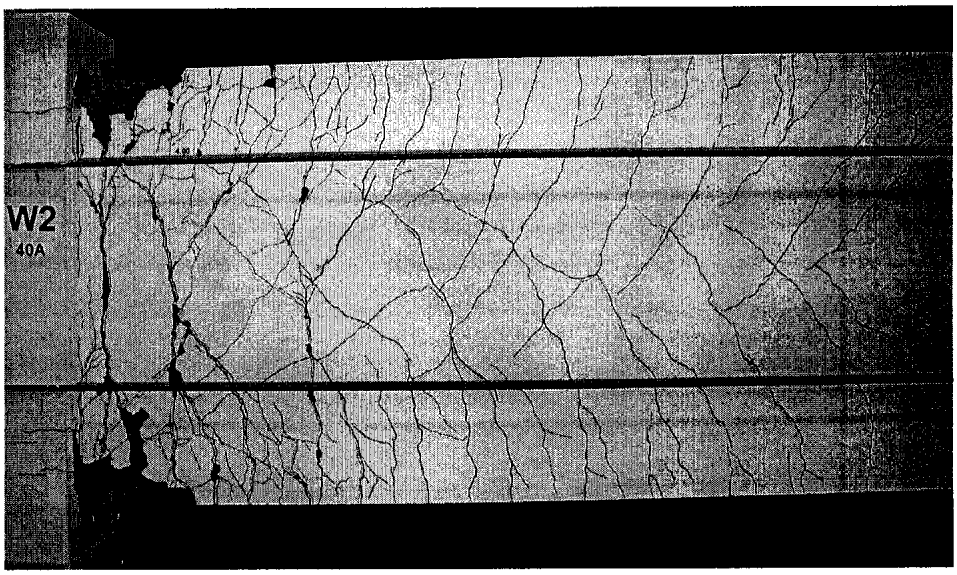

Figure A.93: LiuW2: DS4b - cracking after cycle 40a

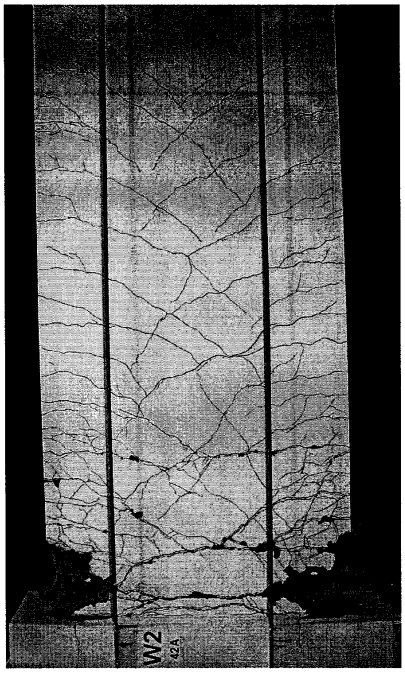

Figure A.94: LiuW2: DS4f - photo at failure

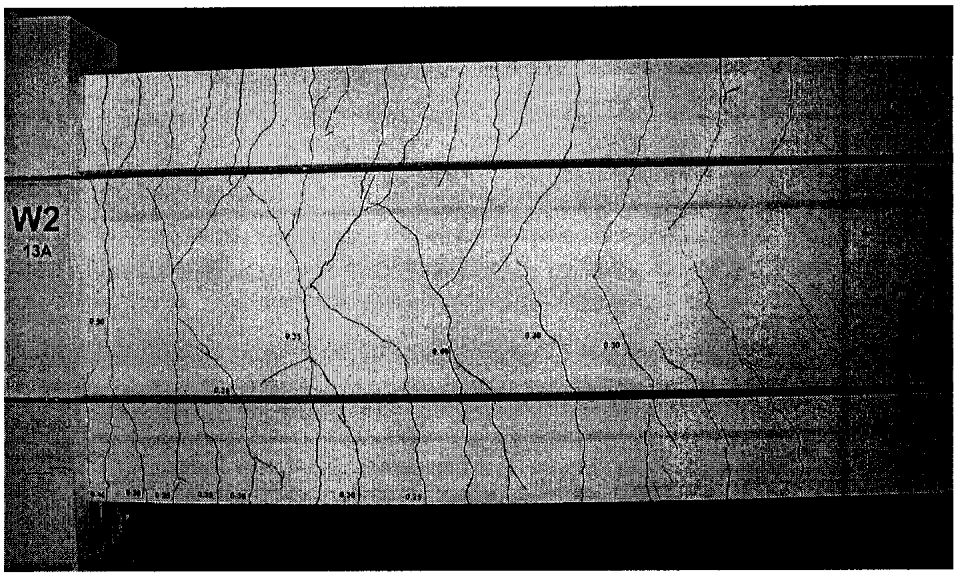

Figure A.95: LiuW2: DSr1 - cracking of first yield

A.48 AliW1

Table A.82: AliW1 damage information

MOR	DS	% Drift	Force, kips (kN)	Description	Figure
1	DS1b	-0.26%	-16.5 (-73.4)	Cycles 1 and 2 flexural cracking in b.e. lower two stories grew into shear cracks (p. 32)	
	DS1c	-0.26%	-16.5 (-73.4)	Cycles 1 and 2 flexural cracking in b.e. lower two stories grew into shear cracks (p. 32)	
	DS1d	0.75%	31.0 (137.7)	As determined from moment-curvature analysis	
2	DS2a	-1.54%	-31.7 (-141.0)	Cycle 9: minor crushing in east boundary element that spalled of in next cycle (p. 34-35)	Fig. A.97, **??**, **??**
	DSr10	-2.57%	-35.2 (-156.6)	Cycle 13/14: largest crack measuring 0.2 inches (p. 35)	
	DSr9	-2.06%	-33.3 (-148.1)	Cycle 11/12: largest crack measuring 0.12 inches (p. 35)	

Table A.83: AliW1 crack width information

					Crack Width, in (mm)	
DS	% Drift	Force, kips (kN)	Exact/Max	Crack Type	Max.	Resid.
DSr9	-2.06%	-33.3 (-148.1)	Max	Shear	0.12 (3)	
DSr10	-2.57%	-35.2 (-156.6)	Max	Shear	0.2 (5.1)	
C1	-0.77%	-29.3 (-130.3)	Max	Shear	0.025 (0.64)	
C2	-0.77%	-29.3 (-130.3)	Max	Shear	0.04 (1)	
C3	-1.03%	-31.3 (-139.2)	Max	Shear	0.06 (1.5)	
C4	-2.06%	-33.3 (-148.1)	Max	Shear	0.12 (3)	
C5	-2.57%	-35.2 (-156.6)	Max	Shear	0.2 (5.1)	

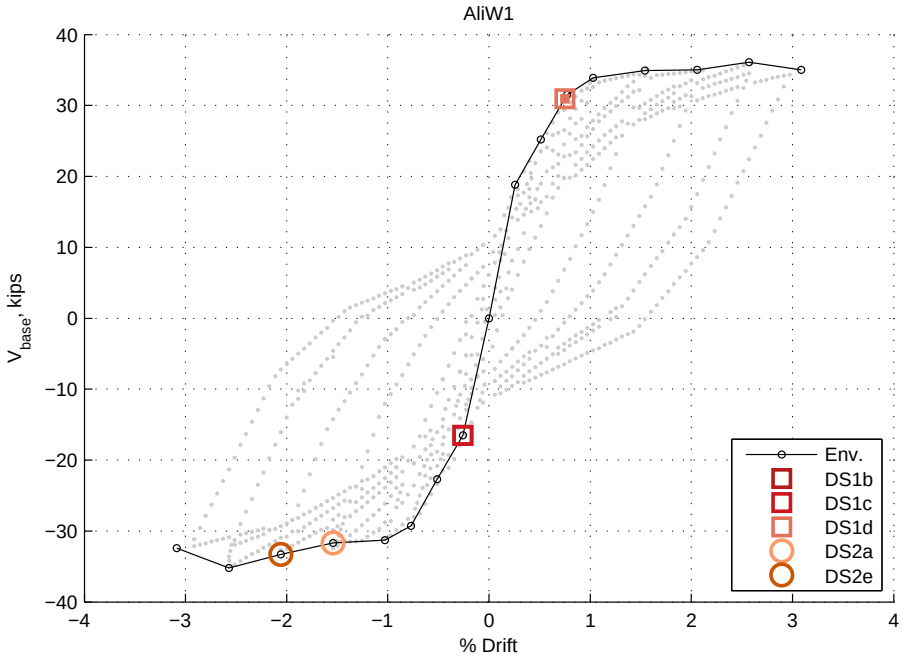

Figure A.96: Envelope for AliW1

Figure A.97: AliW1: DS2a - photo of cylce 9 damage

A.49 TupperW3

Table A.84: TupperW3 damage information

MOR	DS	% Drift	Force, kips (kN)	Description	Figure
1	DS1b	-0.15%	-16.4 (-73.0)	Small hairline flexural cracks; cycle 2(p. 45)	
	DS1c	0.76%	58.9 (262.0)	cycle 4(p. 45)	
	DS1d	0.72%	56.9 (253.2)	As determined from moment-curvature analysis	
	DS1e	0.76%	58.9 (262.0)	Compression yield of b.e. reinforcement; cycle 4(p. 45)	
2	DS2a	1.60%	75.3 (334.9)	Stated as crushing in compression zone, interpretted to be cover spalling; cycle 7(p. 46)	Fig. A.99
4	DS4f	2.92%	71.3 (317.1)	'it is clear that failure occurred due to severe distress in the compression zone, with concrete crushing, rupturing of one of the confining hoops and local buckling of the longitudinal bars"; cycle 10(p. 46-47)	Fig. A.100
	DSr1	0.72%	56.5 (251.2)	Reported tensile yield; value given in report is said to be estimate; cycle 4(p. 45)	

Table A.85: TupperW3 crack width information

					Crack Width, in (mm)	
DS	% Drift	Force, kips (kN)	Exact/Max	Crack Type	Max.	Resid.
DS2a	1.60%	75.3 (334.9)	Max	Shear	0.059 (1.5)	
C1	1.09%	72.4 (322.1)	Max	Flexure	0.016 (0.4)	
C2	1.99%	74.0 (329.0)	Max	Flexure	0.059 (1.5)	

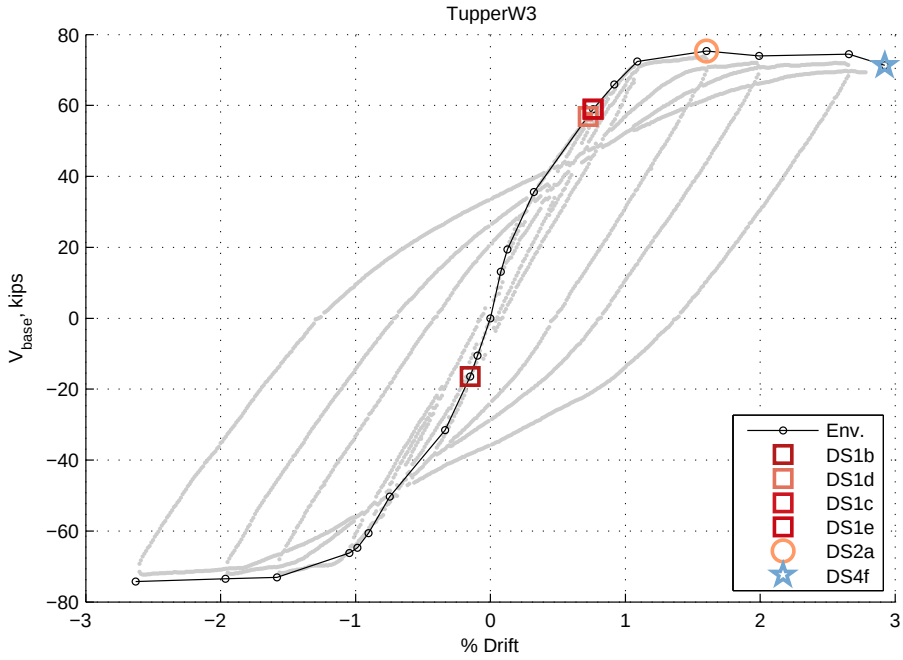

Figure A.98: Envelope for TupperW3

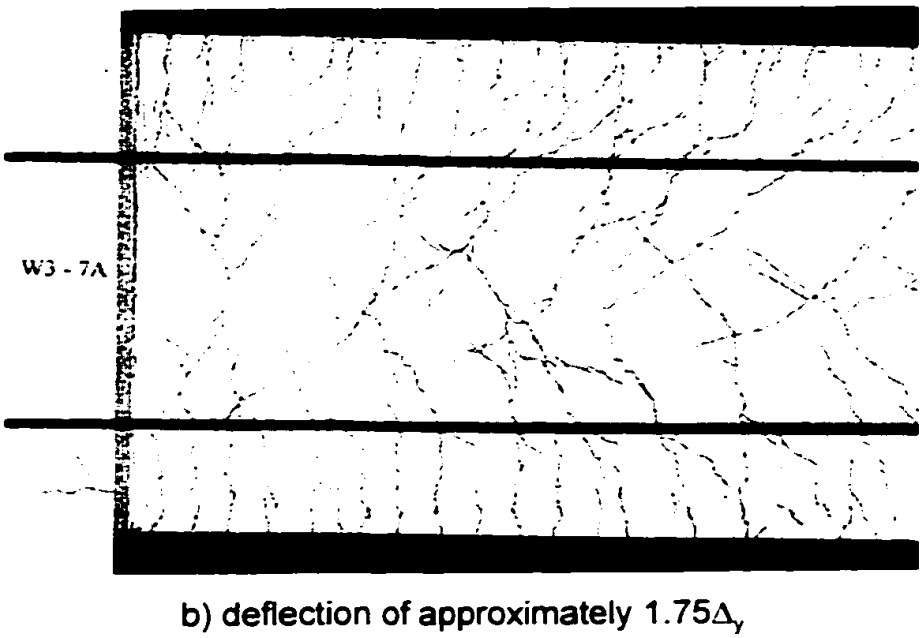

Figure A.99: TupperW3: DS2a - deflection of approximately 1.75 Deltay

Figure A.100: TupperW3: DS4f - final damage of wall

A.50 MobeenW1

Table A.86: MobeenW1 damage information

MOR	DS	% Drift	Force, kips (kN)	Description	Figure
1	DS1a	0.08%	34.2 (152.0)	Initial cracking; second cycle at 3mm drift level; 238mm above base of wall (p. 101)	
	DS1d	-0.51%	-74.3 (-330.6)	As determined from moment-curvature analysis	
	DS1e	0.67%	81.8 (363.7)	Reported compression yield; 24mm displacement level, nearly all extreme vertical bars yielded in tension and compression (p. 101)	
2	DS2a	1.17%	84.1 (374.3)	Spalling started at 42mm disp level, not stated if exposes reinforcement (p. 102)	
4	DS4b	1.85%	85.5 (380.4)	Large chunks of concrete spalled off revealing buckled visible bars at approx. 125 mm above base (p. 102)	
	DS4e	-2.18%	-68.1 (-303.0)	Moving towards negative 78mm, bar fracture in southwest corner caused drop in lateral load (p. 102)	
	DSr1	0.35%	59.5 (264.7)	Reported tensile yield; 12mm displacement level vertical reinforcement just beyond yield strain (p. 101)	
	DSr11	-3.85%	-67.8 (-301.6)	Maximum crack width at end of test is 8.5mm (p. 108)	Fig. A.102
	DSr14	-1.51%	-82.8 (-368.5)	Stirrups first yielded on north side near base at 54mm disp (p. 102)	

Table A.87: MobeenW1 crack width information

					Crack Width, in (mm)	
DS	% Drift	Force, kips (kN)	Exact/Max	Crack Type	Max.	Resid.
DSr1	0.35%	59.5 (264.7)	Max	Any	0.016 (0.4)	
DS1e	0.67%	81.8 (363.7)	Max	Any	0.024 (0.6)	
DS2a	1.17%	84.1 (374.3)	Max	Any	0.059 (1.5)	
DSr11	-3.85%	-67.8 (-301.6)	Max	Any	0.33 (8.5)	

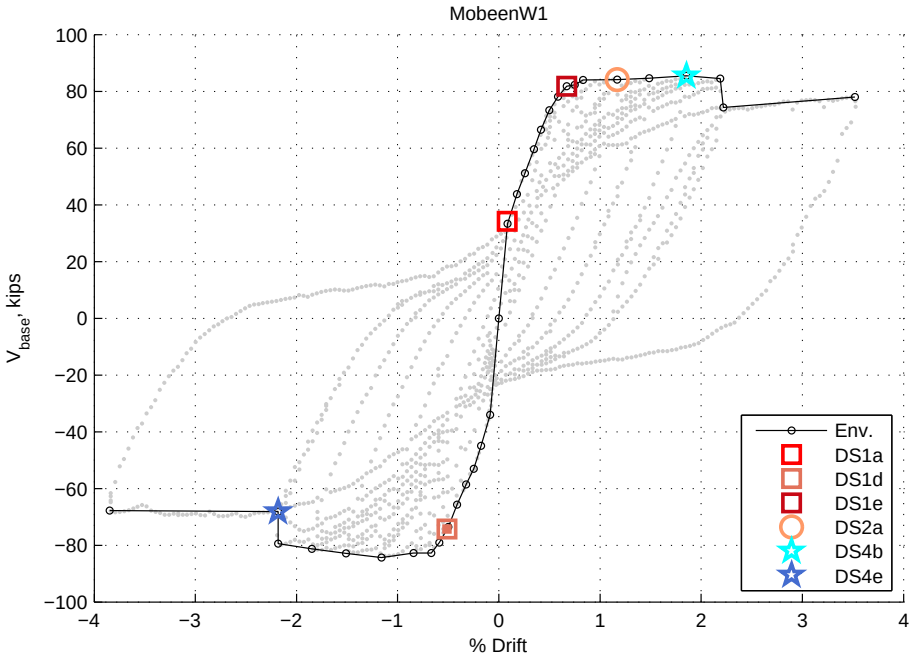

Figure A.101: Envelope for MobeenW1

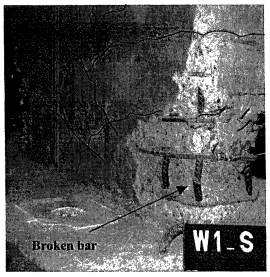

Figure 4.21 South side view of W-1 after test with broken bar visible

Figure 4.22 North side view of W-1 after test with buckled bars

Figure A.102: MobeenW1: DSr11 - Final damage of wall (close up of boundary element)

A.51 RivaW1

Table A.88: RivaW1 damage information

MOR	DS	% Drift	Force, kips (kN)	Description	Figure
1	DS1d	-0.48%	-100.5 (-447.2)	As determined from moment-curvature analysis	
2	DS2d	-2.09%	-181.2 (-806.0)	Vertical crack close to the ground floor	
4	DS4e	3.14%	150.2 (667.9)	Bar fracture of longitudinal web reinforcement when unloading from positive peak of cycle 30 to the negative peak; fracture was described as a tensile failure with necking	
	DSr1	-1.06%	-131.7 (-585.8)	Yield assummed to occur in cycles 25 due to presentation of results	
	DSr11	-3.17%	-173.6 (-772.4)	10mm wide crack in boundary element	

Table A.89: RivaW1 crack width information

					Crack Width, in (mm)	
DS	% Drift	Force, kips (kN)	Exact/Max	Crack Type	Max.	Resid.
DSr1	-1.06%	-131.7 (-585.8)	Max	Any	0.031 (0.8)	
DSr11	-3.17%	-173.6 (-772.4)	Max	Shear	2 (50)	
				Flexure	0.39 (10)	

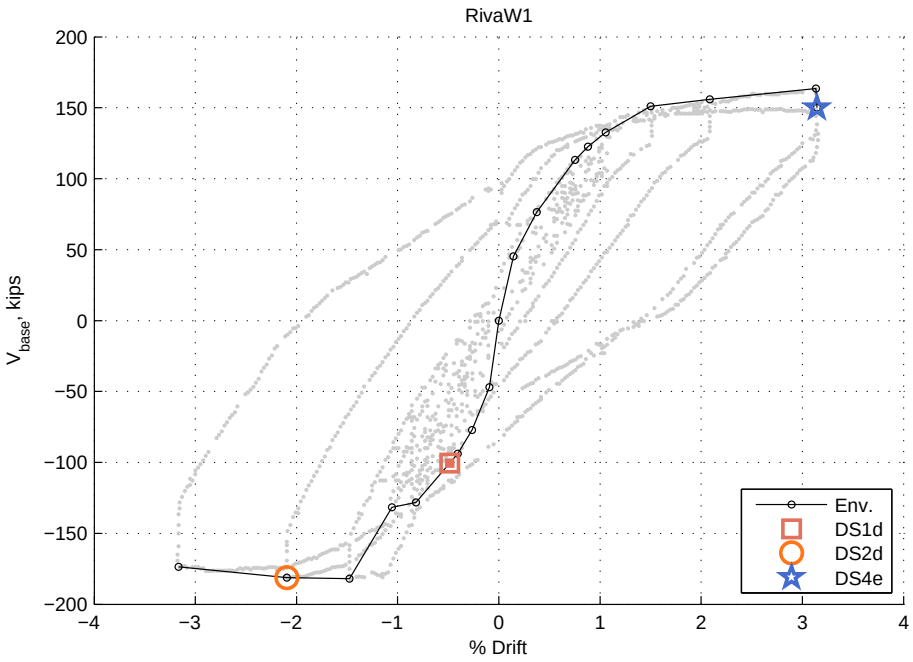

Figure A.103: Envelope for RivaW1

A.52 ShiuC1

Table A.90: ShiuC1 damage information

MOR	DS	% Drift	Force, kips (kN)	Description	Figure
1	DS1a	0.14%	15.1 (67.2)	Initial cracking occurred at 15.1 kips (p. B4)	Fig. A.105
	DS1d	0.52%	47.4 (211.0)	As determined from moment-curvature analysis	
4	DS4b	2.86%	74.8 (332.5)	Buckling of flexural reinforcement in spalled regions at base of wall at end of test((p. B6)	Fig. A.107
	DS4i	2.86%	74.8 (332.5)	Loss of lateral load carrying capacity due to sliding shear failure (severe distress in boundary element at main horizontal crack) (p. 23); exact point not included because occurs at lower drift than max historic	Fig. A.107
	DSr1	0.97%	62.4 (277.6)	Initial yielding occurred at 15.1 kips (p. B4)	

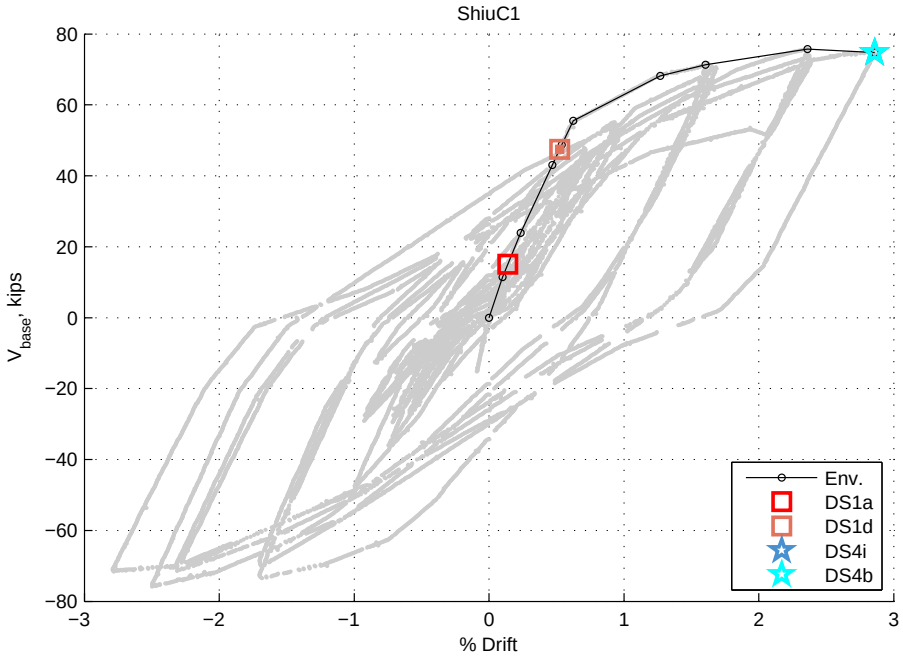

Figure A.104: Envelope for ShiuC1

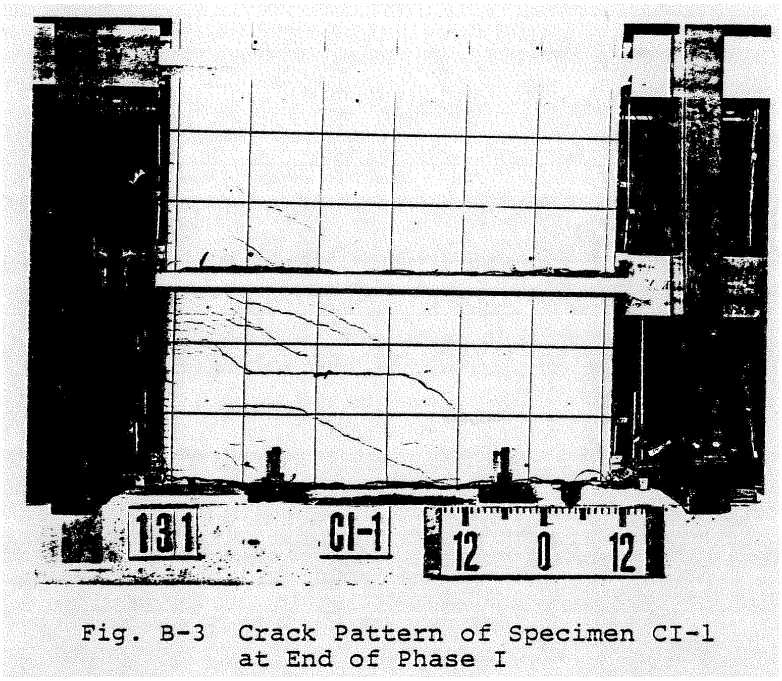

Figure A.105: ShiuC1: DS1a - crack pattern following first phase of testing

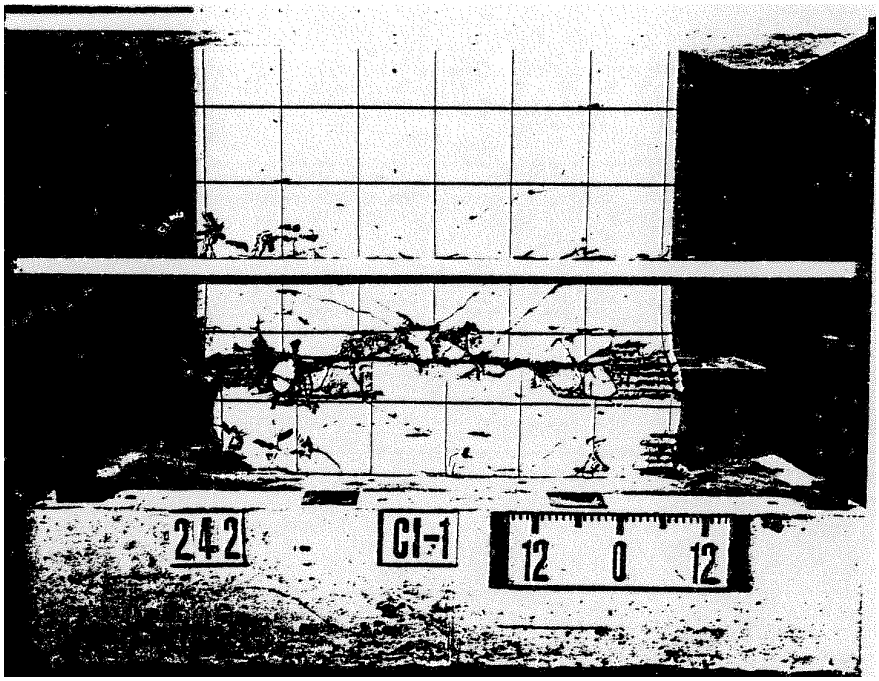

Figure A.106: ShiuC1: DS4b - final damage of wall

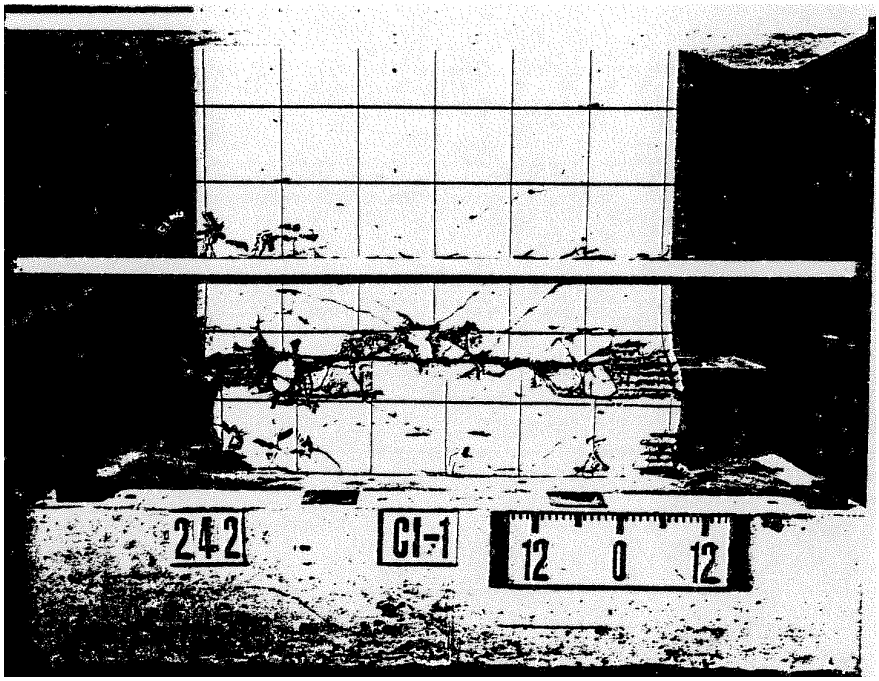

Figure A.107: ShiuC1: DS4i - final damage of wall

A.53 KhaC1

Table A.91: KhaC1 damage information

MOR	DS	% Drift	Force, kips (kN)	Description	Figure
1	DS1b	0.10%	6.7 (30.0)	Tension cracks at bottom and mid-height of wall	
	DS1c	1.48%	67.7 (301.0)	Pairs of diagonal cracks formed	
	DS1d	NaN%	NaN (NaN)	As determined from moment-curvature analysis	
4	DS4i	-2.57%	-67.6 (-300.8)	Shear failure occurred at 363 kN, but recorded as max neg. peak as this is the largest drift experienced; failure accompanied by large diagonal cracks from corner to corner, crushing of concrete at toe, and buckling vertical steel (no yielding)	

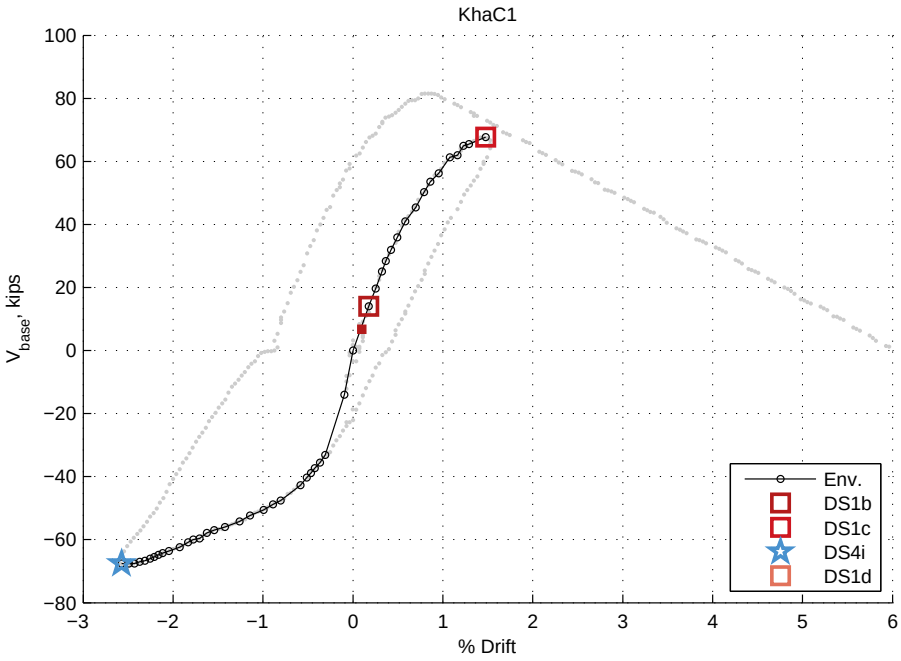

Figure A.108: Envelope for KhaC1

A.54 ElnCW2

Table A.92: ElnCW2 damage information

MOR	DS	% Drift	Force, kips (kN)	Description	Figure
1	DS1b	0.06%	10.0 (44.7)	Tension cracks developed near base of wall	
	DS1d	NaN%	NaN (NaN)	As determined from moment-curvature analysis	
4	DS4o	0.21%	22.1 (98.2)	Premature failure of wall due to bond slip of lap splice	

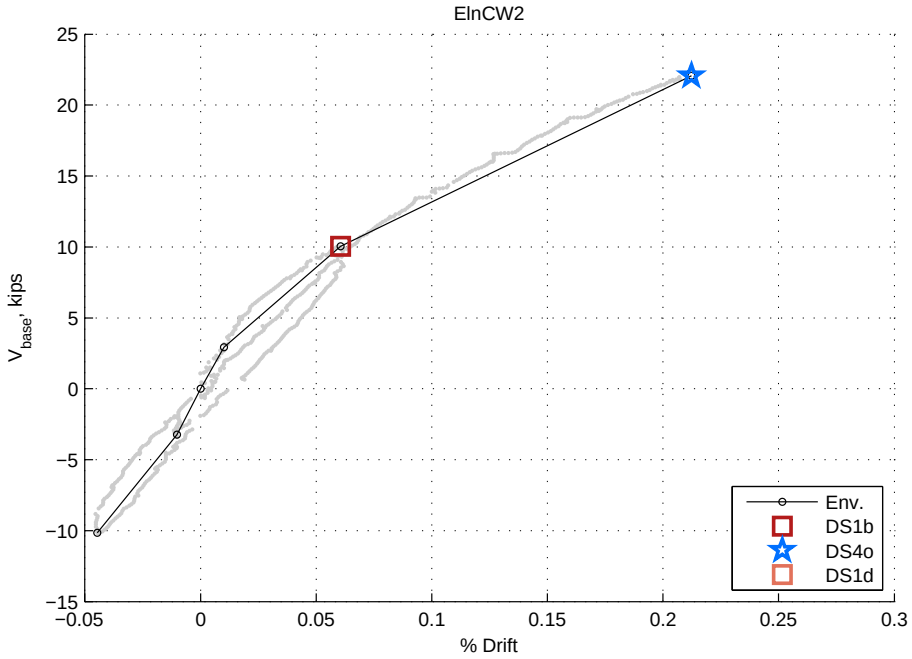

Figure A.109: Envelope for ElnCW2

A.55 ElnCW3

Table A.93: ElnCW3 damage information

MOR	DS	% Drift	Force, kips (kN)	Description	Figure
1	DS1b	0.04%	15.1 (67.0)	Horizontal cracks observed at base of wall	
	DS1c	0.10%	34.8 (155.0)	Diagonal cracks observed in both directions	
	DS1d	NaN%	NaN (NaN)	As determined from moment-curvature analysis	
4	DS4o	0.30%	44.5 (198.0)	Wall failed due to bond slip of lap splice	
	DSr5	0.24%	43.8 (195.0)	Diagonal cracks extended from corner to corner in both diagonal directions	

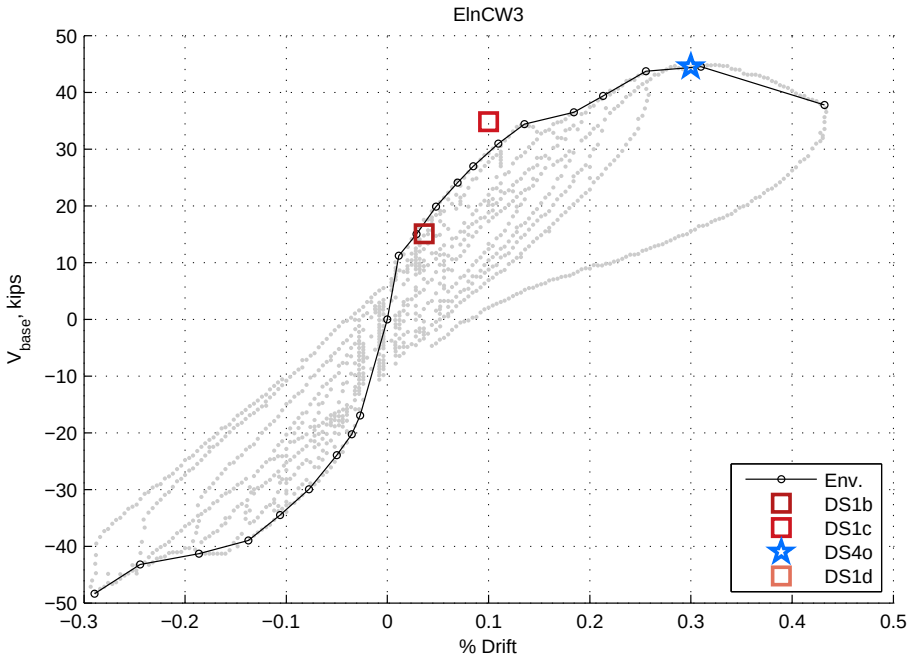

Figure A.110: Envelope for ElnCW3

A.56 IleX

Table A.94: IleX damage information

MOR	DS	% Drift	Force, kips (kN)	Description	Figure
1	DS1a DS1d	0.28% 0.43%	150.1 (667.7) 169.7 (754.9)	First cracking As determined from moment-curvature analysis	
4	DS4b DS4g	2.05% -3.08%	205.5 (914.1) -189.6 (-843.4)	Buckling at ends of flanges Rupture of previously buckled bars (some stirrups also ruptured)	

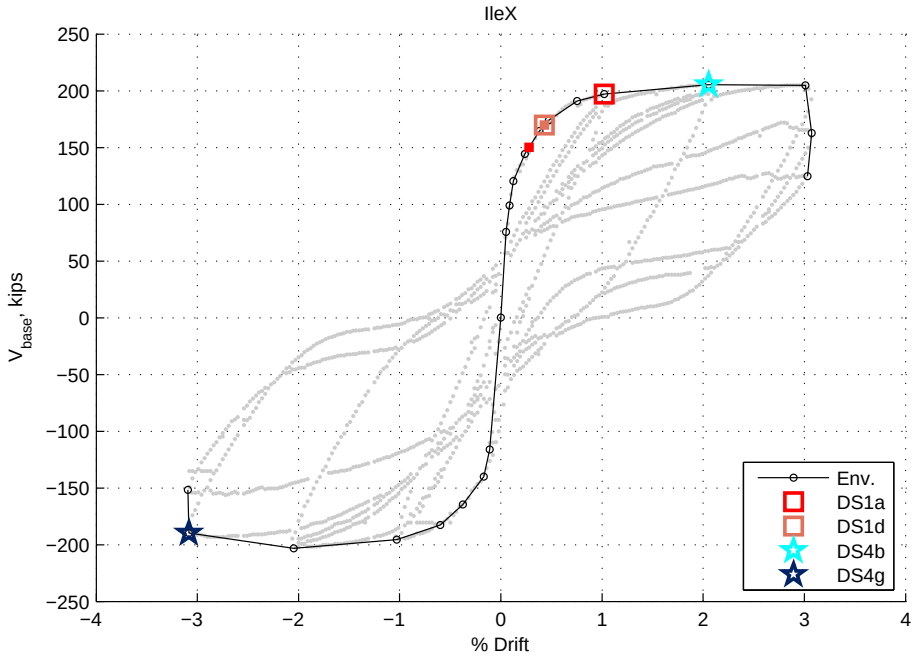

Figure A.111: Envelope for IleX

A.57 IleY

Table A.95: IleY damage information

MOR	DS	% Drift	Force, kips (kN)	Description	Figure
1	DS1b	-0.56%	-156.2 (-694.6)	Horizontal web cracks	
	DS1c	0.56%	137.8 (612.8)	First inclined cracking at base of flanges	
	DS1d	-0.23%	-123.2 (-548.2)	As determined from moment-curvature analysis	
4	DS4b	-1.02%	-170.9 (-760.3)	Steel bars at edges of flanges tended to buckle	
	DS4f	-3.07%	-142.4 (-633.4)	Drop in lateral load carrying capacity dictated by bar buckling at base of one flange extremity where one stirrup was missing (pos direction); bars buckle on corner of u-shape wall web (neg direction)	
	DSr1	0.36%	118.3 (526.3)	Initial yielding at 1.3cm	

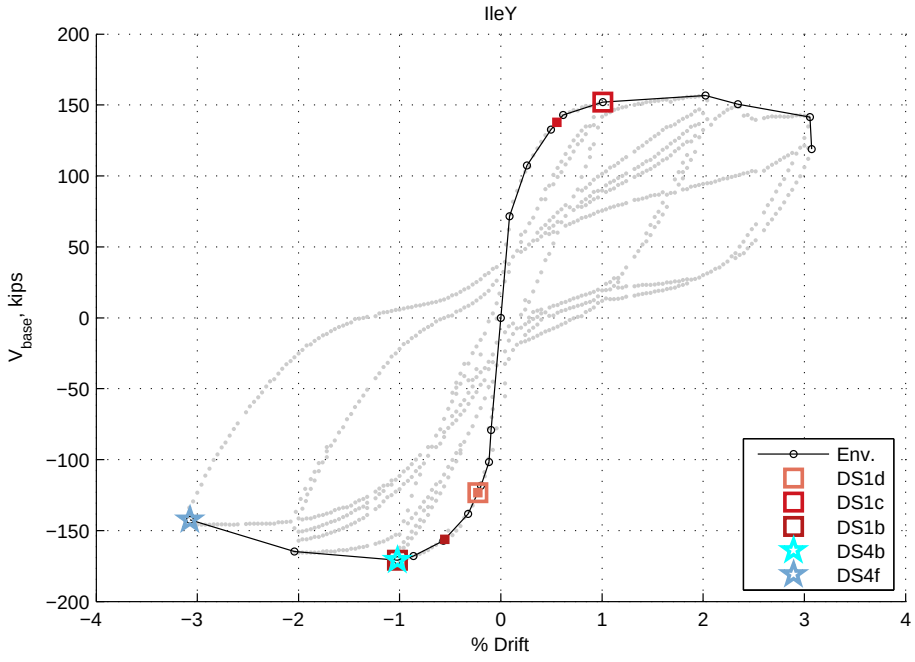

Figure A.112: Envelope for IleY

A.58 IleXY

Table A.96: IleXY damage information

MOR	DS	% Drift	Force, kips (kN)	Description	Figure
1	DS1d	0.58%	-170.2 (-757.0)	As determined from moment-curvature analysis	
4	DS4e	2.03%	-101.8 (-452.6)	During final 'fly' of 8cm displacement cycle, previously buckled bars fractured when straightening out; a shear failure of the flange was said to follow	Fig. A.114

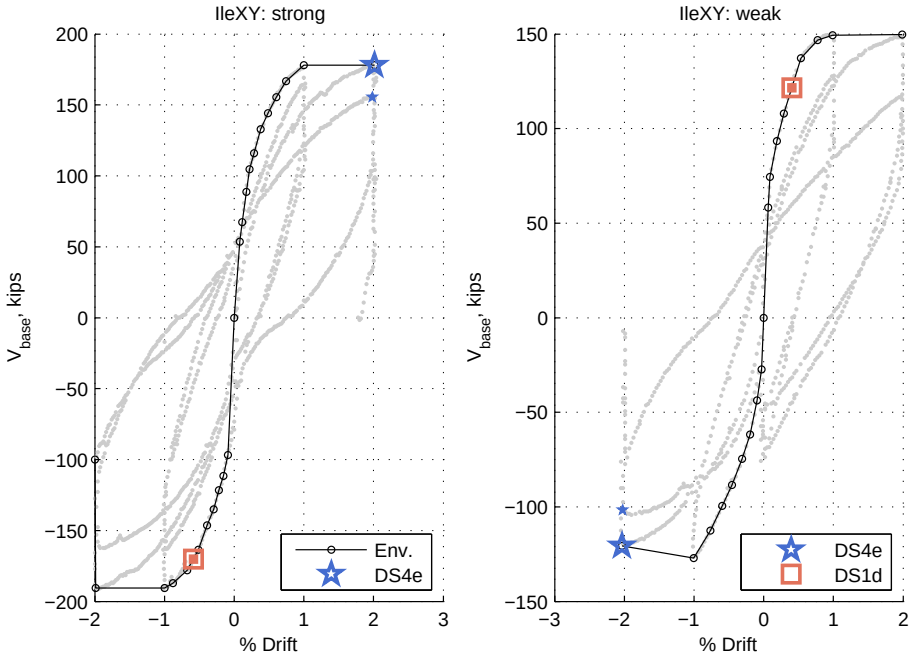

Figure A.113: Envelope for IleXY

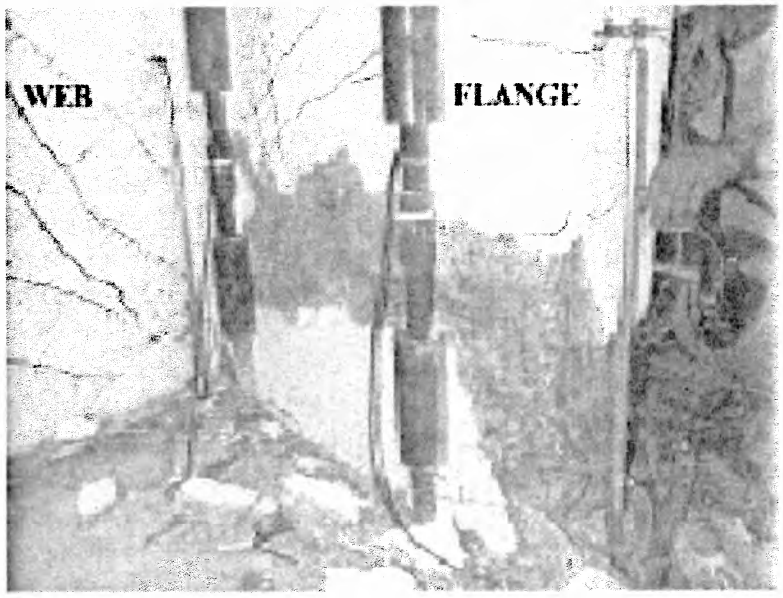

Fig. 14. Shear failure of one flange at the end of the XY direction test.

Figure A.114: IleXY: DS4e - Shear failure of flange

A.59 TUA

Table A.97: TUA damage information

MOR	DS	% Drift	Force, kips (kN)	Description	Figure
1	DS1d	0.49%	-96.8 (-430.5)	As determined from moment-curvature analysis	
2	DS2a	1.17%	87.7 (390.1)	Limited spalling following cycles at ductility=3	
4	DS4b	1.89%	-104.3 (-463.8)	Bar buckling first during diagonal cycle to ductility of -6	
	DS4e	2.51%	99.9 (444.2)	Bar fracture of D6 bars in west flange at ductility of 8 in positive strong axis bending (other cycles entered at ductility of 6)	
	DS4k	3.10%	77.7 (345.7)	Unconfined concrete in web and flanges 'decomposed'	

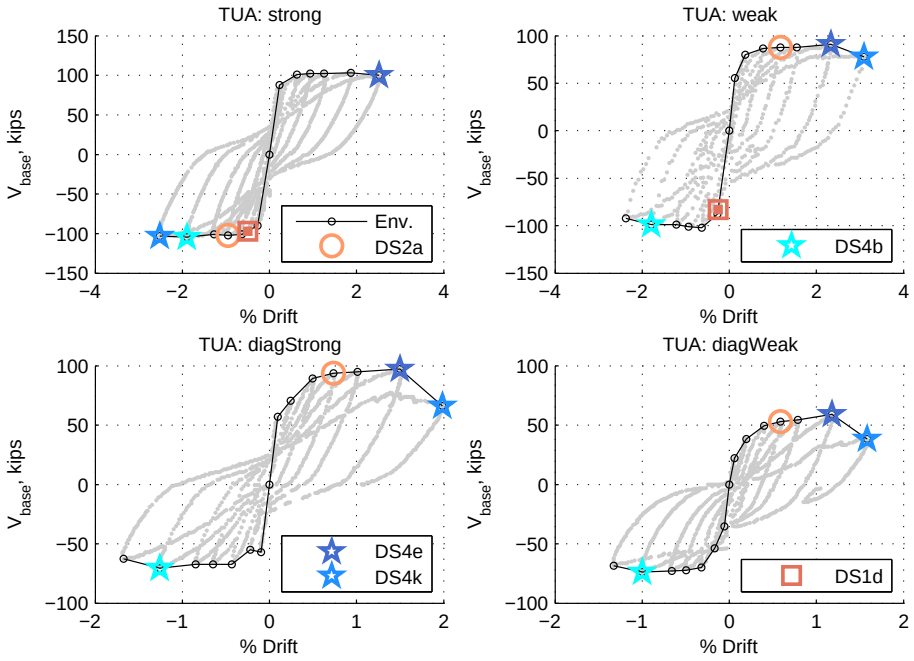

Figure A.115: Envelope for TUA

A.60 TUB

Table A.98: TUB damage information

MOR	DS	% Drift	Force, kips (kN)	Description	Figure
1	DS1d	0.66%	-94.4 (-419.8)	As determined from moment-curvature analysis	
2	DS2a	0.91%	78.9 (350.9)	Initial spalling (no exposed rebar) at ductility=2	
3	DS3a	1.80%	81.1 (360.7)	Spalling revealing longitudinal reinforcement at ductility=4 (NS cycles)	
4	DS4b	2.72%	83.3 (370.6)	Buckling during diagonal cycle to position E; two D12 bars in flange end buckled	
	DS4m	2.72%	83.3 (370.6)	Crushing of diagonal compression strut in web during sweeping cycle	

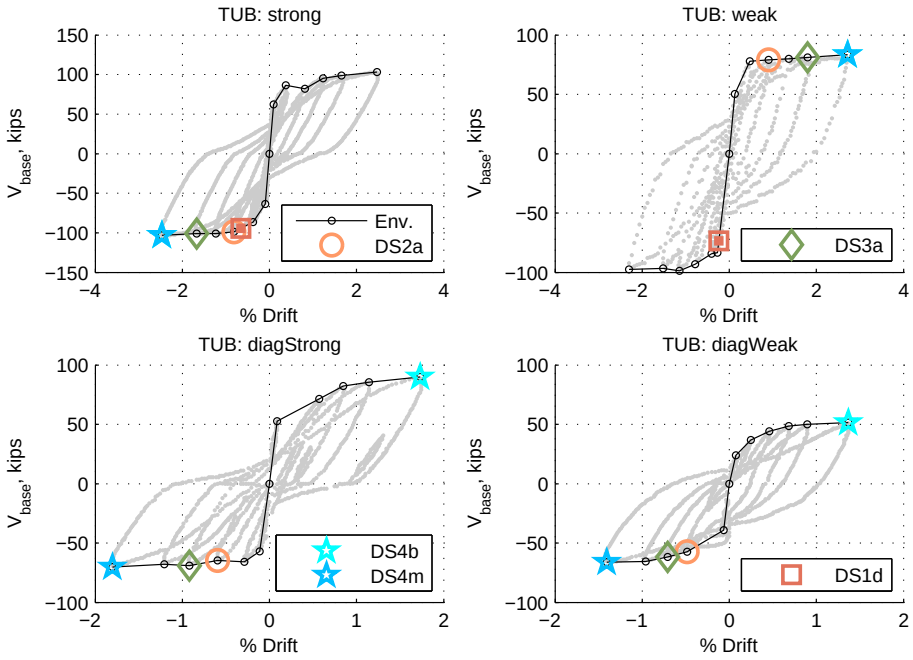

Figure A.116: Envelope for TUB

A.61 NTW1

Table A.99: NTW1 damage information

MOR	DS	% Drift	Force, kips (kN)	Description	Figure
1	DS1b	0.10%	37.4 (166.4)	Flex. cracks in web tip when flange in compression (flex. cracks in flange begin at next drift level and thus not entered)	
	DS1c	0.14%	-67.7 (-301.1)	Shear cracks in web under FC/FT loading	
	DS1d	1.93%	-72.5 (-322.5)	As determined from moment-curvature analysis	
2	DS2a	1.63%	-224.3 (-997.9)	Spalling of cover at base of web tip when flange is in tension (cracks equal to 1/8 inch at same step)	
4	DS4a	2.22%	-207.2 (-921.7)	Core crushing at third cycle in drift level	
	DS4b	2.22%	-207.2 (-921.7)	Bars buckled in web tip in first ramp of hourglass load cycle	
	DS4e	4.45%	-36.9 (-163.9)	Bar fracture and buckling in flange tips after first peak at drift level (weak axis bending); Bar fracture in web tip on next strong axis bending cycle	
	DS4m	0.99%	-29.5 (-131.4)	Web crushing while attempting to reach peak, unable to sustain gravity load	
	DS4p	4.44%	58.6 (260.5)	Core crushing flange tips under weak axis bending	
	DSr10	1.63%	-224.3 (-997.9)	cracks equal to 1/8 inch in middle two feet of flange (same point at which spalling occurs)	

Table A.100: NTW1 crack width information

DS	% Drift	Force, kips (kN)	Exact/Max	Crack Type	Crack Width, in (mm) Max.	Resid.
DS2a	-1.63%	-224.3 (-997.9)	Max	Shear	0.06 (1.5)	
				Flexure	0.13 (3.2)	
DSr10	-1.63%	-224.3 (-997.9)	Max	Shear	0.06 (1.5)	
				Flexure	0.13 (3.2)	
C1	-0.38%	-117.0 (-520.4)	Max	Shear	0.02 (0.51)	
C2	0.28%	62.3 (277.1)	Max	Shear	0.016 (0.41)	
C4	-0.10%	-26.1 (-116.2)	Max	Shear	0.01 (0.25)	
C5	-0.07%	-8.8 (-39.3)	Max	Shear	0.013 (0.33)	
C6	0.09%	29.6 (131.6)	Max	Shear	0.005 (0.13)	
C7	-0.07%	-8.8 (-39.3)	Max	Shear	0.013 (0.33)	
C8	-0.38%	-110.5 (-491.4)	Max	Shear	0.025 (0.64)	
C9	0.28%	62.3 (277.1)	Max	Shear	0.016 (0.41)	
C10	0.31%	71.4 (317.7)	Max	Shear	0.02 (0.51)	
C11	0.17%	50.4 (224.2)	Max	Shear	0.02 (0.51)	
C12	-0.07%	-8.8 (-39.3)	Max	Shear	0.013 (0.33)	
C13	-0.55%	-144.6 (-643.3)	Max	Shear	0.025 (0.64)	
C14	0.41%	80.9 (360.0)	Max	Shear	0.03 (0.76)	
				Flexure	0.007 (0.18)	
C15	-0.73%	-175.0 (-778.4)	Max	Shear	0.035 (0.89)	
				Flexure	0.035 (0.89)	
C16	0.54%	95.0 (422.6)	Max	Shear	0.025 (0.64)	
				Flexure	0.01 (0.25)	
C17	-1.13%	-212.5 (-945.4)	Max	Shear	0.06 (1.5)	
				Flexure	0.013 (0.33)	
C18	0.82%	108.4 (482.0)	Max	Shear	0.05 (1.3)	
				Flexure	0.025 (0.64)	
C19	-1.13%	-212.5 (-945.4)	Max	Shear	0.06 (1.5)	
				Flexure	0.13 (3.2)	
C20	0.82%	106.1 (472.1)	Max	Shear	0.03 (0.76)	
				Flexure	0.03 (0.76)	

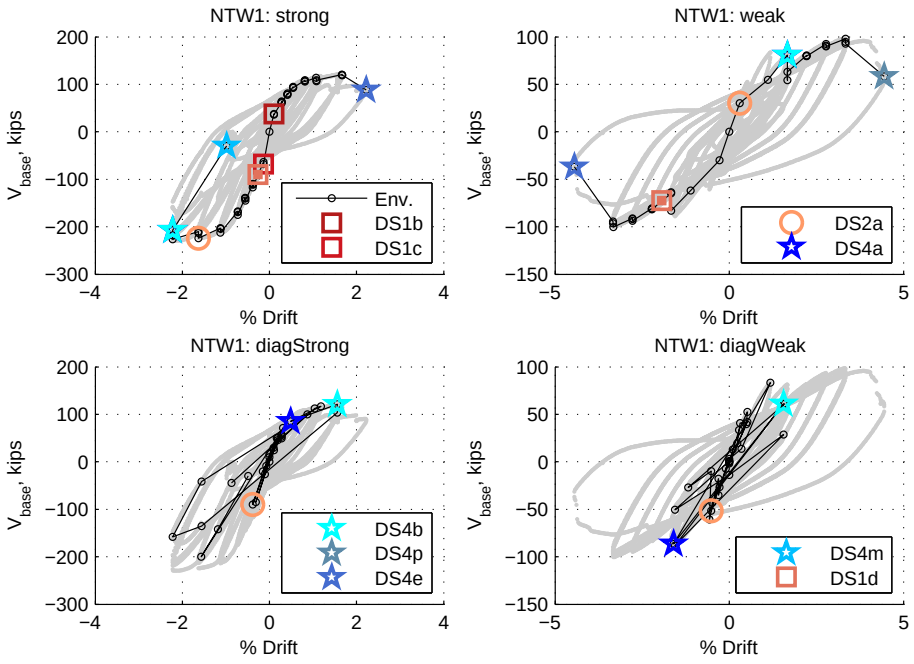

Figure A.117: Envelope for NTW1

A.62 NTW2

Table A.101: NTW2 damage information

MOR	DS	% Drift	Force, kips (kN)	Description	Figure
1	DS1b	0.04%	30.1 (133.9)	Flex. cracks in web tip when flange in compression)	
	DS1c	0.05%	-44.0 (-195.8)	Shear cracks in web under FC/FT loading	
	DS1d	0.24%	-103.5 (-460.3)	As determined from moment-curvature analysis	
2	DS2a	1.67%	-238.1 (-1058.9)	Spalling of cover at base of web tip when flange is in tension	
	DS2d	2.19%	-208.0 (-925.1)	Vertical cracks in flange tips during figure-eight cycle (not specified when)	
4	DS4b	2.19%	-208.0 (-925.1)	Bars buckled in web tip (4 endmost); accompanied by stirrup fracture	
	DS4e	2.70%	-212.2 (-944.0)	Previously buckled bars fractured in web tip after cycling	
	DS4q	2.19%	-208.0 (-925.1)	Fractured confining hoops 8 inches above foundation in web tip (and bars buckled)	
	DSr10	2.19%	-218.3 (-971.1)	shr cracks equal to 1/8 in. when flange is in tension (flex. cracks nearly 1/16, but not quite)	
	DSr9	1.71%	130.2 (579.0)	shr cracks equal to 0.10 in. when flange is in compression	

Table A.102: NTW2 crack width information

					Crack Width, in (mm)	
DS	% Drift	Force, kips (kN)	Exact/Max	Crack Type	Max.	Resid.
DS2a	-1.67%	-238.1 (-1058.9)	Max	Shear	0.06 (1.5)	
				Flexure	0.04 (1)	
DSr9	1.71%	130.2 (579.0)	Max	Shear	0.1 (2.5)	
				Flexure	0.035 (0.89)	
DS4b	1.93%	132.1 (587.6)	Max	Shear	0.13 (3.2)	
				Flexure	0.06 (1.5)	
DS4q	1.93%	132.1 (587.6)	Max	Shear	0.13 (3.2)	
				Flexure	0.06 (1.5)	
C1	0.04%	21.2 (94.2)	Max	Shear	0.02 (0.51)	
C2	-0.35%	-138.5 (-615.9)	Max	Shear	0.025 (0.64)	
C3	0.21%	63.4 (281.8)	Max	Shear	0.013 (0.33)	
				Flexure	0.005 (0.13)	
C4	-0.51%	-177.8 (-791.0)	Max	Shear	0.03 (0.76)	
				Flexure	0.0013 (0.033)	
C5	0.43%	106.3 (472.6)	Max	Shear	0.04 (1)	
				Flexure	0.035 (0.89)	
C7	1.09%	123.6 (549.7)	Max	Shear	0.035 (0.89)	
				Flexure	0.013 (0.33)	
C9	0.49%	91.8 (408.2)	Max	Shear	0.035 (0.89)	
				Flexure	0.04 (1)	
C10	-2.19%	-232.3 (-1033.4)	Max	Shear	0.13 (3.2)	
				Flexure	0.06 (1.5)	
C11	1.71%	131.7 (585.7)	Max	Shear	0.1 (2.5)	
				Flexure	0.035 (0.89)	
C12	1.93%	132.1 (587.6)	Max	Shear	0.13 (3.2)	
				Flexure	0.06 (1.5)	

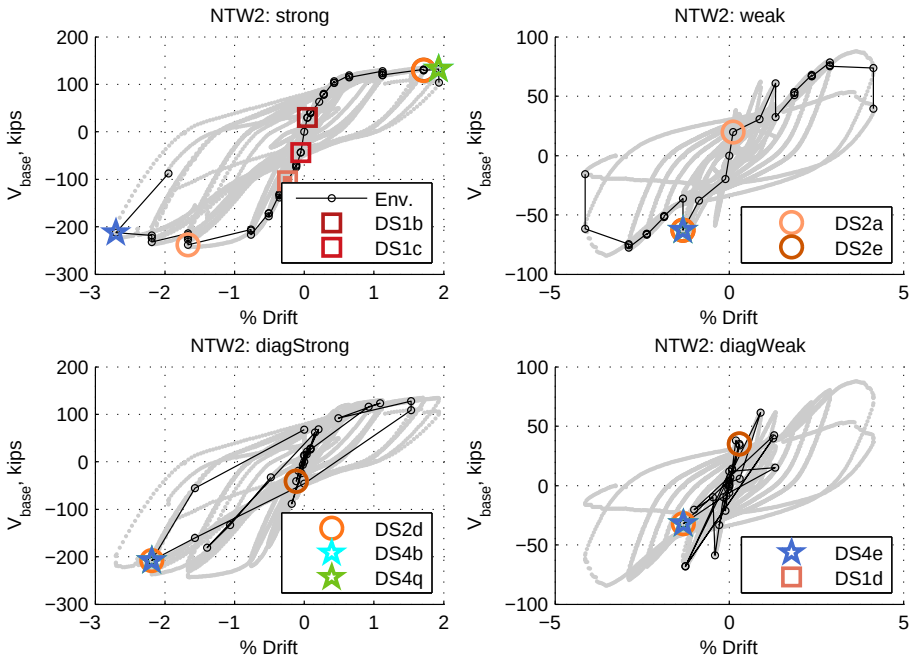

Figure A.118: Envelope for NTW2

A.63 PW1

Table A.103: PW1 damage information

MOR	DS	% Drift	Force, kips (kN)	Description	Figure
1	DS1b	-0.11%	-69.5 (-309.4)		
	DS1c	-0.11%	-69.5 (-309.4)		
	DS1d	0.62%	167.9 (746.7)	As determined from moment-curvature analysis	
2	DS2a	0.56%	170.6 (758.9)		
	DS2d	-0.54%	-157.0 (-698.2)		
3	DS3a	-0.79%	-173.4 (-771.4)		
4	DS4a	1.47%	171.9 (764.8)		
	DS4b	1.47%	187.7 (834.9)		
	DS4e	-1.53%	-83.8 (-372.7)		

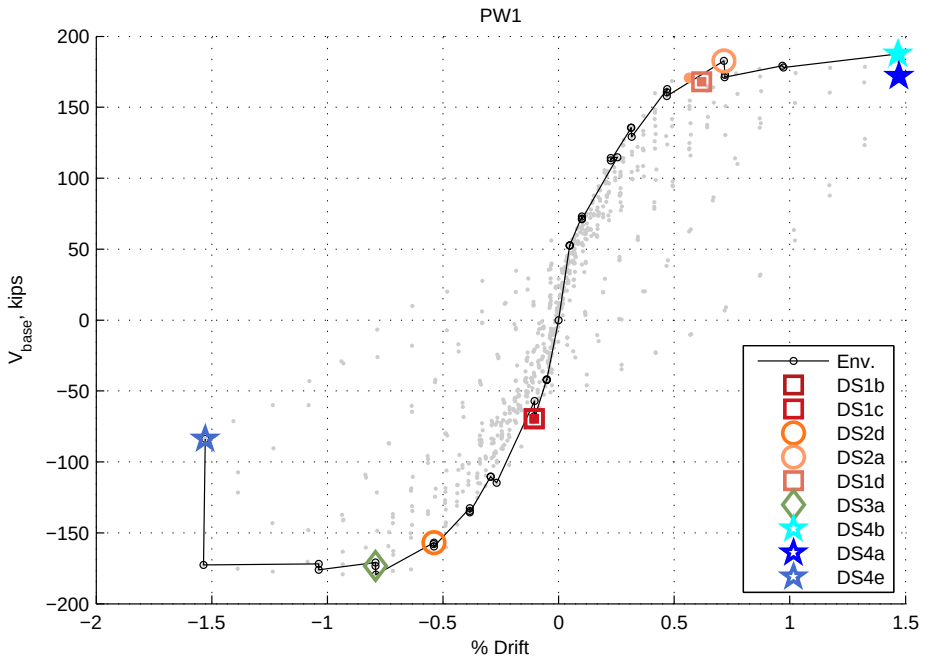

Figure A.119: Envelope for PW1

A.64 PW2

Table A.104: PW2 damage information

MOR	DS	% Drift	Force, kips (kN)	Description	Figure
1	DS1b	-0.10%	-107.0 (-476.0)		
	DS1c	-0.10%	-107.0 (-476.0)		
	DS1d	0.75%	254.1 (1130.2)	As determined from moment-curvature analysis	
2	DS2a	0.76%	260.9 (1160.5)		
	DS2d	0.35%	194.7 (866.2)		
3	DS3a	-0.76%	-260.2 (-1157.5)		
4	DS4a	1.50%	253.7 (1128.6)		
	DS4b	-1.10%	-3.7 (-16.5)		
	DS4k	-1.10%	-3.7 (-16.5)		

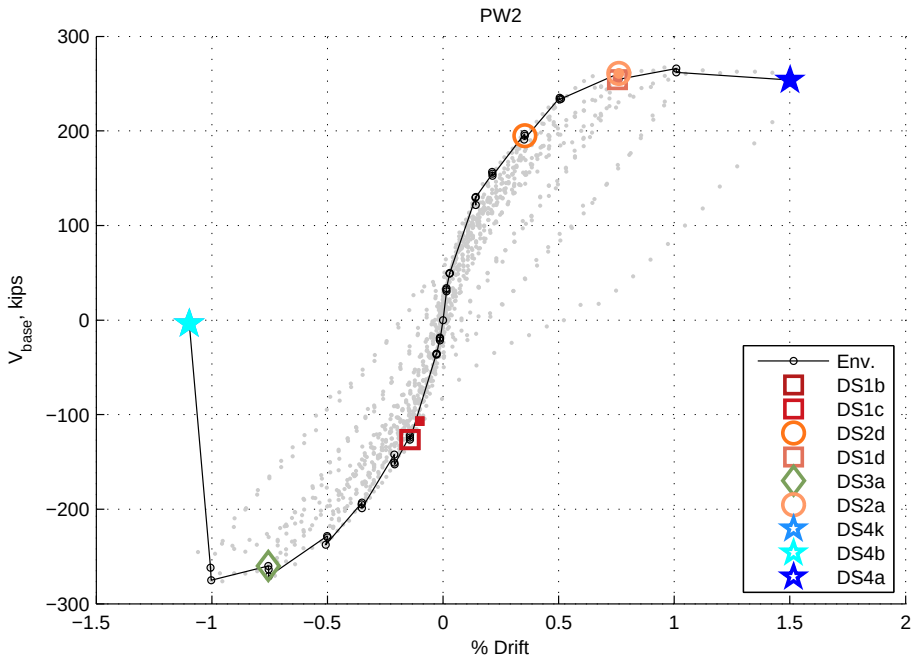

Figure A.120: Envelope for PW2

A.65 PW3

Table A.105: PW3 damage information

MOR	DS	% Drift	Force, kips (kN)	Description	Figure
1	DS1b	-0.06%	-77.6 (-345.0)		
	DS1c	-0.08%	-93.3 (-415.0)		
	DS1d	-0.37%	-185.8 (-826.3)	As determined from moment-curvature analysis	
2	DS2a	-0.40%	-188.1 (-836.9)		
	DS2d	-0.30%	-170.8 (-759.7)		
3	DS3a	0.75%	210.2 (934.9)		
4	DS4a	-1.00%	-205.9 (-915.8)		
	DS4b	1.00%	211.1 (939.1)		
	DS4k	-1.00%	-205.9 (-915.8)		
	DSr9	0.50%	201.0 (894.2)	From testing notes	

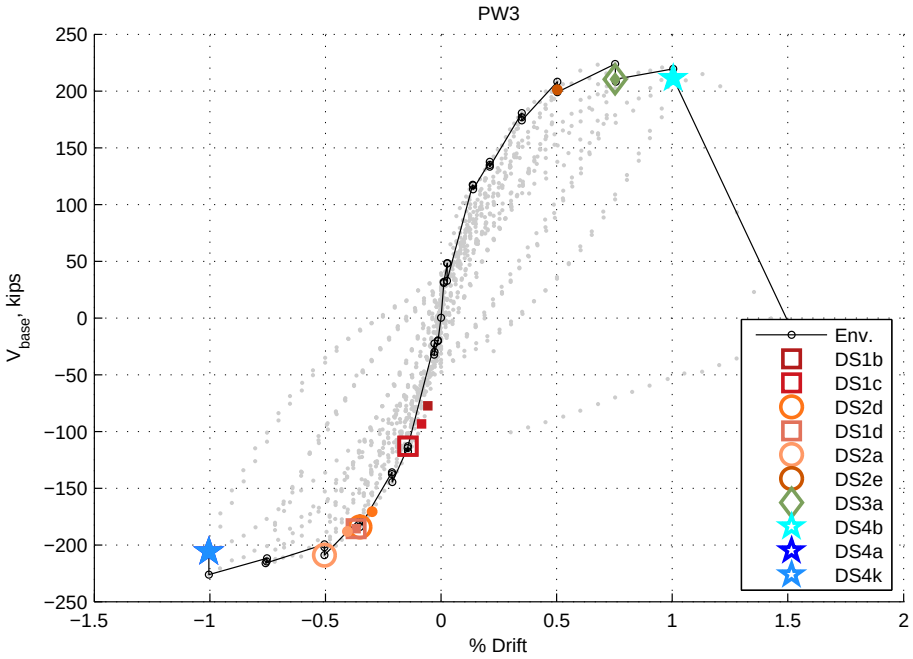

Figure A.121: Envelope for PW3

A.66 PW4

Table A.106: PW4 damage information

MOR	DS	% Drift	Force, kips (kN)	Description	Figure
1	DS1b	-0.09%	-80.2 (-356.7)		
	DS1c	-0.07%	-72.2 (-321.4)		
	DS1d	NaN%	NaN (NaN)	As determined from moment-curvature analysis	
2	DS2a	0.51%	199.2 (886.2)		
	DS2d	0.51%	199.2 (886.2)		
3	DS3a	-0.76%	-213.5 (-949.9)		
4	DS4a	-0.75%	-206.7 (-919.6)		
	DS4b	1.00%	75.4 (335.4)		
	DS4k	1.00%	75.4 (335.4)		
	DSr9	-1.01%	-217.8 (-968.6)	From testing notes	

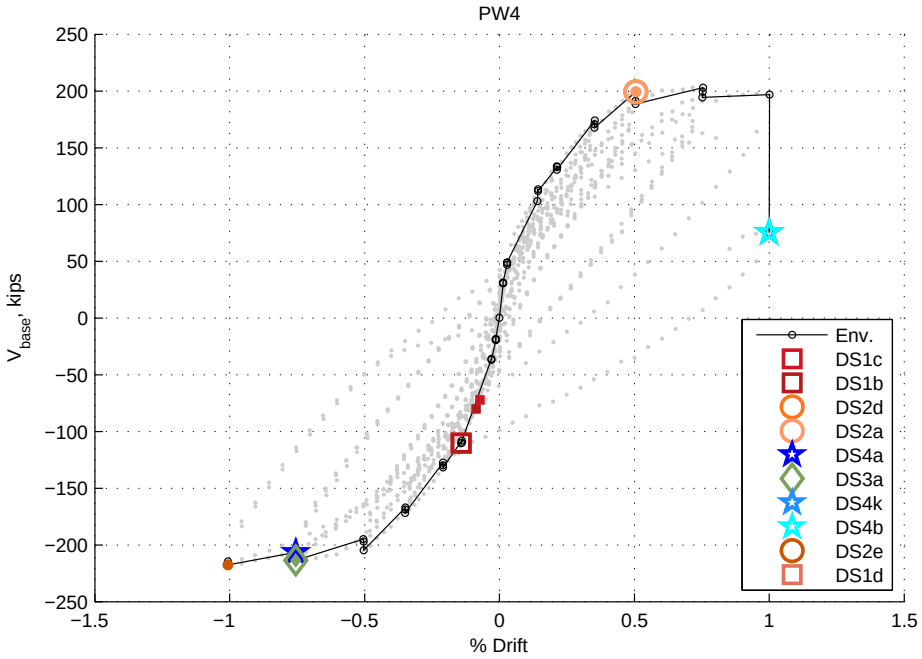

Figure A.122: Envelope for PW4